AD-767 561

STOL TACTICAL AIRCRAFT INVESTIGATION. VOLUME II. DESIGN COMPENDIUM

J. Hebert, Jr., et al

General Dynamics

Prepared for:

Air Force Flight Dynamics Laboratory

May 1973

DISTRIBUTED BY:

NTIS
National Technical Information Service
U. S. DEPARTMENT OF COMMERCE
5285 Port Royal Road, Springfield Va. 22151

AFFDL-TR-73-21-Vol. II

STOL TACTICAL AIRCRAFT INVESTIGATION

VOLUME II ✦ DESIGN COMPENDIUM

J. Hebert, Jr.
E. S. Levinsky
J. C. Ramsey
E. C. Laudeman
H. G. Altman
L. G. Barbee

Convair Aerospace Division of
General Dynamics Corporation

TECHNICAL REPORT AFFDL-TR-73-21

May 1973

Approved for public release; distribution unlimited

Air Force Flight Dynamics Laboratory
Air Force Systems Command
Wright-Patterson Air Force Base, Ohio

273

AIR FORCE/56780/13 September 1973 — 150

FOREWORD

The Design Compendium was prepared by the Convair Aerospace Division of General Dynamics Corporation under USAF Contract F33615-71-C-1754, Project 643A, "STOL Tactical Aircraft Investigation." This contract was sponsored by the Prototype Division of the Air Force Flight Dynamics Laboratory. The USAF Project Engineer was G. Oates (PT) and the Convair Aerospace Program Manager was J. Hebert. H. G. Altman, L. G. Barbee, E. C. Laudeman, E. S. Levinsky, N. A. Ponomareff, and J. C. Ramsey were the principal contributors.

The research reported was conducted during the period 7 June 1971 through 31 January 1973. This report was submitted by the author on 28 February 1973 under contractor report number GDCA-DHG73-001.

This report has been reviewed and is approved.

E. J. Cross Jr.

E. J. CROSS, JR.
Lt. Col USAF
Chief, Prototype Division

DOCUMENT CONTROL DATA - R & D

(Security classification of title, body of abstract and indexing annotation must be entered when the overall report is classified)

1. ORIGINATING ACTIVITY (Corporate author)
Convair Aerospace Division
General Dynamics Corporation
San Diego, California 92138

2a. REPORT SECURITY CLASSIFICATION
Unclassified

2b. GROUP

3. REPORT TITLE
STOL Tactical Aircraft Investigation
Volume II - Design Compendium

4. DESCRIPTIVE NOTES (Type of report and inclusive dates)
Final Report (7 June 1971 to 31 January 1973)

5. AUTHOR(S) (First name, middle initial, last name)
J. Hebert, Jr., E. S. Levinsky, J. C. Ramsey, E. C. Laudeman, H. G. Altman, L. G. Barbee

6. REPORT DATE
May 1973

7a. TOTAL NO. OF PAGES
~~274~~

7b. NO. OF REFS
41

8a. CONTRACT OR GRANT NO.
F33615-71-C-1754

b. PROJECT NO.
643A - Task 0001

c.

d.

9a. ORIGINATOR'S REPORT NUMBER(S)
GDCA-DHG73-001

9b. OTHER REPORT NO(S) (Any other numbers that may be assigned this report)
AFFDL TR-73-21-Vol. II

10. DISTRIBUTION STATEMENT
Approved for Public Release
Distribution Unlimited

11. SUPPLEMENTARY NOTES
---

12. SPONSORING MILITARY ACTIVITY
Air Force Flight Dynamics Laboratory (PTA)
Wright Patterson AFB, Ohio 45433

13. ABSTRACT

The Design Compendium presents methods for estimating the aerodynamic and stability and control characteristics of mechanical flaps and the three lift/propulsion systems: Mechanical Flaps Plus Vectored Thrust, Externally Blown Flaps, and Internally Blown Flaps.

A review of various theoretical approaches is presented to form a basis for the generalized methods that are developed to estimate lift, drag, pitching moment, downwash, and the lateral-directional stability derivatives. Sample problems are presented to allow the most advantageous utilization of the methodology. The data correlations shown at the end of the major sections verify and substantiate the selected approaches.

A general methodology has been developed for predicting the low speed aerodynamic and stability characteristics of STOL transport aircraft. The methodology is applicable to the EBF, IBF, and MF/VT STOL concepts. The basic procedures, which predict the lift curve versus angle of attack, maximum lift coefficient, induced drag, thrust recovery, pitching moment, and downwash angle are easily hand-calculated for a single case or programmed on a small computer to calculate a large number of configurations.

Security Classification

14. KEY WORDS	LINK A		LINK B		LINK C	
	ROLE	WT	ROLE	WT	ROLE	WT
1. Aerodynamics						
2. Externally Blown Flaps						
3. High Lift Systems						
4. Internally Blown Flaps						
5. Lift/Propulsion Concepts						
6. Mechanical Flap/Vectored Thrust						
7. Methodology						
8. Stability and Control						
9. STOL Aircraft						
10. Wind Tunnel Data						

*U.S.Government Printing Office: 1973 -- 758-426/80

Security Classification

ABSTRACT

The Design Compendium presents methods for estimating the aerodynamic and stability and control characteristics of mechanical flaps and the three lift/propulsion systems:

1. Mechanical Flaps Plus Vectored Thrust
2. Externally Blown Flaps
3. Internally Blown Flaps

The mechanical flap has a propulsion system below the wing that is vectored down away from the flap or wing. Lift augmentation is mainly obtained from the vertical component of the jet thrust vector. Additional circulation lift and the accompanying moment was minimized by properly locating the vectored thrust component.

The externally blown flap system has an external jet nozzle mounted below the wing. The propulsion system exhausts a jet stream toward the flap, which spreads spanwise along the wing with the jet flowing through the flap slots and deflected down by the flap. The lift augmentation of this system is analogous to the internally blown flap.

The internally blown flap system has high-velocity air ejected from the vicinity of the knee of the flap in a direction such that the flow will attach to the upper surface of the flap. Lift augmentation is obtained with this system not only from the vertical component of the thrust vector, but also by increasing circulation around the airfoil.

The Data Analysis Report, Volume IV, summarizes the force and rake information measured during the 1,087 hours of low speed wind tunnel testing conducted by the Convair Aerospace Division of General Dynamics during the STOL Tactical Aircraft Investigation. Over 2,730 data runs were generated on 242 major configuration variables that covered the above concepts. This data and subsequent analyses were used to develop the methodology presented herein.

A review of various theoretical approaches is presented to form a basis for the generalized methods that are developed to estimate lift, drag, pitching moment, downwash, and the lateral-directional stability derivatives. Sample problems are presented under the two-digit sections to allow the most

advantageous utilization of the methodology. The data correlations shown at the end of the major sections verify and substantiate the selected approaches. The methodology was developed with a capability that allows it to be broadened into a universal program applicable to mechanical flaps or any lift/propulsion system.

A general methodology has been developed for predicting the low speed aerodynamic and stability characteristics of STOL transport aircraft. The methodology is applicable to the EBF, IBF and MF/VT STOL concepts. The basic procedures, which predict the lift curve versus angle of attack, maximum lift coefficient, induced drag, thrust recovery, pitching moment, and downwash angle are easily hand-calculated for a single case or programmed on a small computer to calculate a large number of configurations. The methodology has been evaluated by comparing its results with wind tunnel test data obtained under the current STOL program for EBF, IBF and MF/VT configurations over a range of jet momentum coefficients from zero to four and with a wide variety of jet nacelle locations and trailing flap configurations.

TABLE OF CONTENTS

TABLE OF CONTENTS, Contd

LIST OF ILLUSTRATIONS

LIST OF ILLUSTRATIONS, Contd

LIST OF ILLUSTRATIONS, Contd

LIST OF ILLUSTRATIONS, Contd

LIST OF ILLUSTRATIONS, Contd

LIST OF ILLUSTRATIONS, Contd

LIST OF ILLUSTRATIONS, Contd

LIST OF ILLUSTRATIONS, Contd

LIST OF TABLES

NOMENCLATURE

Symbol		Units
A or Æ	Aspect ratio of wing	
A'	Aspect ratio of the extended wing area	
b	Wing span	In. or Ft.
c	Airfoil section chord, flap and leading edge retracted	In. or Ft.
c'	Airfoil chord with leading and/or trailing-edge flaps extended	% c
c, c_W	Mean aerodynamic chord	In. or Ft.
C_D	Drag coefficient	
c_d	Section (2-dimensional) drag coefficient	
C_{D_i}	Power-on induced drag coefficient	
C_{D_P}	Power-on minimum profile drag coefficient	
$C_{D_{P_o}}$	Power-off minimum profile drag coefficient of the total aircraft including thrust recovery from leading-edge blowing	
$C_{D_{RAM}}$	Momentum loss coefficient due to the inlet ram drag	
$C'_{D_{RAM}}$	Ram drag based on the extended wing area	
c_{exp}	Exposed mean aerodynamic chord	In. or Ft.
c_{f_i}	Flap chord	% c

NOTE: Primed coefficients are based on the extended wing area.

NOMENCLATURE, Contd

Symbol		Units
c_{f_n}	Trailing-edge flap chord (subscripts denote	% c
C_L	Lift coefficient	
$\Delta C_{L_{LE}}$	Lift coefficient increment due to leading-edge device	
$\Delta C'_{L_{TE}}$	Lift coefficient increment due to the deflection and trailing-edge blowing	
$\Delta C'_{L_{wing}}$	Total increment in lift coefficient due to trailing-edge flap deflection, trailing-edge blowing, leading-edge high-lift device deflection, and leading-edge blowing at zero angle of attack	
c_ℓ	Section (2-dimensional) lift coefficient	
c_{ℓ_o}	Lift coefficient at zero angle of attack for the basic cambered airfoil	
$\Delta c'_{\ell LE}$	Leading-edge flap section lift increment at zero angle attack	
$\Delta c'_{\ell_{TE}}$	Power-on trailing edge flap section lift increment at $\alpha = 0$	
$\Delta c'_{\ell_{TE_o}}$	Power-off trailing edge flap section lift increment at $\alpha = 0$	
$C_{L_{aero}}$	Aerodynamic lift (total lift minus direct thrust component)	
$C_{L_{PT}}$	Direct thrust lift component	
c_{LE}	Leading-edge device chord	% c

NOMENCLATURE, Contd

Symbol		Units
$\bar{c}'_{j_n}$	Average extended wing chord at the spanwise station of the nth jet	% c
$C_{L_{MAX}}$	Maximum lift coefficient	
$C'_{L_{MAX}}$	Power-on lift coefficient at the power-on stall angle of attack	
$C'_{L_{MAX_o}}$	Power-off maximum lift coefficient	
$C_{L_{MAX_a}}$	Maximum lift of the basic clean airfoil	
$\Delta C'_{L_{MAX_{LE}}}$	Increment in maximum lift due to the deflection and blowing of a leading-edge high-lift device	
$\Delta C'_{L_{MAX_{TE}}}$	Increment in maximum lift due to the deflection and blowing of a trailing-edge flap system	
$\left.\Delta C'_{L_{MAX_{LE}}}\right)_{PWR}$	Increment in maximum lift coefficient due to leading-edge blowing	
$\left.\Delta C'_{L_{MAX_{TE}}}\right)_{o}$	Power-off maximum lift coefficient increment due to the deflection of the trailing-edge flap system	
$\left.\Delta C'_{L_{MAX_{TE}}}\right)_{PWR}$	Maximum lift coefficient increment due to blowing on the trailing-edge flap system	
$c_{\ell_{max}}$	Section (2-dimensional) maximum lift coefficient	
$c_{\ell_{max_a}}$	Two-dimensional maximum lift coefficient as estimated from DATCOM (Paragraph 4.1.1.4)	
$\left.\Delta c'_{\ell_{max}}\right)_{LE}$	Two-dimensional increment in maximum lift coefficient	

NOMENCLATURE, Contd

Symbol		Units
$\left.\Delta c'_{\ell_{\max_{TE}}}\right)_o$	Increment in the two-dimensional maximum lift coefficient, power-off	
C'_{L_α}	Lift curve slope	/Deg
$\left.C'_{L_\alpha}\right)_o$	Power-off lift curve slope measured at the angle of zero lift	/Deg
$\left.C'_{L_\alpha}\right)_\alpha$	Lift curve slope angle-of-attack, "α"	/Deg
$\left.C'_{L_\alpha}\right)_{\alpha_{o_L}}$	Lift-curve slope evaluated at angle of zero lift	/Deg
c'_{ℓ_α}	Two-dimensional lift curve slope	/Deg
$\left.c'_{\ell_\alpha}\right)_o$	Two-dimensional power-off lift-curve slope	/Deg
$c'_{\ell_{\alpha_{th}}}$	Two-dimensional theoretical lift curve slope	/Deg
C_{ℓ_β}	Rolling moment due to sideslip	/Deg
c_{ℓ_δ}	Rate of change of lift with flap deflection at constant angle of attack	/Deg
$c_{\ell_{\delta_i}}$	Lift effectiveness for the i^{th} flap segment	/Deg
$\left.c'_{\ell_\delta}\right)_{LE}$	Theoretical leading edge lift effectiveness parameter	/Deg
C_m	Moment coefficient based on free-stream velocity	
Δc_m	Two-dimensional pitching moment increment	

NOMENCLATURE, Contd

Symbol		Units
$\Delta c'_{m_{TE}}$	Trailing-edge flap pitching moment increment at zero angle of attack	
C_N	Normal force coefficient based on free-stream velocity	
C_{n_β}	Yawing moment due to sideslip	Deg
c_r	Root chord	In. or Ft.
c_x	Distance from the leading edge to the leading edge of first flap segment	% c
C_{y_β}	Side force due to sideslip	/Deg
C_μ	Overall gross jet momentum coefficient at the blowing nozzle for an IBF, or at the jet exit for EBF and MF/VT systems	
$C_{\mu_{LE}}$	Leading-edge blowing momentum coefficient	
C_{μ_J}	Bowing momentum coefficient of engine blowing system	
C'_{μ_J}	Blowing momentum coefficient of engine	
C'_{μ_o}	Portion of the engine blowing momentum coefficient captured by the trailing edge flap	
C_{μ_T}	Blowing momentum coefficient of the trailing edge blowing system (IBF)	
$C'_{\mu_{TE}}$	Blowing momentum coefficient at the trailing edge flap	
$\left. C'_{\mu_T} \right)_{TE}$	Momentum coefficient of EBF system measured at the T.E.	

NOMENCLATURE, Contd

Symbol		Units
c_μ	Section (2-dimensional) momentum coefficient	
c'_{μ_c}	Section blowing momentum coefficient captured by the trailing edge flap based on the wing area spanned by the blowing per engine	
c_{μ_L}	Section (2-dimensional) leading edge blowing momentum coefficient	
c_{μ_T}	Section (2-dimensional) trailing edge blowing momentum coefficient	
DSF32	Double slotted flap configuration No. 32	
d_{j_n}	Diameter of the nth jet stream at the flap trailing edge assuming a six-degree jet expansion angle due to mixing	In. or Ft.
EBF	Externally blown flap	
e	Induced drag factor (aerodynamic efficiency), which depends on blowing coefficient and the type of STOL system	
e_o	Power-off aerodynamic efficiency	
gap_i	Gap between successive flap elements	% c
h_{noz}	Height of the blowing slot	In.
h_1, h_2	Engine buttock line locations	In. or Ft.
I	Number of slots or segments in the flap system	
IBF	Internally blown flap	
i	Subscript that indicates the 1st, 2nd, 3rd, etc. flap segment of double- or triple-slotted flap	

NOMENCLATURE, Contd

Symbol		Units
i_e	Engine incidence angle relative to mean chord plane (MCP)	Deg
K_b or k	Partial span flap factor	
$K_{b_{LE}}$	Leading-edge partial-span factor	
ΔK_{b_n}	Partial-span blowing factor	
ΔK_{b_o}	Power-off partial-span flap factor	
K_{PWR}	Ratio of the power-on to power-off lift curve slope	
k_{pwr}	Theoretical ratio of the 2-dimensional powered to the unpowered lift curve slope	
K_{MAX}	Correlating constant based on the leading-edge configuration	
K_T	Equal to 2.0 for IBF and MF/VT systems and equal to 1.0 for EBF systems	
M	Mach number	
MF/VT	Mechanical Flap/Vectored Thrust	
m	Number of flap segments	
N	Total number of engine nacelles contributing to flap blowing (EBF only)	
n	Nacelle location	% b
n_e	Number of engines	
overlap_i	Overlap between successive elements	% c
PBF	Plain blown flap	

NOMENCLATURE, Contd

Symbol		Units
R_e	Nozzle radius	In. or Ft.
R'	Jet efflux radius	In. or Ft.
r	Thrust recovery factor	
S	Basic wing reference area	Sq. Ft.
S'	Extended wing area including the chord extension due to both trailing- and leading-edge high-lift devices	Sq. Ft.
SSF2	Single slotted flap, Configuration No. 2	
S_{exp}	Exposed wing area	Sq. Ft.
S'_j	Extended wing area spanned by the blowing nozzle	Sq. Ft.
S_W	Wing area	Sq. Ft.
s	Spreading angle of jet efflux	Deg.
TSF 311	Triple slotted flap, Configuration No. 311	
t/c	Airfoil thickness ratio	
V_e	Engine exhaust velocity	Ft./Sec.
V_∞	Free-stream velocity	Ft./Sec.
X	$\cos^{-1}\left[2\ (x_S/c') - 1\right]$	
X_e	Horizontal distance from leading edge to engine exhaust plane	In. or Ft.
X_H	Longitudinal displacement from 0.25 $\bar{c}_W$ in body-axis system	In. or Ft.
X_{ref}	Moment reference center as a fraction of the mean aerodynamic chord	In. or Ft.

NOMENCLATURE, Contd

Symbol		Units
Z	Vertical displacement from the wing wake	In. or Ft.
Z_e	Average vertical distance from MCP to center of engine at the exhaust plane	In. or Ft.
Z_H	Vertical displacement from $0.25\ \bar{c}_W$ in body-axis system	In. or Ft.
z_e	Actual vertical distance from MCP to centerline of engine at the exhaust plane	In. or Ft.
RATIO		
$\bar{A}_c/A_j$	Average jet capture ratio	
$\left(\frac{b'}{b}\right)$	Ratio of vortex span to geometric span	
$\frac{C_{L_{MAX}}}{c_{\ell_{max}}}$	Empirical factor used to correct section maximum lift coefficient for finite wings, including corrections for wing sweep and leading-edge radius	
$\left(\frac{C_{\ell_\beta}}{C_L}\right)_A$	Aspect ratio contribution to C_{ℓ_β}, power off	/Deg
$\left(\frac{C_{\ell_\beta}}{C_L}\right)_\Lambda$	Sweep contribution to C_{ℓ_β}, power off	/Deg
$\left(\frac{\Delta C_{\ell_\beta}}{C_{L_{aero}}}\right)_A$	Incremental aspect ratio contribution to C_{ℓ_β} due to power	/Deg

NOMENCLATURE, Contd

Symbol		Units
$\left(\frac{\Delta C_{\ell_\beta}}{C_{L_{aero}}}\right)_\Lambda$	Incremental sweep contribution to C_{ℓ_β} due to power	/Deg
$\left(\frac{\Delta C_{\ell_\beta}}{C_{L_{aero}}}\right)_\Lambda$	Incremental sweep contribution to C_{ℓ_β} due to power	/Deg
$\left(\frac{C_{n_\beta}}{C_L}\right)_A$	Aspect ratio contribution to C_{n_β}, power off	/Deg
$\left(\frac{C_{n_\beta}}{C_L}\right)_\Lambda$	Sweep contribution to C_{n_β}, power off	/Deg
$\left(\frac{C_{n_\beta}}{C_{L_{aero}}}\right)_A$	Incremental aspect ratio contribution to C_{n_β} due to power	/Deg
$\left(\frac{\Delta C_{n_\beta}}{C_{L_{aero}}}\right)_\Lambda$	Incremental sweep contribution to C_{n_β} due to power	/Deg
$\left(\frac{C_{y_\beta}}{C_L}\right)_A$	Aspect ratio contribution to C_{y_β}, power off	/Deg
$\left(\frac{C_{y_\beta}}{C_L}\right)_\Lambda$	Sweep contribution to C_{y_β}, power off	/Deg
$\left(\frac{\Delta C_{y_\beta}}{C_{L_{aero}}}\right)_A$	Incremental aspect ratio contribution to C_{y_β} due to power	/Deg

NOMENCLATURE, Contd

Symbol		Units
$\left(\frac{\Delta C_{y_\beta}}{C_{L_{aero}}}\right)_\Lambda$	Incremental sweep contribution to C_{y_β} due to power	/Deg
c'_f/c'	Extended trailing edge flap chord to overall extended wing chord ratio	
c'_{LE}/c'	Extended leading edge flap chord to overall extended wing chord	
$c_{\ell_\alpha}/c_{\ell_{\alpha th}}$	Reynolds-number-dependent correction for boundary layer displacement effects	
$\left(\frac{c_{m_\delta}}{c_{\ell_\delta}}\right)_{theory\ LE}$	Leading edge flap center of pressure location from thin airfoil theory	
$\left(\frac{c_{m_\delta}}{c_{\ell_\delta}}\right)_{theory\ TE}$	Trailing-edge flap center of pressure location from thin airfoil theory	
$\left(\frac{h_H}{\bar{c}_W}\right)$	Vertical displacement from 0.25 $\bar{c}_W$ reference point in stability axes	
$\left(\frac{h_H}{\bar{c}_W}\right)_{vortex}$	Vertical displacement of horizontal tail from vortex sheet	
$\left(\frac{\Delta h}{\bar{c}_W}\right)_{wake}$	Incremental displacement of the vortex sheet	
$\frac{dK_b}{d\eta}$	Slope of the partial span flap factor curve	
$(1 - \Delta C_\mu/C_\mu)$	Estimated fraction of the IBF jet momentum remaining at the flap trailing edge and based on the ratio of the flap chord to the jet nozzle height, h_{noz} (scrubbing loss)	

NOMENCLATURE, Contd

Symbol		Units
$(1 - 0.12\ c'_j/c)$	Estimated fraction of the EBF jet momentum remaining at the flap trailing edge and based on the total flap chord ratio, c'_f/c (scrubbing loss)	
GREEK		
α	Angle of attack of the wing root chord with respect to the forward velocity	Deg
$\Delta\alpha_{i_{pwr}}$	Change in induced angle of attack (downwash angle) due to power and is to be evaluated at the power-on stall angle of attack and with the flaps extended	Deg
α_{o_L}	Zero-lift angle of attack for an untwisted wing	Deg
$\alpha_{o_{L_o}}^*$	Power-off angle of zero lift with full BLC	Deg
$\alpha_{o_{L_{pwr}}}$	Power-on angle of zero lift	Deg
Δ_{α_S}	Change in stall angle of attack due to power	Deg
$\alpha^*_{s_o}$	Power-off angle of attack at maximum lift with full BLC	Deg
$\Delta\alpha_t$	Angle of attack effect of wing twist	Deg
α_W	Wing angle of attack	Deg
$\Delta\alpha_o/\theta$	Change in wing zero-lift angle of attack due to a unit change in linear wing twist	
β	Equal to $\sqrt{1-M^2}$	
δ_f	Trailing-edge flap deflection	Deg
δ_{f_1}	Angle between successive chord planes	Deg
δ_{f_i}	Flap deflection of the i^{th} flap segment	Deg

NOMENCLATURE, Contd

Symbol		Units
$\delta_H)_{EFF}$	Effective deflection angle of the leading-edge device and is expressed in terms of the geometric leading-edge device deflection angle, δ_H	Deg
δ_{LE}	Leading-edge high-lift device deflection angle	Deg
δ_T	Deflection angle of the engine tailpipes, measured relative to the wing reference plane	Deg
$\delta*_T$	Effective jet turning angle	Deg
ϵ	Average spanwise wing downwash angle at infinity	Deg
ϵ_o	Downwash angle in the vortex plane	Deg
$\Delta\epsilon_A$	Downwash angle increment for wing aspect ratio effects	Deg
$\Delta\epsilon_{EBF}$	Downwash angle increment for an EBF configuration	Deg
$\Delta\epsilon_{IBF}$	Downwash angle increment for an IBF configuration	Deg
$\Delta\epsilon_{MF/VT}$	Downwash angle increment for an MF/VT configuration ($\delta_T \approx 90$ degrees)	Deg
$\Delta\epsilon_\Lambda$	Downwash angle increment for wing sweep angle effects	Deg
η_i	Efficiency factor for a flap segment	
η_{max} and η_δ	Empirical factors to correlate available test data on airfoils with trailing edge flaps	
η_p	Plain flap efficiency factor depending on the flap deflection angle, δ_f, plus the upper surface angle at the flap trailing edge, ϕ_{TE}	

NOMENCLATURE, Contd

Symbol		Units
η_S	Static turning efficiency	
$\eta_{S_{I_i}}$	Slotted flap efficiency factor for the i^{th} flap segment	
θ	Twist of the wing tip with respect to the root section in degrees (negative for washout)	/Deg
θ_f	$\cos^{-1}\left[1 - 2\,(c_f'/c')\right]$	/Deg
θ_{LE}	$\cos^{-1}\left[1 - 2\,(c_{LE}/c')\right]$	/Deg
θ_S	Static turning angle	/Deg
$\Lambda'_{c/2}$	Mid-chord sweep angle of the extended wing	
$\Lambda_{c/4}$	Sweep of quarter chord line of the basic wing	/Deg
λ	Wing taper ratio	
ϕ_{TE}	Upper surface trailing edge angle	/Deg

SECTION 1

INTRODUCTION

The overall objective of this Phase I effort was to produce a generalized methodology for estimating the aerodynamic and stability and control characteristics of mechanical flaps and three STOL lift/propulsion systems:

1. Mechanical Flap Plus Vectored Thrust (MF/VT) — Normal force components due to conventional wing lift and to direct engine thrust vectoring independent of wing system.
2. Externally Blown Flap (EBF) — Normal force components due to conventional wing lift, deflected thrust, and augmented wing lift by high-energy, external blowing.
3. Internally Blown Flap (IBF) — Normal force components due to conventional wing lift, augmented lift, and vectored thrust by high-energy blowing through wing duct system.

The mechanical flap with vectored thrust has a propulsion system located beneath the wing whose thrust is vectored down away from the flap or wing. Lift augmentation is mainly obtained from the vertical component of the jet thrust vector. Additional lift due to increased circulation may be obtained by properly locating the vectored thrust component.

The externally blown flap system is limited to an external jet nozzle mounted beneath the wing. The propulsion system exhausts a jet stream toward the flap; the jet spreads spanwise along the wing with part of the jet flowing through the flap slots, the remainder deflected down by the flap. The lift augmentation of this system is analogous to the internally blown flap and full spreading is assumed.

The internally blown flap system is defined as a jet flap, where high-velocity air is ejected from the vicinity of the knee of the flap in a direction such that the flow will attach to the upper surface of the flap. Lift augmentation is obtained with this system not only from the vertical component of the thrust vector, but also by increasing circulation around the airfoil.

The results of an analysis of aerodynamic and stability and control data obtained from a series of wind tunnel tests of a 1/20-scale STOL transport model conducted at the General Dynamics Low Speed Wind Tunnel in San Diego during the summer and fall of 1972 are utilized in the development of the methodology. The tests consisted of over 2,700 runs totaling 1,087 hours of testing time for the three lift/propulsion systems designed for use with STOL transport configurations. A vast assortment of interchangeable model components permitted testing of over 240 wing, leading edge, trailing edge, and engine nacelle combinations. The model was also equipped with three independent air systems for engine, leading edge, and trailing edge blowing simulation. Most of the runs were made with a rake of pressure probes capable of measuring flow velocity and deflection at possible tail locations.

A review of various theoretical approaches is presented to form a basis for the generalized methods that are developed to estimate lift, drag, pitching moment, downwash, and the lateral-directional stability derivatives.

SECTION 2

GEOMETRY

The important geometries used in Sections 4 through 9 are presented in this section. Basic definitions of the two-dimensional high-lift systems, which are the basis of the methodology, are given in Figures 2-1 through 2-5. Geometry for triple-slotted, double-slotted, single-slotted, and plain trailing-edge flaps is illustrated. Similar information is shown for the leading-edge slat and Krueger flap.

Jet stream capture area is shown in Figure 2-6. The example shows a propulsion stream tube with the assumed six-degree plume angle and the associated jet capture area at the end of the extended chord.

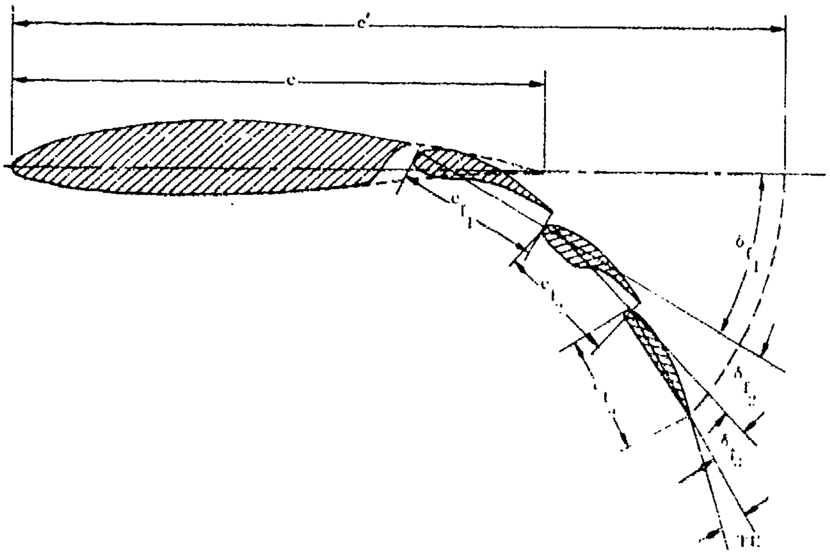

Figure 2-1. Triple-Slotted Flap

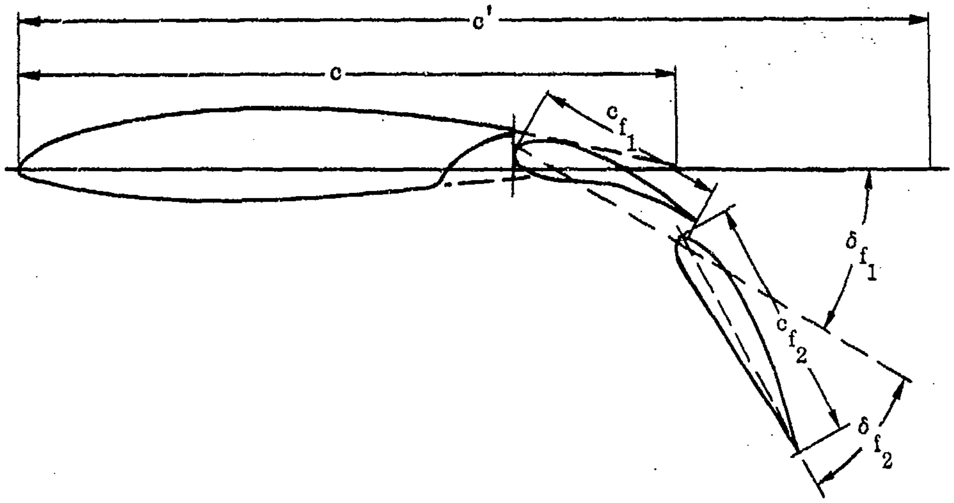

Figure 2-2. Double-Slotted Flap

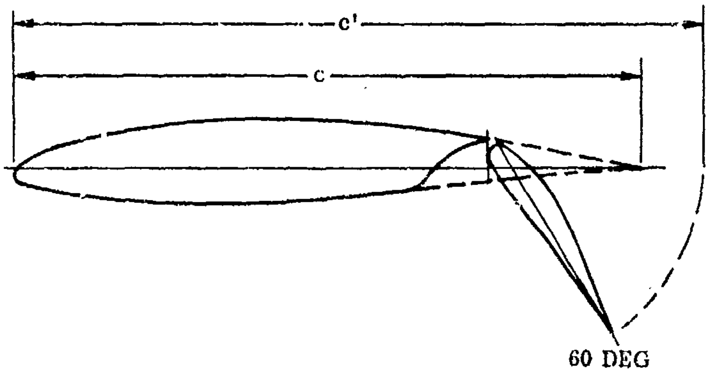

Figure 2-3. Single-Slotted Flap

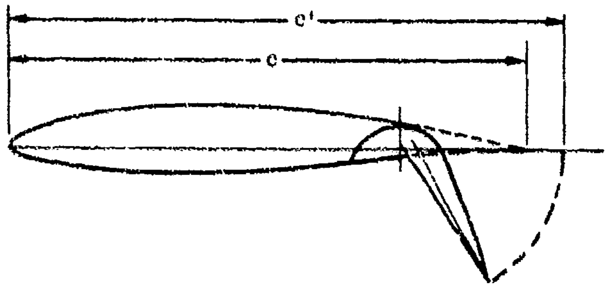

Figure 2-4. Plain Flap

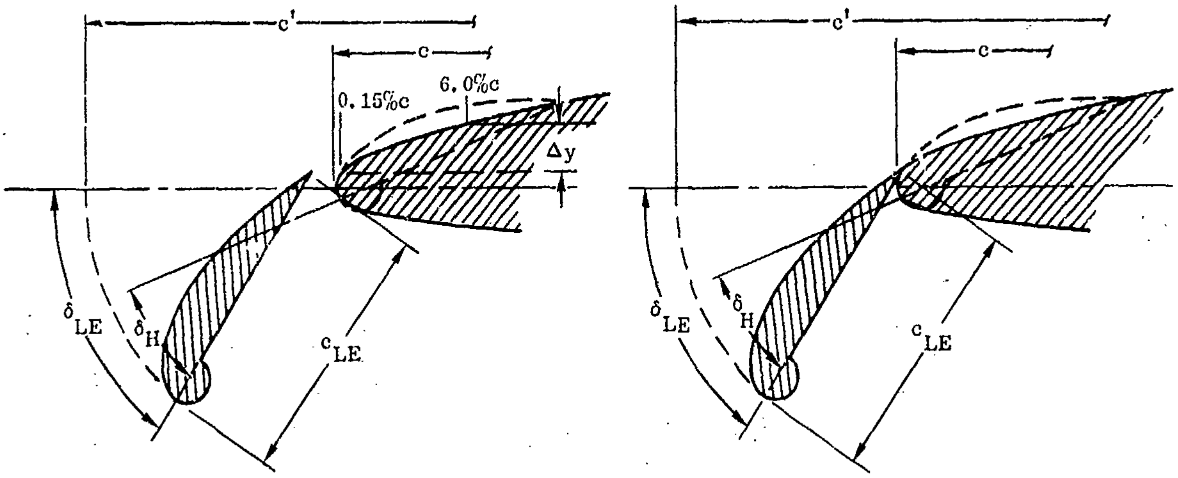

Leading Edge Slat

Leading Edge Krueger Flap

Figure 2-5. Leading Edge Slat & Flap

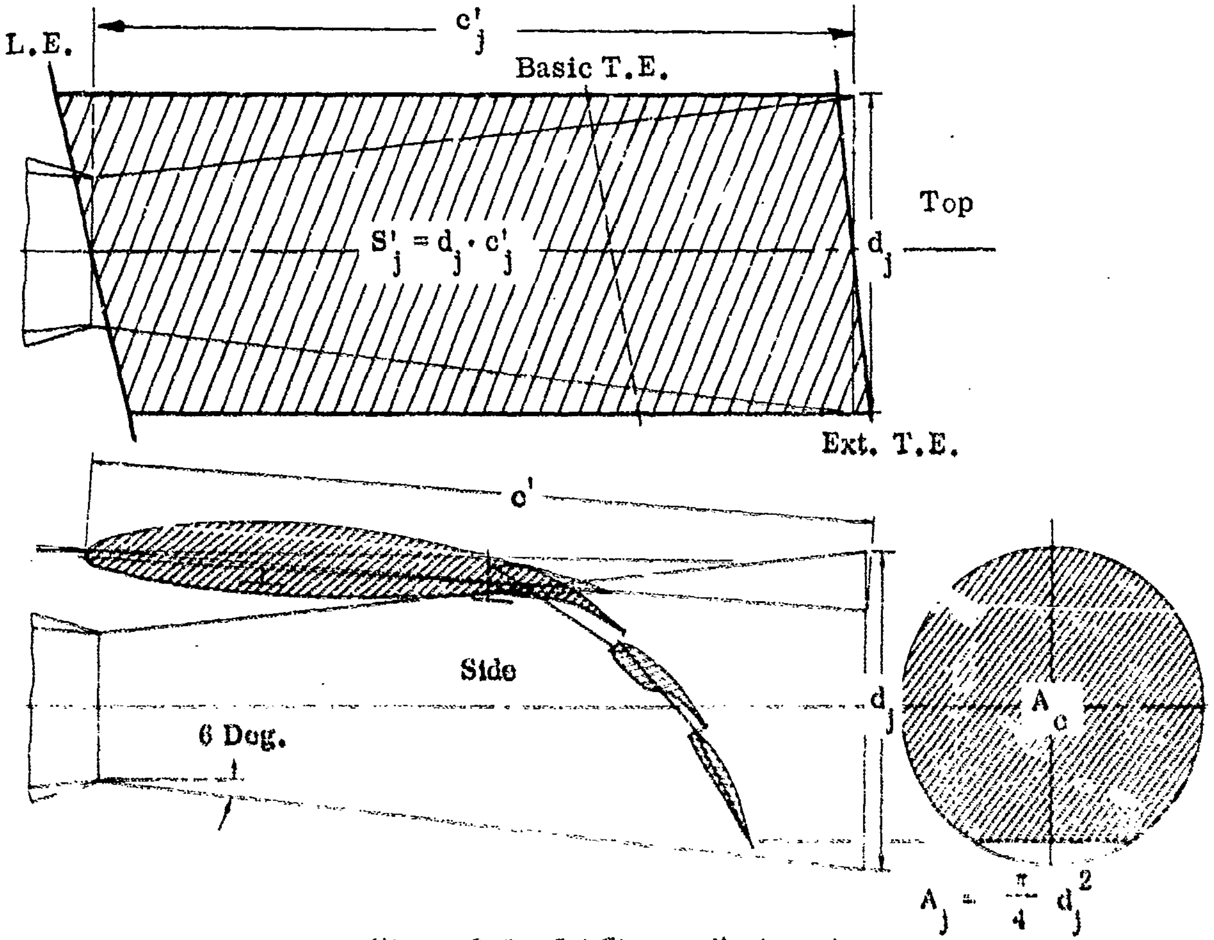

Figure 2-6. Jet Stream Capture Area

SECTION 3

REVIEW OF PREDICTION METHODS

Among the objectives of the current research program dealing with STOL technology is the formulation and substantiation of a generalized methodology for predicting the aerodynamic characteristics of STOL transport aircraft. The methods to be developed should be applicable for the MF/VT, IBF, and EBF concepts and should be economical so that they may be used for correlating the numerous wind tunnel configurations tested. In addition, the methodology should be simple and suitable for incorporation into USAF DATCOM, Reference 3-1.

Prior to developing the desired methodology, several available methods and computer programs were evaluated and compared with wind tunnel data to assess their suitability for incorporation into the generalized method. For the MF/VT concept, comparisons were made with the idealized lifting line equations and with a Convair Aerospace nonlinear span loading computer program, Reference 3-2. For the IBF concept, comparisons were made with several idealized jet flapped wing expressions (References 3-3, 3-4, and 3-5), with a recent modification of the Convair Aerospace nonlinear program to include jet sheet effects (Reference 3-6) and with a computer program based on the lifting surface method of Das (Reference 3-7). For the EBF concept, test data was compared with a Convair Aerospace wing-in-jet method and computer program (References 3-8 and 3-9) and with calculations using the EBF/IBF analogy method (Reference 3-9). Several of these comparisons are discussed in the following paragraphs.

3.1 MECHANICAL FLAPS

The nonlinear span loading program and the idealized lifting line equations are compared with power-off test data in Figure 3-1. The configuration consists of a wing and fuselage, with and without four underslung podded nacelles. The wing aspect ratio was 8 and the quarter chord sweep was 12.5 degrees. Data is shown with flaps retracted, and with triple-slotted flaps extended 60 degrees and the leading-edge Krueger at 55 degrees.

Both methods agree well with the test results in the linear region with the flap retracted. Of special interest is the ability of the nonlinear spanload program to predict the stalling characteristics for this condition. As discussed in References 3-2 and 3-9, the nonlinear program uses two-dimensional airfoil section data that must be stacked along the span at a sufficient number of spanwise control stations. An iteration procedure is used to obtain the circulation along the lifting line. Reference 3-2 also presents a semi-empirical procedure that modifies two-dimensional section characteristics in regions of large spanwise flow, such as occurs with partial span flaps and in the region of the fuselage/wing juncture. The calculations presented using the nonlinear spanload program treat the fuselage as an unflapped wing section that has the same two-dimensional values of $c_{\ell_{max}}$ as the clean airfoil; hence, modifications for spanwise flow effects in the fuselage region were made only with the flaps extended.

As seen from Figure 3-1, the idealized lifting line equations and the nonlinear program agree well with the flaps-extended test data in the linear regions. Agreement of the nonlinear program with test data through stall with flaps extended, although still relatively good, is somewhat dependent on the semi-empirical fuselage correction for $c_{\ell max}$.

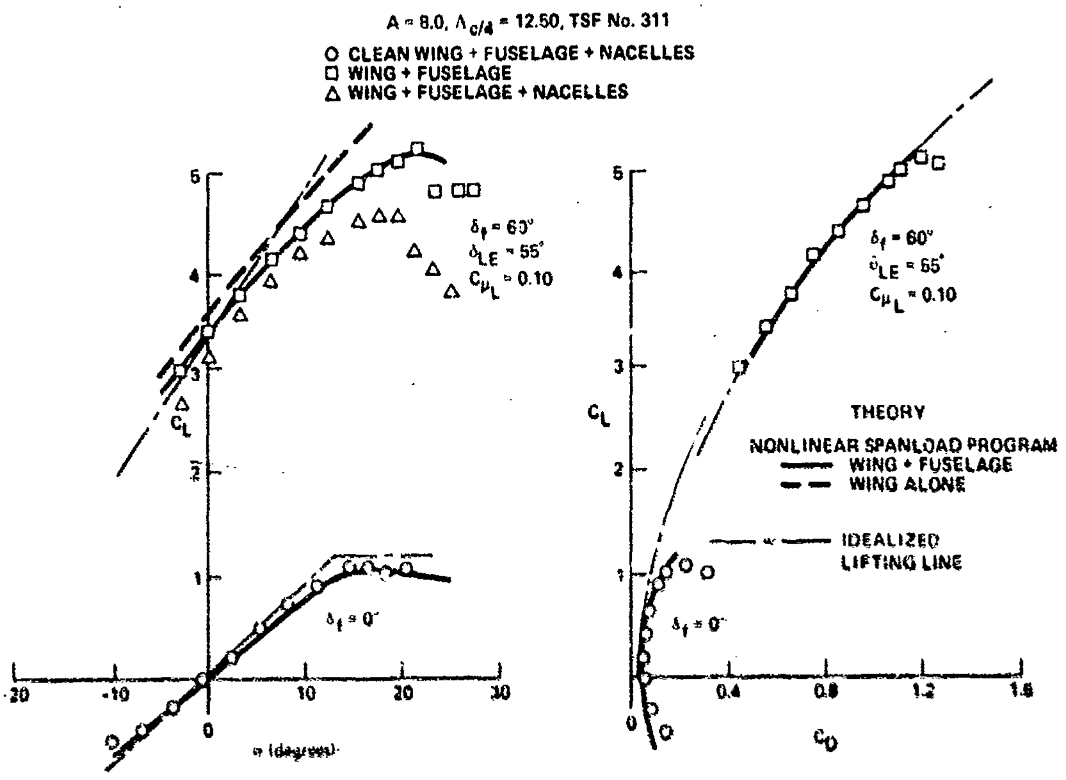

Figure 3-1. MF Test Data Correlation with Nonlinear Span Loading and Lifting Line Theoretical Methods

As noted previously, the nonlinear program requires two-dimensional airfoil and flap data (lift, drag, and pitching moment) through the stall in order to be used for predicting the corresponding nonlinear three-dimensional wing characteristics. Data of this type is shown in Figure 3-2 for the basic NACA-64 series airfoil with a triple-slotted trailing-edge flap deflected 60 degrees, with and without a blown leading-edge flap ($c_{\mu_{LE}} \simeq 0.1$). The data in Figure 3-2 was measured in the two-dimensional wind tunnel test described in Reference 3-10, and represents various amounts of blowing over the trailing-edge flap ($0 \leq c_\mu \leq 3.0$). Thus, the section data may be used to

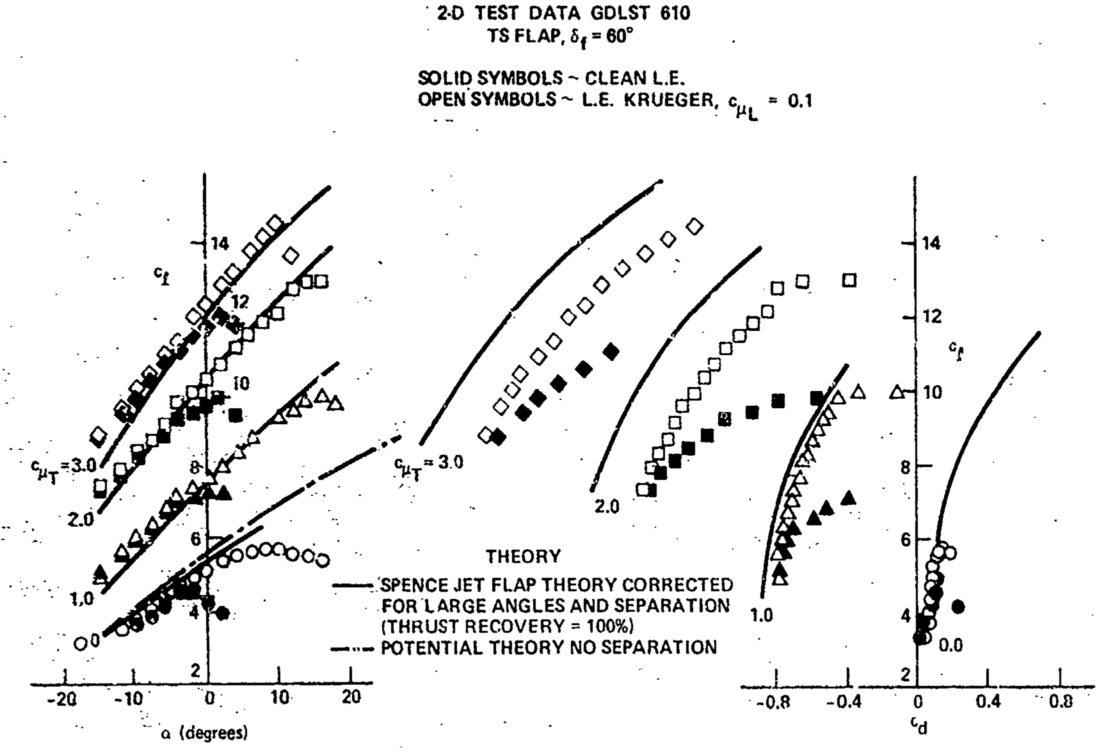

Figure 3-2. Two-Dimensional Test Data Required for Nonlinear Span Loading Program

estimate the three-dimensional IBF characteristics assuming that the nonlinear program (Reference 3-[illegible] remains valid for the IBF concept.

A considerable data bank of two-dimensional data for various flap configurations and blowing conditions is required if the nonlinear program is to be used to predict the stalling characteristics of mechanical flaps or lift/propulsive flap concepts. In lieu of a data bank of the required scope, analytical methods may be used to estimate the aerodynamic section characteristics, at least for the linear range. Calculations of this type, using full potential theory for a $c_\mu = 0$ and the Spence thin airfoil theory for $c_\mu > 0$, are also shown in Figure 3-2. Good agreement with the two-dimensional wind tunnel data is obtained for the blowing coefficients indicated.

3.2 INTERNALLY BLOWN FLAPS

The nonlinear span-loading method was applied to calculate the aerodynamic characteristics of a wing with an aspect ratio of 8 and a triple-slotted IBF at 60 degrees. The experimental section data from Figure 3-2 was used in the nonlinear span load to predict the results compared with the three-dimensional test data in Figure 3-3. Reasonably good agreement is shown for $C_{L_{max}}$ for all blowing coefficients. A semi-empirical method is used to estimate the section characteristics of that part of the wing buried in the fuselage. Predicted lift and lift curve slope values are found to

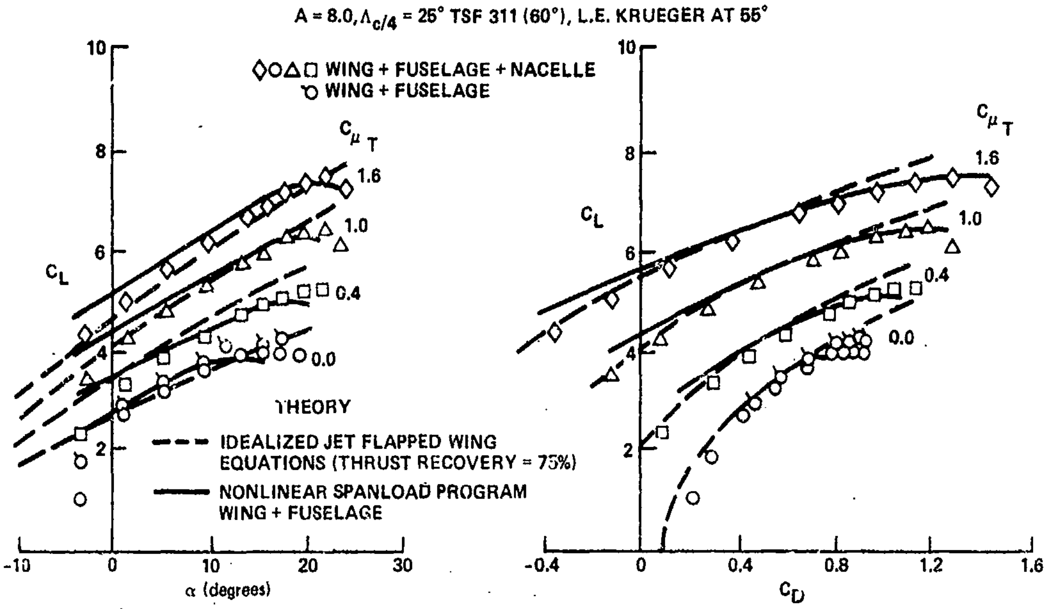

Figure 3-3. IBF Test Data Correlation with Nonlinear Span Loading and Idealized Jet Flap Theory Methods

depart somewhat from test data at the higher blowing coefficients. This possibly could be attributable to the jet sheet effects being neglected in the nonlinear program. A modification for jet sheet effects was inserted into the nonlinear span load program and will be subsequently discussed in connection with Figure 3-4. The nonlinear program is shown to agree with the drag data for all blowing coefficients.

Also shown in Figure 3-3 are calculations using the idealized jet flapped wing equations from References 3-3 and 3-4. These equations yield a reasonably good agreement with lift and induced drag in the linear range. A thrust recovery of 75 percent and a flap cutout for the fuselage (partial-span flap factors taken from mechanical flap calculations) were used in the idealized calculations. The corresponding assumption on thrust recovery is not needed when using the nonlinear spanload program, because the experimental two-dimensional thrust recovery (drag) may be used directly from Figure 3-2.

The nonlinear span load program, after modification for jet sheet effects according to Reference 3-6, has been compared with test data in Figure 3-4 for a plain IBF wing with an aspect ratio of 8 and a quarter chord sweep of 25 degrees. In addition, calculations are shown using the idealized jet flapped-wing equations from References 3-3 and 3-4 and using a computer program based on the linearized lifting surface method of Das as described in Reference 3-7. Experimental two-dimensional section data was not available for the plain IBF. Hence, the modified nonlinear span loading program was based on estimated linear section characteristics and no computation of nonlinear stall could be made.

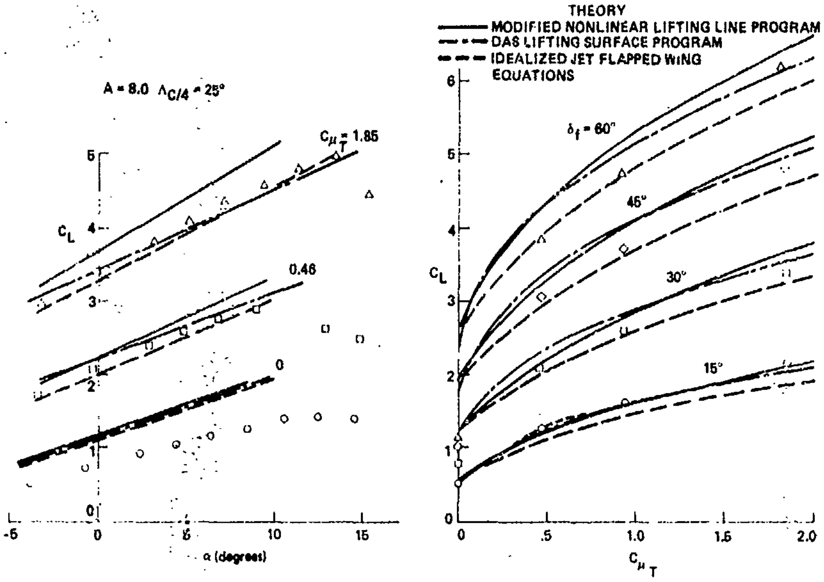

a. 30-Degree Flap Deflection

b. Zero Angle of Attack, Flap Deflections of 15, 30, 45, and 60 Degrees

Figure 3-4. IBF Test Data Correlation with Three Theoretical Methods

All three methods overpredicted the power-off lift and lift curve slopes for a flap deflection of 30 degrees because of separation over the flaps. Empirical corrections for flap separation are therefore required in the two-dimensional methodology to be recommended. Corrections due to flap separation generally disappear at blowing coefficients approaching 1.0 because of the beneficial effects of boundary layer control.

The modified nonlinear span loading program appears to overpredict the lift and lift curve slopes at the higher blowing coefficients. This may be due to an over-correction in the program for the effects of the jet sheet. The idealized jet flapped wing equations from References 3-3 and 3-4, although relatively simple to apply, seem to underpredict the lift at zero angle of attack at the highest blowing coefficients. The Das-type computer program is a lifting surface method that satisfies tangential flow boundary conditions on the wing and dynamic boundary conditions on the jet sheet at eight spanwise control stations. In principle, at least, the Das method should be the most accurate of the three methods for the IBF concept. Comparisons with test data in Figure 2-4 are somewhat inconclusive. Limitations in the Das approach stem from his assumption of a zero chord jet flap, specification of the jet-induced vorticity distribution, and the limitation to eight predetermined spanwise locations for satisfying boundary conditions. The Das method also includes the usual small deflection angle and small thickness linearity assumptions.

Extensive correlations with IBF test data, as performed in Reference 3-11, show that the idealized jet flap wing equations in References 3-3 and 3-4 consistently underestimate the blowing effects on the lift curve slope. On the other hand, a somewhat improved agreement has been obtained by using an alternative equation for the power-on lift curve slope as derived by Kerney (Reference 3-5) that uses matched asymptotic expansions. This may be seen in Figure 3-5, where the methods described in References 3-18, 3-4, 3-5 and 3-7 are compared with the ratio K_{PWR} of the power-on to power-off lift curve slope for test data on an internally blown flap with 15 degrees of deflection (Reference 3-11). Test data from Reference 3-11 for wings of various sweeps and aspect ratios and flap deflection angles up to 60 degrees shows even higher values of K_{PWR} than predicted by Reference 3-5. On the basis of these comparisons, the idealized jet flap equations will be based on Reference 3-5 for power-on lift curve slope. Figure 3-5 also shows that K_{PWR}, when based on Reference 3-5, is near the two-dimensional value:

$$K_{PWR} \simeq k_{pwr} = c'_{\ell\alpha} / c'_{\ell\alpha_0} \tag{3-1}$$

The approximation, which is applicable to the wing aspect ratios and jet momentum coefficients encountered for STOL transports, will be used in the methodology presented in Section 4.1.2.

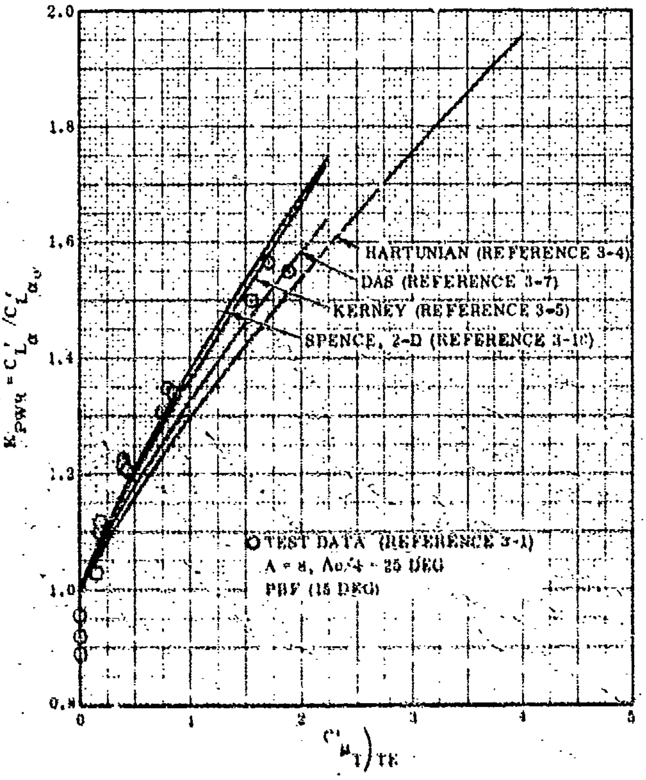

Figure 3-5. Comparison of Several Theories with Test Data for the Ratio of Powered to Unpowered Lift Curve Slopes

The Das-type computer program was used to generate the IBF partial-span factor, K_b, for lift. The results shown in Figure 3-6 indicate that, for the range of parameters considered, the IBF partial-span factor corresponds closely to the mechanical flap (MF) partial-span factor. The MF partial-span factor has therefore been employed in the generalized STOL methodology.

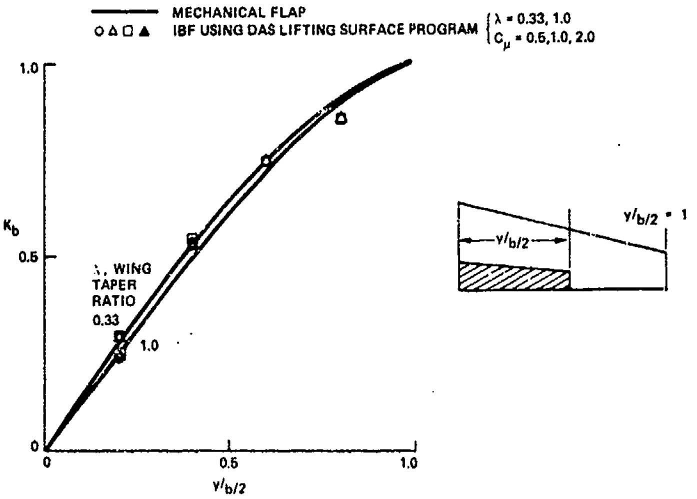

Figure 3-6. Evaluation of IBF Partial-Span Flap Factors

3.3 EXTERNALLY BLOWN FLAPS

A wing-in-jet (WJ) method was developed to estimate aerodynamic characteristics of STOL aircraft with EBF systems. This method is based on analytical procedures for calculating the interaction between a wing and propeller slipstream, and has been described in detail in Reference 3-8.

As depicted in Figure 3-7, the WJ method is a multiple-lifting-line vortex lattice potential theory method. Horseshoe vortex elements of strength Γ_{hi} are distributed over the wing, where h and i are indices referring to the chordwise row and spanwise position of the element. In addition, horseshoe vortex elements of strength Γ'_{hm} and Γ''_{hm} are distributed around the inside and outside, respectively, of each of the jets. Here h and m are indices referring to chordwise and angular locations on the jet surfaces. The usual flow tangency boundary conditions are satisfied at control points on the wing and flap surfaces as shown in Figure 3-7. In addition, boundary conditions of constant static pressure and constant normal flow angle across the jet surfaces are satisfied at control points on the jets (Figure 3-7).

At present, the computer program for the WJ method is limited to consideration of a single chordwise lifting line and to jets of circular cross section. Reduction of the

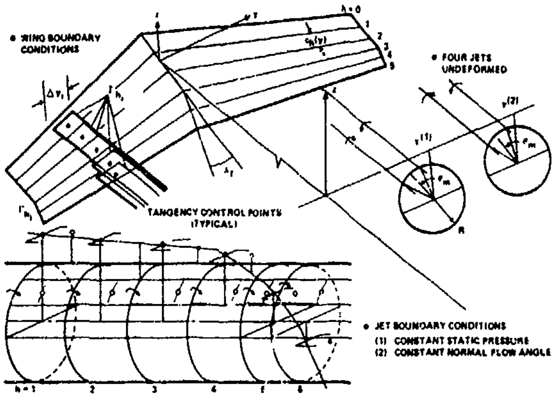

Figure 3-7. Wing-in-Jet Method for EBF, Multiple-Lifting-Line Model

WJ method to a single lifting line representation is depicted in Figure 3-8. The wing and flap systems are taken at an effective angle of attack, α_{EFF}, which may vary across the span. The effective angle of attack is found from thin airfoil theory as:

$$\alpha_{EFF} = \alpha \cdot \alpha_{\delta} (C_{\mu}, \text{ flap geometry}) \cdot \delta_f \qquad (3\text{-}2)$$

where α_{δ} must include effects of power in addition to the usual geometric parameters. Methods to calculate α_{δ} with power-on are included in Reference 3-8.

As illustrated in Figure 3-8, the single-lifting-line model should be adequate for lift and drag for full capture, since for this condition the lifting line tends to be buried at a representative depth inside the jet as sketched in Figure 3-8a. However, for partial capture (viz., jets that lie below the wing and/or for small flap deflections), the single-lifting-line model will prove inadequate when for the condition sketched in Figure 3-8b, the trailing edge of

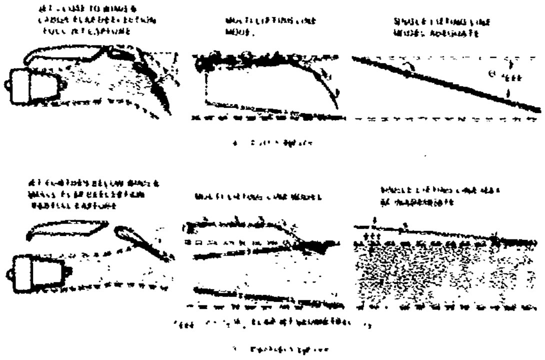

Figure 3-8. Simplification of Wing-in-Jet Method for EBF, Single-Lifting-Line Model

the flap is still buried inside the jet and the single-lifting-line representation shows the bound vortex and control point to be outside the jet. Calculations using the single-lifting-line model have exhibited high sensitivity to the assumed vertical location of the lifting line with respect to the jet surface for the partial-capture condition.

The WJ method is compared with EBF test data in Figure 3-9. The data shown is for jet engines in Position A (high and forward) and for triple-slotted flaps deflected 60 degrees, as shown in Figure 3-10a. Essentially full capture was achieved for this condition. As shown in Figure 3-9a, the assumption of a six-degree jet expansion angle gave improved agreement with test results. All subsequent calculations by the WJ method have been performed using this expansion angle.

Computations at $C_\mu = 0$ were performed with the α_δ values over the wing reduced from theoretical values for flow separation over the flaps. For $C_\mu > 0$, full theoretical α_δ values were assumed over the entire wing span. Thus, it was assumed that the jet efflux spread spanwise over the upper wing surface to a degree sufficient to provide full BLC. This assumption appears reasonable since, as seen in Figure 3-10, the jet intercepts just below the first slot of the triple-slotted flap for Engine Position A.

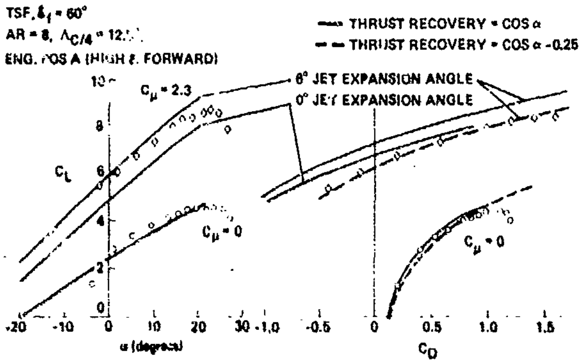

a. Data from GDLST 600

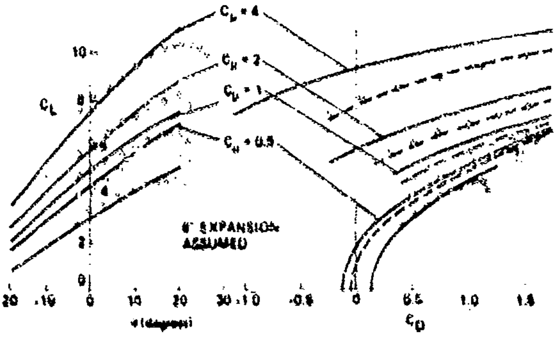

b. Data from GDLST 612

Figure 3-9. EBF Test Data Correlation with the Wing-in-Jet Theoretical Method - Full Capture

a. Jets in High Position, Full Capture

(Eng. pos. A - Ref 3-11)

b. Jets in Low Position, Partial Capture

(Eng. pos. F - Ref 3-11

Figure 3-10. Effect of Jet Height on Capture and BLC

Good agreement is shown for drag when the thrust recovery factor, r, is assumed to be:

$$r = \cos \alpha - 0.25 \qquad (3\text{-}3)$$

where the cosine term represents thrust recovery of the jet engines at inclination α and the 0.25 term corresponds to a loss of 25 percent of the jet momentum in passing over the flaps. The computed induced drag values included in Figure 3-9 are higher than would be expected on the basis of the idealized jet flapped-wing expressions, which assume a constant downwash distribution across the span because of the low aspect ratio of the sections buried in the jets. This higher induced drag is in agreement with EBF test results.

A comparison between the WJ method and EBF test data is shown in Figure 3-11 for jets that have been lowered to Position F, resulting in only partial capture. (See also Figure 3-10b.) The calculations assuming full BLC effectiveness when $C_\mu > 0$ in Figure 3-11a now appear to overpredict the lift at the lower values of C_μ. Calculations assuming full BLC only on the wing sections immersed in the jets are shown in Figure 3-11b. These computations agree better with the test data at low values of C_μ, but underpredict the lift at the higher values. Thus, only limited BLC effectiveness was achieved for Position F. This corresponds with results obtained when the jets do not pass through the two upper flap slots, as shown in Figure 3-10.

As noted previously, the computer program for the WJ method treats the jets as circular in cross section, with no spanwise spreading or distortion due to the flap system. (The six-degree jet expansion is attributed to viscous mixing effects.) The WJ program therefore yields a highly peaked span load distribution as shown in Figure 3-12 for Engine Positions A and F at $C_\mu = 4$. Recent NASA test data (References 3-12 and 3-13) seems to confirm this type of spanload distribution and therefore suggests that EBF jet spreading may be relatively minor, except for BLC effects. Some lift augmentation is predicted by the WJ method over parts of the wing outside the jets due to upwash from the jets, from the highly loaded sections immersed in the jets,

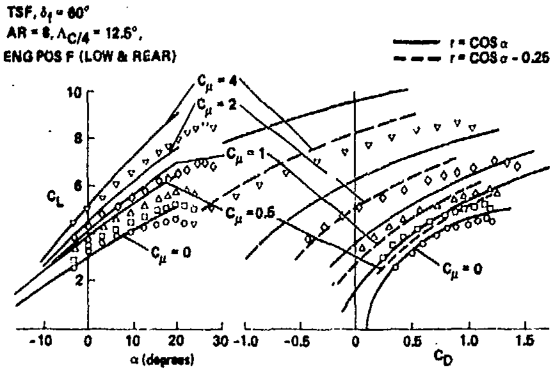

a. Full BLC Effectiveness when $C_\mu > 0$

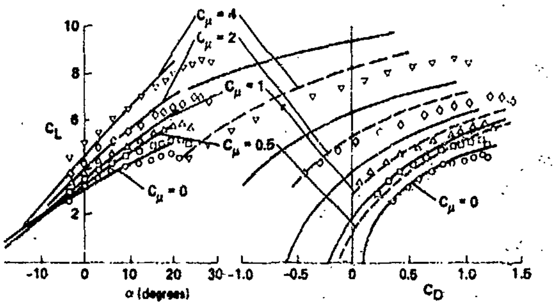

b. No BLC Outside Jets, Full BLC Inside Jets, Revised α_δ According to 2D-EBF

Figure 3-11. EBF Test Data Correlation with the Wing-in-Jet Theoretical Method - Partial Capture

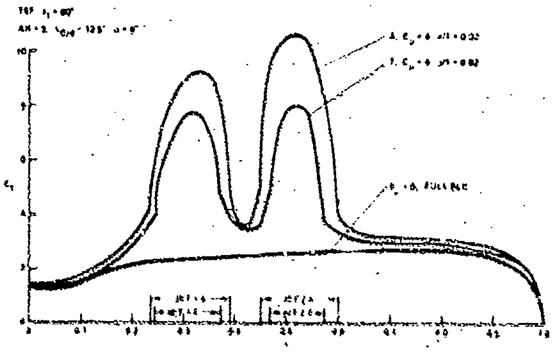

Figure 3-12. Calculated Span Load Distributions by the Wing-in-Jet Method for EBF

and from the establishment of BLC effectiveness as discussed in the preceding paragraphs.

A second and much simpler procedure for predicting aerodynamic characteristics of EBF systems is the analogy method. A discussion of the analogy method, with sample results, is given in Reference 3-9. In brief, the analogy method (pictured in Figure 3-13)

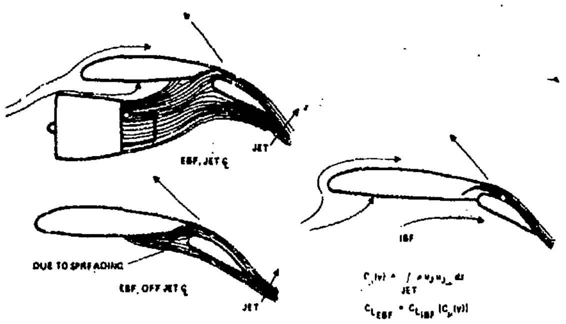

- MATHEMATICAL JUSTIFICATION: TING, LIU, & KLEINSTEIN - AIAA, 1972
- EXPERIMENTAL JUSTIFICATION: TESTS 1DLST 600 & 612

Figure 3-13. EBF/IBF Analogy for EBF

assumes that the EBF jet spreads laterally after impinging on the flap and finally leaves the flap trailing edge tangentially as a thin jet sheet, in much the same manner as for an IBF jet. A necessary requirement for the use of the analogy method is a knowledge of the spanwise distribution of jet momentum coefficient, C_μ.

Wind tunnel data with a triple-slotted flap deflected to 60 degrees and tested as an IBF and an EBF system are shown in Figure 3-14. The EBF data, which is for a 100-percent capture condition (Engine Position A), clearly substantiates the analogy for lift and drag, at least for the configuration investigated.

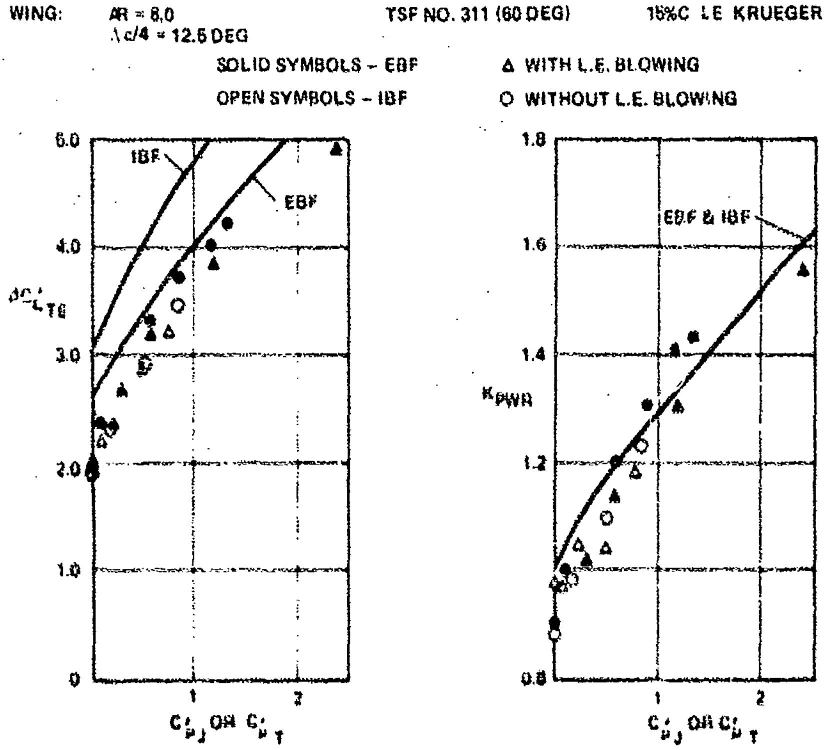

Figure 3-14. EBF Test Data Correlation with the EBF/IBF Analogy Method

A mathematical justification for the analogy method may be obtained by following the systematic expansion procedure in Reference 3-14. The expansion procedure is performed in terms of the chord-to-span ratio (assumed small). Jet thickness is assumed to be of the same order as the chord. This procedure results in an inner two-dimensional solution for a flapped airfoil which is decoupled from an outer three-dimensional solution for the lifting line and jet sheet. The outer first-order solution is unaffected by details of the interaction between the thick jet and flap, and would be identical for the EBF and IBF concepts.

The inner two-dimensional solution defines the section lift chracteristics, $c_\ell(\alpha)$ and $c_m(\alpha)$, which are to be used with the outer solution. The values $c_\ell(\alpha)$ and $c_m(\alpha)$ depend on the airfoil and jet geometry and on the jet and free-stream velocity characteristics. Methods given in Reference 3-14 for obtaining section characteristics are based on two-dimensional airfoil theory in nonuniform sheared flows (References 3-15 and 3-18). These two-dimensional methods use finite-difference and iteration techniques to numerically solve Poisson's equation for the stream function with appropriate boundary conditions, and require extensive use of digital computers. A nonlinear numerical method for treating the interaction between jets and airfoils, and which includes an iteration procedure for determining the shape and location of the jet boundary, has been documented in Reference 3-17.

A highly simplified linearized treatment of the interaction between a flapped airfoil and jet is also included in References 3-8 and 3-9, and has been shown to reduce to the Spence thin jet flap results (Reference 3-8) as the jet thickness approaches zero. The Spence theory may be used as the inner solution for obtaining the two-dimensional powered section characteristics, provided that the jet sheet is thin and adjacent to the flap. This corresponds to 100-percent jet capture, as discussed previously, and results in a correspondence between EBF and IBF aerodynamic characteristics.

3.4 SELECTED GENERALIZED STOL METHODOLOGY

Several of the methods described previously will be used to form the basis of the simplified generalized STOL methodology. Neither the original nor the revised version (modified for jet sheet effects of the nonlinear span-loading program has been used as part of the generalized methodology. The nonlinear program requires a two-dimensional data bank to predict nonlinear stall characteristics which is not readily available. Additional data is required to account for fuselage interference effects on $C_{L_{max}}$ with large flap deflections and with blowing. The Das computer program is linear and was not used directly for the IBF method. It handles only eight previously prescribed spanwise control stations and uses a jet sheet corresponding to a pure jet flap.

Nevertheless, the Das program was used to calculate the partial-span lift factor for the IBF concept and to verify the use of the mechanical flap values for this factor up to a local C_μ value of 2. For the EBF concept, the wing-in-jet method was not incorporated into the generalized methodology because only the single-lifting-line approximation of the WJ method has been programmed. As mentioned previously, this model is sensitive to the vertical location of the lifting line with respect to the jet boundaries and requires an auxiliary two-dimensional, powered, flapped airfoil calculation for α_{EFF}.

The generalized methodology presented may be used to predict lift and net horizontal force coefficients for either the MF/VT, IBF, or EBF concepts. This methodology also includes an estimate of lift curve nonlinearities and of $C_{L_{max}}$.

For the MF concept, the generalized methodology was based on the idealized lifting-line equations with the partial-span lift factor, K_b. The VT effects on lift and induced drag are included in the methodology, assuming zero lift augmentation, provided that the jets do not impinge on the flaps. For partial or total jet impingement on the flaps, lift augmentation is included according to the EBF formulation described. The thrust recovery factor is based on an empirical fit of the test data in terms of the effective jet turning angle for the VT concept.

The generalized methodology reduces to the idealized jet flapped-wing equations for lift and induced drag for the IBF system. The matched asymptotic expansion method of Reference 3-5 is used for the lift curve slope. Partial-span flap factors used for lift are the same as those for the MF equations, as noted previously. Partial-span blowing effects on induced drag have been combined into the thrust recovery factor, r, which is shown to exceed the static turning efficiency at low values of C_μ and to approach it at the higher C_μ values.

The generalized methodology uses the analogy method for the EBF concept. For full impingement of the jets on the flaps (full capture), lift augmentation and induced drag are found from the IBF formulation, except for the effects of jet spreading on lift coefficient at zero angle of attack. For the partial-capture condition (viz., when the capture area of the jet stream captured by the flaps is less than the total jet stream cross-section), the effective C_μ for the EBF calculation is reduced by the area ratio. The remaining fraction of the jet momentum, not captured by the flap, is treated as vectored thrust. The effect of jet spanwise spreading on lift coefficient at zero angle of attack is included in the formulation as a partial-span lift factor.

For minimum spreading, the lateral extent of each jet is found by allowing a six-degree expansion of the jet diameter from the jet exit plane to the flap trailing edge. Distribution of jet momentum captured by the flap is assumed constant over this lateral distance. For maximum spreading, the total lateral distance covered by all jets is set equal to the wing span covered by the flaps (excluding the fuselage). Because of the lack of an explicit theory or test results for predicting spreading, calculations are generally performed for the minimum and maximum spreading limits. The methodology for maximum spreading then reduces to that used in the data analysis report (Reference 3-11).

In addition to considerations of jet capture and spreading, BLC effects are included in the generalized methodology. The BLC effects are introduced through modification of the two-dimensional lift characteristics when part of the jet passes through the flap slots. Thrust recovery for the EBF concept is shown to be similar to the static turning efficiency and exceeds the cosine of the jet turning angle for triple-slotted flaps.

Generally, similar deficiencies were uncovered in reviewing the prediction techniques related to stability and control characteristics. In addition to the large bank of two-dimensional section data needed for the nonlinear span load program, it and the Das program had the inherent defect of not adequately predicting $\Delta C_m)_{\alpha=0}$. However, it does predict the slope of the C_m/C_L curve. Thus, attention was primarily directed toward predicting the pitching moment increments. From the combination of the two programs, the C_m/C_L curve can be constructed.

The generalized methodology includes multiple-slotted flap configurations. For mechanical flaps, linear thin airfoil theory is extended to include multiple-slotted flaps. Agreement is generally best for triple-slotted flaps, since the flap segment chords are small and the flow is gradually turned.

Spence's two-dimensional theory is used for the internally blown flaps. Blowing has the beneficial effect of causing the flow to approach the theoretical potential. Excellent agreement has been found between calculated and test results for internally blown flaps.

Alternative methods were evaluated for the externally blown flaps but were found unsuitable. The present EBF method subsequently developed has shown good agreement with test data for flap configurations in which a large flap area is captured.

Early in the program, data analysis indicated that simple lifting-line theory provided downwash values that were in excellent agreement with the test values. The nonlinear span load program could only provide similar results at the cost of added complexity and it was not totally operative in the asymmetric mode. It was felt that the asymmetric case would reduce the confidence level when using the program to predict lateral-directional derivatives. The generalized methods presented to obtain the lateral-directional derivatives are extensions of the C_{ℓ_β} method employed in DATCOM.

SECTION 4

LIFT CURVE

Three basic assumptions have been made to develop an expression that represent the lift coefficient curve, C_L versus α. These assumptions are:

1. The lift curve is most nearly represented by a sine curve.
2. The reference area used in the lift and momentum coefficients is the predominant area contributing to producing the force.
3. The portion of the jet momentum not captured by the trailing-edge flap system is treated as a vectored thrust term.

All equations required to estimate the lift curve in the linear range are included in Figure 4-1, together with paragraph numbers and equation numbers of this report where a more detailed explanation of the terms may be found. The generalized lift curve as defined in Figure 4-1 is expressed as:

$$C_L = \frac{S'}{S}\left[\left.C'_{L_\alpha}\right)_o \cdot K_{PWR} \cdot \sin\left(\alpha - \alpha_{o_L} - \Delta\alpha_t\right) + \Delta C'_\mu \sin\left(\alpha + \delta_T\right)\right] \qquad (4\text{-}1)$$

where:

S	is the basic wing reference area.
S'	is the extended wing area including the chord extension due to both trailing- and leading-edge high-lift devices.
$\left.C'_{L_{\alpha}}\right)_o$	is the power-off lift curve slope measured at the angle of zero lift and based on the extended wing area (Paragraph 4.1.1).
K_{PWR}	is the ratio of the power-on to power-off lift curve slope (Paragraph 4.1.2).
α	is the angle of attack referenced to wing root chord for which the lift coefficient will be estimated.
α_{o_L}	is the zero-lift angle of attack for an untwisted wing and is given by:

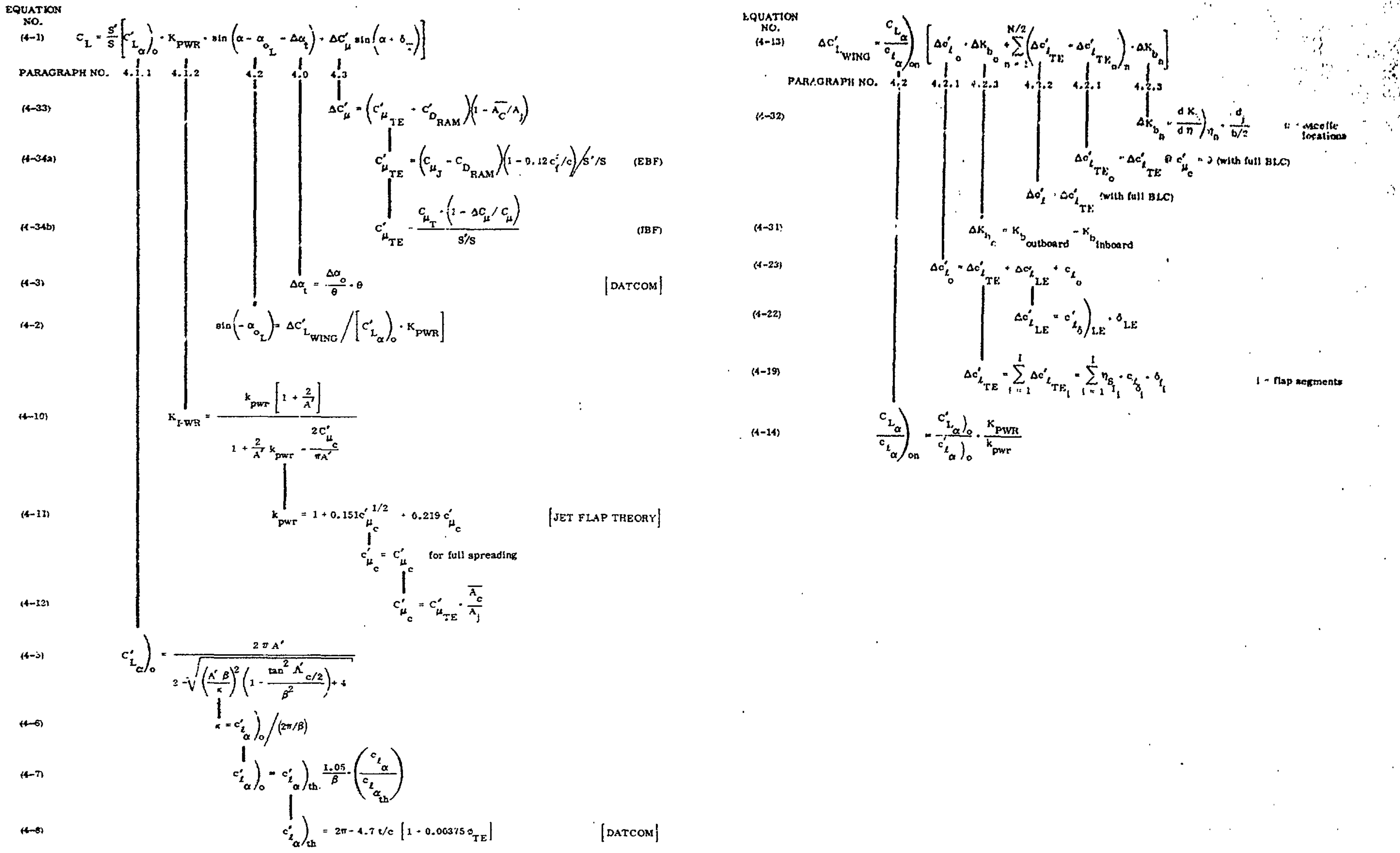

(4-1) $$C_L = \frac{S'}{S}\left[C'_{L_\alpha}\Big)_o \cdot K_{PWR} \cdot \sin\left(\alpha - \alpha_{o_L} - \Delta\alpha_t\right) + \Delta C'_\mu \sin\left(\alpha + \delta_{-}\right)\right]$$

(4-33) $$\Delta C'_\mu = \left(C'_{\mu_{TE}} + C'_{D_{RAM}}\right)\left(1 - \overline{A_C}/A_j\right)$$

(4-34a) $$C'_{\mu_{TE}} = \left(C_{\mu_J} - C_{D_{RAM}}\right)\left(1 - 0.12\, c'_f/c\right)\Big/ S'/S$$ (EBF)

(4-34b) $$C'_{\mu_{TE}} = \frac{C_{\mu_T} \cdot \left(1 - \Delta C_\mu / C_\mu\right)}{S'/S}$$ (IBF)

(4-3) $$\Delta\alpha_t = \frac{\Delta\alpha_o}{\theta} \cdot \theta$$ [DATCOM]

(4-2) $$\sin\left(-\alpha_{o_L}\right) = \Delta C'_{L_{WING}} \Big/ \left[C'_{L_\alpha}\Big)_o \cdot K_{PWR}\right]$$

(4-10) $$K_{I\text{-}WR} = \frac{k_{pwr}\left[1 + \frac{2}{A'}\right]}{1 + \frac{2}{A'} k_{pwr} - \frac{2C'_{\mu_c}}{\pi A'}}$$

(4-11) $$k_{pwr} = 1 + 0.151 c'^{\,1/2}_{\mu_c} + 0.219\, c'_{\mu_c}$$ [JET FLAP THEORY]

$$c'_{\mu_c} = C'_{\mu_c}$$ for full spreading

(4-12) $$C'_{\mu_c} = C'_{\mu_{TE}} \cdot \frac{\overline{A_c}}{A_j}$$

(4-5) $$C'_{L_\alpha}\Big)_o = \frac{2\pi A'}{2 + \sqrt{\left(\frac{A'\beta}{\kappa}\right)^2\left(1 - \frac{\tan^2 \Lambda'_{c/2}}{\beta^2}\right) + 4}}$$

(4-6) $$\kappa = c'_{\ell_\alpha}\Big)_o \Big/ \left(2\pi/\beta\right)$$

(4-7) $$c'_{\ell_\alpha}\Big)_o = c'_{\ell_\alpha}\Big)_{th} \cdot \frac{1.05}{\beta} \cdot \left(\frac{c_{\ell_\alpha}}{c_{\ell_{\alpha_{th}}}}\right)$$

(4-8) $$c'_{\ell_\alpha}\Big)_{th} = 2\pi - 4.7\, t/c\,\left[1 + 0.00375\, \phi_{TE}\right]$$ [DATCOM]

(4-13) $$\Delta C'_{L_{WING}} = \frac{C_{L_\alpha}}{c_{\ell_\alpha}}\Bigg)_{on}\left[\Delta c'_{\ell_o} \cdot \Delta K_{b_o} + \sum_{n=1}^{N/2}\left(\Delta c'_{\ell_{TE}} - \Delta c'_{\ell_{TE_o}}\right)_n \cdot \Delta K_{b_n}\right]$$

(4-32) $$\Delta K_{b_n} = \frac{dK_b}{d\eta}\Bigg)_{\eta_n} \cdot \frac{d_j}{b/2}$$ n = nacelle locations

$$\Delta c'_{\ell_{TE_o}} = \Delta c'_{\ell_{TE}} \;@\; c'_{\mu_c} = 0$$ (with full BLC)

$$\Delta c'_\ell = \Delta c'_{\ell_{TE}}$$ (with full BLC)

(4-31) $$\Delta K_{b_c} = K_{b_{outboard}} - K_{b_{inboard}}$$

(4-23) $$\Delta c'_{\ell_o} = \Delta c'_{\ell_{TE}} + \Delta c'_{\ell_{LE}} + c_{\ell_o}$$

(4-22) $$\Delta c'_{\ell_{LE}} = c'_{\ell_\delta}\Big)_{LE} \cdot \delta_{LE}$$

(4-19) $$\Delta c'_{\ell_{TE}} = \sum_{i=1}^{I} \Delta c'_{\ell_{TE_i}} = \sum_{i=1}^{I} \eta_{\delta_i} \cdot c_{\ell_{\delta_i}} \cdot \delta_{f_i}$$ I = flap segments

(4-14) $$\frac{C_{L_\alpha}}{c_{\ell_\alpha}}\Bigg)_{on} = \frac{C'_{L_\alpha}\Big)_o}{c'_{\ell_\alpha}\Big)_o} \cdot \frac{K_{PWR}}{k_{pwr}}$$

Figure 4-1. Lift Curve Methodology

$$\sin\left(-\alpha_{o_L}\right) = \Delta C'_{L_{WING}} \Big/ \left[\left(C'_{L_\alpha}\right)_o \cdot K_{PWR}\right] \qquad (4\text{-}2)$$

where:

$\Delta C'_{L_{wing}}$	is the total increment in lift coefficient due to trailing-edge flap deflection, trailing-edge blowing, leading-edge high-lift device deflection, and leading-edge blowing at zero angle of attack (Section 4.2).

$\Delta\alpha_t$ is the effect of wing twist and is given by:

$$\Delta\alpha_t = \frac{\Delta\alpha_o}{\theta} \cdot \theta \qquad (4\text{-}3)$$

where:

$\Delta\alpha_o/\theta$	is the change in wing zero-lift angle of attack due to a unit change in linear wing twist (Figure 4-2).
θ	is the twist of the wing tip with respect to the root section in degrees (negative for washout). A linear distribution with span is assumed.

$\Delta C'_\mu$ is the portion of the jet momentum that is not used to augment the wing lift (not captured by the flap system) and is treated as vectored thrust according to Section 4.3.

All primed coefficients are based on the extended wing area, S', whereas the unprimed coefficients are based on the reference wing area, S.

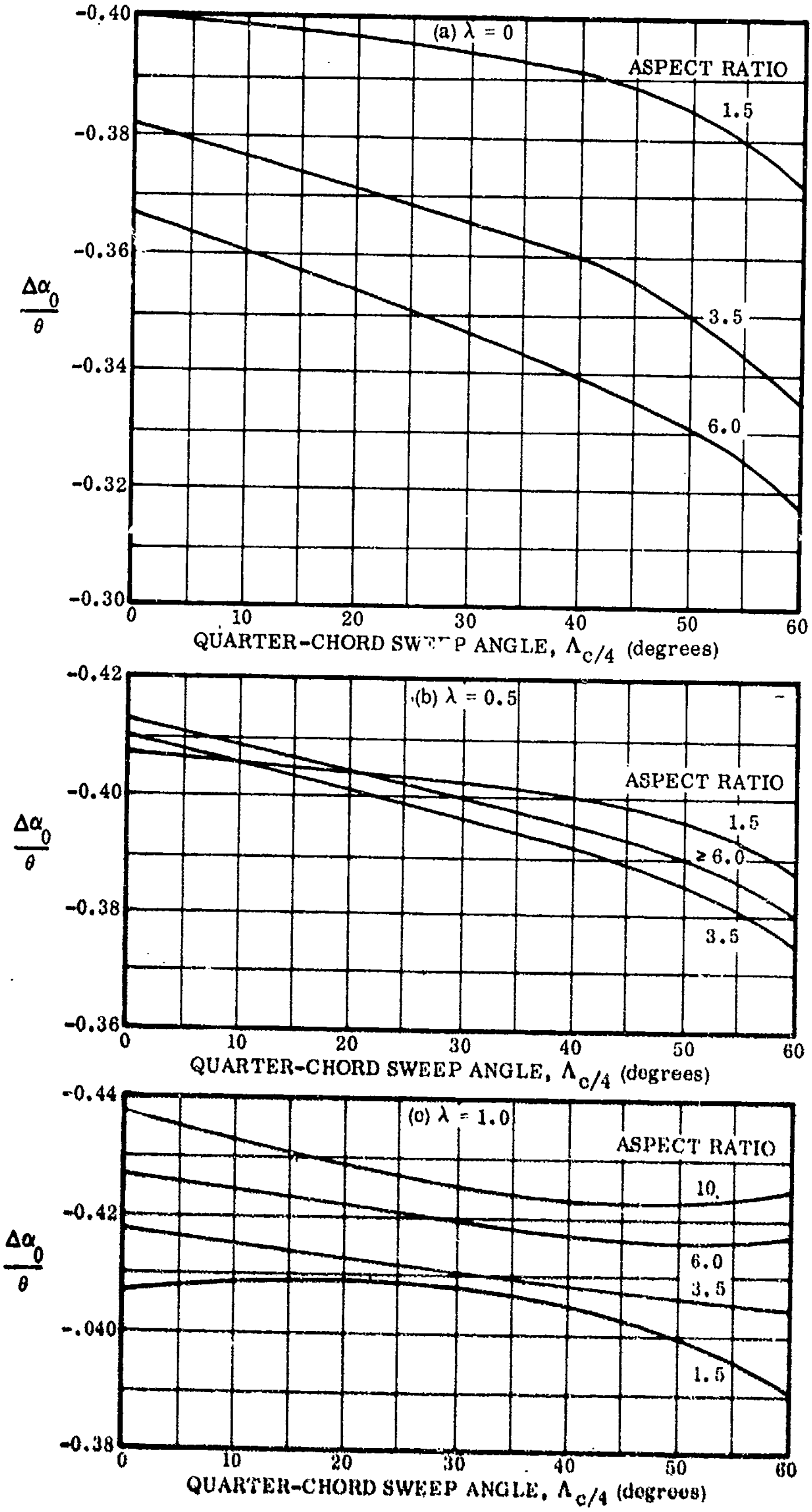

Figure 4-2. Effect of Linear Twist on Wing Angle of Attack for Zero Lift

4.1 LIFT CURVE SLOPE

The procedure for estimating the lift curve slope is based on estimating the three-dimensional power-off lift curve slope and then calculating the factor K_{PWR} to account for the change in lift curve slope due to blowing. Only that portion of the jet momentum captured by the flaps is included in K_{PWR}. The change in lift curve slope due to the uncaptured portion of the jet momentum, which is included in the last term of Equation 4-1, is discussed in Section 4.3.

The calculation for lift curve slope, which is performed using expressions from linearized thin airfoil and lifting line theories, are valid only at the angle of attack of zero lift, α_{0_L}. The lift curve slope, C'_{L_α}, may be obtained at other angles of attack, α, (below stall) by using the sine curve representation, which gives:

$$C'_{L_\alpha}\Big)_\alpha = C'_{L_\alpha}\Big)_{\alpha_{0_L}} \cos\left(\alpha - \alpha_{0_L}\right) \tag{4-4}$$

Equation 4-4 is applicable for both power-off and power-on conditions, except for the contribution from vectored thrust. In the following discussions, all expressions for lift curve slope are at the angle of attack for zero lift, even though not explicitly indicated.

4.1.1 LIFT CURVE SLOPE - POWER OFF. The three-dimensional power-off lift curve slope, $C'_{L_\alpha}\Big)_0$, is based on DATCOM (Reference 3-1, Paragraph 4.1.3.2), which expresses the lift curve slope as a function of wing aspect ratio, mid-chord sweep angle, Mach number, and section lift curve slope. The subscript $\Big)_0$ refers to the power-off value. In the present methodology:

$$C'_{L_\alpha}\Big)_0 = \frac{2\pi A'}{2 + \sqrt{\left(\frac{A'\beta}{\kappa}\right)^2\left(1 + \frac{\tan^2 \Lambda'_{c/2}}{\beta^2}\right) + 4}} \tag{4-5}$$

where:

A' is the aspect ratio of the extended wing area

$\Lambda'_{c/2}$ is mid-chord sweep angle of the extended wing

β is equal to $\sqrt{1-M^2}$, where M is free-stream Mach number

$$\kappa = c'_{\ell_\alpha}\Big)_0 \Big/ \left(2\pi/\beta\right) \tag{4-6}$$

where $c'_{\ell_\alpha}\Big)_0$ is the two-dimensional power-off lift-curve slope.

For wings with spanwise variations in section characteristics, it is recommended that values at the MAC station be used in lieu of spanwise averaging.

Equation 4-5, for the power-off lift curve slope, has been compared with test data from numerous Convair Aerospace and NASA wind tunnel tests in Figure 4-3. Good correlation is shown for aspect ratios between ten and four. Equation 4-5 is consistent with the idealized lifting line expression for large aspect ratios and reduces to the slender body theory limit for small aspect ratios, as shown in Figure 4-3.

The two-dimensional power-off lift curve slope, $\left.c'_{\ell_\alpha}\right)_o$, is estimated for clean airfoils by the method outlined in DATCOM (Paragraph 4.1.1.2), which gives:

$$\left.c'_{\ell_\alpha}\right)_o = \left.c'_{\ell_\alpha}\right)_{th} \frac{1.05}{\beta} \cdot \left(\frac{c_{\ell_\alpha}}{c_{\ell_{\alpha_{th}}}}\right) \quad (4\text{-}7)$$

where:

$$\left.c'_{\ell_\alpha}\right)_{th} = 2\pi + 4.7\ t/c\ \left[1 + 0.00375\,\phi_{TE}\right] \quad (4\text{-}8)$$

(based on the Kutta-Joukouski hypothesis of finite velocity at the trailing edge) where ϕ_{TE} is the total trailing edge angle in degrees.

$c_{\ell_\alpha}/c_{\ell_{\alpha_{th}}}$ is a Reynolds-number-dependent correction for boundary layer displacement effects given in Figure 4-4 and is dependent on the location of transition, which was assumed at the leading edge for Figure 4-4.

Equation 4-7 is also used for estimating the power-off lift curve slope for flapped airfoils of the type applicable to STOL transports. With the flaps extended, however, the ratio $c_{\ell_\alpha}/c_{\ell_{\alpha_{th}}}$ should be set equal to 0.75 for all Reynolds numbers. If full boundary layer control is obtained, as with adequate tangential blowing, the factor $c_{\ell_\alpha}/c_{\ell_{\alpha_{th}}}$ should be set equal to one. This would be the case with flaps either retracted or extended.

4.1.2 LIFT CURVE SLOPE - POWER ON. The power-on lift curve slope for an augmented system (i.e., either an IBF or an EBF with partial capture) is based on the results of two-dimensional and three-dimensional jet flap theory; e.g., References 4-1 through 4-3, 3-18, and 3-5. Except for thrust vector effects, the power-on three-dimensional lift curve slope, C'_{L_α}, is expressed in Equation 4-1 as:

$$C'_{L_\alpha} = C'_{L_\alpha}\Big)_o \cdot K_{PWR} \tag{4-9}$$

where

K_{PWR} is the ratio of the power-on to power-off lift curve slope.

This factor is obtained from Equation 26 Reference 3-5 as:

$$K_{PWR} = \frac{k_{pwr}\left[1 + \frac{2}{A'}\right]}{1 + \frac{2}{A'}\,k_{pwr} - \frac{2C'_{\mu_c}}{\pi A'}} \tag{4-10}$$

and:

k_{pwr} is the theoretical ratio of the two-dimensional powered to unpowered lift curve slope and is given by the Spence jet flap theory in Reference 4-3 as

$$k_{pwr} = 1 + 0.151 c'^{\,1/2}_{\mu_c} + 0.219\, c'_{\mu_c} \tag{4-11}$$

For the range of aspect ratios and jet momentum coefficients encountered with STOL transports, Equation 4-10 may be approximated by:

$$K_{PWR} = k_{pwr} \tag{4-10a}$$

The momentum coefficient, C'_{μ_c}, used in the expression for K_{PWR} is based on the captured fraction of the total jet momentum coefficient at the flap trailing edge. $C'_{\mu_{TE}}$ from Equation 4-34a and is defined as:

$$C'_{\mu_c} = C'_{\mu_{TE}} \cdot \frac{\overline{A}_c}{A_j} \tag{4-12}$$

where

$\tilde{A}_c/A_j$ is the average jet capture ratio as defined in Section 2.

The present methodology, which is based on the EBF/IBF analogy, uses Equation 4-10 as a single expression for K_{PWR} for all three STOL concepts (IBF, EBF, and MF/VT). The capture ratio $\tilde{A}_c/A_j$ used in Equation 4-12 must correspond to the specific STOL system, as summarized below:

$$\text{IBF} \qquad \bar{A}_c/A_j = 1.0$$

$$\text{EBF} \qquad 0 < \bar{A}_c/A_j < 1.0$$

$$\text{MF/VT} \qquad \bar{A}_c/A_j = 0$$

The two-dimensional momentum coefficient, c'_{μ_c}, used in Equation 4-11 for k_{pwr} is assumed equal to C'_{μ_c}, which is equivalent to assuming either full spreading of the jetstream over the wing span or that the lift curve slope is independent of the spanwise extent of the jet. This assumption is consistent with the theory for mechanical flaps (i.e., lift curve slope is nearly independent of the spanwise variation of flap deflection angle). Based on results from the Das computer program, Reference 3-7, this assumption has been shown to be approximately true for the IBF concept at low values of C'_{μ_c}. This is also consistent with the experimentally observed EBF/IBF analogy for the lift curve slope as shown in Figure 4-5a.

Blowing over the trailing-edge flaps can have an effect on the lift curve slope ratio by providing boundary layer control (BLC) as well as supercirculation. This has been observed at low momentum coefficient in the test data of Reference 3-11. This BLC effect is negligible for vectored thrust configurations and EBF configurations with low capture ratios for which very little if any of the jet efflux passes through the first flap slot. For these cases, the ratio $c_{\ell_\alpha}/c_{\ell_{\alpha_{th}}}$ used in determination of the unpowered lift curve slope, $\left.C'_{L_\alpha}\right)_o$, should be held equal to 0.75 for all blowing coefficients. On the other hand, for IBF configurations and EBF configurations with high capture ratios, full BLC is generally obtained at blowing coefficient values greater than 1.0. Under these conditions, the ratio $c_{\ell_\alpha}/c_{\ell_{\alpha_{th}}}$ should be taken equal to 1.0. The variation of $c_{\ell_\alpha}/c_{\ell_{\alpha_{th}}}$ with C'_{μ_c} would depend on the particular flap/slot/jet geometry and may be obtained for IBF flaps from data of the type shown in Figure 4-5b. A similar variation may be assumed for EBF flaps of the same geometry according to the analogy assumption.

Equations 4-10 and 4-11 for K_{PWR} and k_{pwr} have been plotted in Figures 4-5a and 4-5b as a convenience in estimating the lift curve slope ratios. Included in Figure 4-5a are IBF and EBF test data from Reference 3-11, where the EBF is for the fully captured case, viz. $\overline{A_c}/A_j \simeq 1$. The correspondence of both types of blown flap data with the theory for this case is clearly shown. Numerous correlations of IBF, EBF, and MF/VT test results with Equation 4-10 are presented in Reference 3-11. Other correlations of K_{pwr} from Reference 3-11 are shown in Figures 4-5c and 4-5d for a triple-slotted EBF and a plain IBF, respectively. The EBF data again compares favorably with Equation 4-10, although some of the IBF data at large flap deflections shows larger K_{pwr} values than predicted by Equation 4-10.

SAMPLE PROBLEM

GIVEN:

$\frac{S'}{S} = 1.609$

$A = 8.0$

$\Lambda_{c/4} = 25$ deg

$t/c' = 0.125$

$M = 0.10$

$A' = 4.972$ (from DATCOM)

$\Lambda'_{c/2} = 20.01$ deg

$\Phi_{TE} = 14.1$ deg

$c_f/h_{noz} = 260$

$c_f/c = 0.706$

$\left.\frac{\bar{A}c}{Aj}\right)_{EBF} = 0.935$

$\left.\frac{\bar{A}c}{Aj}\right)_{IBF} = 1.00$

$\left.\frac{\bar{A}c}{Aj}\right)_{MF/VT} = 0.0$

CALCULATE:

1. β with Equation 4-7.

$$\beta = \sqrt{1 - M^2}$$

$$\beta = \sqrt{1 - .01}$$

$$\beta = 0.995$$

2. Two-dimensional theoretical power-off lift curve slope with Equation 4-8.

$$\left.c'_{\ell_\alpha}\right)_{TH/o} = 2\pi + 4.7\ t/c' \left[1 + 0.00375\ \Phi_{TE}\right]$$

$$= 2\pi + 4.7\ (0.125) \left[1 + 0.00375\ (14.1)\right]$$

$$= 6.902\ \text{rad}^{-1}$$

3. Two-dimensional power-off lift curve slope with Equation 4-7.

A. EBF and IBF

$$c'_{\ell_\alpha}\Big)_o = c'_{\ell_{\alpha_{TH}}}\Big)_o \cdot \frac{1.05}{\beta} \cdot \left[\frac{c_{\ell_\alpha}}{c_{\ell_{\alpha_{TH}}}}\right]_o$$

$$\frac{c_{\ell_\alpha}}{c_{\ell_{\alpha_{TH}}}} = 1.00 \text{ (Full BLC effect is assumed)}$$

$$c'_{\ell_\alpha}\Big)_o = 6.902 \left(\frac{1.05}{0.995}\right) (1.00)$$

$$= 7.284 \text{ rad}^{-1}$$

B. MF/VT

$$c'_{\ell_\alpha}\Big)_o = c'_{\ell_{\alpha_{TH}}}\Big)_o \cdot \frac{1.05}{\beta} \cdot \left[\frac{c_{\ell_\alpha}}{c_{\ell_{\alpha_{TH}}}}\right]_o$$

$$\frac{c_{\ell_\alpha}}{c_{\ell_{\alpha_{TH}}}} = 0.75 \text{ (Zero BLC effect)}$$

$$c'_{\ell_\alpha}\Big)_o = (6.902) \left(\frac{1.05}{0.995}\right) (0.75)$$

$$= 5.4626 \text{ rad}^{-1}$$

4. κ with Equation 4-6.

A. EBF and IBF

$$\kappa = \frac{c'_{\ell_\alpha}\Big)_o}{2\pi/\beta}$$

$$= \frac{7.284 \times 0.995}{2\pi}$$

$$= 1.1534$$

B. MF/VT

$$\kappa = \frac{5.4626 \times 0.995}{2\pi}$$

$$= 0.8651$$

5. Lift curve slope, power off, with Equation 4-5.

$$\left.C'_{L_\alpha}\right)_o = \frac{2\pi A'}{2 + \sqrt{\left(\frac{A'\beta}{\kappa}\right)^2 \left(1 + \frac{\tan^2 \Lambda'_{c/2}}{\beta^2}\right) + 4}}$$

A. EBF and IBF

$$\left.C'_{L_\alpha}\right)_o = \frac{2\pi(4.972)}{2 + \sqrt{\left(\frac{4.972 \times 0.995}{1.1534}\right)^2 \left(1 + \frac{\tan^2 20.01}{0.99}\right) + 4}}$$

$$= 4.473 \text{ rad}^{-1}$$

B. MF/VT

$$\left.C'_{L_\alpha}\right)_o = \frac{2\pi(4.972)}{2 + \sqrt{\left(\frac{4.972 \times 0.995}{0.8651}\right)^2 \left(1 + \frac{\tan^2 20.01}{0.99}\right) + 4}}$$

$$= 3.715 \text{ rad}^{-1}$$

6. Capture fraction of the total jet momentum coefficient at the flap trailing edge.

A. EBF (Equation 4-34a)

$$C'_{\mu_{TE}} = \frac{\left(C_{\mu_J} - C_{D_{RAM}}\right)\left(1 - 0.12\ c'_f/c\right)}{S'/S}$$

$$C'_{\mu_{TEm}} = \frac{(1 - 0.17)\ [(1 - 0.12\ (0.706)]}{1.609}$$

$$= 0.472$$

B. IBF (Equation 4-34b)

$$C'_{\mu_{TE}} = \frac{C_{\mu_T} \cdot (1 - \Delta C_\mu / C_\mu)}{S'/S}$$

$\Delta C_\mu / C_\mu = 0.16$ (From Figure 4-17)

$$C'_{\mu_{TE}} = \frac{(1.0)\ (1 - 0.16)}{1.609}$$

$$= 0.5221$$

C. MF/VT (Equation 4-34a without the $1 - 0.12\ c'_f/c$ terms)

$$C'_{\mu_{TE}} = \frac{C_J - C_{D_{RAM}}}{S'/S}$$

$$= \frac{1 - 0.123}{1.609}$$

$$= 0.5451$$

7. C'_{μ_c} with Equation 4-12.

A. EBF

$$C'_{\mu_c} = C'_{\mu_{TE}} \left(\frac{\bar{A}_c}{A_j} \right)$$

$$= (0.472)\ (0.935)$$

$$= 0.441$$

B. IBF

$$C'_{\mu_c} = C'_{\mu_{TE}} \left(\frac{\bar{A}_c}{A_j}\right)$$

$$\frac{\bar{A}_c}{A_j} = 1.0 \text{ (IBF Concept)}$$

$$C'_{\mu_c} = 0.5221$$

C. MF/VT

$$C'_{\mu_c} = C'_{\mu_{TE}} \left(\frac{\bar{A}_c}{A_j}\right)$$

$$\frac{\bar{A}_c}{A_j} = 0.0 \text{ (MF/VT Concept)}$$

$$C'_{\mu_c} = 0.0$$

8. Ratio of the two-dimensional powered to unpowered lift curve slope with Equation 4-11.

A. EBF

$$k_{pwr} = 1 + 0.151\, c'_{\mu_c}{}^{1/2} + 0.219\, c'_{\mu_c}$$

$$= 1 + 0.151\,(0.441)^{1/2} + 0.219\,(0.441)$$

$$= 1.1969$$

then

$$K_{PWR} = k_{pwr} \text{ from Equation 4-10a}$$

$$= 1.1969$$

B. IBF

$$k_{pwr} = 1 + 0.151 \quad c'_{\mu_c}{}^{1/2} + 0.219\, c'_{\mu_c}$$

$$= 1 + (0.151)\,(\,0.5221)^{1/2} + (0.219)\,(\,0.5221)$$

$$K_{PWR} = k_{pwr} = 1.2234$$

C. MF/VT

$$k_{pwr} = 1 + 0.151 \quad c'_{\mu_c}{}^{1/2} + 0.219\, c'_{\mu_c}$$

$$= 1 + (0.151)\,(0.0) + (0.219)\,(0.0)$$

$$K_{PWR} = k_{pwr} = 1.00$$

9. The power-on lift curve slope with Equation 4-9.

A. EBF

$$C'_{L_\alpha} = C'_{L_\alpha}\Big)_o \cdot K_{PWR}$$

$$C'_{L_\alpha} = (4.473/\text{rad})\,(1.1969)$$

$$= 5.35 \text{ rad}^{-1}$$

B. IBF

$$C'_{L_\alpha} = C'_{L_{\alpha\, o}} \cdot K_{PWR}$$

$$C'_{L_\alpha} = (4.473/\text{rad})(1.2234)$$

$$= 5.471 \text{ rad}^{-1}$$

C. MF/VT

$$C'_{L_\alpha} = C'_{L_\alpha}\Big)_o \cdot K_{PWR}$$

$$= (3.715)\,(1.00)$$

$$= 3.715 \text{ rad}^{-1}$$

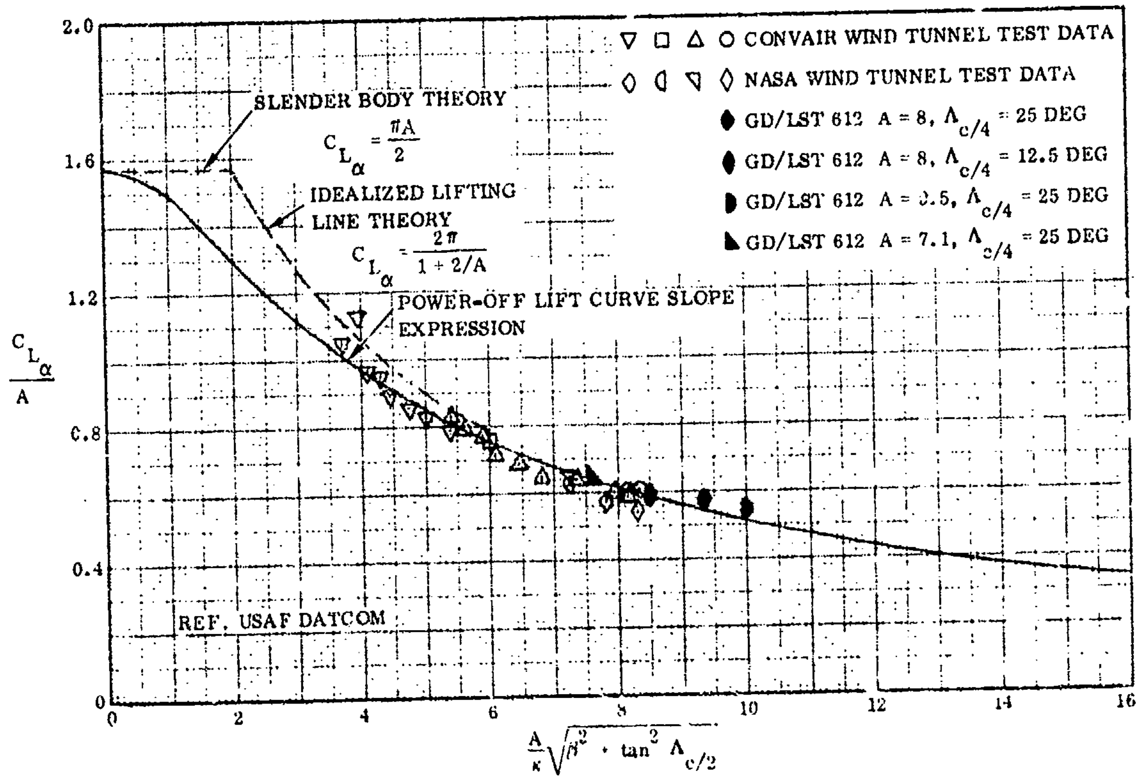

Figure 4-3. Clean Airfoil Lift Curve Slope Correlation

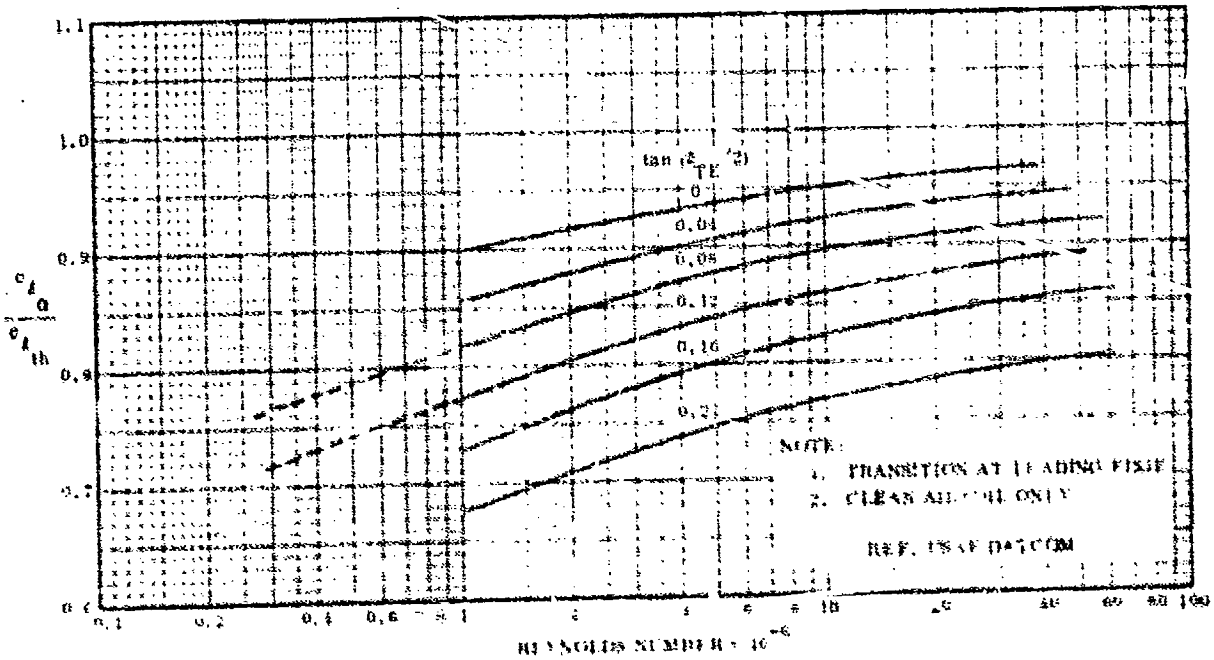

Figure 4-4. Two-Dimensional Lift Curve Slope Correction for Reynolds Number

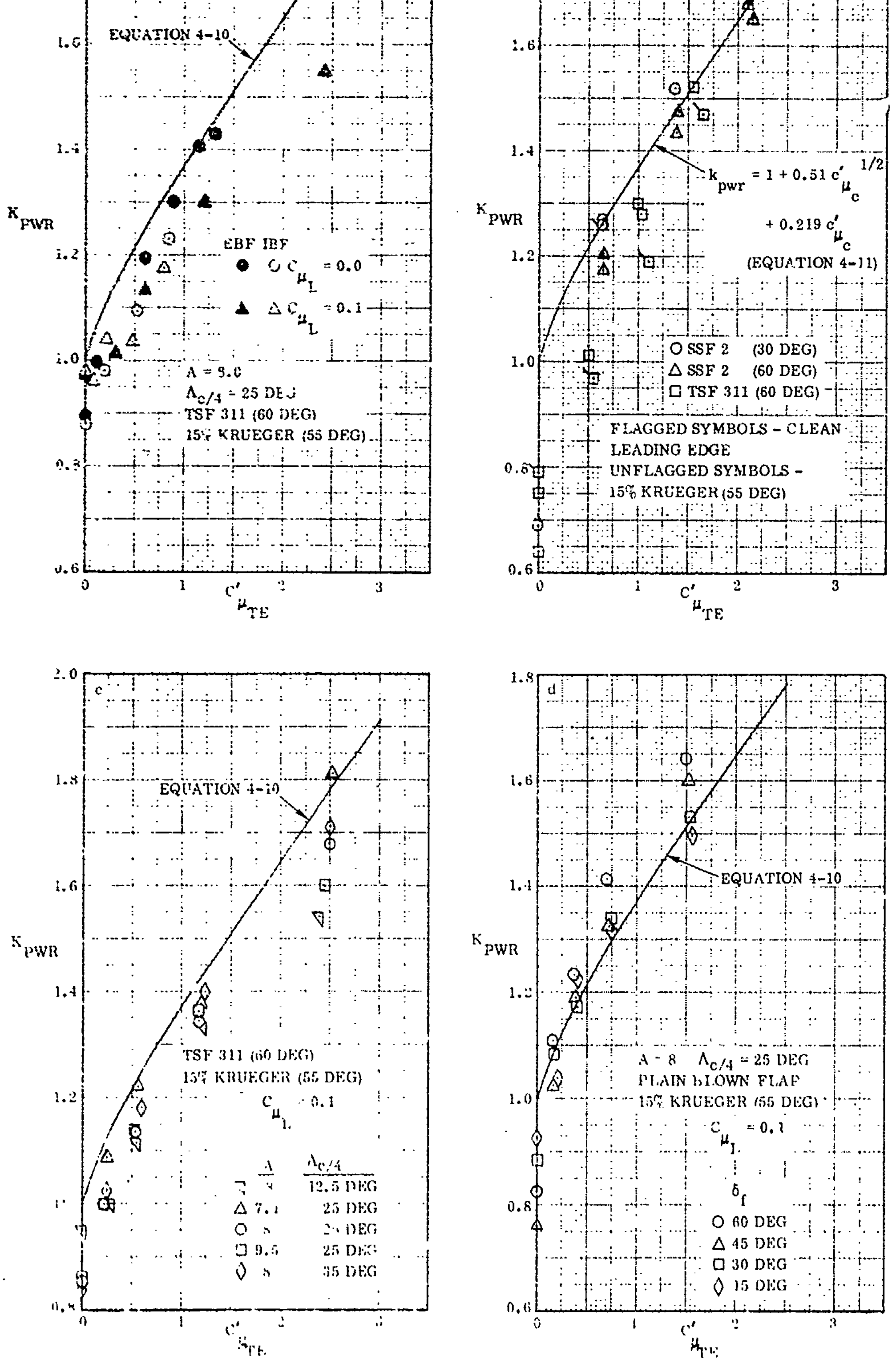

Figure 4-5. Correlation of Lift Curve Slope Power Ratio

4.2 LIFT AT ZERO ANGLE OF ATTACK

The method for estimating the increment in lift coefficient at zero angle of attack due to leading- and trailing-edge high-lift devices is based on thin airfoil theory extended to include the effects of blowing by Spence's jet flap theory (Reference 3-18). The generalized expression for this increment including the effects of jet stream capture ratio and spreading is:

$$\Delta C'_{L_{WING}} = \left.\frac{C_{L_\alpha}}{c_{\ell_\alpha}}\right)_{on} \left[\Delta c'_{\ell_o} \cdot \Delta K_{b_o} + \sum_{n=1}^{N/2} \left(\Delta c'_{\ell_{TE}} - \Delta c'_{\ell_{TE_o}} \right)_n \cdot \Delta K_{b_n} \right] \qquad (4\text{-}13)$$

where

$$\left.\frac{C_{L_\alpha}}{c_{\ell_\alpha}}\right)_{on} = \frac{\left.C'_{L_\alpha}\right)_o}{\left.c'_{\ell_\alpha}\right)_o} \cdot \frac{K_{PWR}}{k_{pwr}} \qquad (4\text{-}14)$$

and

$\left.C'_{L_\alpha}\right)_o$ is from Equation 4-5.

$\left.c'_{\ell_\alpha}\right)_o$ is from Equation 4-7.

K_{PWR} is from Equation 4-10.

k_{pwr} is from Equation 4-11.

$\Delta c'_{\ell_o}$ is the power-off section lift increment at $\alpha = 0$, discussed in Paragraph 4.2.1.

ΔK_{b_o} is the power-off partial-span flap factor discussed in Paragraph 4.2.3.

$\Delta c'_{\ell_{TE}}$ is the power-on trailing edge flap section lift increment at $\alpha = 0$, discussed in Paragraph 4.2.2

$\Delta c'_{\ell_{TE_o}}$ is the power-off trailing edge flap section lift increment at $\alpha = 0$ with the same amount of BLC effect as used to determine $\Delta c_{\ell_{TE}}$ discussed in Paragraph 4.2.1.

ΔK_{b_n} is the partial-span blowing factor discussed in Paragraph 4.2.3.

N	is the total number of engine nacelles contributing to flap blowing (EBF only).
n	is the nacelle location.

The effects of capture ratio and BLC are accounted for in the method by adjusting the estimate of the two-dimensional lift coefficients at zero angle of attack. The effects of jet spreading for the EBF system are included in the method with partial span factors in the limiting cases of minimum and maximum spreading.

For an IBF system equation 4-13 will simplify to:

$$\Delta C'_{L_{WING}} = \left.\frac{C_{L_\alpha}}{c_{\ell_\alpha}}\right)_{ON} \left[\Delta c'_{\ell_{TE}} \cdot K_{b_o}\right] \tag{4-13a}$$

when the flap span and blowing span are assumed the same.

4.2.1 POWER-OFF LIFT INCREMENT. The lift effectiveness of plain trailing-edge flaps can be defined from thin airfoil theory. The rate of change of lift with flap deflection (power off) at a constant angle of attack is given by:

$$c_{\ell_\delta} = 2 \left[\theta_f + \sin \theta_f\right] \tag{4-15}$$

where

$$\cos \theta_f = 1 - 2(c'_f/c') \tag{4-16}$$

This expression is plotted in Figure 4-6 as a function of flap chord ratio. The theory considers only a bent flap plate and does not include effects of thickness or large deflection angles. These effects are accounted for by introducing the empirical flap efficiency factors shown in Figures 4-7 through 4-10. The lift increment of a plain flap may now be expressed as indicated in Reference 4-4 as:

$$\Delta c_{\ell_{TE}} = \eta_P \cdot c_{\ell_\delta} \cdot \delta_f \tag{4-17}$$

where

η_P	is the plain flap efficiency factor from Figure 4-7 depending on the flap deflection angle, δ_f , plus the upper surface angle at the flap trailing edge, ϕ_{TE}.
c_{ℓ_δ}	is the rate of change of lift with flap deflection at constant angle of attack from Equation 4-15 or from Figure 4-6.
δ_f	is the flap deflection angle in radians.

This procedure is extended to single-slotted flaps with Fowler motion by simply basing the lift coefficient on the extended chord and evaluating c_{ℓ_δ} at a flap chord ratio based on the extended chord. The flap efficiency factors, η_{S_1}, given in Figure 4-8 are to be used for this case. Thus, for single-slotted flaps with Flower motion, the flap lift increment becomes:

$$\Delta c'_{\ell_{TE}} = \eta_{S_1} \cdot c_{\ell_\delta} \cdot \delta_f \qquad (4-18)$$

A further extension of the procedure is made to include the incremental lift for double- and triple-slotted Fowler flaps with different deflections of the individual flap segments. The lift increment is obtained for these multiple-slotted flaps by using the principle of superposition; i.e., by summing the incremental lift increments for each flap segment for the respective deflection angles, δ_{f_i}, and overall flap chord ratios, c'_{f_i}/c'. The result is:

$$\Delta c'_{\ell_{TE}} = \sum_{i=1}^{I} \Delta c'_{\ell_{TE_i}} = \sum_{i=1}^{I} \eta_{S_{I_i}} \cdot c_{\ell_{\delta_i}} \cdot \delta_{f_i} \qquad (4-19)$$

where

i	is a subscript that indicates the 1st, 2nd, 3rd, etc. flap segment of double- or triple-slotted flap.
I	is the number of slots or segments in the flap system.
$\eta_{S_{I_i}}$	is the slotted flap efficiency factor from Figures 4-9 and 4-10 for the i^{th} flap segment as a function of δ'_{f_i}
$c_{\ell_{\delta_i}}$	is the lift effectiveness from Figure 4-6 for the i^{th} flap segment (function of c'_{f_i}/c').
δ_{f_i}	is the flap deflection of the i^{th} flap segment.

The principle of superposition and the geometry definition required to evaluate Equation 4-19 is shown in Figure 4-11.

It should be noted that the chord lines, c_{f_i}, for each flap segment, shown in Figure 4-11 as well as Figure 2-1, is the chord line that will coincide with the basic airfoil chord line when the flap segments are retracted. The flap deflection, δ_{f_i}, therefore is defined as the angular travel this chordline makes with respect to the preceding flap segment as shown in Figure 4-11.

The effects of leading-edge high-lift devices on the wing lift at zero angle of attack can also be estimated by using thin airfoil theory. The resulting theoretical leading-edge lift effectiveness parameter, $c'_{\ell_\delta}\Big)_{LE}$, as plotted in Figure 4-12 is:

$$c'_{\ell_\delta}\Big)_{LE} = 2\,(\sin\theta_{LE} - \theta_{LE}) \qquad (4\text{-}20)$$

where

$$\cos\theta_{LE} = 1 - 2(c_{LE}/c') \qquad (4\text{-}21)$$

Unlike trailing-edge flaps, the deflection of a nose flap causes a loss in lift at zero angle of attack. The decremental lift coefficient, $\Delta c'_{\ell_{LE}}$, is:

$$\Delta c'_{\ell_{LE}} = c'_{\ell_\delta}\Big)_{LE} \cdot \delta_{LE} \qquad (4\text{-}22)$$

where

$c'_{\ell_\delta}\Big)_{LE}$ is from Equation 4-20 or Figure 4-12.

δ_{LE} is the leading-edge deflection angle in radians as defined in Section 2, positive nose down; therefore, $c'_{\ell_\delta}\Big)_{LE}$ is negative.

The summation of the trailing-edge and leading-edge flap lift increments gives the total power-off section lift increment due to deployment of high-lift devices shown below:

$$\Delta c'_{\ell_o} = \Delta c'_{\ell_{TE}} + \Delta c'_{\ell_{LE}} + c_{\ell_o} \qquad (4\text{-}23)$$

where

$\Delta c'_{\ell_{TE}}$ is from Equations 4-17, 4-18, or 4-19.

$\Delta c'_{\ell_{LE}}$ is from Equation 4-22.

c_{ℓ_o} is the lift coefficient at zero angle of attack for the basic cambered airfoil. (See DATCOM Paragraph 4.1.1.1 for method of estimation.)

The two-dimensional power-off lift increment at zero angle of attack estimated from Equation 4-23 may be converted directly to a three-dimensional value by using Equation 4-13 with all of the power-on terms set equal to zero. The equation below results:

$$\Delta C'_{L_{wing}}\Big)_o = \frac{C'_{L_\alpha}\Big)_o}{c'_{\ell_\alpha}\Big)_o} \left[\Delta c'_{\ell_o} \cdot \Delta K_{b_o}\right] \qquad (4\text{-}24)$$

In the above equation and also in Equation 4-13, the flap partial span factor is used to correct the entire increment in lift at zero angle of attack. This is approximately correct since $\Delta c'_{\ell_{TE}}$ and c_{ℓ_o} in Equation 4-23 are very small compared to $\Delta c'_{\ell_{TE}}$. These two terms generally have opposite signs and therefore tend to cancel each others effect.

The increment in lift at zero angle of attack due to the trailing edge flap, $\Delta C'_{L_{TE}}$, which is by far the largest portion of the total increment, $\Delta C'_{L_{wing}}$, is correlated with test data in Figure 4-13 for many flap configurations and wing planforms.

4.2.2 POWER-ON LIFT INCREMENT. The lift effectiveness, c_{ℓ_δ}, of plain trailing-edge tangentially blown flaps was developed by Spence, Reference 3-18. Assuming thin airfoil potential flow theory (no flow separation) and with the additional assumptions that the trailing jet remains thin and shallow in downward displacement, Spence obtained the following equation for lift effectivess power on:

$$c_{\ell_\delta} = 2\left(\theta_f + \sin\theta_f\right) + 4\pi D_o \qquad (4\text{-}25)$$

θ_f is defined in Equation 4-16.

D_o is the Fourier series coefficient defined as a function of jet momentum coefficient and flap chord to wing chord ratio.

This equation is plotted in Reference 3-18 for various values of flap chord ratio and over a range of jet momentum coefficients from 0 to 5. For convenience, these results are presented in Figure 4-14. The cross-plot of c_{ℓ_δ} versus flap chord ratio at a jet momentum coefficient of zero is identical to the power-off thin airfoil theory shown in Figure 4-6.

The two-dimensional trailing-edge flap lift increments, $\Delta c'_{\ell_{TE}}$, for an airfoil with a blown flap (either IBF or EBF) is determined from the same set of equations used for power-off calculations; i.e., Equations 4-17, 4-18, and 4-19. However, the power-on values of the flap effectiveness parameter, c_{ℓ_δ}, are obtained from Figure 4-14.

The power-on flap efficiency factors η_P η_S, and η_{S_I} are taken as equal to 1.0 for IBF systems and for EBF systems with full BLC effectiveness. EBF systems without full BLC effectiveness are discussed at the close of this section. For the IBF with upper-surface blowing, the deflection angle used to estimate the power-on c_{ℓ_δ} is the deflection angle of the flap, δ_f, plus the upper surface angle, ϕ_{TE}. For the EBF, the normal flap deflection angle defined previously in connection with the power-off case (e.g., Figure 4-11) is used.

Correlation of two-dimensional test data for single- and triple-slotted blown flaps with the jet flap theory just discussed is presented in Figure 4-15. Agreement is relatively good except at low values of momentum coefficient, where the BLC effect is not fully developed on the airfoil. The method tends to underpredict slightly the test data at high momentum coefficients.

A two-dimensional jet momentum coefficient, c'_{μ_c}, is used to determine two-dimensional flap effectiveness values from Figure 4-14. The value of c'_{μ_c} is obtained from the corresponding three-dimensional jet momentum coefficient, C'_{μ_c}, based on S' through the relationship:

$$c'_{\mu_c} = \frac{S'}{S'_j} \cdot C'_{\mu_c} \qquad (4\text{-}26)$$

where for IBF systems

S'_j is equal to the extended wing area spanned by the blowing nozzle.

and for EBF systems

S'_j is equal to the area that is bounded by the extent of the wing span over which the jet stream has spread.

For maximum spreading, this area is the exposed extended-wing area (i.e., the same area as for a full span IBF). This assumes that the jet stream from all of the engines spreads uniformly over the entire exposed span of the wing. For a minimum spreading, c'_{μ_c} differs for each jet and must be based on the area S'_{j_n}, n = 1, 2, ..N, covered by the jets from each of the N engines. Thus, for minimum spreading:

$$\left.c'_{\mu_c}\right)_n = \frac{C'_{\mu_c}}{N} \cdot \frac{S'}{S'_{j_n}} \qquad (4\text{-}27)$$

where S'_{j_n} shown in Figure 2-6 is defined as:

$$S'_{j_n} = d_{j_n} \cdot c'_{j_n} \qquad (4\text{-}28)$$

and

d_{j_n} is the diameter of the nth jet stream at the flap trailing edge assuming a six-degree jet expansion angle due to mixing. (See Section 2.)

c'_{j_n} is the average extended wing chord at the spanwise station of the nth jet.

Equations 4-26 and 4-27 assume that the adjacent jets do not overlap.

Total lift increment due to power is obtained by summing the incremental parts for each engine nacelle, giving:

$$\Delta c'_{\ell_{pwr}} = \sum_{n=1}^{N/2} \left(\Delta c'_{\ell_{TE}} - \Delta c'_{\ell_{TE_o}}\right)_n \qquad (4\text{-}29)$$

where

$\Delta c'_{\ell_{TE}}$ is the power-on increment due to trailing-edge flap deflection and blowing from Equations 4-17, 4-18, or 4-19 with full BLC.

$\Delta c'_{\ell_{TE_o}}$ is the power-off increment due to trailing-edge flap deflection and blowing from Equations 4-17, 4-18, or 4-19 with full BLC at $c'_{\mu_c} = 0$.

n is a subscript that denotes each nacelle location on a wing semi-span.

The summation is taken over only one wing panel because of lateral symmetry.

As discussed in connection with the lift curve slope in Section 4.1, full BLC effectiveness is not achieved on EBF configurations when sufficient jet efflux does not pass through the flap slots and onto the upper flap surface. This lack of BLC effectiveness generally occurs for low engine positions without upward jet deflectors and/or with small flap deflection angles, as used during takeoff. Even for these configurations, however, partial BLC effectiveness may occur at the higher values of jet momentum coefficient if sufficient jet momentum penetrates through the slots and reattaches to the upper-surface flap boundary layer. Partial BLC effectiveness may also occur at very high angles of attack because the jet tends to be deflected up into the flap slots.

As yet, a quantitative methodology for estimating the extent of BLC effectiveness for EBF systems with arbitrary engine and flap geometry has not been developed. In lieu of such a method, the methodology for the EBF lift curve slope has been presented in Section 4.1 for the limiting cases of full and zero BLC effectiveness. Similar limiting conditions must also be assumed when estimating the flap lift increment at zero angle of attack.

The limiting condition of full power-on BLC effectiveness was discussed in the preceding section. To obtain the flap lift increment, $\Delta C'_{L_{wing}}$, for the zero BLC effectiveness limit, the term $C_{L_\alpha}/c_{\ell_\alpha})_{on}$ and the term involving $\Delta c'_{\ell_0}$ in Equation 4-13 should be based on zero BLC values. Thus, the power-off flap efficiency factors from Figures 4-7 through 4-10 are used in estimating this $\Delta c'_{\ell_0}$ term. On the other hand, the summation term in Equation 4-13, which contains $\Delta c'_{\ell_{TE_0}}$ is assumed unaffected by BLC. This is equivalent to assuming that the two-dimensional flap lift increment due to power as given by Equation 4-29 remains unaffected by BLC.

4.2.3 PARTIAL SPAN FLAP AND BLOWING. The method for estimating partial span effects on flap lift effectiveness is outlined in DATCOM for unblown flap systems. By using a linear spanload program for jet flapped wings (Reference 3-7), these effects were found also to be applicable to partial-span blowing. The effects of partial span are presented in the form of span factors, K_b, in Figure 4-16, where:

$$\Delta C'_L\Big)_{\substack{part\\span}} = \Delta K_b \cdot \Delta C'_L\Big)_{\substack{full\\span}} \tag{4-30}$$

The span factors in Figure 4-16 were obtained for wings with aspect ratios from 1.5 through 12 on sweeps of zero through 45 degrees. For flap spans or blowing spans that do not extend to the aircraft centerline (fuselage cutouts) or to the wing tip (aileron cutouts), the factor ΔK_b is determined as shown in Figure 4-16:

$$\Delta K_{b_o} = K_{b_{outboard}} - K_{b_{inboard}} \tag{4-31}$$

In the present methodology, these same span factors are used not only for power-off flap configurations and IBF systems, but for EBF systems with less than full span spreading. For ease in estimating ΔK_b for short blowing spans (such as EBF with minimum spreading), the slopes $dK_b/d\eta$ are plotted in Figure 4-16. The partial span factor for an individual engine nacelle becomes:

$$\Delta K_{b_n} = \frac{d\,K_b}{d\,\eta}\Big)_{\eta_n} \cdot \frac{d_j}{b/2} \tag{4-32}$$

where:

$\frac{dK_b}{d\eta}\Big)_{\eta_n}$ is obtained from Figure 4-16 for a value η_n at the jet centerline.

SAMPLE PROBLEM

GIVEN:

$\delta_{f_1} = 28.4$ deg

$\delta_{f_2} = 16.4$ deg

$\delta_{f_3} = 15.0$ deg

$c_{f_1}'/c' = 0.439$

$c_{f_2}'/c' = 0.269$

$c_{f_3}'/c' = 0.1326$

$\Phi_{upper} = 12.2$ deg

$N = 4$

$\delta_{LE} = 51$ deg

$c_{f_{LE}}/c' = 0.145/1.609$
$= 0.0901$

Outboard Flap End = 0.99

Inboard Flap End = 0.10

$\lambda = 0.333$

$\eta_1 = 0.325$

$\eta_2 = 0.550$

$\Delta\eta_1 = \left.\frac{d_j}{b/2}\right)_1 = 0.1688$

$\Delta\eta_2 = \left.\frac{d_j}{b/2}\right)_2 = 0.1539$

CALCULATE:

1. Ratio of lift curve slope (3-D to 2-D) from Equation 4-14.

$$\left.\frac{C_{L_\alpha}}{c_{\ell_\alpha}}\right)_{on} = \frac{\left.C'_{L_\alpha}\right)_o}{\left.c'_{\ell_\alpha}\right)_o} \cdot \frac{K_{PWR}}{k_{pwr}}$$

A. EBF

$\left.C'_{L\alpha}\right)_o = 4.473$

$\left.c'_{\ell\alpha}\right)_o = 7.284$

$\frac{K_{PWR}}{k_{pwr}} = 1.00$

From Sample Problem in Section 4.1

$$\left.\frac{C_{L_\alpha}}{c_{\ell_\alpha}}\right)_{on} = \frac{4.473}{7.284}\ (1.0)$$

$$= 0.6141$$

B. IBF

$$\left.\begin{array}{l} \left.C'_{L_\alpha}\right)_o = 4.473 \\ \left.c'_{\ell_\alpha}\right)_o = 7.284 \\ \dfrac{K_{PWR}}{k_{pwr}} = 1.00 \end{array}\right\} \text{From Sample Problem in Section 4.1}$$

$$\left.\frac{C_{L_\alpha}}{c_{\ell_\alpha}}\right)_{on} = \left(\frac{4.473}{7.284}\right)(1.0)$$

$$= 0.6141$$

C. MF/VT

$$\left.\begin{array}{l} \left.C'_{L_\alpha}\right)_o = 3.715 \\ \left.c'_{\ell_\alpha}\right)_o = 5.463 \\ \dfrac{K_{PWR}}{k_{pwr}} = 1.00 \end{array}\right\} \text{From Sample Problem in Section 4.1}$$

$$\left.\frac{C_{L_\alpha}}{c_{\ell_\alpha}}\right)_{on} = \left(\frac{3.715}{5.463}\right)(1.00)$$

$$= 0.680$$

2. Two-dimensional lift coefficient at $\alpha = 0$ for EBF, IBF and MF/VT.

$c_{\ell_o} = 0.25$ from DATCOM

3. **Increment of lift coefficient for trailing edge flap with Equation 4-19.**

A. EBF and IBF

$$\Delta c'_{\ell_{TE}} = \sum_{i=1}^{I} \eta_{S_{I_i}} \cdot c_{\ell_{\delta_i}} \cdot \delta_{f_i}$$

$$\left.\begin{aligned} \eta_{S_{3_1}} &= 1.0 \\ \eta_{S_{3_2}} &= 1.0 \\ \eta_{S_{3_3}} &= 1.0 \end{aligned}\right\} \text{Full BLC effect assumed.}$$

$$\left.\begin{aligned} c_{\ell_{\delta_1}} &= 4.87 \\ c_{\ell_{\delta_2}} &= 3.94 \\ c_{\ell_{\delta_3}} &= 2.84 \end{aligned}\right\} \text{From Figure 4-6.}$$

$$\Delta c'_{\ell_{TE}} = (1.0)(4.87)\left(\frac{28.4}{57.295}\right)+(1.0)(3.94)\left(\frac{16.4}{57.295}\right)+(1.0)(2.84)\left(\frac{15}{57.295}\right)$$

$$= 2.4139 + 1.128 + 0.743$$

$$= 4.285$$

B. MF/VT

$$\eta_{S_{3_1}} = 0.77$$

$$\eta_{S_{3_2}} = 0.77$$

$$\eta_{S_{3_3}} = 0.608$$

$$\Delta c'_{\ell_{TE}} = (0.77)(4.87)\left(\frac{28.4}{57.295}\right)+ (0.77)(3.94)\left(\frac{16.4}{57.295}\right)+ (0.608)(2.84)\left(\frac{15}{57.295}\right)$$

$$= 1.8587 + 0.8684 + 0.4521$$

$$= 3.179$$

4. Increment of lift coefficient for a leading edge flap with Equation 4-22 for EBF, IBF and MF/VT.

$$\Delta c'_{\ell_{LE}} = c'_{\ell_\delta}\Big)_{LE} \cdot \delta_{LE}$$

$$c'_{\ell_\delta}\Big)_{LE} = -0.073 \qquad \text{From Figure 4-12}$$

$$\Delta c'_{\ell_{LE}} = (-0.073)\left(\frac{51}{57.295}\right)$$

$$= -0.065$$

5. Total power-off section lift increment with Equation 4-23.

$$\Delta c'_{\ell_o} = \Delta c'_{\ell_{TE}} + \Delta c'_{\ell_{LE}} + c_{\ell_o}$$

A. EBF and IBF

$$\Delta c'_{\ell_o} = 4.285 - 0.065 + 0.250$$

$$= 4.470$$

B. MF/VT

$$\Delta c'_{\ell_o} = 3.179 - 0.065 + 0.250$$

$$= 3.364$$

6. Partial span flap factor for EBF, IBF and MF/VT using Equation 4-31.

$$\Delta K_{b_o} = K_{b_{outboard}} - K_{b_{inboard}}$$

$$K_{b_{outboard}} = 0.996 \qquad \text{From Figure 4-16}$$

$$K_{b_{inboard}} = 0.138 \qquad \text{From Figure 4-16}$$

$$\Delta K_{b_o} = 0.858$$

7. Partial span blowing factor with Equation 4-32 (n = 1,2).

$$\Delta K_{b_n} = \frac{d\,K_b}{d\,\eta}\Big)_{\eta_n} \cdot \frac{d_j}{b/2}$$

A. EBF

$$\left.\frac{dK_b}{d\eta}\right)_1 = 1.250$$ From Figure 4-16

$$\left.\frac{dK_b}{d\eta}\right)_2 = 1.051$$ From Figure 4-16

$$\Delta K_{b_1} = 1.250 \cdot 0.1688$$

$$= 0.211$$

$$\Delta K_{b_2} = 1.051 \cdot 0.1539$$

$$= 0.1617$$

B. IBF and MF/VT -- Not Applicable.

8. Local jet momentum coefficient with Equation 4-27.

A. EBF

$$\left.c'_{\mu_c}\right)_n = \frac{c'_{\mu_c}}{N} \cdot \frac{S'}{S'_{J_n}}$$

where:

$c'_{\mu_c} = 0.441$ From sample problem in Section 4.1

$S'/S'_{J_1} = 2.491$

$S'/S'_{J_2} = 3.230$

$$c'_{\mu_{c_1}} = 0.441 \cdot 2.481$$

$$= 1.0941$$

$$c'_{\mu_{c_2}} = 0.441 \cdot 3.230$$

$$= 1.424$$

B. IBF

$c_{\mu_c} = 0.5221$ From Section 4.1.

C. MF/VT — Not Applicable.

9. Theoretical lift effectiveness using power-off geometry.

A. EBF

$$\left.c_{\ell_{\delta_1}}\right)_1 = 7.69$$

$$\left.\begin{array}{l} \left.c_{\ell_{\delta_2}}\right)_1 = 6.69 \\ \left.c_{\ell_{\delta_3}}\right)_1 = 5.78 \\ \left.c_{\ell_{\delta_1}}\right)_2 = 8.10 \end{array}\right\} \text{From Figure 4-14.}$$

$$\left.c_{\ell_{\delta_2}}\right)_2 = 7.32$$

$$\left.c_{\ell_{\delta_3}}\right)_2 = 6.45$$

B. IBF

$$\left.\begin{array}{l} c_{\ell_{\delta_1}} = 6.31 \\ c_{\ell_{\delta_2}} = 5.47 \\ c_{\ell_{\delta_3}} = 4.48 \end{array}\right\} \text{From Figure 4-14.}$$

C. MF/VT – Not Applicable.

10. Power-on lift increment for the trailing-edge flaps from Equation 4-19.

$$\Delta c'_{\ell_{TE}} = \sum_{i=1}^{I} \Delta c'_{\ell_{TE_i}} = \sum_{i=1}^{I} \eta_{S_{I_i}} \cdot c_{\ell_{\delta_i}} \cdot \delta_{f_i}$$

A. EBF

Inboard Jet (n = 1)

$$\Delta c'_{\ell} = (7.69)\left(\frac{28.4}{57.295}\right) + (6.69)\left(\frac{16.4}{57.295}\right) + (5.78)\left(\frac{15}{57.295}\right)$$

$$= 3.812 + 1.915 + 1.513$$

$$= 7.240$$

Outboard Jet

$$\Delta c'_{\ell} = (8.10)\left(\frac{28.4}{57.295}\right) + (7.32)\left(\frac{16.4}{57.295}\right) + (6.45)\left(\frac{15}{57.295}\right)$$

$$= 4.015 + 2.095 + 1.689$$

$$= 7.799$$

B. IBF

$$\Delta c'_{\ell} = (6.31)\left(\frac{28.4}{57.295}\right) + (5.47)\left(\frac{16.4}{57.295}\right) + (4.48)\left(\frac{15+12.2}{57.295}\right)$$

$$= 3.1277 + 1.5657 + 2.1268$$

$$= 6.8202$$

C. MF/VT — Not Applicable.

11. Power-on lift increment, $\Delta c'_{\ell_{PWR}}$, using the following terms extracted from Equation 4-13.

$$\sum_{n=1}^{N/2} \left(\Delta c'_{\ell_{TE}} - \Delta c'_{\ell_{TE_o}}\right)_n \cdot \Delta K_{b_n}$$

A. EBF

$$\Delta c'_{\ell_{PWR}} = \left(\Delta c'_{\ell} - \Delta c'_{\ell_{TE}}\right) K_{b_1} + \left(\Delta c'_{\ell} - \Delta c'_{\ell_{TE}}\right) K_{b_2}$$

$$= (7.240 - 4.285)(0.211) + (7.799 - 4.285)(0.1617)$$

$$= 0.624 + 0.568$$

$$= 1.192$$

B. IBF

$$\Delta c'_{\ell_{PWR}} = \sum_{n=1}^{2/2} \left(\Delta c'_{\ell_{TE}} - \Delta c'_{\ell_{TE}}\right)_o \cdot K_{b_o}$$

$$= (6.8202 - 4.285)(0.858)$$

$$= 2.1752$$

C. MF/VT — Not Applicable.

12. Power-on incremental lift at zero angle of attack with Equation 4-15.

$$\Delta C'_{L_{WING}} = \left.\frac{C_{L_\alpha}}{c_{\ell_\alpha}}\right)_{on} \left[\Delta c'_{\ell_o} \cdot \Delta K_{b_o} + \sum_{n=1}^{N/2} \left(\Delta c'_{\ell_{TE}} - \Delta c'_{\ell_{TE_o}}\right)_n \cdot \Delta K_{b_n}\right]$$

A. EBF

$$\Delta C'_{L_{WING}} = (0.6141)\left[(4.470)(0.858) + 1.192\right]$$

$$= (0.6141)\left[3.835 + 1.192\right]$$

$$= 3.087$$

B. IBF

$$\Delta C'_{L_{WING}} = (0.6141)\left[(4.470)(0.858) + 2.175\right]$$

$$= (0.6141)\left[3.835 + 2.175\right]$$

$$= 3.691$$

C. MF/VT

$$\Delta C'_{L_{WING}} = (0.680)\ (3.364)(0.858)$$

$$= 1.963$$

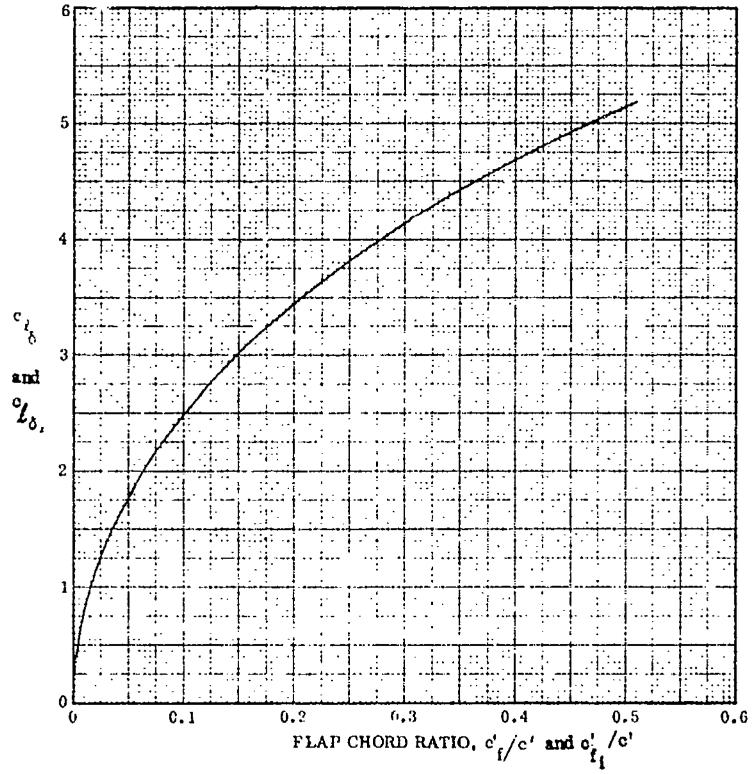

Figure 4-6. Theoretical Lifting Effectiveness of Trailing-Edge Flaps

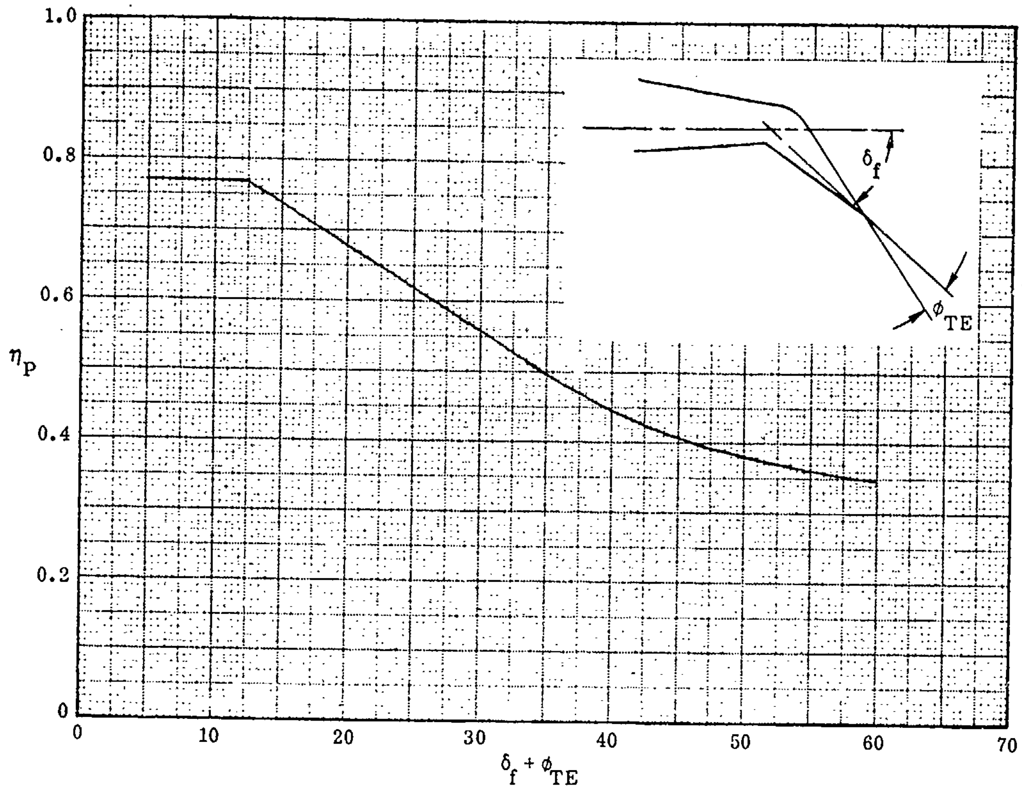

Figure 4-7. Turning Efficiency of Plain Trailing-Edge Flaps

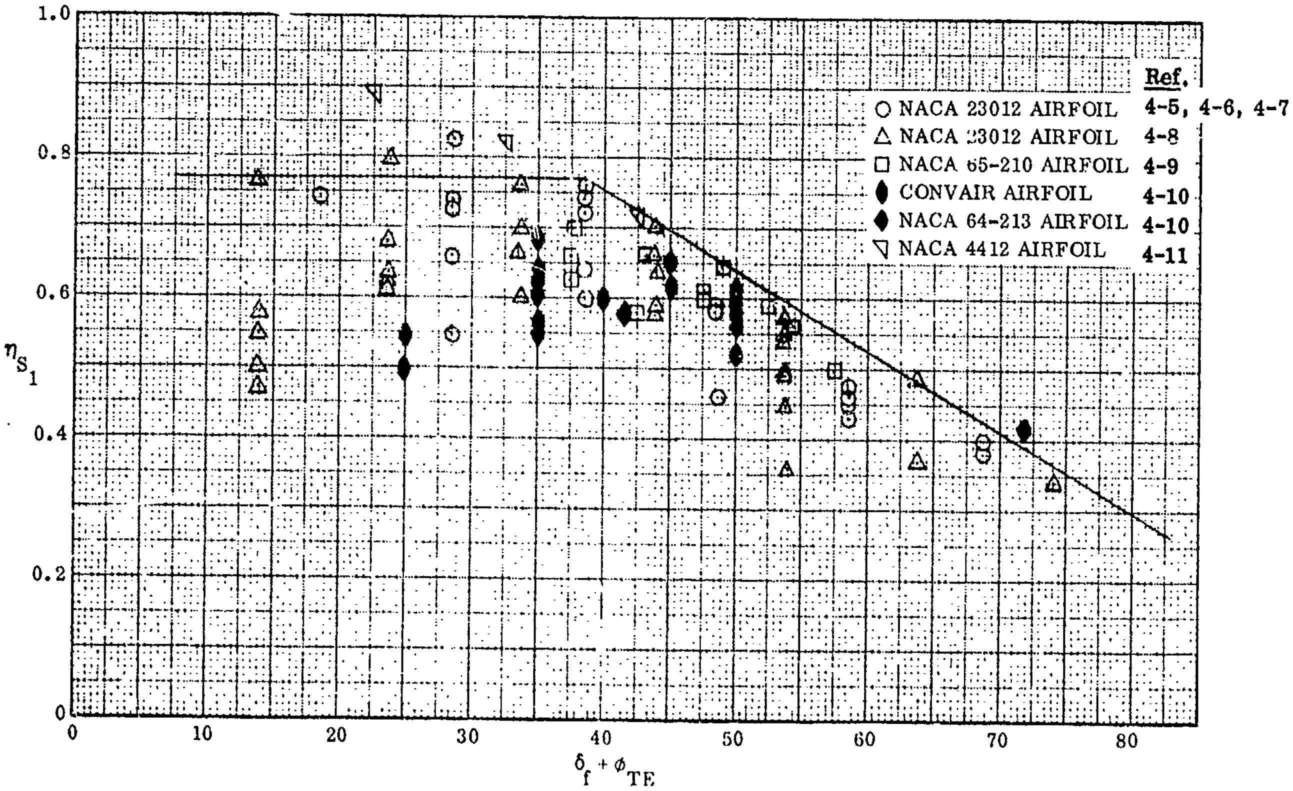

Figure 4-8. Turning Efficiency of Single-Slotted Flaps

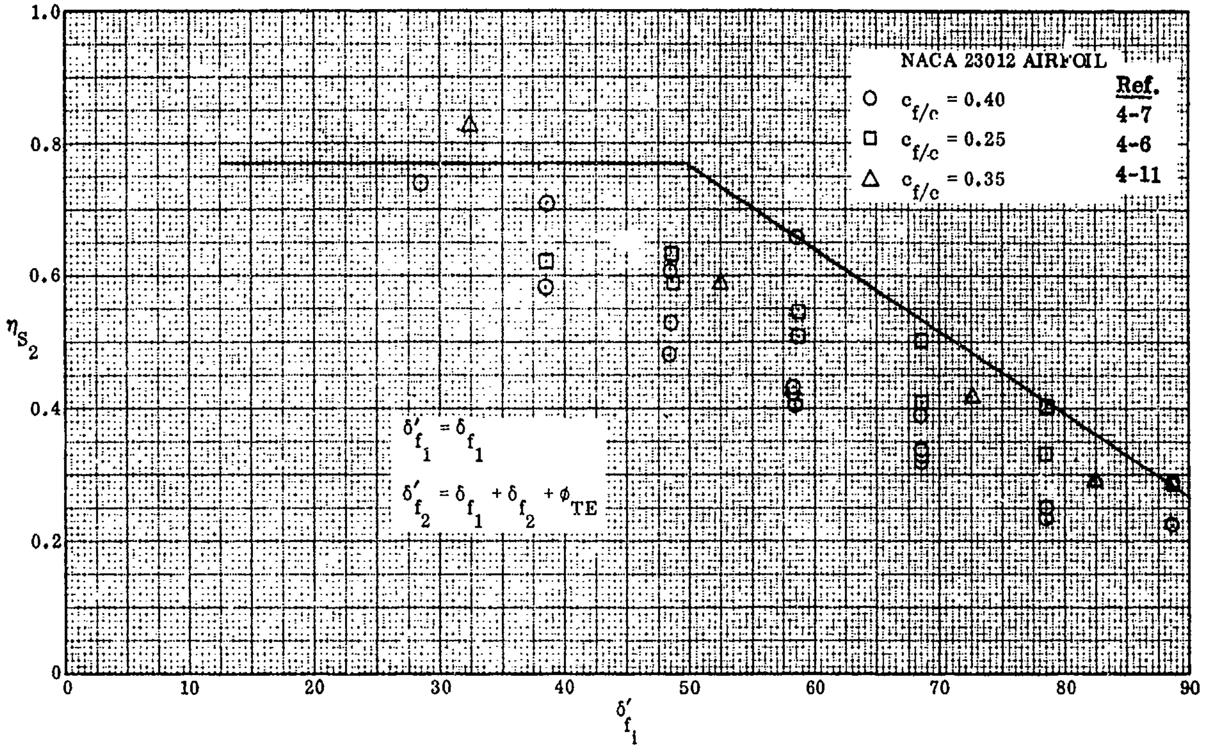

Figure 4-9. Turning Efficiency of Double-Slotted Flaps

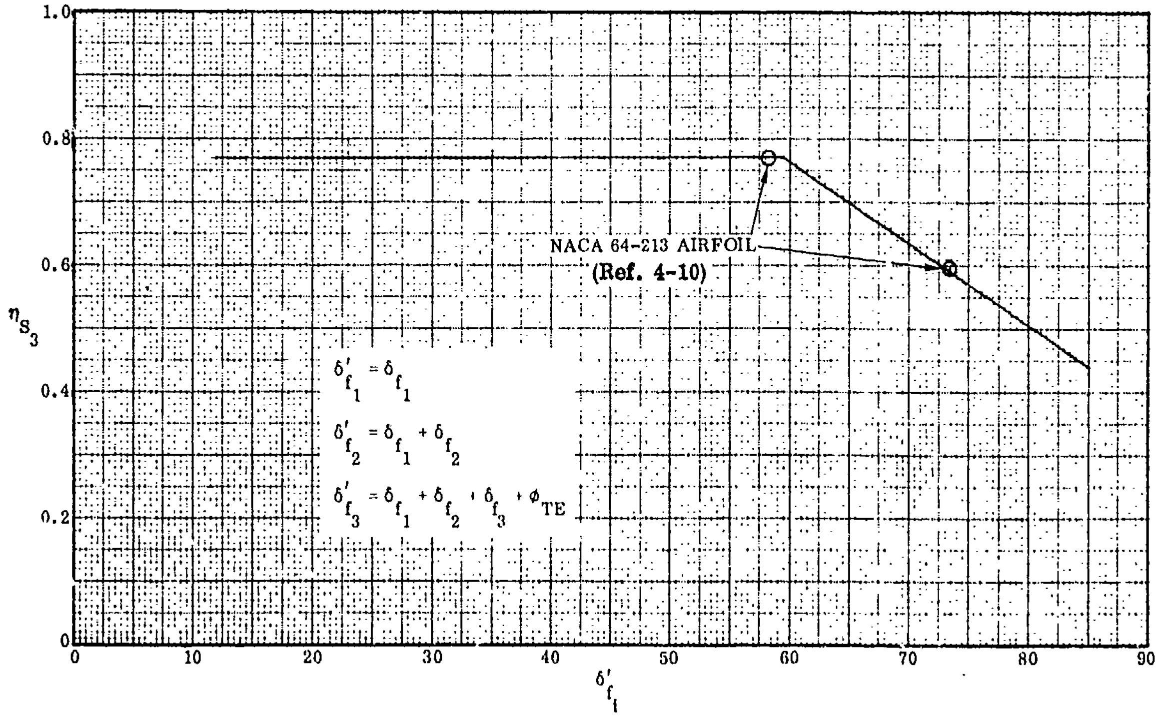

Figure 4-10. Turning Efficiency of Triple-Slotted Flaps

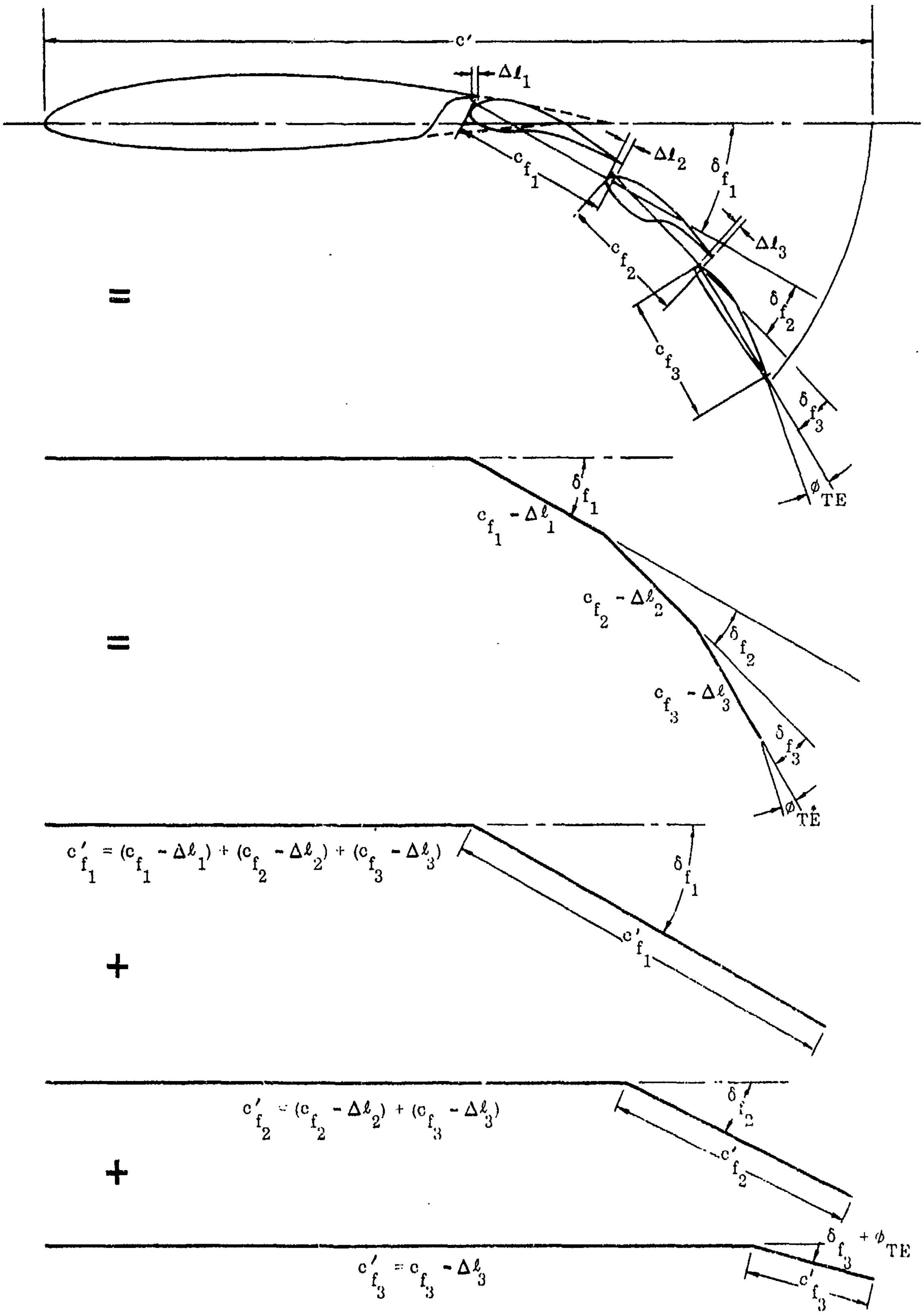

Figure 4-11. Principle of Superposition Theory and Extended Slotted-Flap Geometry

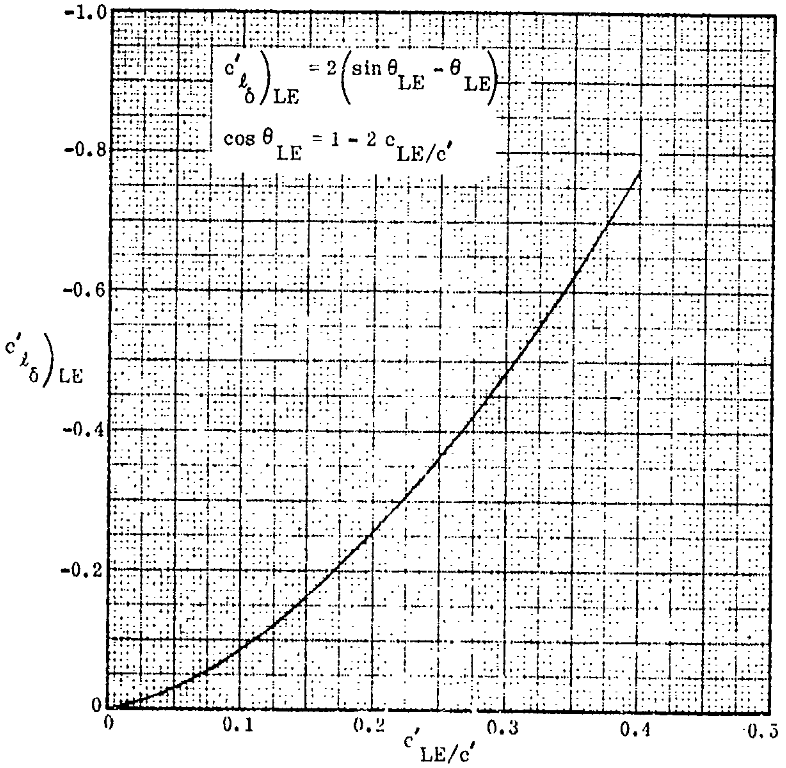

Figure 4-12. Leading-Edge Flap Effectiveness

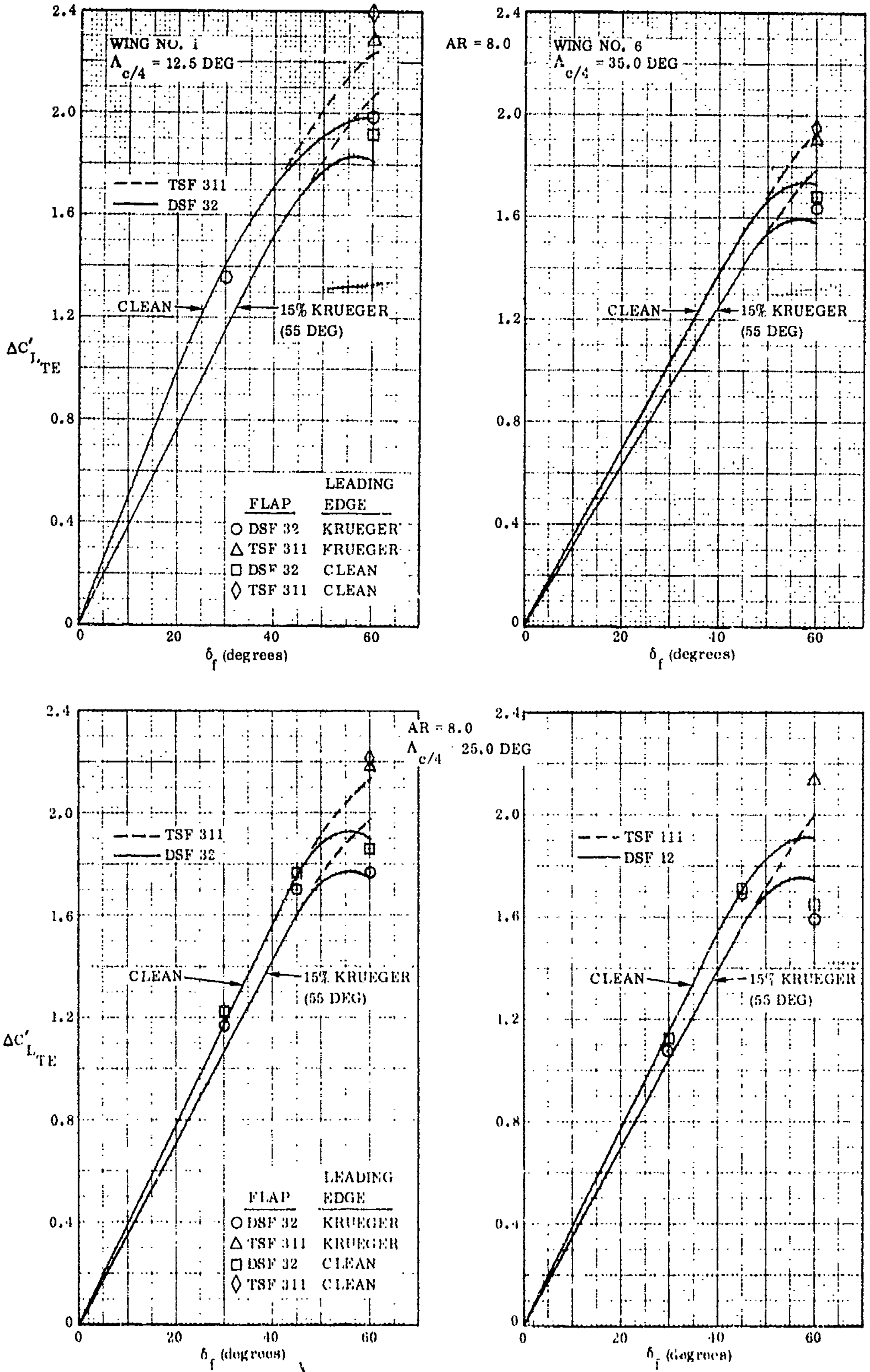

Figure 4-13. Correlation of Lift Effectiveness of Trailing-Edge Flaps

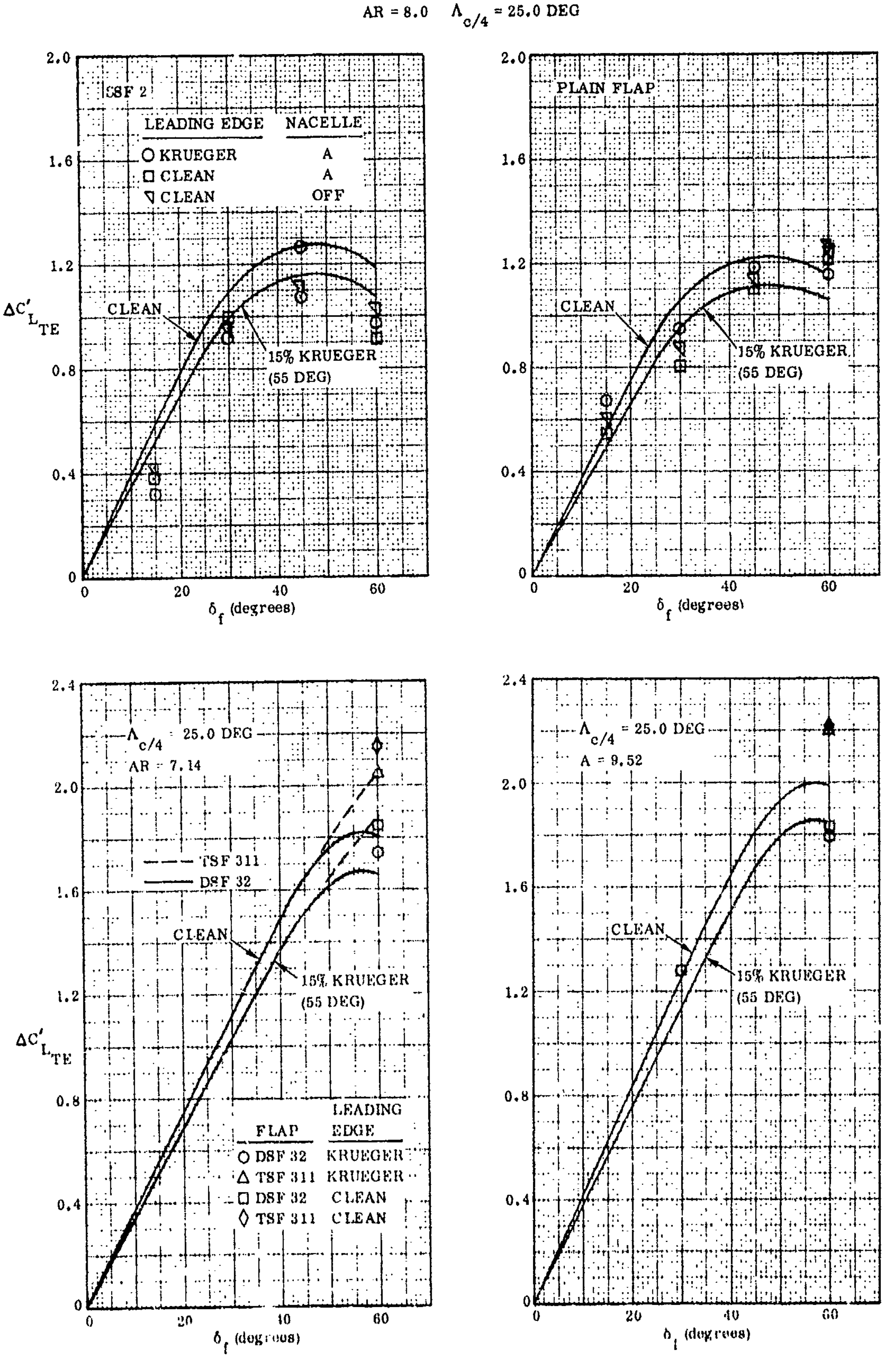

Figure 4-13. Correlation of Lift Effectiveness of Trailing-Edge Flaps (Continued)

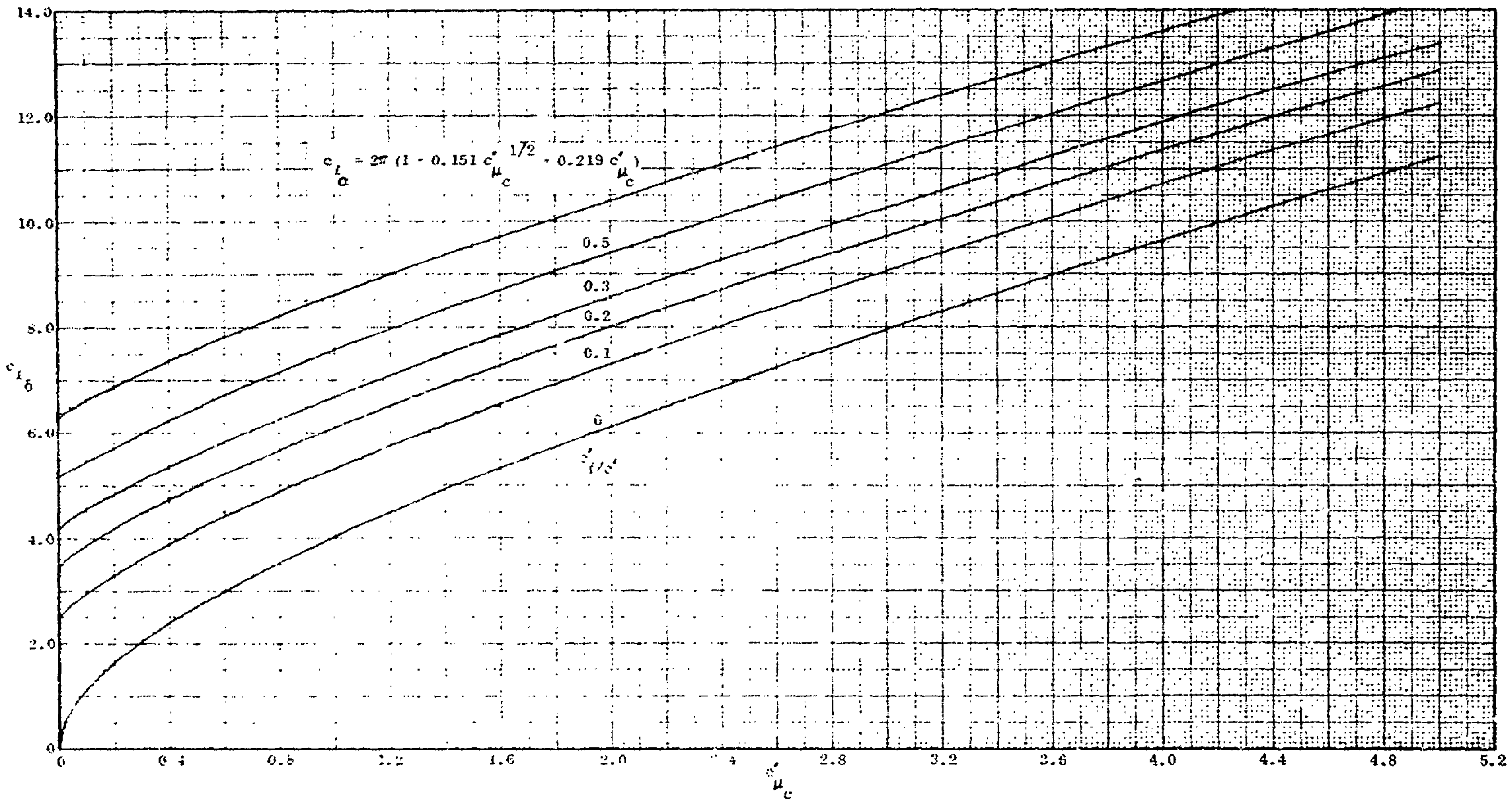

Figure 4-14. Theoretical Lifting Effectiveness of Trailing-Edge Flaps with Blowing

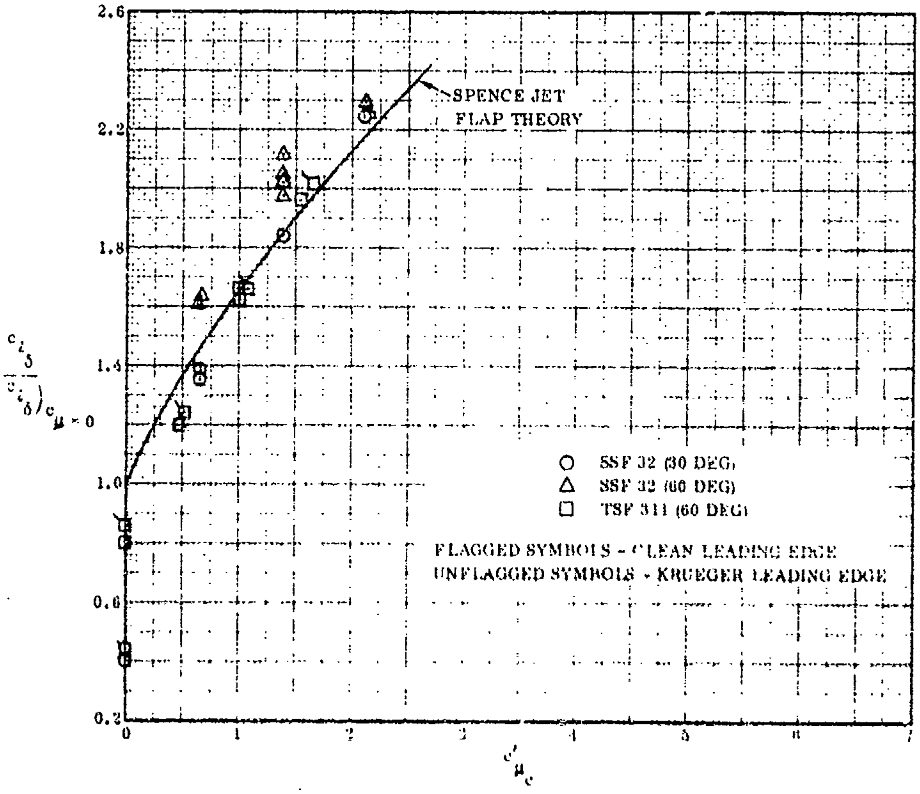

Figure 4-15. Correlation of Lift Effectiveness of Trailing-Edge Flaps

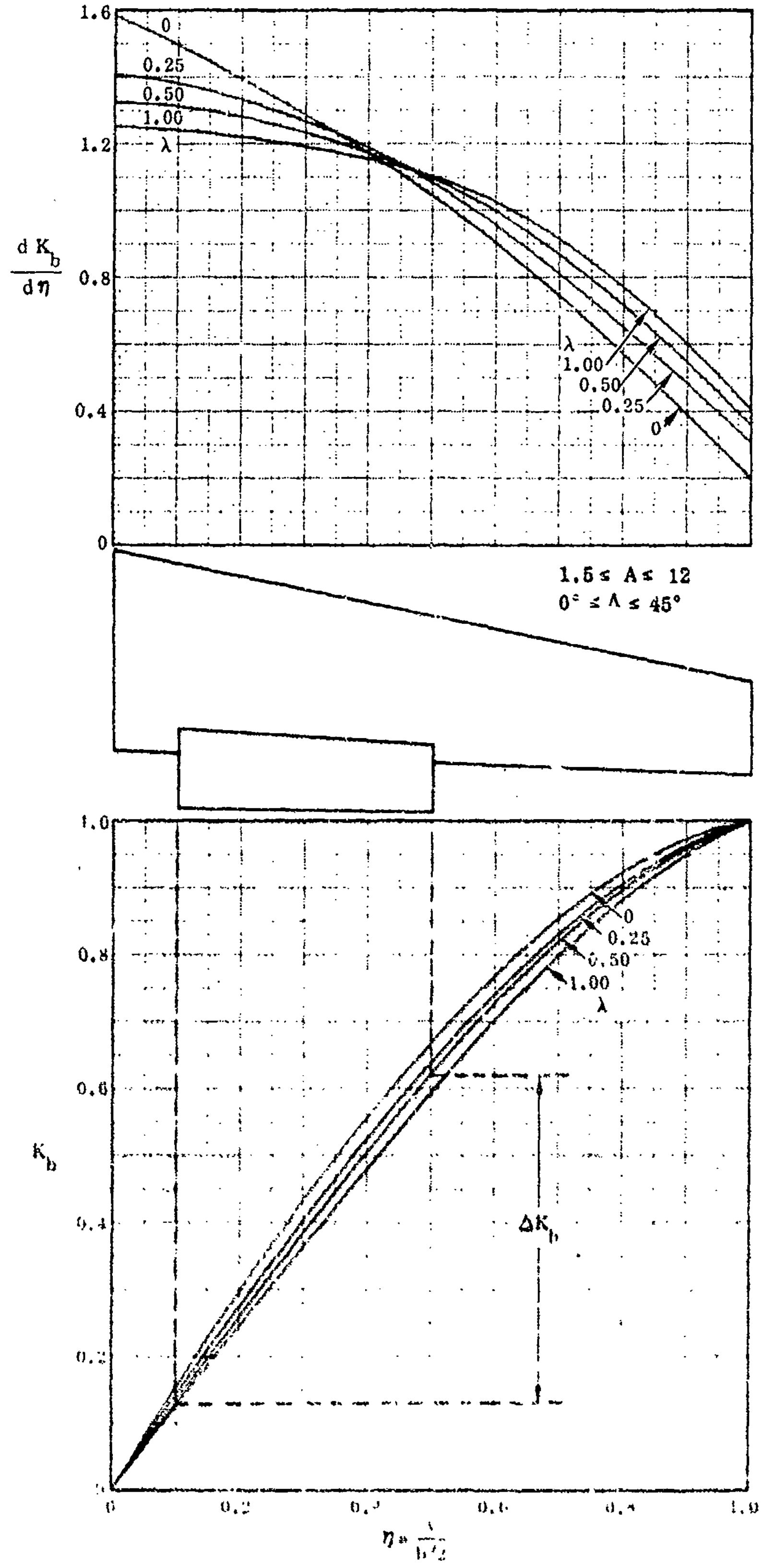

Figure 4-16. Partial-Span Flap Factors

4.3 THRUST VECTOR EFFECT

The final term of the total lift coefficient expression (Equation 4-1) is the thrust vector effect:

$$\Delta C'_\mu \ \sin(\alpha + \delta_T)$$

where

δ_T	is the effective nozzle vectoring thrust angle with respect to the reference line for angle of attack and is taken as positive when the thrust vector points above the horizontal.
$\Delta C'_\mu$	is the incremental gross jet momentum coefficient at the trailing edge of the flap that is neither captured by the flap nor produces supercirculatory lift augmentation.

Therefore:

$$\Delta C'_\mu = \left(C'_{\mu_{TE}} + C'_{D_{RAM}}\right)\left(1 - \bar{A}_C/A_j\right) \qquad (4\text{-}33)$$

For EBF systems

$$C'_{\mu_{TE}} = \left(C_{\mu_J} - C_{D_{RAM}}\right)\left(1 - 0.12\, c'_f/c\right)\Big/ S'/S \qquad (4\text{-}34a)$$

For IBF systems

$$C'_{\mu_{TE}} = \frac{C_{\mu_T} \cdot \left(1 - \Delta C_\mu / C_\mu\right)}{S'/S} \qquad (4\text{-}34b)$$

where

$C'_{D_{RAM}}$	is the ram drag based on the extended wing area.
$\bar{A}_c/A_j$	is the average capture ratio of all engine jets (for IBF, $\bar{A}_c/A_j = 1.0$).
$(1 - 0.12\ c'_f/c)$	is the estimated fraction of the EBF jet momentum remaining at the flap trailing edge and is based on the total flap chord ratio, c'_f/c. (Scrubbing loss.)
$(1 - \Delta C_\mu/C_\mu)$	is the estimated fraction of the IBF jet momentum remaining at the flap trailing edge and is based on the ratio of the flap chord to the jet nozzle height, h_{noz}, as shown in Figure 4-17. (Scrubbing loss.)

SAMPLE PROBLEM

GIVEN:

$\alpha = 10$ deg

$\frac{\bar{A}_c}{A_j} = 0.935$ (EBF case)

$\delta_T = -3.5$ deg (EBF case)

$\frac{\bar{A}_c}{A_j} = 0.0$ (MF/VT case)

$\delta_T = 69$ deg (MF/VT case)

$\frac{\bar{A}_c}{A_j} = 1.00$ (IBF case)

CALCULATE:

1. Jet momentum not captured by the flap, using Equation 4-33.

$$\Delta C'_\mu = \left(C'_{\mu_{TE}} + C'_{D_{RAM}}\right)\left(1 - \bar{A}_C/A_j\right) \tag{4-33}$$

A. EBF

$$\left.\begin{aligned} C'_{\mu_{TE}} &= 0.472 \\ C'_{D_{RAM}} &= 0.105 \end{aligned}\right\}$$ From sample problem in Section 4.1.

$\Delta C'_\mu = (0.472 + 0.105)(1 - 0.935) = 0.038$

B. IBF — Not applicable $\left(\frac{\bar{A}_c}{A_j} = 1.0\right)$

C. MF/VT

$C'_{\mu_{TE}} = 0.5451$

$C'_{D_{RAM}} = 0.076$

$\Delta C'_{\mu} = (0.545 + 0.076)\ (1 - 0.0) = 0.621$

2. Direct thrust vector effect:

$$\Delta C'_{\mu} \sin (\alpha + \delta_T)$$

A. EBF

$$\Delta C'_{\mu} \sin (\alpha + \delta_T) = (0.038) \sin (10 - 3.5) = 0.004$$

B. IBF — Not applicable

C. MF/VT

$$\Delta C'_{\mu} \sin (\alpha + \delta_T) = (0.621) \sin (10 + 69) = 0.610$$

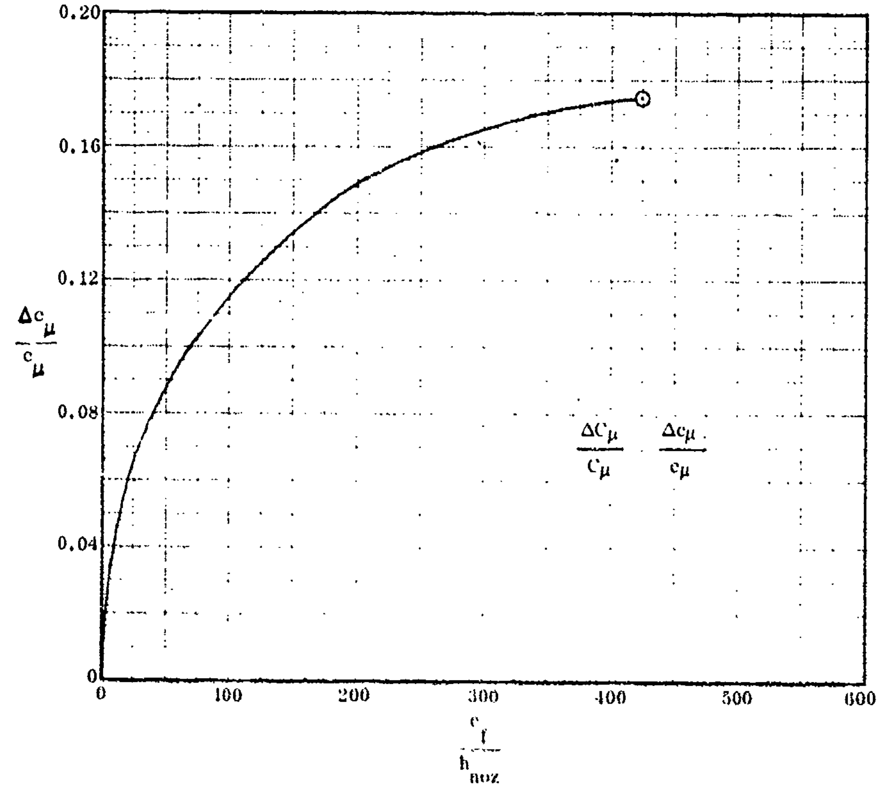

Figure 4-17. Incremental Loss in Blowing Momentum Due to Blowing Over the Flap (IBF)

4.4 LIFT CURVE CORRELATION

The sample problem below shows the method of totaling the various components of the lift to obtain the total lift at the given angle of attack. This problem is for the geometry shown in the sample problems at the end of the preceeding subsections. All of the components of the total lift in the linear range have been calculated in the sample calculations of Sections 4.1, 4.2, 4.3. The procedure for computing a total C_L in the linear range follows.

SAMPLE PROBLEM

GIVEN: $\alpha = 10$ deg

$\Theta = 4.5$ deg

CALCULATE:

1. The angle of attack for zero lift with Equation 4-2.

$$\sin\left(-\alpha_{o_L}\right) = \Delta C'_{L_{WING}} \Big/ \left[\left(C'_{L_\alpha}\right)_o \cdot K_{PWR}\right] \qquad (4\text{-}2)$$

A. EBF

$\Delta C'_{L_{WING}} = 3.087$ from sample problem in Section 4.2.

$\Delta C'_{L_{\alpha_0}} = 4.473$ from sample problem in Section 4.1.

$K_{PWR} = 1.1969$ from sample problem in Section 4.1.

$$-\alpha_{0_L} = \sin^{-1}\left(\frac{3.087}{(4.473)(1.1969)}\right)$$

$$= \sin^{-1}\ (0.5766)$$

$$= 35.21 \text{ deg}$$

B. IBF

$\Delta C'_{L_{WING}} = 3.691$ from sample problem in Section 4.2.

$\Delta C'_{L_{\alpha_0}} = 4.473$ from sample problem in Section 4.1.

$K_{PWR} = 1.2234$ from sample problem in Section 4.1.

$$-\alpha_{0_L} = \sin^{-1}\left(\frac{3.691}{(4.473)(1.2234)}\right)$$

$$= \sin^{-1}\ (0.6745)$$

$$= 42.41 \text{ deg}$$

C. MF/VT

$\Delta C'_{L_{WING}} = 1.963$ from sample problem in Section 4.2.

$\Delta C'_{L_{\alpha_0}} = 3.715$ from sample problem in Section 4.1.

$K_{PWR} = 1.00$ from sample problem in Section 4.1.

$$-\alpha_{0_L} = \sin^{-1}\left(\frac{1.963}{(3.715)(1.00)}\right)$$

$$= \sin^{-1}\ (0.5284)$$

$$= 31.89 \text{ deg}$$

2. The effect of wing twist, given by Equation 4-3, for EBF, IBF and MF/VT.

$$\Delta\alpha_t = \frac{\Delta\alpha_0}{\theta}\cdot\theta \qquad (4\text{-}3)$$

$[\Delta\alpha_0/\Theta] = -0.3875$ from Figure 4-2.

$\Delta\alpha_T = (-0.3875)(-4.5) = 1.74$ deg

3. The total wing lift at an angle of attack, using Equation 4-1.

$$C_L = \frac{S'}{S}\left[\left(C'_{L_\alpha}\right)_o \cdot K_{PWR} \cdot \sin\left(\alpha - \alpha_{o_L} - \Delta\alpha_t\right) + \Delta C'_\mu \sin\left(\alpha + \delta_T\right)\right] \qquad (4\text{-}1)$$

A. EBF

$C'_{L_{\alpha_0}}$ = 4.473 from sample problem in Section 4.1.

K_{PWR} = 1.1969 from sample problem in Section 4.1.

$\Delta C'_\mu$ = 0.038 from sample problem in Section 4.3.

$$C_{L_{\alpha = 10\text{ deg}}} = (1.609)[(4.473)(1.1969)\sin(10 + 35.21 - 1.74) + (0.038)\sin(10 - 3.5)]$$

$$= (1.609)[(4.473)(1.1969)\sin(43.47) + (0.038)\sin(6.5)]$$

$$= (1.609)\ [3.683 + 0.004]$$

$$= 5.932$$

B. IBF

$C'_{L_{\alpha_0}}$ = 4.473 from sample problem in Section 4.1.

K_{PWR} = 1.2234 from sample problem in Section 4.1.

$\Delta C'_\mu$ = 0.0 from sample problem in Section 4.3.

$$C_L = (1.609)\ [(4.473)(1.2234)\sin(10 + 42.41 - 1.74)]$$

$$= (1.609)(4.473)(1.2234)(0.7735)$$

$$= 6.811$$

C. MF/VT

$C'_{L_{\alpha_0}}$ = 3.715 from sample problem in Section 4.1.

K_{PWR} = 1.00 from sample problem in Section 4.1.

$\Delta C'_\mu$ = 0.621 from sample problem in Section 4.3.

$$C_L = (1.609)\ [(3.715)(1.00)\sin(10 + 31.89 - 1.74) + (0.621)\sin(10 + 69)]$$

$$= (1.609)\ [(3.715)(0.6448) + (0.621)(0.9816)]$$

$$= (1.609)(3.005)$$

$$= 4.835$$

CORRELATIONS

The correlations presented herein are for a wing with aspect ratio of 8, quarter-chord sweep of 25 degrees, and taper ratio of 0.33. This wing was tested with a wide variety of nacelle positions, flap configurations, and blowing systems. All of the configurations used for correlations are with leading-edge Krueger flaps deflected 55 degrees and with a leading-edge jet momentum coefficient equal to 0.10.

The EBF calculations for the wing with a triple-slotted flap (δ_f = 60 deg) are compared with test results in Figures 4-18 through 4-20. Figure 4-18, which is with the engines in the high position (Position A) for which the capture ratio is 0.935, shows good agreement with the test data (power-on) when assuming full BLC. Although the power-on calculations for lift with full spreading lie somewhat closer to the test data than do the calculations based on a minimum spreading angle of 6 degrees, the relative insensitivity of the spreading assumption on the lift is encouraging. All subsequent calculations to be presented for EBF comparisons have therefore been based on minimum spreading. The power-off calculation for lift at a blowing coefficient of zero is shown with full BLC effectiveness (no flow separation) and without BLC effectiveness (flow separation based on the flap efficiency factors in Figure 4-10). Test data indicates that flap separation is slightly less severe than predicted.

Figure 4-19 depicts a similar comparison but with the engines lowered to Position E, for which the capture ratio has been reduced to 0.579. In this case, the jet efflux no longer passes through the first flap slot, and all computations are based on the same degree of flow separation as for the power-off case. The test data shows somewhat higher lift curve slopes at all values of blowing coefficient, C_μ, than do the computations. Computed lift curve slopes are assumed to be reduced from full potential flow theory values by 25 percent because of flow separation, as discussed in Paragraph 4.1.2.

Figure 4-20 compares the methodology and test results when the engines in Position E are tilted upward by 15 degrees so that the capture ratio is increased from 0.579 to 0.997. In this case, the methodology is similar to that for Figure 4-18; therefore, full BLC effectiveness has been assumed for the power-on computations.

Comparisons for double-slotted EBF systems of 30- and 60-degree deflections are shown in Figures 4-21 and 4-22, respectively. The engines are in Position A (high), for which the jets pass through the first flap slot. All power-on computations have therefore been based on full BLC effectiveness. The discrepancy in the power-off lift curve in Figure 4-21 may once again be attributed to smaller effects of flow separation in the data than predicted by the methodology. The comparisons shown for the 60-degree double-slotted flaps in Figure 4-22 indicate that full BLC effectiveness was not approached for this flap configuration until the C_{μ_T} values exceeded 1.0.

Figures 4-23 and 4-24 compare the methodology with test data for low-capture-ratio single-slotted flaps of 30 and 60 degrees of deflection, respectively. Although the jets are still in the high position, zero BLC effectiveness was assumed for power-on, because the jet efflux failed to pass through the single flap slot. The power-off lift data in Figure 4-23 is again somewhat higher in the linear range than predicted by the methodology. The nonlinearity in the test results at low angles of attack is due to separation on the underside of the leading-edge Krueger flap, which is not included in the methodology. This type of separation occurs under conditions of low angles of attack, small flap deflections, small flap chords, and low effective blowing coefficients, and has been negligible for the previous comparisons. Thus, with increased flap angle and capture ratio, as in Figure 4-24, the extent of the linear region is increased and the correlation between methodology and lift data is improved. In this case, the methodology appears to slightly overpredict the power-off separation effects on lift.

Figures 4-25 through 4-28 present correlations between methodology and test data for IBF systems with plain flaps of 15, 30, 45, and 60 degrees of deflection, respectively. For the IBF computations, the full BLC effect was assumed for power-on conditions, whereas power-off lift estimates were based on plain flap efficiencies from Figure 4-7. As indicated in Figure 4-25, the methodology agrees reasonably well with the overall lift data for the 15-degree flap deflection. Similar agreement is shown in Figure 4-26 for the 30-degree flap deflection, except that full BLC effectiveness is apparently not achieved for C_{μ_T} values below 0.5. In addition, use of η_p from Figure 4-7 appears to somewhat overestimate flap efficiency for the power-off condition. Similar results are shown in Figure 4-27 for the 45-degree flap deflection, except that the power-off lift estimate using Figure 4-7 lies closer to the test data. Comparisons for the 60-degree flap deflection IBF configuration are shown in Figure 4-28 and once again indicate that full BLC effectiveness is established at $C_{\mu_T} \approx 0.5$. In this case, good agreement is also indicated for the power-off lift in the linear range of the test data.

Figures 4-29 and 4-30 compare methodology and test data for MF/VT configurations with the jets in a low and rearward position (Position F). The comparison in Figure 4-29 is for a double-slotted flap with 30 degrees of deflection and with an effective thrust vectoring angle of 37 degrees. Power-off data and calculations are similar to the power-off EBF comparison for the flap shown in Figure 4-21. Power-on computations for lift assume no supercirculation or BLC effect for the jets, and lie consistently below the test results in the linear region. This discrepancy is probably due to underestimating flap turning efficiency as discussed in connection with Figure 4-21. Test data for lift in the linear region also shows a somewhat higher lift curve slope at the higher C_μ values than is predicted by the methodology. Thus, a small favorable interference effect is observed. The drop-off in test data for lift at low angles is believed due to leading-edge separation, as discussed previously.

The comparisons in Figure 4-30 are for a triple-slotted flap with 60 degrees of deflection and with an effective thrust vectoring angle of 69 degrees. No power-on BLC effect or supercirculation is assumed. The power-off data is similar to the power-off EBF data obtained with the same flap system and shown in Figures 4-18 to 4-20. The power-on lift data lies somewhat above the prediction and exhibits higher lift curve slopes in the linear range for the reasons mentioned in connection with Figure 4-29.

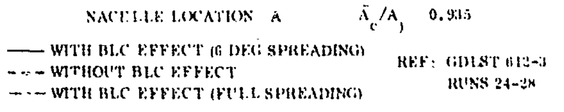

Figure 4-18. Correlation of Lift Generalized Methodology with EBF Test Data, A = 8, $\Lambda_{c/4}$ = 25 Degrees, Triple-Slotted Flap (δ_f = 60 Degrees), Nacelles High

Correlations between the lift curve from the methodology and test data for two additional aspect ratios (7.1 and 9.5) with wing sweep of 25 degrees are shown in Figures 4-31 and 4-32. This data is with the triple-slotted EBF at 60 degrees. The theory underpredicts the test data at an aspect ratio of 7.1 (Figure 4-31) and shows a slight overprediction at an aspect of 9.5 Figure 4-32).

Correlations between the lift curve from the methodology and test data for wings with quarter-chord sweeps of 12.5 and 35 degrees, with aspect ratio constant at 8, are shown in Figures 4-33 and 4-34. This data is also with the triple-slotted EBF at 60 degrees. The correlation is good at all blowing coefficients at both wing sweeps.

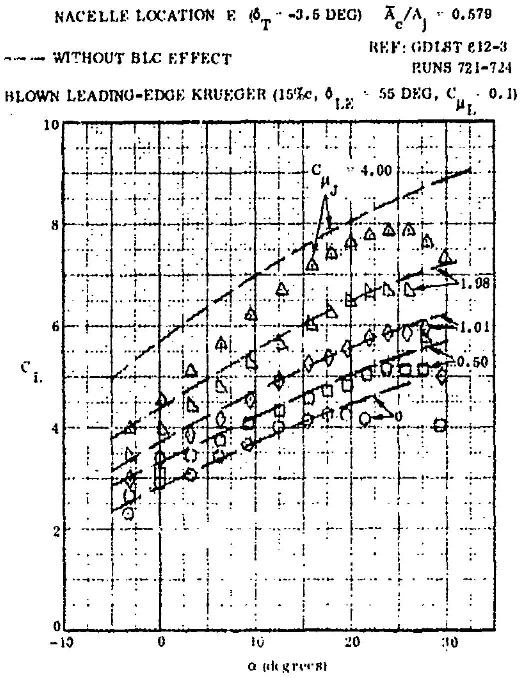

Figure 4-19. Correlation of Lift Generalized Methodology with EBF Test Data, A = 8, $\Lambda_{c/4}$ = 25 Degrees, Triple-Slotted Flap (δ_f = 60 Degrees), Nacelles Low

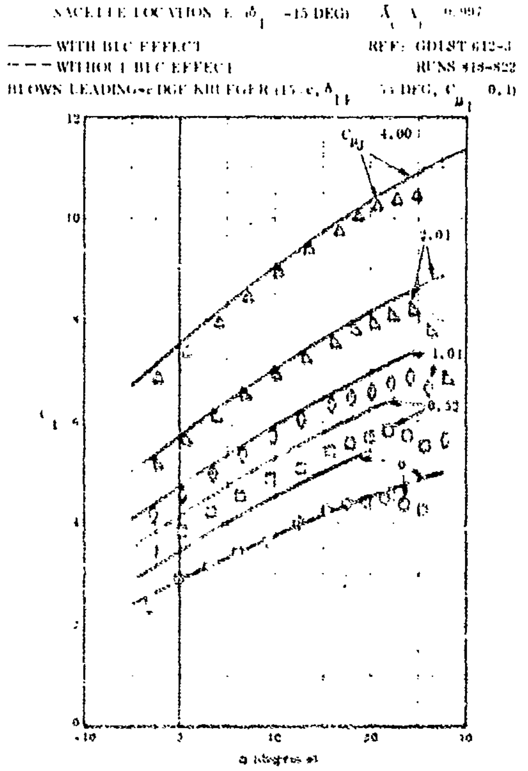

Figure 4-20. Correlation of Lift Generalized Methodology with EBF Test Data, A = 8, $\Lambda_{c/4}$ = 25 Degrees, Triple-Slotted Flap (δ_f = 60 Degrees), Nacelles Low with Thrust Deflected Upward 15 Degrees

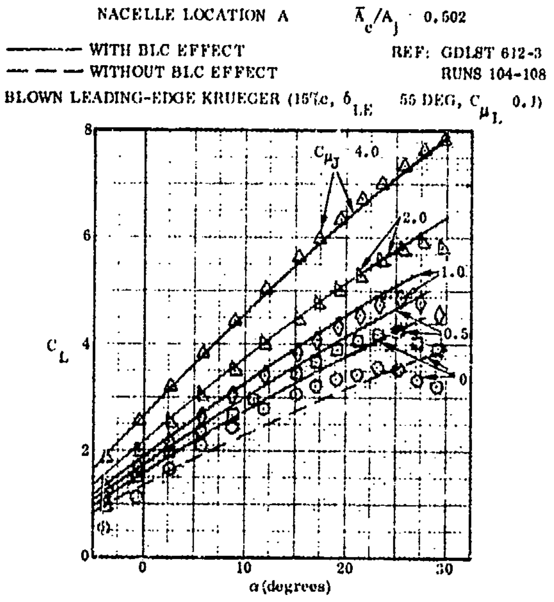

Figure 4-21. Correlation of Lift Generalized Methodology with EBF Test Data, A = 8, $\Lambda_{c/4}$ = 25 Degrees, Double-Slotted Flap (δ_f = 30 Degrees)

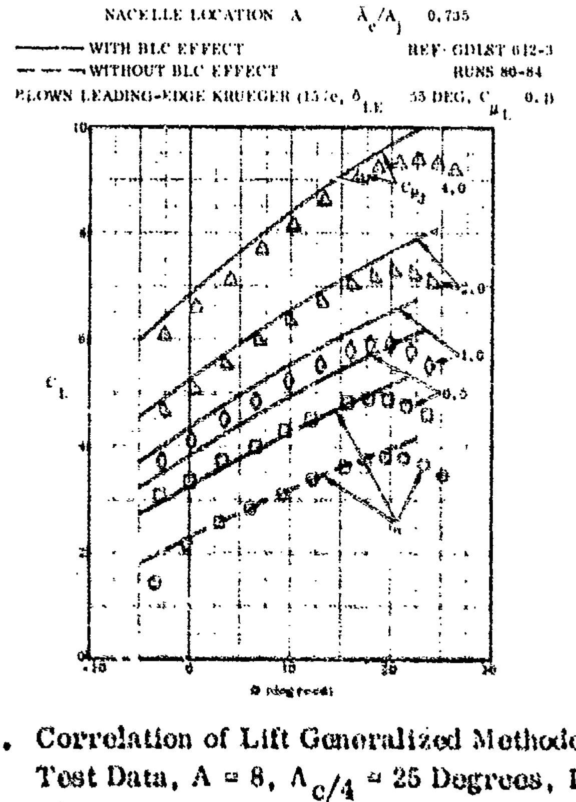

Figure 4-22. Correlation of Lift Generalized Methodology with EBF Test Data, A = 8, $\Lambda_{c/4}$ = 25 Degrees, Double-Slotted Flap (δ_f = 60 Degrees)

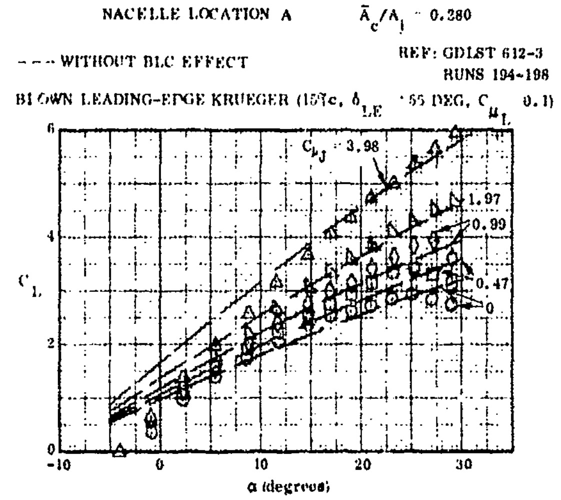

Figure 4-23. Correlation of Lift Generalized Methodology with EBF Test Data, A = 8, $\Lambda_{c/4}$ = 25 Degrees, Single-Slotted Flap (δ_f = 30 Degrees)

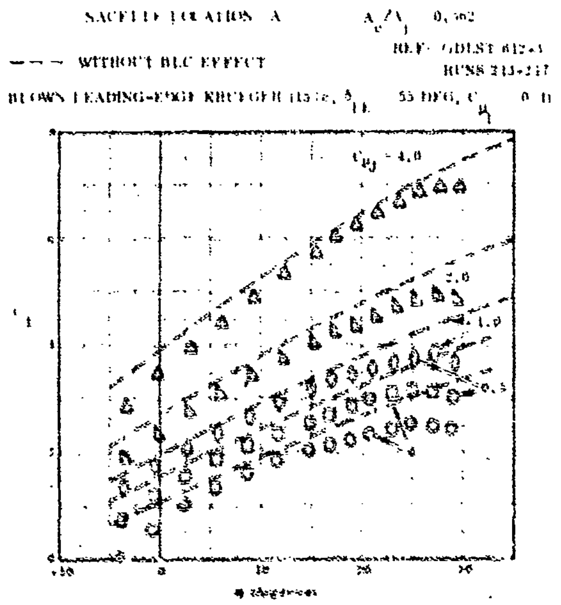

Figure 4-24. Correlation of Lift Generalized Methodology with EBF Test Data, A = 8, $\Lambda_{c/4}$ = 25 Degrees, Single-Slotted Flap (δ_f = 60 Degrees)

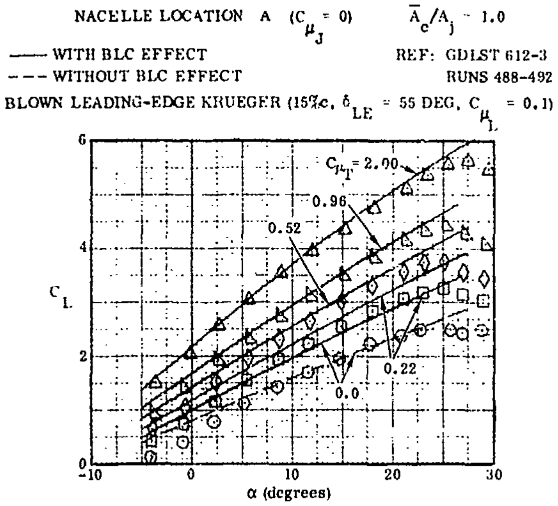

Figure 4-25. Correlation of Lift Generalized Methodology with IBF Test Data, A = 8, $\Lambda_{c/4}$ = 25 Degrees, Plain Blown Flap (δ_f = 15 Degrees)

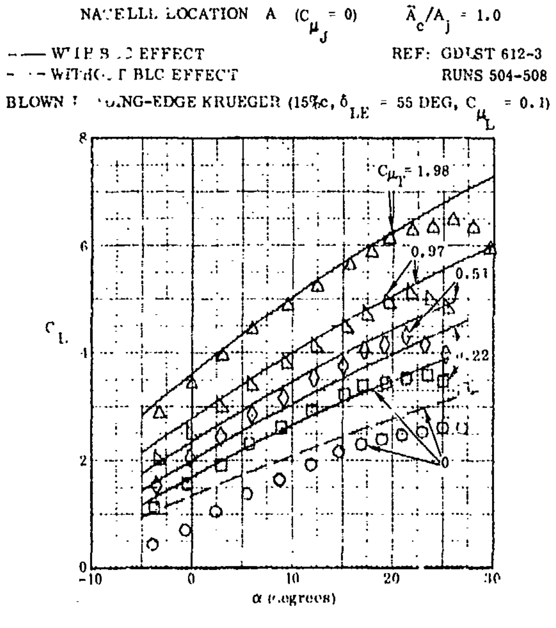

Figure 4-26. Correlation of Lift Generalized Methodology with IBF Test Data, A = 8, $\Lambda_{c/4}$ = 25 Degrees, Plain Blown Flap (δ_f = 30 Degrees)

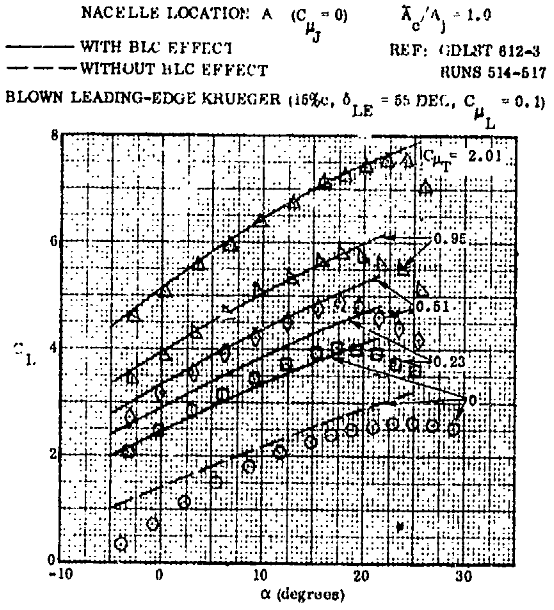

Figure 4-27. Correlation of Lift Generalized Methodology with IBF Test Data, A = 8, $\Lambda_{c/4}$ = 25 Degrees, Plain Blown Flap (δ_f = 45 Degrees)

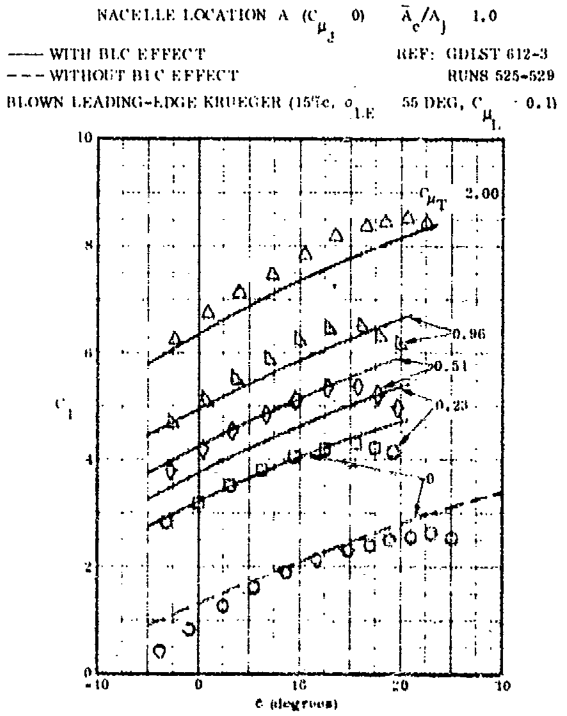

Figure 4-28. Correlation of Lift Generalized Methodology with IBF Test Data, A = 8, $\Lambda_{c/4}$ = 25 Degrees, Plain Blown Flap (δ_f = 60 Degrees)

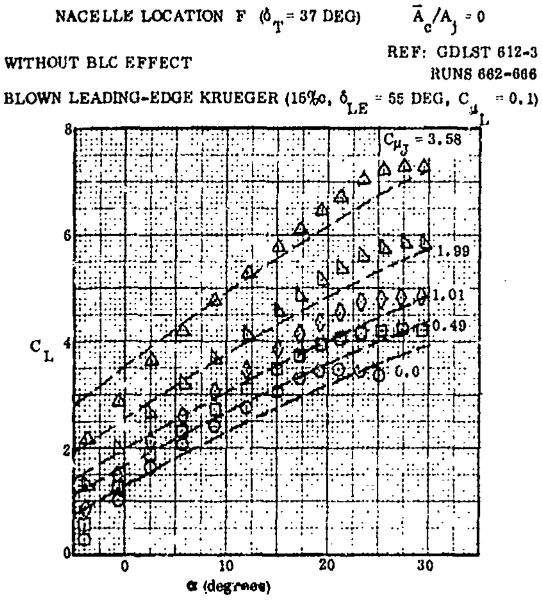

Figure 4-29. Correlation of Lift Generalized Methodology with MF/VT Test Data, A = 8, $\Lambda_{c/4}$ = 25 Degrees, Double-Slotted Flap (δ_f = 30 Degrees), Thrust Vectored Downward 37 Degrees

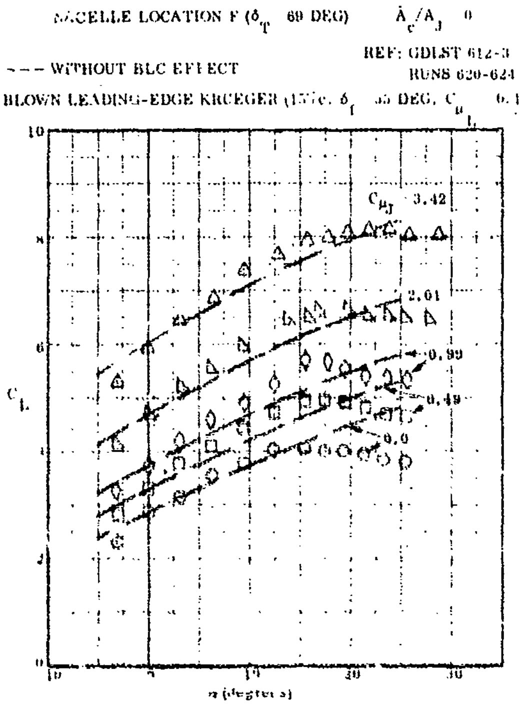

Figure 4-30. Correlation of Lift Generalized Methodology with MF/VT Test Data, A = 8, $\Lambda_{c/4}$ = 25 Degrees, Triple-Slotted Flap (δ_f = 60 Degrees), Thrust Vectored Downward 69 Degrees

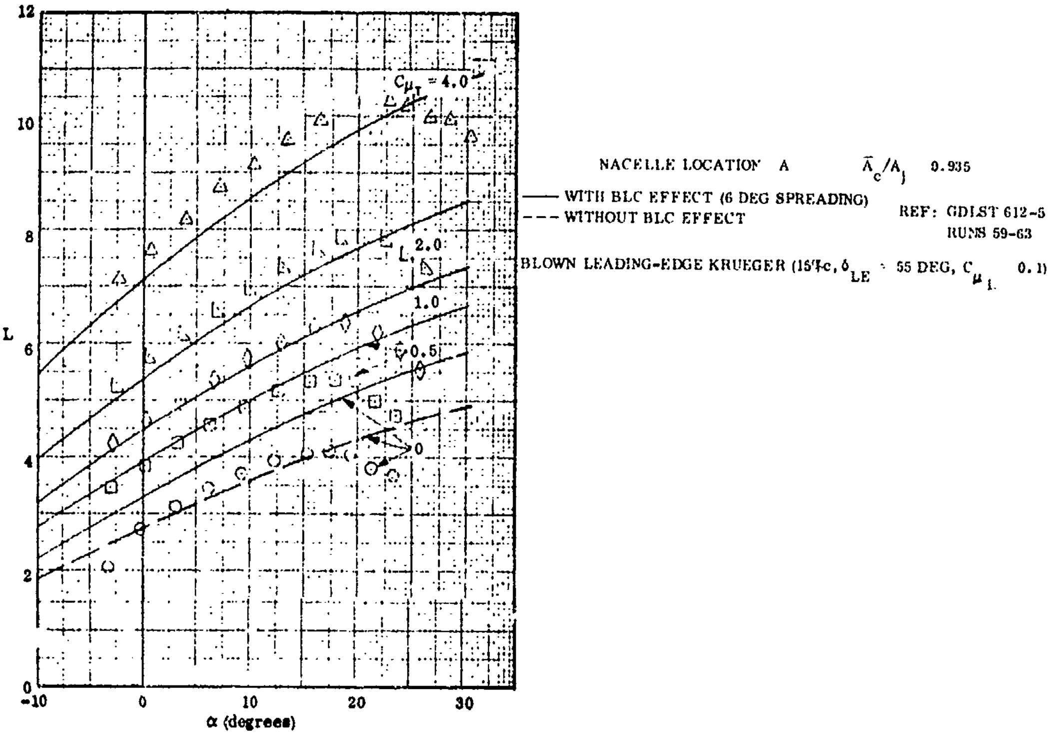

Figure 4-31. Correlation of Lift Generalized Methodology with EBF Test Data, A = 7.1, $\Lambda_{c/4}$ = 25 Degrees, Triple-Slotted Flap (δ_f = 60 Degrees)

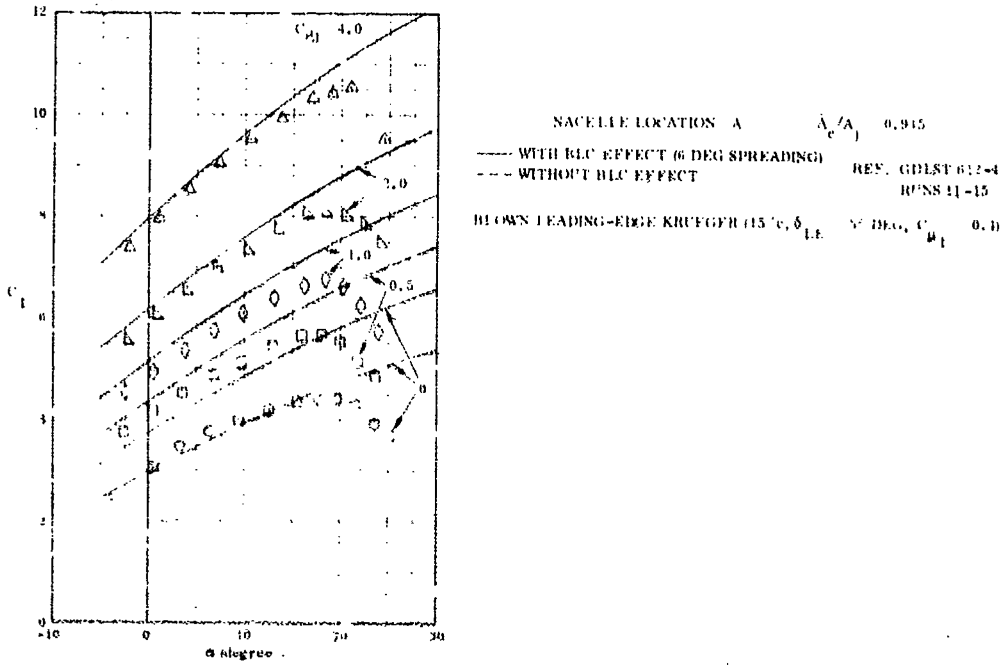

Figure 4-32. Correlation of Lift Generalized Methodology with EBF Test Data, A = 9.5, $\Lambda_{c/4}$ = 25 Degrees, Triple-Slotted Flap (δ_f = 60 Degrees)

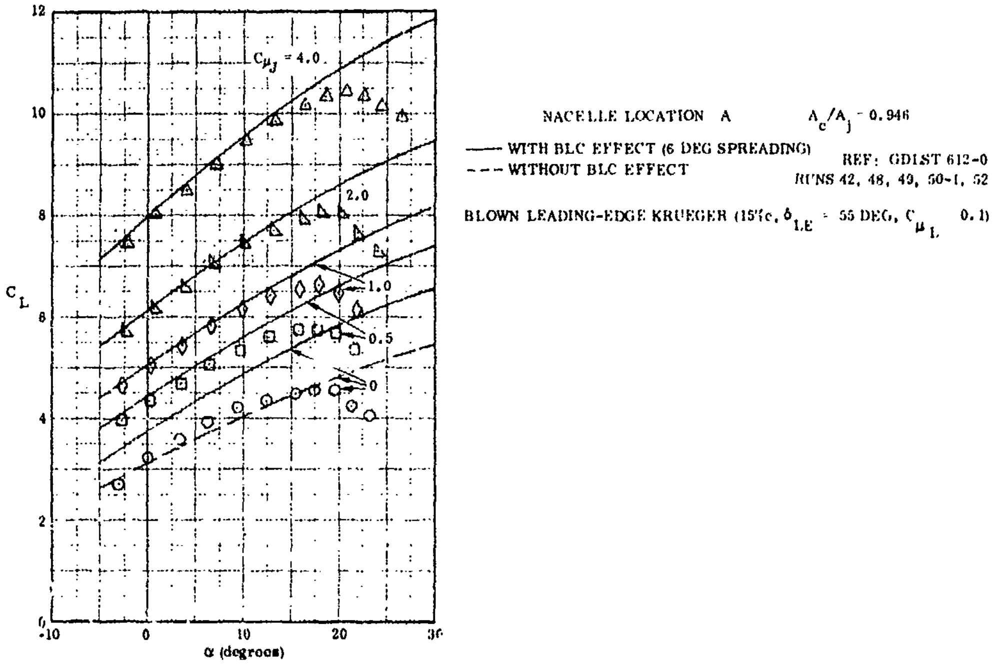

Figure 4-33. Correlation of Lift Generalized Methodology with EBF Test Data, A = 8.0, $\Lambda_{c/4}$ = 12.5 Degrees, Triple-Slotted Flap (δ_f = 60 Degrees)

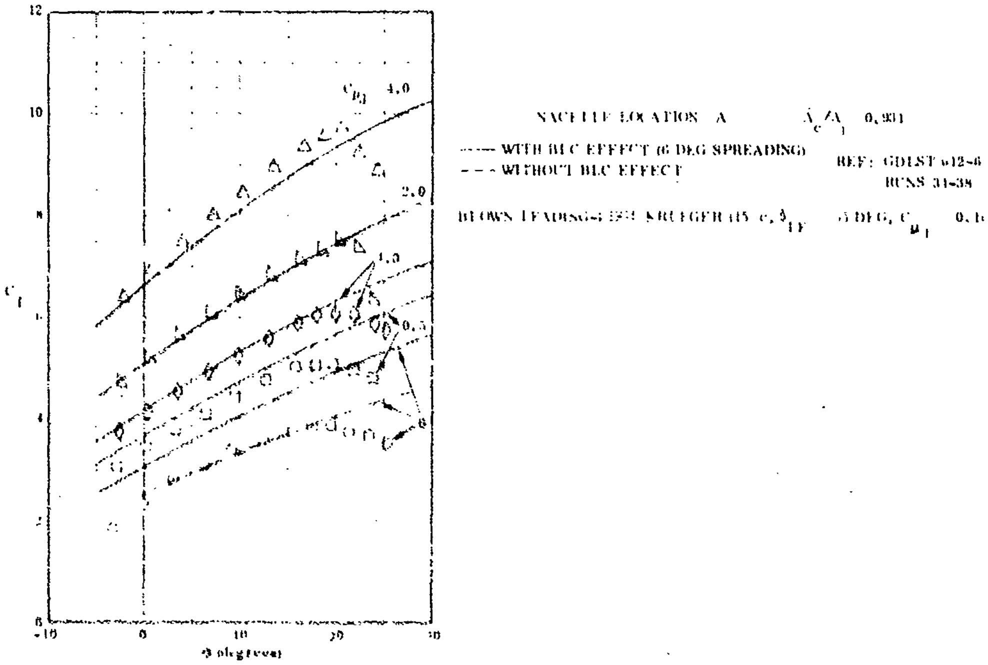

Figure 4-34. Correlation of Lift Generalized Methodology with EBF Test Data, A = 8.0, $\Lambda_{c/4}$ = 35 Degrees, Triple-Slotted Flap (δ_f = 60 Degrees)

SECTION 5

MAXIMUM LIFT

The maximum lift coefficient is estimated by assuming that $C_{L_{MAX}}$ is built up as shown in Figure 5-1 from the sum of the three components indicated in the following expression:

$$C_{L_{MAX}} = \frac{S'}{S}\left[C_{L_{MAX_o}} + \Delta C'_{L_{MAX_{LE}}} + \Delta C'_{L_{MAX_{TE}}}\right] \tag{5-1}$$

where:

$C_{L_{MAX_o}}$	is the maximum lift of the basic clean airfoil (Section 5.1).
$\Delta C'_{L_{MAX_{LE}}}$	is the increment in maximum lift due to the deflection and blowing of a leading-edge high-lift device. This increment is measured without a trailing edge (Section 5.2) and is based on extended wing area.
$\Delta C'_{L_{MAX_{TE}}}$	is the increment in maximum lift due to the deflection and blowing of a trailing-edge flap system. This increment is measured with or without flaps, slats, and/or blowing on the leading edge (Section 5.3) and is based on extended wing area.

All equations required to estimate the various terms in Equation 5.1 are also shown in Figure 5-1. The figure indicates the paragraphs that furnish a more detailed explanation of the terms.

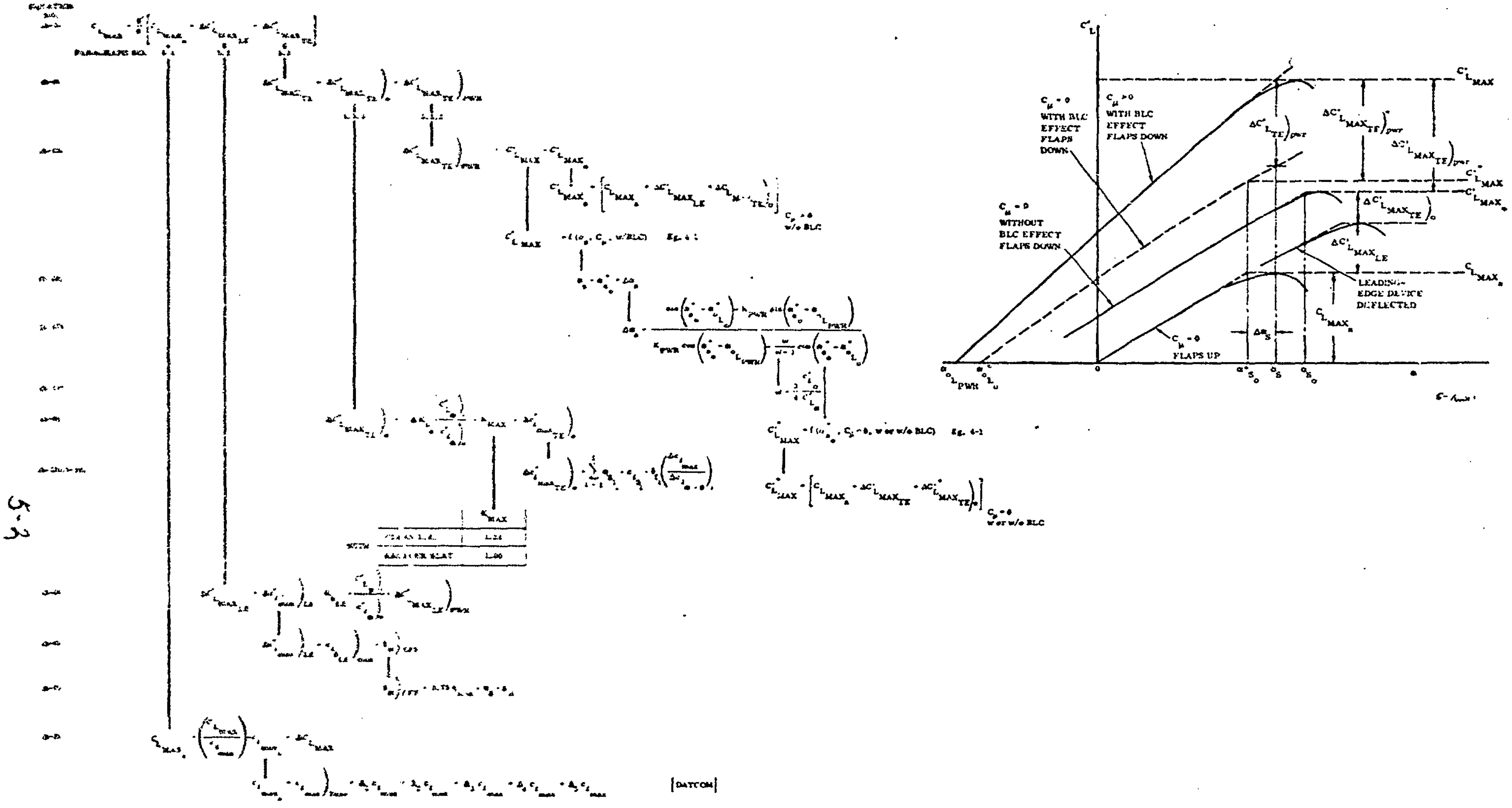

Figure 5-1. Maximum Lift Methodology

5-2

5.1 MAXIMUM LIFT - CLEAN WING

An empirical method for estimating the maximum lift coefficient for a clean three-dimensional wing is presented in USAF DATCOM, Paragraph 4.1.3.1. This method, which requires the estimation of the two-dimensional section maximum lift from DATCOM Paragraph 4.1.1.4, is based on experimental data from high-aspect-ratio, untwisted, constant-section (symmetrical or cambered) wings. The generalized maximum lift coefficient is expressed as:

$$C_{L_{MAX_a}} = \left(\frac{C_{L_{MAX}}}{c_{\ell_{max}}}\right) \cdot c_{\ell_{max_a}} + \Delta C_{L_{MAX}} \tag{5-2}$$

where:

$\Delta C_{L_{MAX}}$ is the empirical maximum lift increment shown in DATCOM (Paragraph 4.1.3.4) due to Mach number changes.

$\frac{C_{L_{MAX}}}{c_{\ell_{max}}}$ is the empirical factor used to correct section maximum lift coefficient for finite wings, including corrections for wing sweep and leading-edge radius (Figure 5-2).

$c_{\ell_{max_a}}$ is the two-dimensional maximum lift coefficient as estimated from DATCOM (Paragraph 4.1.1.4) as shown in Figure 5-1.

Estimating the two-dimensional maximum lift coefficient $c_{\ell_{max_a}}$ at the low Reynolds numbers normally associated with powered lift testing requires that the empirical data in DATCOM be extrapolated to Reynolds numbers of less than one million. Test data in this Reynolds number range is presented in Figure 5-3. Included is data for the NACA 64A213 airfoil which was used on the basic Convair powered model. This data is provided as a guide for estimating $c_{\ell_{max_a}}$ at the lower test Reynolds numbers.

Using the value $c_{\ell_{max_a}}$ for maximum section lift coefficient from Figure 5-3 which corresponds to Convair test Reynolds number, the wing maximum lift coefficient, $C_{L_{MAX_a}}$, was obtained for the five wings tested and the estimated results are compared with the test values in Table 5-1.

Table 5-1. Comparison of Theoretical Maximum Lift Coefficients With Test Data

Wing	Aspect Ratio	Leading Edge Sweep	Δy	$\frac{C_{L_{MAX}}}{c_{\ell_{max}}}$ (Figure 5-2)	$C_{L_{MAX_a}}$		$\frac{C_{L_{MAX}}}{c_{\ell_{max}}}$ (Test Data)
					Theory	Test	
1	8	15.4	3.1	0.85	1.025	1.091	0.90
3	8	27.9	3.1	0.80	0.965	1.075	0.88
4	9.5	27.9	3.1	0.80	0.965	1.070	0.88
5	7.1	27.9	3.1	0.80	0.965	1.065	0.88
6	8	37.8	3.1	0.74	0.893	1.078	0.89

Better correlation is obtained if the value of the ratio $C_{L_{MAX}}/c_{\ell_{max}}$ were taken as 0.89 instead of the values indicated in Figure 5-2. This difference could be attributed to the spanwise twist, thickness, and camber variations that are built into these wings and not included in the empirical correlations in DATCOM.

SAMPLE PROBLEM

GIVEN:

64A213 Airfoil

$\Lambda_{LE} = 27.9$ deg

$\Delta y = 3.1$

$M = 0.1$

$c_{\ell_{max_a}} = 1.21$ from DATCOM Paragraph 4.1.1.4.

$\Delta C_{L_{max}} = 0$ from DATCOM Paragraph 4.1.3.4.

CALCULATE:

Maximum lift coefficient for the clean wing, using Equation 5-2, for EBF, IBF, and MF/VT.

$$C_{L_{MAX_a}} \quad \left(\frac{C_{L_{MAX}}}{c_{\ell_{max}}}\right) \cdot c_{\ell_{max_a}} + \Delta C_{L_{MAX}} \tag{5-2}$$

$\dfrac{C_{L_{MAX}}}{c_{\ell_{max}}} = 0.80$ from Figure 5.2.

$C_{L_{MAX_a}} = (1.21)\,(0.80)$

$= 0.968$

Note: This value has been increased by $\Delta C_{L_{MAX_a}} = 0.10$ to account for twist and camber effects on the basis of test data.

$C_{L_{MAX_a}} = 1.068$

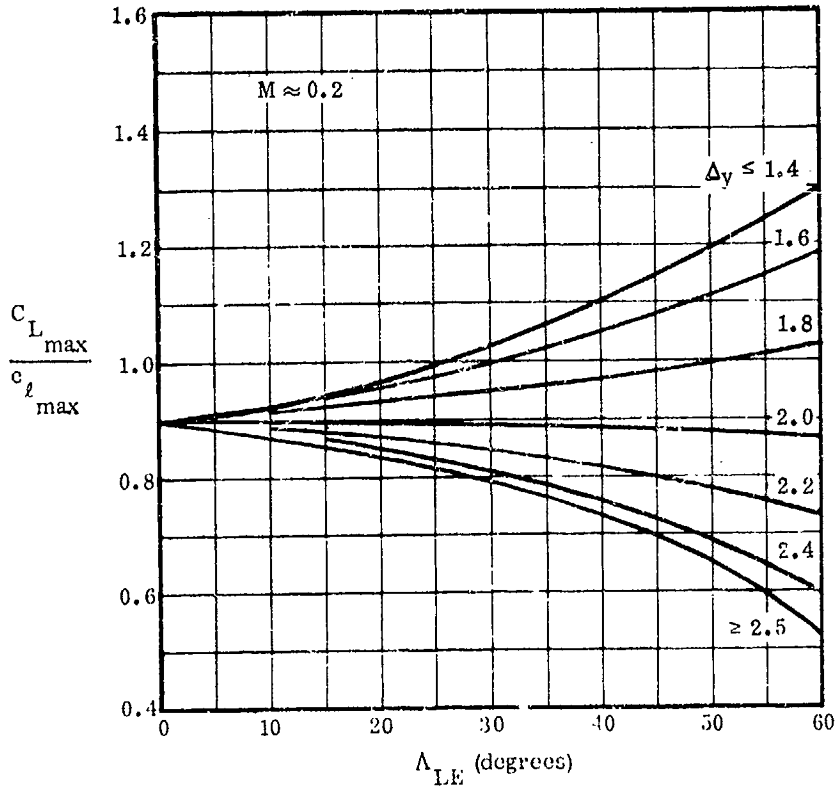

Figure 5-2. Subsonic Maximum Lift of High-Aspect-Ratio Wings

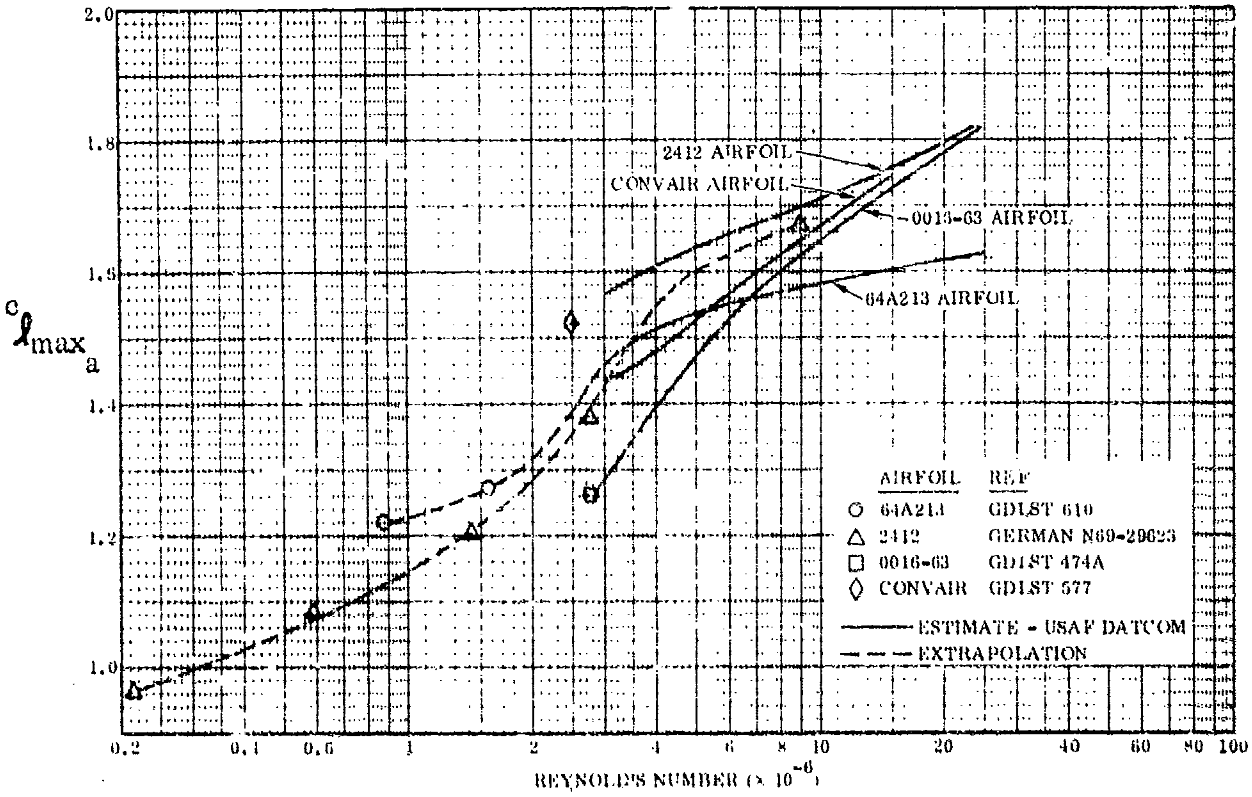

Figure 5-3. Effect of Reynolds Number on Two-Dimensional Maximum Lift Coefficient

5.2 MAXIMUM LIFT INCREMENT DUE TO LEADING-EDGE DEVICES

Leading-edge devices increase the maximum lift capability of airfoils by increasing static pressures (reducing suction) near the nose at a given angle of attack, thereby delaying leading-edge stall to higher angles of attack. This is accomplished without significantly affecting the trailing-edge flow conditions, and is most effective on thin airfoils.

The present method for estimating the lift coefficient increment, $\Delta C'_{L_{MAX_{LE}}}$, assumes that maximum lift on the airfoil without blowing is achieved when the static pressure near the leading edge of the leading-edge device approximates the static pressure near the leading edge of the basic airfoil just prior to stall. The method used for estimating the maximum lift increment for leading edge high lift devices is therefore based on Reference 4-4 and given by the following expression:

$$\Delta C'_{L_{MAX_{LE}}} = \left.\Delta c'_{\ell_{max}}\right)_{LE} \cdot K_{b_{LE}} \cdot \frac{\left.C'_{L_{\alpha}}\right)_o}{\left.c'_{\ell_{\alpha}}\right)_o} + \left.\Delta C'_{L_{MAX_{LE}}}\right)_{PWR} \qquad (5\text{-}3)$$

where:

$\left.\Delta c'_{\ell_{max}}\right)_{LE}$	is the two-dimensional increment in maximum lift coefficient from Equation 5-4.
$K_{b_{LE}}$	is the leading-edge partial-span factor shown in Figure 5-4.
$\left.C'_{L_{\alpha}}\right)_o$	is the three-dimensional lift curve slope defined in Paragraph 4.1.1.
$\left.c'_{\ell_{\alpha}}\right)_o$	is the two-dimensional lift curve slope defined in Paragraph 4.1.1.
$\left.\Delta C'_{L_{MAX_{LE}}}\right)_{PWR}$	is the increment in maximum lift coefficient due to leading-edge blowing shown in Figure 5-5.

The two-dimensional increment in maximum lift coefficient is based on thin airfoil theory as follows:

$$\Delta c'_{\ell_{\max}}\Big)_{LE} = c_{\ell_{\delta_{LE}}}\Big)_{\max} \cdot \delta_H\Big)_{EFF} \tag{5-4}$$

where, as presented in Figure 5-6 as a function of leading-edge high-lift device chord c_{LE}/c'

$$c_{\ell_{\delta_{LE}}}\Big)_{\max} = 2 \sin \Theta_{LE} \tag{5-5}$$

and

$$\cos \Theta_{LE} = (1 - 2\, c_{LE}/c') \tag{5-6}$$

$\delta_H\Big)_{EFF}$ is the effective deflection angle of the leading-edge device and is expressed in terms of the geometric leading-edge device deflection angle, δ_H, as defined in Section 2:

$$\delta_H\Big)_{EFF} = 0.75\, \eta_{\max} \cdot \eta_\delta \cdot \delta_H \tag{5-7}$$

where:

$\eta_{\max}$ and η_δ	are empirical factors introduced in Reference 4-4 to correlate Equation 5-4 with available test data on airfoils with trailing edge flaps (Figures 5-7 and 5-8).
0.75	is a factor introduced to furnish better correlation with the clean trailing-edge test data from Reference 3-11.

The maximum lift efficiency factor, $\eta_{\max}$, depends on the type of leading-edge device and on the ratio of the leading-edge radius to the maximum airfoil thickness; η_δ is an efficiency factor that accounts for large leading-edge flap deflections.

The term $C'_{L_{MAX,\ LE}}\big)_{pwr}$ accounts for the effect of blowing from a spanwise slot at the rear of a Krueger flap. The increments were obtained from test data on three wings with aspect ratios of 8.0 and sweeps of 12.5, 25 and 35 degrees and are presented in Figure 5-1 as a function of the jet momentum coefficient, $C'_{\mu_L}\big)_{noz}$, at the nozzle exit.

The method for estimating $\Delta C'_{L_{MAX_{LE}}}$ is compared with test data from Reference 3-11 in Figure 5-9. Test data is included for both slats and Krueger flaps. The data is correlated as a function of effective leading-edge deflection angle, $\delta_H\big)_{EFF}$ (as obtained from Equation 5-3 and 5-4) versus the geometric deflection angle, δ_H. The theoretical values are plotted in terms of the same parameters with $\delta_H\big)_{EFF}$ defined by Equation 5-7.

SAMPLE PROBLEM

GIVEN:

$\frac{LER}{t/c} = 0.098$

$\delta_H = 51$ deg

$\frac{c_{LE}}{c'} = 0.1266$

$\frac{b_{LE}}{b} = 0.905$

$C_{\mu_I} = 0.10$

CALCULATE:

1. Effective leading-edge deflection angle, using Equation 5-7, for EBF, IBF, and MF/VT.

$$\left.\delta_H\right)_{EFF} = 0.75\,\eta_{max} \cdot \eta_\delta \cdot \delta_H \tag{5-7}$$

$\eta_\delta = 0.55$ (Figure 5-8)

$\eta_{max} = 1.730$ (Figure 5-7)

$$\left.\delta_H\right)_{EFF} = (0.75)\,(1.730)\,(0.55)\left(\frac{51}{57.295}\right) = 0.635 \text{ rad}$$

2. The two-dimensional power-off increment in maximum lift due to the leading edge, using Equation 5-4 for EBF, IBF, and MF/VT.

$$\left.\Delta c'_{\ell_{max}}\right)_{LE} = \left.c_{\ell_{\delta_{LE}}}\right)_{max} \cdot \left.\delta_H\right)_{EFF} \tag{5-4}$$

$$\left.c_{\ell_{\delta_{LE}}}\right)_{max} = 1.34 \text{ from Figure 5-6.}$$

$$\left.\Delta c'_{\ell_{max}}\right)_{LE} = (1.34)\ (0.635)$$

$$= 0.851$$

3. The leading-edge device partial-span factor from Figure 5-4 for EBF, IBF, and MF/VT.

$$K_{b_{LE}} = 0.842$$

4. The increment in maximum lift due to leading-edge BLC blowing from Figure 5-5 for EBF, IBF, and MF/VT.

$$\left.\Delta C'_{L_{MAX_{LE}}}\right)_{PWR} = 0.60$$

5. The maximum lift increment due to leading-edge devices, using Equation 5-3, for EBF, IBF, and MF/VT.

$$\Delta C'_{L_{MAX_{LE}}} = \left.\Delta c'_{\ell_{max}}\right)_{LE} \cdot K_{b_{LE}} \cdot \frac{\left.C'_{L_\alpha}\right)_o}{\left.c'_{\ell_\alpha}\right)_o} + \left.\Delta C'_{L_{MAX_{LE}}}\right)_{PWR} \tag{5-3}$$

$$\frac{\left.C'_{L_\alpha}\right)_o}{\left.c_{\ell_\alpha}\right)_o} = 0.7519$$

From Section 4.2 sample problem. This ratio is based on the clean wing with LE device $\Lambda_{c/2}$ and A to be consistent with the buildup method of Equation 5-1 and is calculated using Equations 4-6 and 4-8.

$$\Delta C'_{L_{MAX_{LE}}} = (0.851)\ (0.842)\ (0.7519) + 0.600$$

$$= 0.539 + 0.600$$

$$= 1.139$$

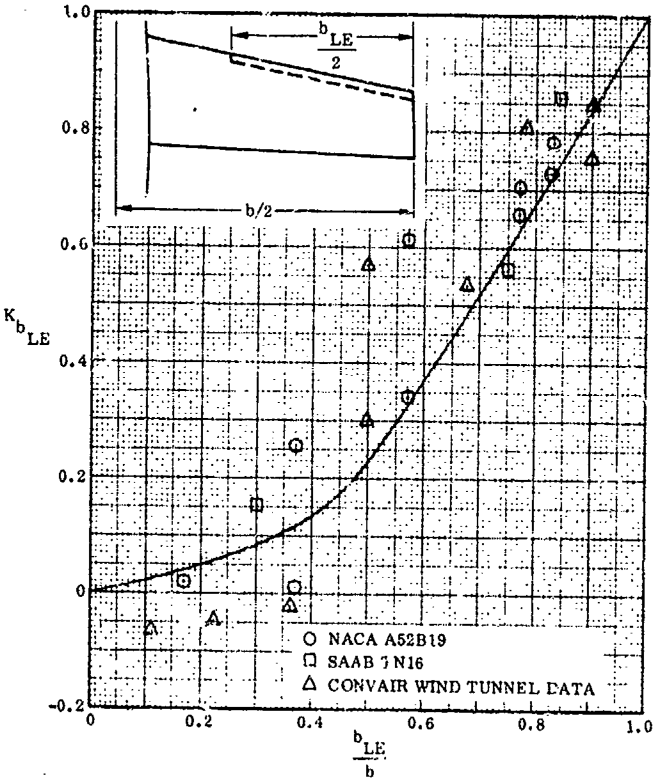

Figure 5-4. Leading-Edge Device Maximum Lift Span Factor

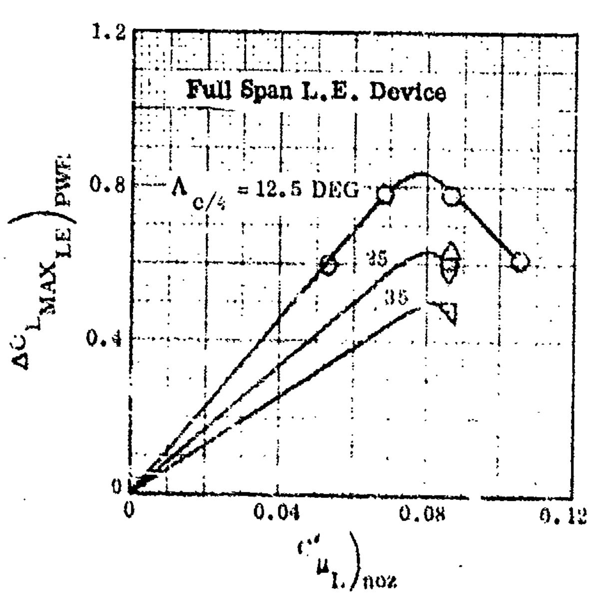

Figure 5-5. Incremental Maximum Lift Due to Leading-Edge Blowing

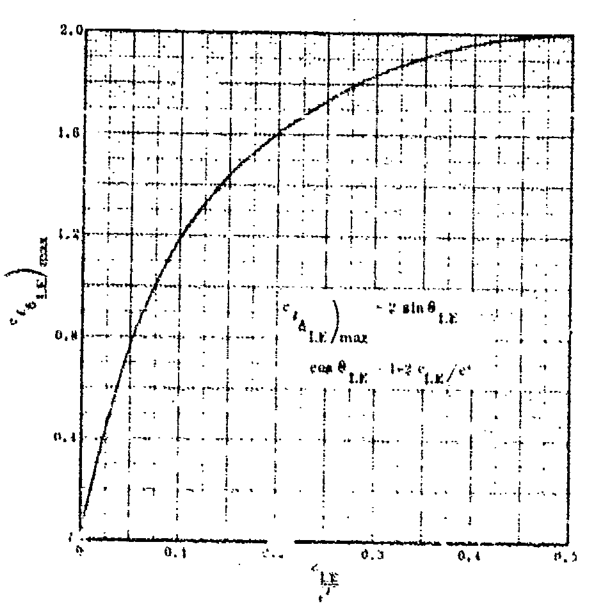

Figure 5-6. Leading Edge Flap Maximum Lift Effectiveness

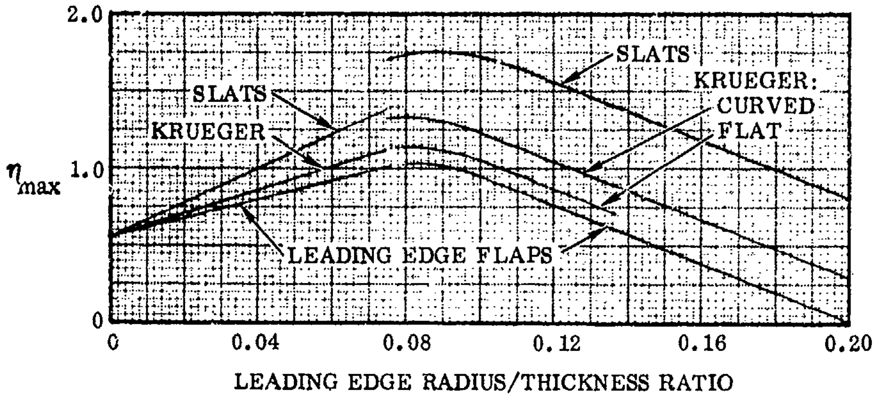

Figure 5-7. Maximum Lift Efficiency for Leading-Edge Devices

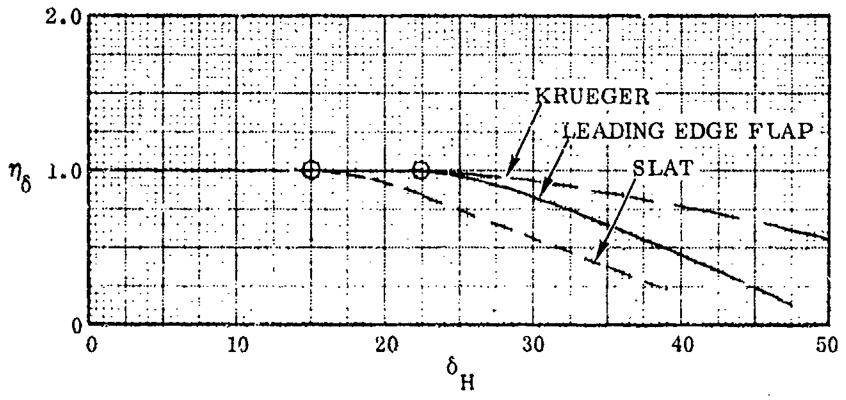

Figure 5-8. Leading Edge Device Deflection Angle Correction Factor

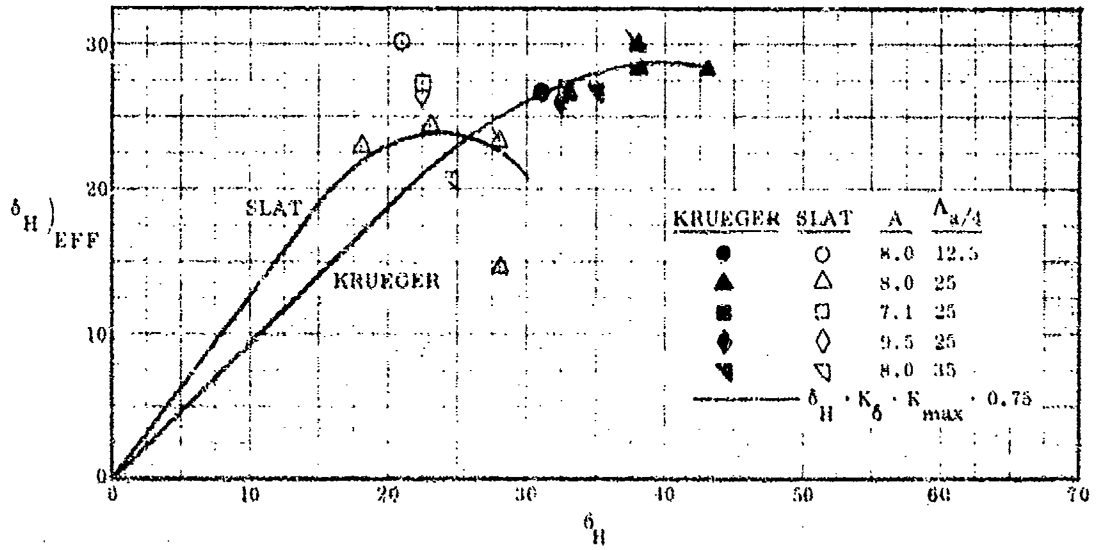

Figure 5-9. Correlation of Leading Edge Device Effective Deflection Angle

5.3 MAXIMUM LIFT INCREMENT DUE TO TRAILING-EDGE FLAPS

The increment in maximum lift coefficient due to a trailing-edge flap system is determined by summing increments due to flap deflection and due to blowing over the flap as follows.

$$\Delta C'_{L_{MAX_{TE}}} = \Delta C'_{L_{MAX_{TE}}}\Big)_o + \Delta C'_{L_{MAX_{TE}}}\Big)_{PWR} \qquad (5\text{-}8)$$

where

$\Delta C'_{L_{max_{TE}}}\Big)_o$ is the power-off maximum lift coefficient increment due to the deflection of the trailing-edge flap system.

$\Delta C'_{L_{max_{TE}}}\Big)_{PWR}$ is the maximum lift coefficient increment due to blowing on the trailing-edge flap system.

These two terms are discussed in the following paragraphs.

5.3.1 POWER-OFF MAXIMUM LIFT INCREMENT DUE TO TRAILING-EDGE FLAPS.

The method for estimating maximum lift increment for a flapped airfoil is based on Reference 4-4 and given by the following expression.

$$\Delta C'_{L_{MAX_{TE}}}\Big)_o = \Delta K_{b_o} \cdot \frac{C'_{L_\alpha}\Big)_o}{c'_{\ell_\alpha}\Big)_o} \cdot K_{MAX} \cdot \Delta c'_{\ell_{max_{TE}}}\Big)_o \qquad (5\text{-}9)$$

where:

ΔK_{b_o} is the flap span factor (Equation 4-31).

$C'_{L_\alpha}\Big)_o$ is the power-off three-dimensional lift curve slope based on extended wing area (Equation 4-5).

$c'_{\ell_\alpha}\Big)_o$ is the power-off two-dimensional lift curve slope based on extended chord (Equation 4-7).

K_{MAX} is a correlating constant based on the leading-edge configuration.

and:

K_{MAX} = 1.21 for a clean leading edge.

K_{MAX} = 1.00 for a slat or Krueger leading edge.

$\left.\Delta c'_{\ell_{max_{TE}}}\right)_o$ is the increment in the two-dimensional maximum lift coefficient, power-off (Equation 5-13 or 5-14).

Using thin airfoil theory and assuming that stall is sensitive only to the leading-edge loading, the increment in the two-dimensional maximum lift coefficient, $\left.\Delta c'_{\ell_{max_{TE}}}\right)_o$, is estimated by first obtaining the ratio $\Delta c_{\ell_{max}}/\Delta c_{\ell_{\alpha=0}}$ as:

$$\frac{\Delta c_{\ell_{max}}}{\Delta c_{\ell_{\alpha=0}}} = \frac{\sin \theta_f}{\theta_f + \sin \theta_f} \tag{5-10}$$

where:

$$\cos \theta_f = (1 - 2\, c'_f/c') \qquad \text{(Equation 4-16)}$$

Equation 5-10 is plotted in Figure 5-10. This expression assumes that separation occurs at the leading edge of the airfoil, but this is not always the case, especially on airfoils with large leading-edge radii or with highly efficient leading-edge devices. The thin airfoil theory was modified to account for an arbitrary separation point, x_S/c', and Equation 5-10 became:

$$\frac{\Delta c_{\ell_{max}}}{\Delta c_{\ell_{\alpha=0}}} = 1 - \frac{\theta_f}{\theta_f + \sin \theta_f} \left[1 + \frac{\ln \left| \sin \frac{1}{2}(X + \theta_f) / \sin \frac{1}{2}(X - \theta_f) \right|}{\theta_f \tan X/2} \right] \tag{5-11}$$

where:

$$\cos X = 2(x_S/c') - 1 \tag{5-12}$$

Equation 5-11 is plotted in Figure 5-10 at constant flow-separation values. Lift effectiveness at stall decreases as the flow-separation point on the airfoil moves aft (closer to the flap).

The two-dimensional maximum lift increment, $\left.c'_{\ell_{max_{TE}}}\right)_o$, due to flap deflection is obtained for a single-slotted flap by combining Equations 4-18 and 5-11. The resulting expression is:

$$\Delta c'_{\ell_{\max_{TE}}}\Big)_o = \eta_S \cdot c_{\ell_\delta} \cdot \delta_f \cdot \left(\frac{\Delta c_{\ell_{\max}}}{\Delta c_{\ell_{\alpha=0}}}\right) \tag{5-13}$$

Similarly, for double- and triple-slotted flaps, Equations 4-19 and 5-11 are combined to give:

$$\Delta c'_{\ell_{\max_{TE}}}\Big)_o = \sum_{i=1}^{I} \eta_{S_{I_i}} \cdot c_{\ell_{\delta_i}} \cdot \delta_{f_i} \left(\frac{\Delta c_{\ell_{\max}}}{\Delta c_{\ell_{\alpha=0}}}\right)_i \tag{5-14}$$

where:

I is 2 for double-slotted flaps and 3 for triple-slotted flaps.

The choice of the separation point, x_S/c', to determine maximum lift ratio from Figure 5-10, depends on the leading-edge configuration. For clean leading-edge airfoils, the point of flow separation is assumed at the leading edge, $x_S/c' = 0$. For airfoils with leading-edge high-lift devices, the point of flow separation is assumed to be at the knee of the leading-edge device, $x_S/c' = c_f/c'$.

The preceding method for estimating $\Delta C'_{L_{\max_{TE}}}\Big)_o$ is correlated with test data from Reference 3-11, and the results are shown in Figure 5-11 for several flap and leading-edge configurations and wing planforms. The correlation is generally good for those configurations with attached flow over the flaps up to the condition for leading-edge stall, as postulated in the method. At large flap deflection angles (especially for the plain and single-slotted flaps), however, the stall may also be influenced by flap separation, which is not accounted for in the method. This is shown in Figure 5-11b, where the single-slotted and plain flap test data shows large deviations from the theory at the high deflections, especially with a 15-percent-chord leading-edge Krueger (which delays leading-edge stall).

5.3.2 POWER-ON MAXIMUM LIFT INCREMENT DUE TO TRAILING-EDGE FLAPS. Maximum lift increment due to trailing-edge flap blowing is defined as:

$$\Delta C'_{L_{MAX_{TE}}}\Big)_{PWR} \quad C'_{L\,MAX} - C'_{L\,MAX_o} \tag{5-15}$$

where:

$C'_{L_{MAX}}$	is the power-on lift coefficient at the power-on stall angle of attack, α_s.
$C'_{L_{MAX_o}}$	is the power-off maximum lift coefficient from Equation 5-1

Thin airfoil theory concepts have been developed in References 5-1 and 5-2 to predict the maximum lift increment due to blowing with supercirculation for IBF and EBF systems, respectively. These methods are similar to the procedure discussed in Section 5.3.1 for calculating the increment in maximum lift coefficient due to mechanical flaps in that they assume that stall occurs at the leading edge and at a pressure loading that is independent of the jet momentum coefficient. The mechanical flap and power-on methods are also similar in that they are basically two-dimensional methods, with finite aspect ratio corrections being made by reducing the predicted maximum lift increments by the ratio of the two-dimensional to three-dimensional lift curve slopes. The basic difference between the mechanical flap procedure and the power-on methods of References 5-1 and 5-2 is that pressure loading in the leading-edge region is assumed to be that described by the Spence two-dimensional thin jet theory (Reference 3-18) in the blowing case. An empirical factor equal to 1.8 has been introduced into the EBF method of Reference 5-2 to obtain improved agreement with EBF test data.

The methods of References 5-1 and 5-2, without introduction of empirical factors, predict that the change in maximum lift coefficient $\left.\Delta C'_{L_{max_{TE}}}\right)^*_{pwr}$ due to power equals three-fourths of the change in lift coefficient $\left.\Delta C'_{L_{TE}}\right)_{pwr}$ due to power at the power-on stall angle of attack, α_s. As is shown in Figure 5-1, the increment $\left.\Delta C'_{L_{max_{TE}}}\right)^*_{pwr}$ is to be based on a calculated power-off datum with the same degree of BLC effectiveness (or equivalently of flap separation) as assumed for the power-on calculations. The stall angle of attack for the power-off datum has been designated $\alpha_{s_o}^*$ in Figure 5-1. Figure 5-1 shows that the relationship between $\left.\Delta C'_{L_{max_{TE}}}\right)^*_{pwr}$ and $\left.\Delta C'_{L_{TE}}\right)_{pwr}$ implies that the power-on stall angle of attack, α_s, must decrease with increasing blowing coefficient, a result that is contrary to test results to be discussed in connection with Figure 5-12. To obtain improved agreement with power-on stall data, the methods of References 5-1 and 5-2 have been modified by introducing finite aspect ratio corrections directly into the pressure distribution at the leading edge. Using idealized lifting-line expressions for the induced downwash angle gives the change in maximum lift coefficient due to power as:

$$\Delta C'_{L_{max_{TE}}}\Big)^*_{pwr} = \frac{3}{4}\left[\Delta C'_{L_{TE}}\Big)_{pwr} + 2\pi\Delta\alpha_{i_{pwr}}\right]_{\alpha = \alpha_s} \tag{5-16}$$

where:

$\Delta\alpha_{i_{pwr}}$ is the change in induced angle of attack (downwash angle) due to power and is to be evaluated at the power-on stall angle of attack and with the flaps extended. Equation 5-16 is independent of the form for determining $\Delta\alpha i_{pwr}$.

Equation 5-16 reduces to the result of References 5-1 and 5-2 for the high-aspect-ratio limit in which $\Delta\alpha_{i_{pwr}}$ vanishes.

For the current methodology, Equation 5-16 is expressed in terms of the change in stall angle of attack due to power $(\Delta\alpha_s = \alpha_s - \alpha^*_{s_o})$ rather than in terms of the change in maximum lift coefficient. The expressions for power-off and power-on lift (based on Equations 4-1 and 4-10) and the lifting-line equation for $\Delta\alpha_{i_{pwr}}$ are used and the result is:

$$\Delta\alpha_s = \frac{\sin\left(\alpha^*_{s_o} - \alpha^*_{o_{L_o}}\right) - K_{PWR}\sin\left(\alpha^*_{s_o} - \alpha_{o_{L_{PWR}}}\right)}{K_{PWR}\cos\left(\alpha^*_{s_o} - \alpha_{o_{L_{PWR}}}\right) - \frac{\omega}{\omega - 1}\cos\left(\alpha^*_{s_o} - \alpha^*_{o_{L_o}}\right)} \tag{5-17}$$

where:

$\alpha^*_{s_o}$ is the power-off angle of attack at maximum lift (Equations 4-1 and 5-1).

$\alpha^*_{o_{L_o}}$ is the power-off angle of zero lift (Equation 4-2).

$\alpha_{0_{L_{pwr}}}$ is the power-on angle of zero lift (Equation 4-2).

$$\omega = \frac{3}{4}\frac{c'_{\ell_\alpha}}{C'_{L_\alpha}} \qquad (5\text{-}18)$$

All the other terms were defined previously. The superscript (*) denotes that this power-off term is derived using the same BLC effect as assumed for power-on conditions.

In the infinite aspect ratio limit for which $\omega = 3/4$, Equation 5-18 predicts that the stall angle of attack decreases with increasing momentum coefficient. However, for $\omega = 1$, Equation 5-17 predicts that the stall angle of attack should be independent of momentum coefficient. For values of ω exceeding 1, Equation 5-17 predicts that the stall angle of attack will increase with momentum coefficient. Wind tunnel test data for STOL transport-type configurations in Reference 3-11 shows the parameter ω to vary between 1.09 and 1.22; hence, the power-on stall angle of attack should increase with power.

Equation 5-17 has been compared with IBF and EBF test data from Reference 3-11 in Figure 5-12, and appears to predict the observed variation in stall angle of attack reasonably well, except at the lower momentum coefficient values for which partial BLC effects may influence the test data.

In terms of $\Delta\alpha_s$, the power-on stall angle of attack is given by:

$$\alpha_s = \alpha_{s_0}^{*} + \Delta\alpha_s \qquad (5\text{-}19)$$

and the maximum lift coefficient (power-on) is simply the value of lift coefficient obtained from Equation 4-1 for an angle of attack equal to α_s.

SAMPLE PROBLEM

GIVEN:

$\delta_{f_1} = 28.4$ deg

$\delta_{f_2} = 16.4$ deg

$\delta_{f_3} = 15.0$ deg

$c_{f_1}/c' = 0.439$

$c_{f_2}/c' = 0.269$

$c_{f_3}/c' = 0.1326$

$x_S/c \;\; = 0.10$

CALCULATE:

1. The increment in two-dimensional maximum lift due to the trailing-edge flaps, using Equation 5-13.

$$\left.\Delta c'_{\ell_{\max_{TE}}}\right)_o = \sum_{i=1}^{I} r_{S_{I_i}} \cdot c_{\ell_{\delta_i}} \cdot \delta_{f_i} \left(\frac{\Delta c_{\ell_{\max}}}{\Delta c_{\ell_{\alpha=0}}}\right)_i \tag{5-13}$$

A. EBF and IBF

$$\left.\begin{aligned} c_{\ell_{\delta_1}} &= 4.87 \\ c_{\ell_{\delta_2}} &= 3.94 \\ c_{\ell_{\delta_3}} &= 2.84 \end{aligned}\right\} \text{From Figure 4-6.}$$

$$\left.\frac{\Delta c_{\ell_{\max}}}{\Delta c_{\ell_{\alpha=0}}}\right)_1 = 0.321$$

$$\left.\frac{\Delta c_{\ell_{\max}}}{\Delta c_{\ell_{\alpha=0}}}\right)_2 = 0.378 \quad \Bigg\} \text{ From Figure 5-10.}$$

$$\left.\frac{\Delta c_{\ell_{\max}}}{\Delta c_{\ell_{\alpha=0}}}\right)_3 = 0.415$$

$$\eta_{s_1} = 1.00$$

$$\eta_{s_2} = 1.00 \quad \Bigg\} \text{ Full BLC effect assumed.}$$

$$\eta_{s_3} = 1.00$$

$$\left.\Delta c'_{\ell_{\max_{TE}}}\right)_o = (4.87)(0.321)\left(\frac{28.4}{57.295}\right) + (3.94)(0.378)\left(\frac{16.4}{57.295}\right) + (2.84)(0.415)\left(\frac{15}{57.295}\right)$$

$$= 0.775 + 0.426 + 0.309$$

$$= 1.510$$

B. MF/VT

$$c_{\ell_{\delta_1}} = 4.87$$

$$c_{\ell_{\delta_2}} = 3.94 \quad \Bigg\} \text{ From Figure 4-6.}$$

$$c_{\ell_{\delta_3}} = 2.84$$

$$\left.\frac{\Delta c_{\ell_{max}}}{\Delta c_{\ell_{\alpha=0}}}\right)_1 = 0.321$$

$$\left.\frac{\Delta c_{\ell_{max}}}{\Delta c_{\ell_{\alpha=0}}}\right)_2 = 0.378$$

$$\left.\frac{\Delta c_{\ell_{max}}}{\Delta c_{\alpha=0}}\right)_3 = 0.415$$

From Figure 5-10.

$$\eta_{s_1} = 0.770$$

$$\eta_{s_2} = 0.770$$

$$\eta_{s_3} = 0.608$$

From Figure 4-10.

$$\left.\Delta c'_{\ell_{max_{TE}}}\right)_o = (4.87)\,(0.770)\,(0.321)\left(\frac{28.4}{57.295}\right) + (3.94)\,(0.77)\,(0.378)\left(\frac{16.4}{57.295}\right)$$

$$+ (2.84)\,(0.608)\,(\,0.415)\left(\frac{15}{57.295}\right)$$

$$= 0.597 + 0.328 + 0.188$$

$$= 1.113$$

3. The three-dimensional increment in maximum lift due to trailing edge, using Equation 5-9.

$$\left.\Delta C'_{L_{MAX_{TE}}}\right)_o = \Delta K_{b_o} \cdot \frac{\left.C'_{L_\alpha}\right)_o}{\left.c'_{\ell_\alpha}\right)_o} \cdot K_{MAX} \cdot \left.\Delta c'_{\ell_{max_{TE}}}\right)_o \qquad (5\text{-}9)$$

A. EBF and IBF

$$K_{MAX} = 1.00$$

ΔK_{b_o} = 0.858 From sample problem in Section 4.2.

$\dfrac{\left.C'_{L_\alpha}\right)_o}{\left.c'_{\ell_\alpha}\right)_o}$ = 0.6141 From sample problem in Section 4.2.

$$\left.\Delta C'_{L_{MAX}}\right)_o = (0.858)\,(0.6141)\,(1.00)\,(1.510)$$

$$= 0.796$$

B. MF/VT

$K_{MAX} = 1.00$

ΔK_{b_o} = 0.858 From sample problem in Section 4.2.

$\dfrac{\left.C'_{L_\alpha}\right)_o}{\left.c'_{\ell_\alpha}\right)_o}$ = 0.680 From sample problem in Section 4.2.

$$\Delta C'_{L_{MAX}} = (0.858)\,(0.680)\,(1.00)\,(1.113)$$

$$= 0.649$$

4. The power off maximum lift, using Equation 5-1.

$$C_{L_{MAX}} = \frac{S'}{S}\left[C_{L_{MAX_o}} + \Delta C'_{L_{MAX_{LE}}} + \Delta C'_{L_{MAX_{TE}}}\right] \qquad (5\text{-}1)$$

A. EBF and IBF

$C_{L_{MAX_o}}$ = 1.068 From sample problem in Section 5.1.

$\Delta C'_{L_{MAX_{LE}}}$ = 1.139 From sample problem in Section 5.2.

$$C_{L_{MAX}} = (1.609)\big((1.068) + (1.139) + (0.796)\big)$$

$$= (1.609)\,(3.003)$$

$$= 4.832$$

B. MF/VT

$C_{L_{MAX_o}} = 1.068$ From sample problem in Section 5.1.

$\Delta C'_{L_{MAX_{LE}}} = 1.139$ From sample problem in Section 5.2.

$$C_{L_{MAX}} = (1.609)\left[1.068 + 1.139 + 0.649\right]$$

$$= (1.609)\,(2.856)$$

$$= 4.595$$

5. The power-off lift at zero angle of attack, by eliminating the power effect terms from Equations 4-1 and 4-13. Equation 4-13 reduces to

$$\Delta C'_{L_{wing}} = \left.\frac{C_{\ell_\alpha}}{c_{\ell_\alpha}}\right)_{on} \left[\Delta c'_{\ell_o} \cdot K_{b_o}\right]$$

A. EBF and IBF

$\left.\frac{C'_{L_\alpha}}{c'_{\ell_\alpha}}\right)_{on} = 0.6141$ From sample problem in Section 4.2.

$K_{b_o} = 0.858$ From sample problem in Section 4.2.

$\Delta c'_{\ell_o} = 4.470$ From sample problem in Section 4.2.

$$\Delta C'_{L_{WING}} = (0.6141)\,(4.470)\,(0.858)$$

$$= 2.355$$

B. MF/VT

$\left.\frac{C'_{L_\alpha}}{c_{\ell_\alpha}}\right)_{on}$ = 0.680 From sample problem in Section 4.2.

K_{b_o} = 0.858 From sample problem in Section 4.2.

$\Delta c'_{\ell_o}$ = 3.364 From sample problem in Section 4.2.

$$\Delta C'_{L_{WING}} = (0.680)(3.364)(0.858)$$

$$= 1.963$$

6. Equation 4-3 reduces to

$$-\alpha_{o_L} = \sin^{-1}\left[\Delta C_{L_{WING}} \Big/ \left(C'_{L_{\alpha_o}} \cdot K_{PWR}\right)\right]$$

A. EBF and IBF

$C'_{L_{\alpha_o}}$ = 4.473 From sample problem in Section 4.1.

K_{PWR} = 1.00 Power-off conditions

$$-\alpha_{o_L} = \sin^{-1}\left[2.355/4.473\right]$$

$$= 31.76 \text{ deg}$$

B. MF/VT

$C'_{L_{\alpha_o}}$ = 3.715 From sample problem in Section 4.1.

K_{PWR} = 1.00 From sample problem in Section 4.1.

$$-\alpha_{o_L} = \sin^{-1}\left[1.963/3.715\right]$$

$$= 31.89 \text{ deg}$$

7. The angle of attack for stall, power off, using Equation 4.1 without the power effect terms.

$$C_L = \frac{S'}{S}\left[\left(C'_{L_\alpha}\right)_o \cdot K_{PWR} \cdot \sin\left(\alpha - \alpha_{o_L} - \Delta\alpha_t\right) \right]$$

A. EBF and IBF

$\Delta\alpha_t = 1.74$ deg From sample problem in Section 4.4.

$$C_L = (1.609)\,(4.473)\,(1.0)\,\sin\,(\alpha + 31.76 - 1.74)$$

$$C_L = 7.197\,\sin\,(\alpha + 30.02) = 4.832$$

$$\alpha = \sin^{-1}\left(\frac{4.832}{7.197}\right) - 30.02 \text{ deg}$$

$$\alpha = 12.15 \text{ deg} = \alpha^*_{s_o}$$

B. MF/VT

$\Delta\alpha_t = 1.74$ deg From sample problem in Section 4.4.

$$C_L = (1.609)\,(3.715)\,(1.0)\,\sin\,(\alpha + 31.89 - 1.74)$$

$$C_L = 5.977\,\sin\,(\alpha + 30.15) = 4.595$$

$$\alpha = \sin^{-1}\left(\frac{4.595}{5.977}\right) - 30.15 = 20.08 \text{ deg} = \alpha^*_{s_o}$$

8. Calculate the term ω by Equation 5-18.

$$\omega = \frac{3}{4}\,\frac{c'_{\ell_\alpha}}{C'_{L_\alpha}} \qquad (5\text{-}18)$$

A. EBF and IBF

$$\omega = \frac{3}{4}\left(\frac{7.284}{4.473}\right)$$

$$= 1.221$$

B. MF/VT

$$\omega = \left(\frac{3}{4}\right)\left(\frac{5.4626}{3.715}\right)$$

$$= 1.103$$

9. Calculate the increase in stall angle of attack due to power effects, using Equation 5-17.

$$\Delta\alpha_s = \frac{\sin\left(\alpha^*_{s_o} - \alpha^*_{o_{L_o}}\right) - K_{PWR}\sin\left(\alpha^*_{s_o} - \alpha_{o_{L_{PWR}}}\right)}{K_{PWR}\cos\left(\alpha^*_{s_o} - \alpha_{o_{L_{PWR}}}\right) - \frac{\omega}{\omega - 1}\cos\left(\alpha^*_{s_o} - \alpha^*_{o_{L_o}}\right)} \tag{5-17}$$

A. EBF

K_{PWR} = 1.1969 From sample problem in Section 4.1.

$\alpha^*_{s_o}$ = 12.15 deg

$\alpha^*_{o_{L_o}}$ = -31.76 deg

$\alpha_{o_{L_{PWR}}}$ = -35.21 deg From sample problem in Section 4.4.

$$\Delta\alpha_s = \frac{\sin(12.15 + 31.76) - (1.1969)\sin(12.15 + 35.21)}{(1.1969)\cos(12.15 + 35.21) - \left[\frac{1.221}{1.221-1}\right]\cos(12.15 + 31.76)}$$

$$= \frac{\sin(43.91) - (1.1969)\sin(47.36)}{(1.1969)\cos(47.36) - (5.525)\cos(43.91)}$$

$$= \left(\frac{-0.1869}{-3.1695}\right)$$

$$= 0.0590 \text{ rad} = 3.38 \text{ deg}$$

B. IBF

K_{PWR} = 1.2234 From sample problem in Section 4.1.

$\alpha^*_{s_o}$ = 12.15 deg

$\alpha^*_{o_{L_o}}$ = -31.76 deg

$\alpha^*_{o_{L_{PWR}}}$ = 42.41 deg From sample problem in Section 4.4.

$$\Delta\alpha_s = \frac{\sin(12.15 + 31.76) - (1.2234)\sin(12.15 + 42.41)}{(1.2234)\cos(12.15 + 42.41) - \left[\frac{1.221}{1.221-1}\right]\cos(12.15 + 31.76)}$$

$$= \frac{\sin(43.91) - (1.2234)\sin(54.56)}{(1.2234)\cos(54.56) - 5.525)\cos(43.91)}$$

$$= \left(\frac{-0.3032}{-3.2710}\right)$$

$$= 0.0927 \text{ rad} = 5.31 \text{ deg}$$

C. MF/VT

K_{PWR} = 1.000 From sample problem in Section 4.1.

$\alpha^*_{s_o}$ = 20.08 deg

$\alpha^*_{o_{L_o}}$ = -31.89 deg

$\alpha^*_{o_{L_{PWR}}}$ = -31.89 deg From sample problem in Section 4.4. =

$$\Delta\alpha_s = \frac{\sin(20.08 + 31.89) - (1.00)\sin(20.08 + 31.89)}{(1.00)\cos(20.08 + 31.89) - \left[\frac{1.103}{1.103-1}\right]\cos(20.08 + 31.89)}$$

$$= 0.0 \text{ deg}$$

9. Calculate the power-on stall angle of attack using Equation 5-19.

$$\alpha_s = \alpha^*_{s_0} + \Delta\alpha_s \tag{5-19}$$

A. EBF

$\alpha_s = 12.15 + 3.38$

$= 15.53$ deg

B. IBF

$\alpha_s = 12.15 + 5.31$

$= 17.46$ deg

C. MF/VT

$\alpha_s = 20.08 + 0.0$

$= 20.08$ deg

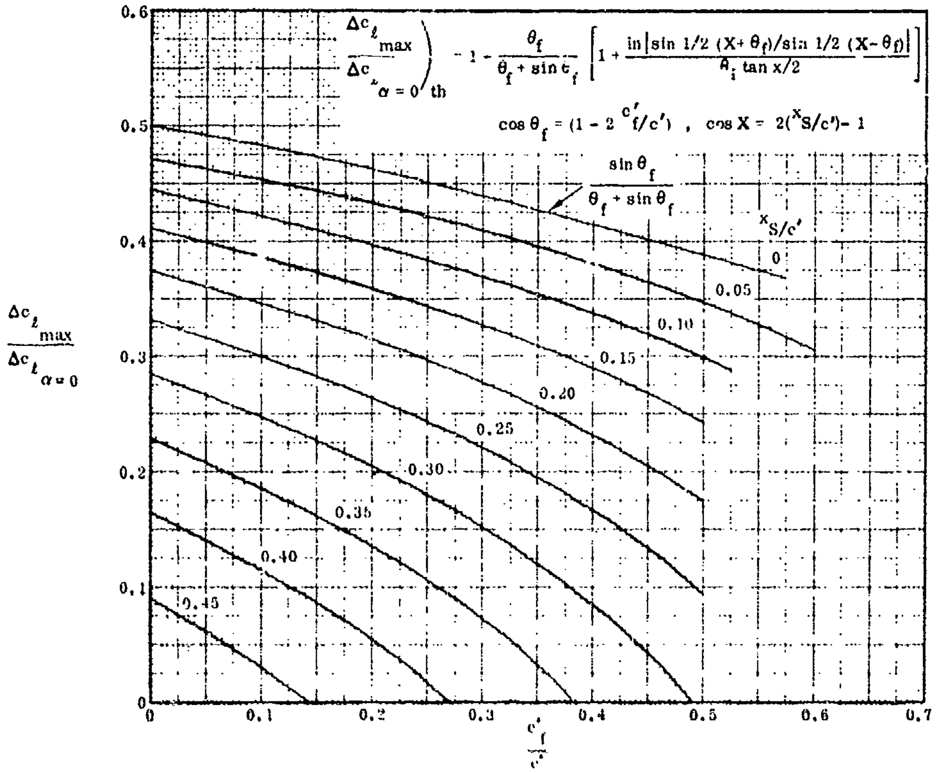

Figure 5-10. Increment in Maximum Lift Coefficient for Trailing-Edge Flaps

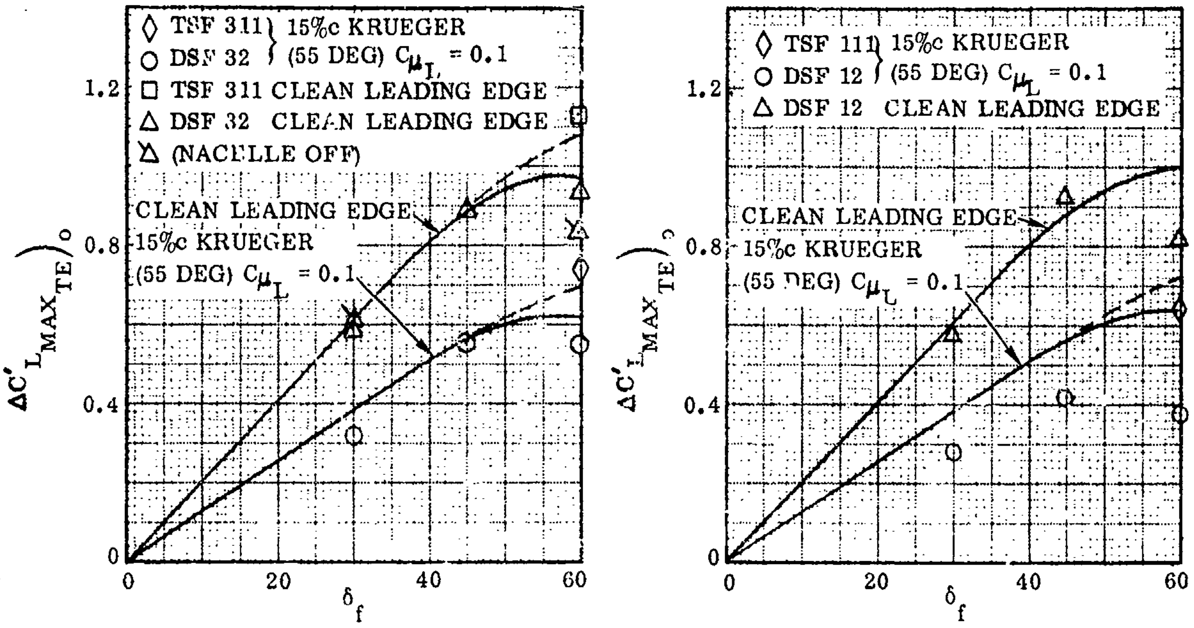

a. Double- and Triple-Slotted Trailing Edge Flaps with Wing Sweep = 25 Degrees, A = 8

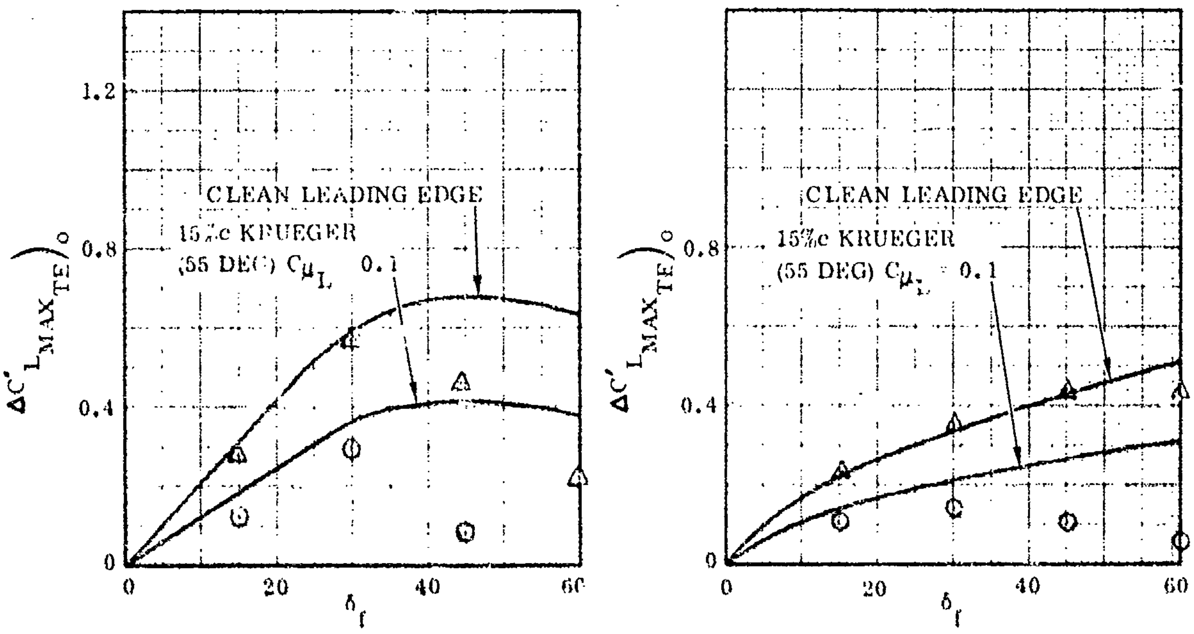

b. Single-Slotted (No. 2) and Plain Trailing Edge Flap with Wing Sweep = 25 Degrees, A = 8

Figure 5-11. Correlation of Methodology With Maximum Lift Increment Due to Flap Deflection

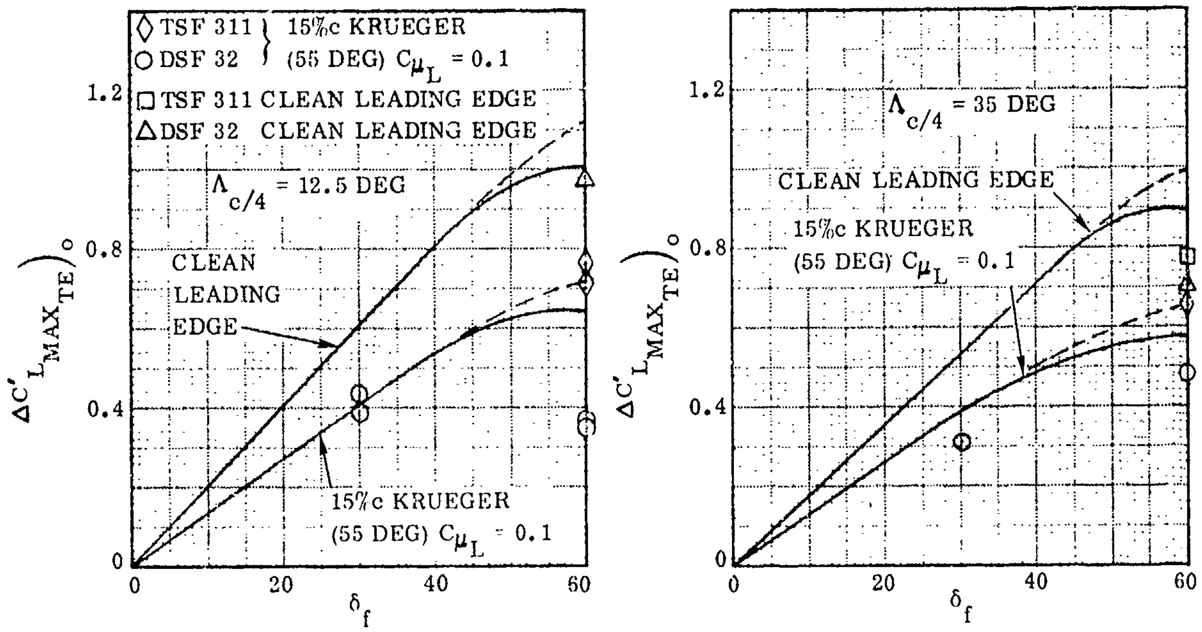

c. Double- and Triple-Slotted Trailing Edge Flap with Wing Sweep - 12.5 and 35 Degrees, A - 8

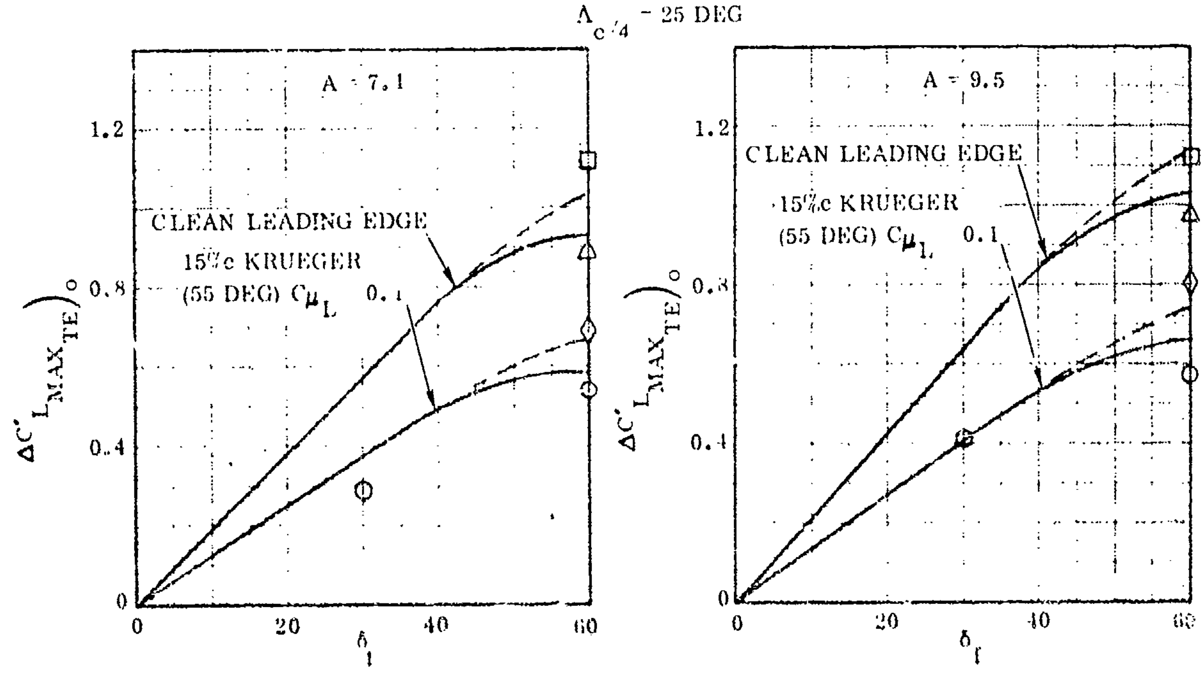

d. Double- and Triple-Slotted Trailing Edge Flap with Wing Sweep 25 Degrees, AR 7.1 and 9.5

Figure 5-11. Correlation of Methodology With Maximum Lift Increment Due to Flap Deflection, Contd

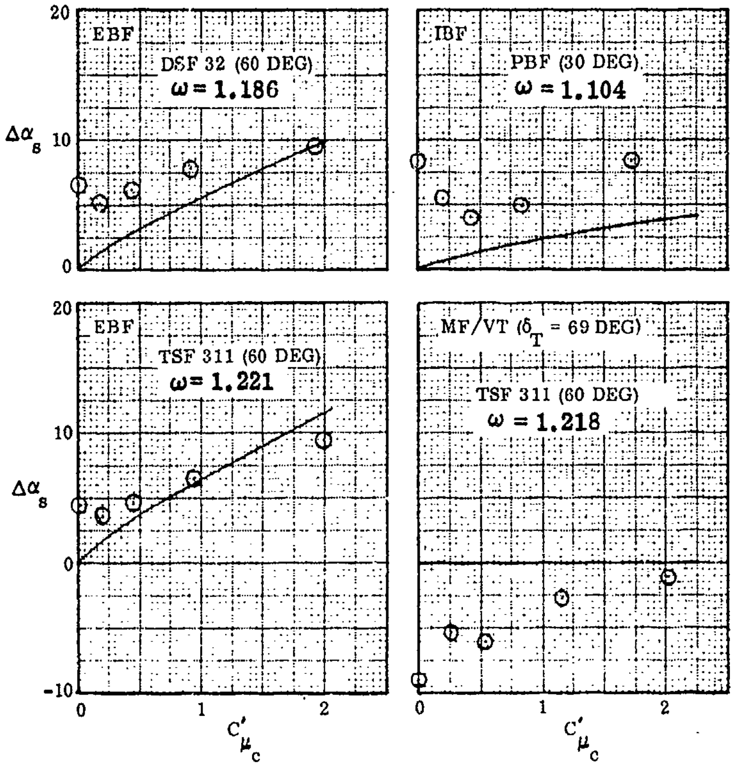

Figure 5-12. Increment in Stall Angle of Attack Due to Power Wing Aspect Ratio = 8.0, Quarter Chord Sweep = 25 deg.

5.4 MAXIMUM LIFT CORRELATION

The sample problem and correlations are for the wings described in Section 4.4.

SAMPLE PROBLEM

GIVEN:

$\alpha = \alpha_{STALL}$

CALCULATE:

1. The power-on maximum lift, using Equation 4-1 at the stall angle of attack.

$$C_L = \frac{S'}{S}\left[\left.C'_{L_\alpha}\right)_o \cdot K_{PWR} \cdot \sin\left(\alpha - \alpha_{o_L} - \Delta\alpha_t\right) + \Delta C'_\mu \sin\left(\alpha + \delta_T\right)\right] \qquad (4\text{-}1)$$

A. EBF

$\Delta\alpha_t = 1.74$ deg from sample problem in Section 4.4.

$\Delta c'_\mu = 0.038$ from sample problem in Section 4.3.

$\left.C'_{L_\alpha}\right)_o = 4.473$ from sample problem in Section 4.1.

$\alpha_{o_L} = 35.21$ deg from sample problem in Section 4.4.

$\alpha = \alpha_s = 15.53$ deg from sample problem in Section 5.3.

$\delta_T = 3.5$ deg

$K_{PWR} = 1.1969$ from sample problem in Section 4.1.

$$C_L = (1.609)\Big[(4.473)(1.1969)\sin(15.53 + 35.21 - 1.74)$$

$$+ (0.038)\sin(15.53 - 3.5)\Big]$$

$$= (1.609)\Big[(4.473)(1.1969)\sin(49.) + (0.038)\sin(12.03)\Big]$$

$$= (1.609)(4.041 + 0.008)$$

$$= 6.515$$

B. IBF

$\Delta\alpha_t$ = 1.74 deg from sample problem in Section 4.4

$\Delta C'_\mu$ = 0.0 from sample problem in Section 4.3.

C'_{L_α} = 4.473 from sample problem in Section 4.1.

α_{o_L} = -42.41 deg from sample problem in Section 4.4.

$\alpha = \alpha_s$ = 17.46 deg from sample problem in Section 5.3.

K_{PWR} = 1.2234 from sample problem in Section 4.1.

δ_T = -3.5 deg.

$$C_L = (1.609)\,[(4.473)(1.2234)\sin(17.46 + 42.41 - 1.74)$$
$$+ (0.0)\sin(17.46 - 3.5)]$$
$$= (1.609)\,[(4.473)(1.2234)\sin(58.13)]$$
$$= (1.609)(4.6473)$$
$$= 7.478$$

C. MF/VT

$\Delta\alpha_t$ = 1.74 deg from sample problem in Section 4.4.

$\Delta C'_\mu$ = 0.621 from sample problem in Section 4.3.

α_{o_L} = -31.89 deg from sample problem in Section 4.4.

$\alpha = \alpha_s$ = 20.08 deg from sample problem in Section 5.3.

K_{PWR} = 1.0 from sample problem in Section 4.1.

δ_T = 69 deg

C'_{L_α} = 3.715 from sample problem in Section 4.1.

$$
\begin{aligned}
C_L &= (1.609)\Big[(3.715)\,(1.00)\,\sin\,(20.08 + 31.89 - 1.74) \\
&\quad + (0.621)\,\sin\,(20.08 + 69)\Big] \\
&= (1.609)\Big[(3.715)\,\sin\,(50.23) + (0.621)\,\sin\,(89.08)\Big] \\
&= (1.609)\,(2.8554 + 0.621) \\
&= 5.594
\end{aligned}
$$

CORRELATIONS

The EBF calculations for the Aspect Ratio 8, 25 degree swept wing with a triple-slotted flap ($\delta_f = 60$ deg) are compared with test results in Figures 5-13 through 5-15. Figure 5-13, which is with the engines in the high position (Position A) for which the capture ratio is 0.935, shows good agreement with the test data (power-on) except at $C_{\mu_J} = 4$ when the methodology overpredicts.

Figure 5-14 depicts a similar comparison but with the engines lowered to Position E, for which the capture ratio has been reduced to 0.579. In this case, the jet efflux no longer passes through the first flap slot, and all computations are based on the same degree of flow separation as for the power-off case. Good agreement is shown for maximum lift coefficient at all C_μ values except $C_{\mu_J} = 4$, where the methodology also overpredicts $C_{L_{MAX}}$.

Figure 5-15 compares the methodology and test results when the engines in Position E are tilted upward by 15 degrees so that the capture ratio is increased from 0.579 to 0.997.

Comparisons for double-slotted EBF systems of 30- and 60-degree deflections are shown in Figures 5-16 and 5-17, respectively. The engines are in Position A (high), for which the jets pass through the first flap slot. Data for the flaps at 30 degrees (Figure 5-16) agrees well with the computations except for the maximum lift value at $C_{\mu_J} = 4$, which is underpredicted by the methodology for this condition.

Figure 5-17 indicates predicted values of maximum lift coefficient somewhat larger than those shown by the test results at all C_μ values, possibly due to flow separation on the flap, which affects the leading-edge stall assumptions in the methodology. A similar effect is shown in Figures 5-19 and 5-23, which are also for flaps with 60-degree deflection.

Figures 5-18 and 5-19 compare the methodology with test data for low-capture-ratio single-slotted flaps of 30 and 60 degrees of deflection, respectively. Although the jets are still in the high position, zero BLC effectiveness was assumed for power-on, because the jet efflux failed to pass through the single flap slot. The predicted values at 60 degrees deflection of $C_{L_{MAX}}$ consistently exceed the test values in Figure 5-19, possibly because separation over the flaps modifies the basic assumption of leading-edge stall in the $C_{L_{MAX}}$ methodology.

Figures 5-20 through 5-23 present correlations between methodology and test data for IBF systems with plain flaps of 15, 30, 45 and 60 degrees of deflection, respectively. The methodology overpredicts $C_{L_{MAX}}$ for the power-off case, possibly due to flap separation effects as mentioned previously in connection with Figures 5-17 and 5-19. On the other hand, the method underpredicts $C_{L_{MAX}}$ at the higher jet momentum coefficients. The latter discrepancy may be due to the delay of stall to higher angles of attack than predicted in the methodology, because of the reattachment of the separated leading-edge flow near the jet slot. This type of flow, with a trapped separation bubble at high angles of attack and high flap deflection angles, has been observed with an internally blown flap in Reference 3-19.

Figures 5-24 and 5-25 compare methodology and test data for MF/VT configurations with the jets in a low and rearward position (Position F). The comparison in Figure 5-24 is for a double-slotted flap with 30 degrees of deflection and with an effective thrust vectoring angle of 37 degrees. The comparisons in Figure 5-25 are for a triple-slotted flap with 60 degrees of deflection and with an effective thrust vectoring angle of 69 degrees.

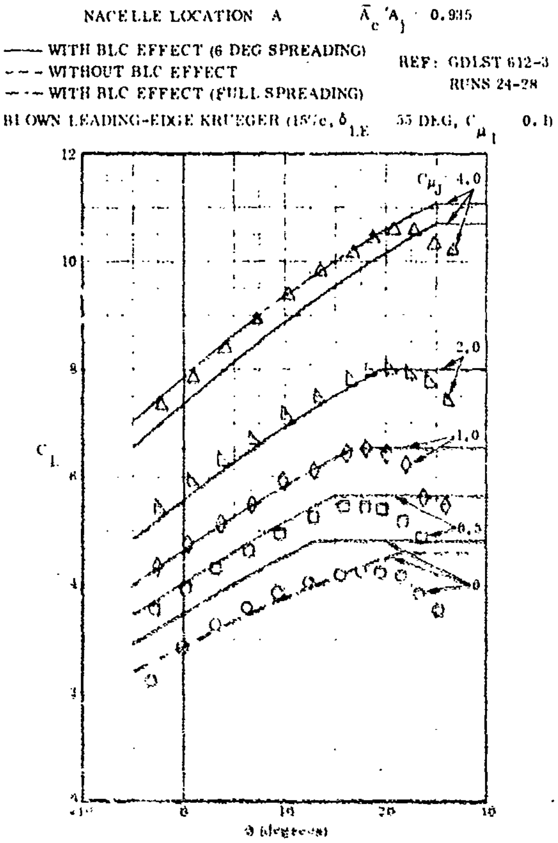

Figure 5-13. Correlation of Maximum Lift Generalized Methodology with EBF Test Data, A = 8, $\Lambda_{c/4}$ = 25 Degrees, Triple-Slotted Flap (δ_f = 30 Degrees), Nacelles High

Maximum lift correlations between the predictions and test data for two additional aspect ratios (7.1 and 9.5) with wing sweep at 25 degrees are shown in Figures 5-26 and 5-27. Good correlation with maximum lift is obtained on this triple-slotted flap data.

Maximum lift correlations between predictions and test data for wing sweeps of 12.5 and 25 degrees with aspect ratio at 8 are shown in Figures 5-28 and 5-29. The theory tends to overpredict the maximum lift for these configurations.

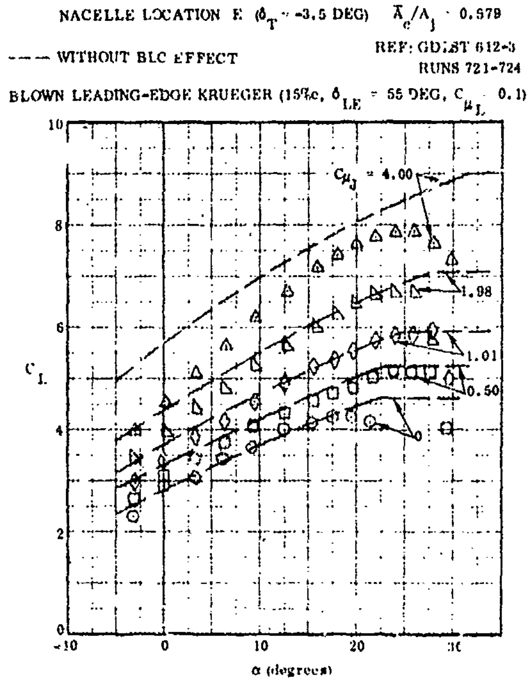

Figure 5-14. Correlation of Maximum Lift Generalized Methodology with EBF Test Data, A = 8, $\Lambda_{c/4}$ = 25 Degrees, Triple-Slotted Flap (δ_f = 60 Degrees), Nacelles Low

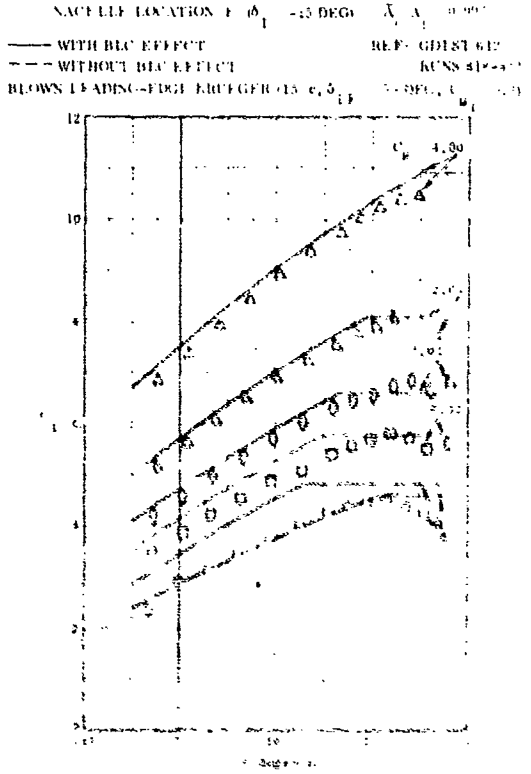

Figure 5-15. Correlation of Maximum Lift Generalized Methodology with EBF Test Data, A = 8, $\Lambda_{c/4}$ = 25 Degrees, Triple-Slotted Flap (δ_f = 60 Degrees), Nacelles Low with Thrust Deflected Upward 15 Degrees

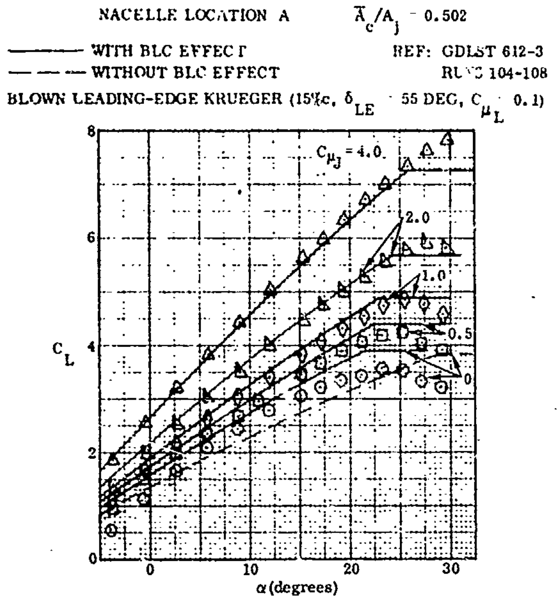

Figure 5-16. Correlation of Maximum Lift Generalized Methodology with EBF Test Data, A = 8, $\Lambda_{c/4}$ = 25 Degrees, Double-Slotted Flap (δ_f = 30 Degrees)

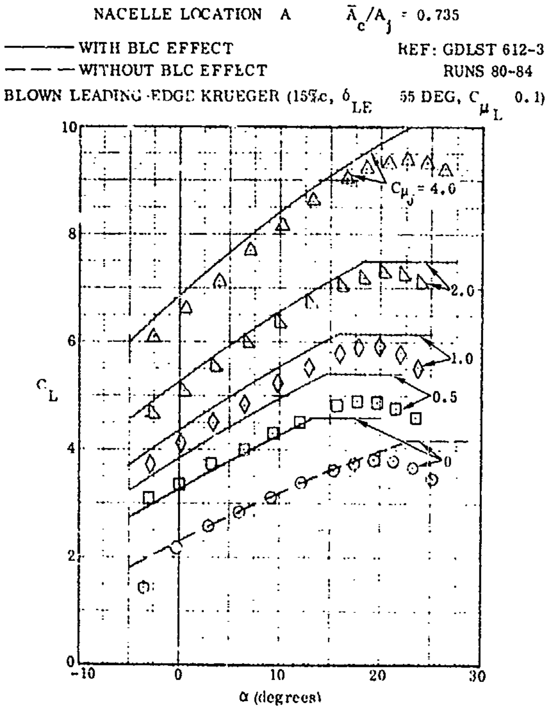

Figure 5-17. Correlation of Maximum Lift Generalized Methodology with EBF Test Data, A = 8, $\Lambda_{c/4}$ = 25 Degrees, Double-Slotted Flap (δ_f = 60 Degrees)

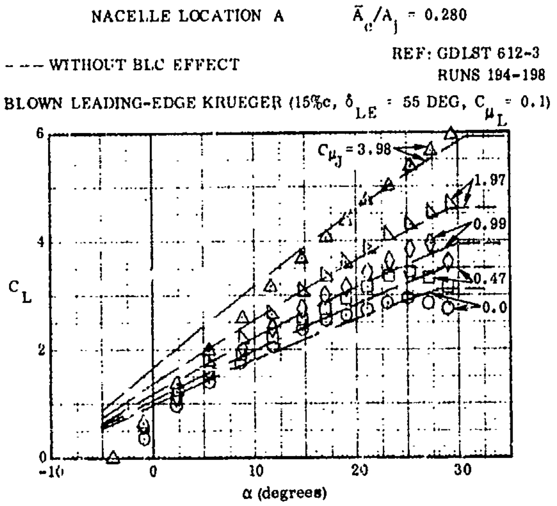

Figure 5-18. Correlation of Maximum Lift Generalized Methodology with EBF Test Data, A = 8, $\Lambda_{c/4}$ = 25 Degrees, Single-Slotted Flap (δ_f = 30 Degrees)

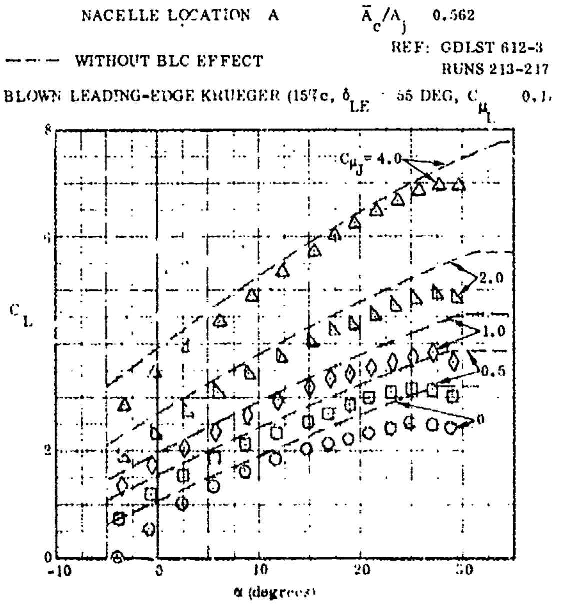

Figure 5-19. Correlation of Maximum Lift Generalized Methodology with EBF Test Data, A = 8, $\Lambda_{c/4}$ = 25 Degrees, Single-Slotted Flap (δ_f = 60 Degrees)

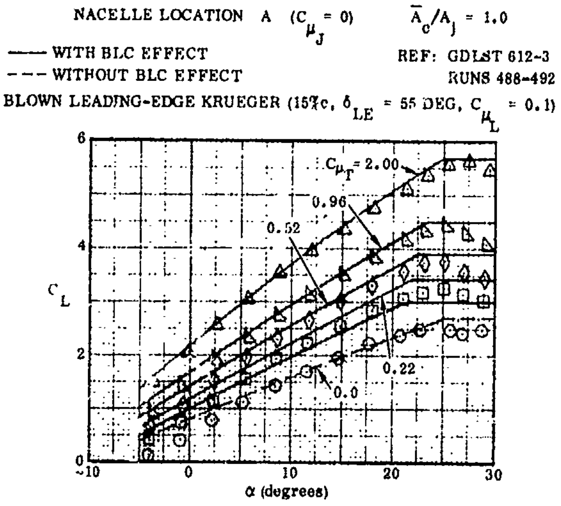

Figure 5-20. Correlation of Maximum Lift Generalized Methodology with IBF Test Data, A = 8, $\Lambda_{c/4}$ = 25 Degrees, Plain Blown Flap (δ_f = 15 Degrees)

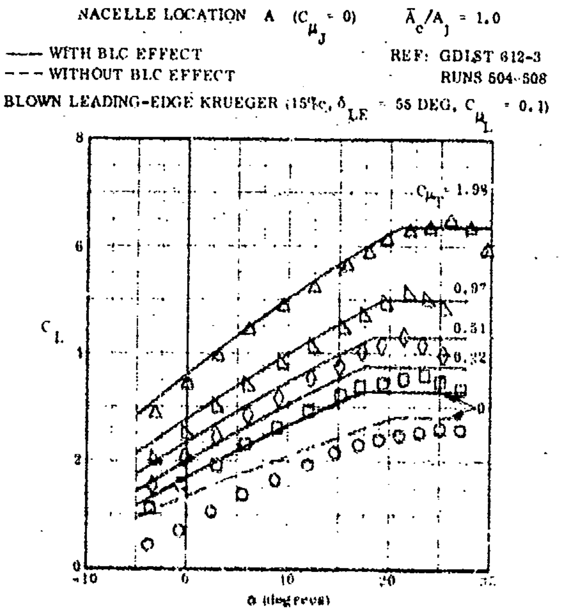

Figure 5-21. Correlation of Maximum Lift Generalized Methodology with IBF Test Data, A = 8, $\Lambda_{c/4}$ = 25 Degrees, Plain Blown Flap (δ_f = 30 Degrees)

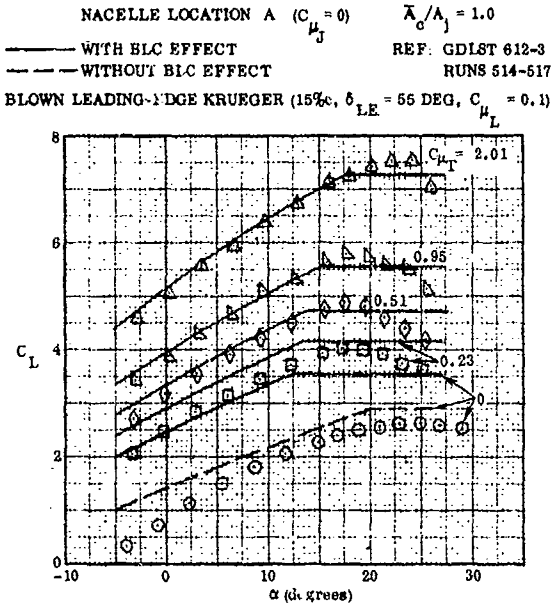

Figure 5-22. Correlation of Maximum Lift Generalized Methodology with IBF Test Data, A = 8, $\Lambda_{c/4}$ = 25 Degrees, Plain Blown Flap (δ_f = 45 Degrees)

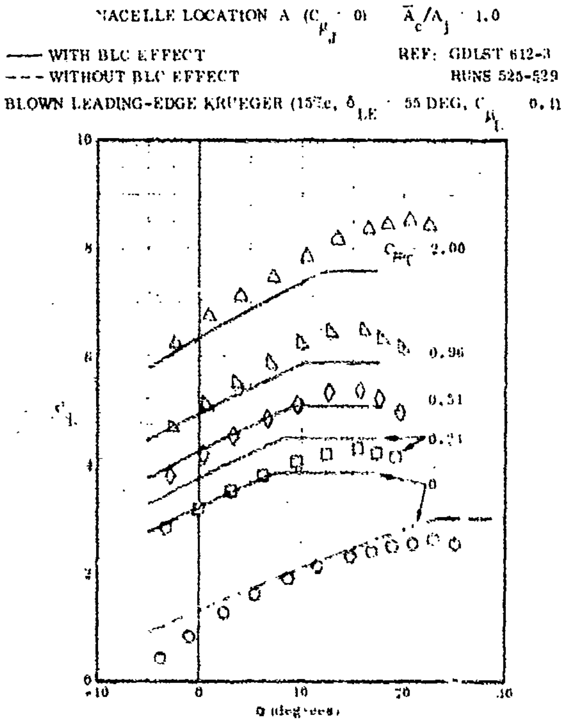

Figure 5-23. Correlation of Maximum Lift Generalized Methodology with IBF Test Data, A = 8, $\Lambda_{c/4}$ = 25 Degrees, Plain Blown Flap (δ_f = 60 Degrees)

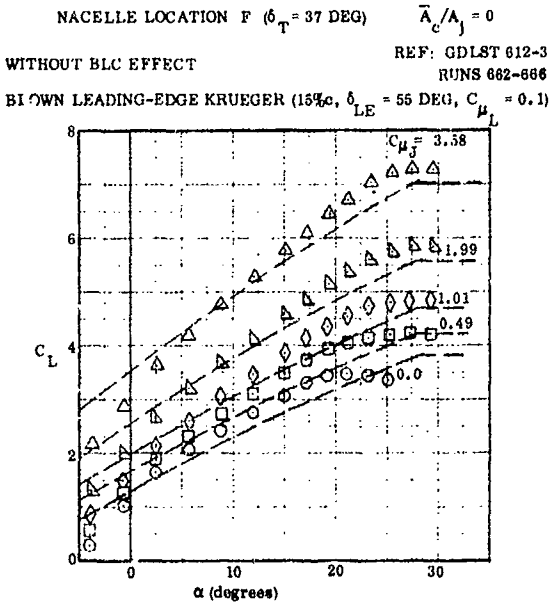

Figure 5-24. Correlation of Maximum Lift Generalized Methodology with MF/VT Test Data, A = 8, $\Lambda_{c/4}$ = 25 Degrees, Double-Slotted Flaps (δ_f = 30 Degrees), Thrust Vectored Downward 37 Degrees

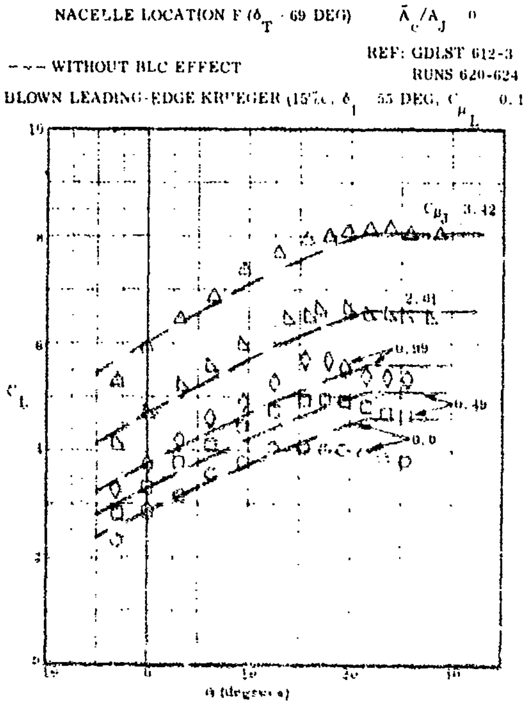

Figure 5-25. Correlation of Maximum Lift Generalized Methodology with MF/VT Test Data, A = 8, $\Lambda_{c/4}$ = 25 Degrees, Triple-Slotted Flap (δ_f = 60 Degrees), Thrust Vectored Downward 69 Degrees

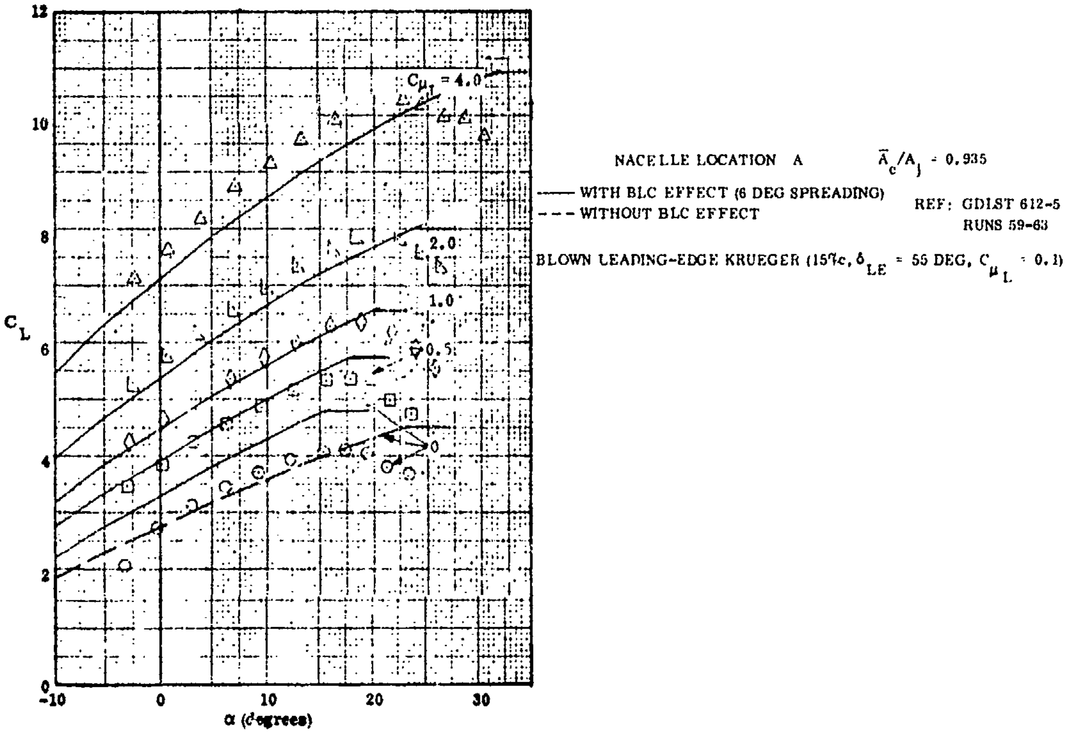

Figure 5-26. Correlation of Maximum Lift Generalized Methodology with EBF Test Data, A = 7.1, $\Lambda_{c/4}$ = 25 Degrees, Triple-Slotted Flap (δ_f = 60 Degrees)

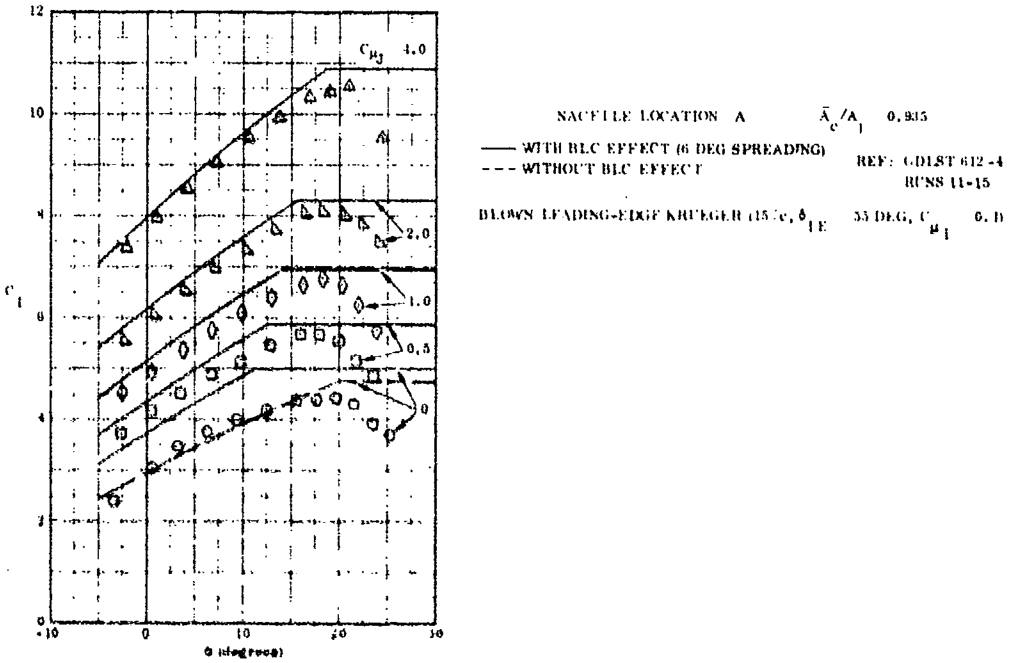

Figure 5-27. Correlation of Maximum Lift Generalized Methodology with EBF Test Data, A = 9.5, $\Lambda_{c/4}$ = 25 Degrees, Triple-Slotted Flap (δ_f = 60 Degrees)

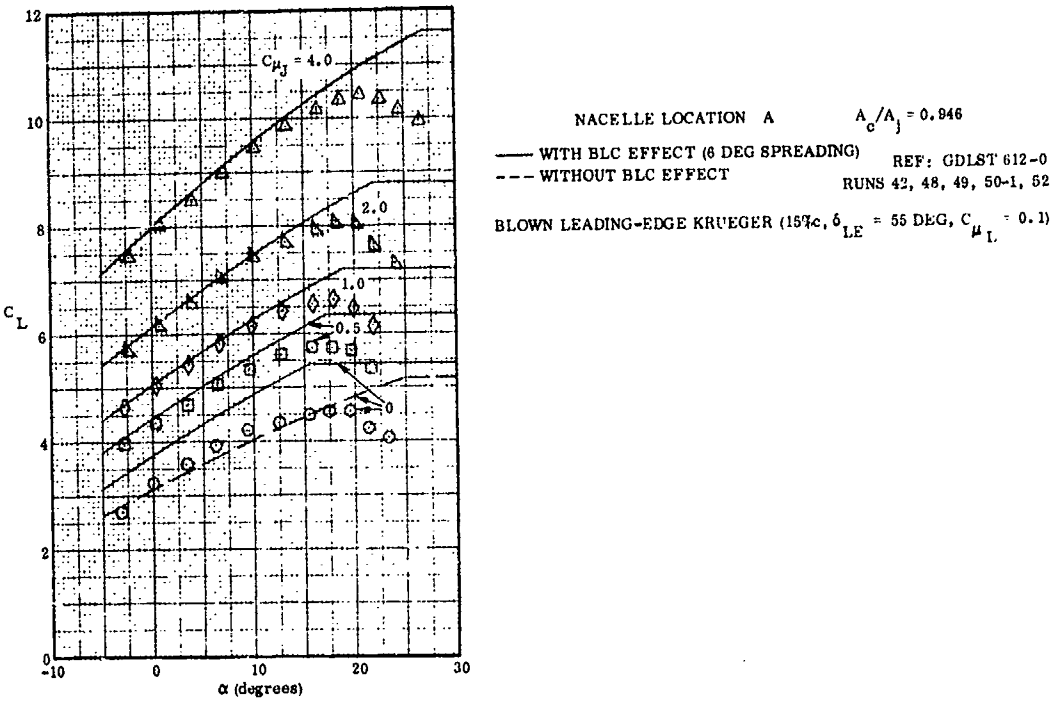

Figure 5-28. Correlation of Maximum Lift Generalized Methodology with EBF Test Data, $A = 8.0$, $\Lambda_{c/4} = 12.5$ Degrees, Triple-Slotted Flap (δ_f = 60 Degrees)

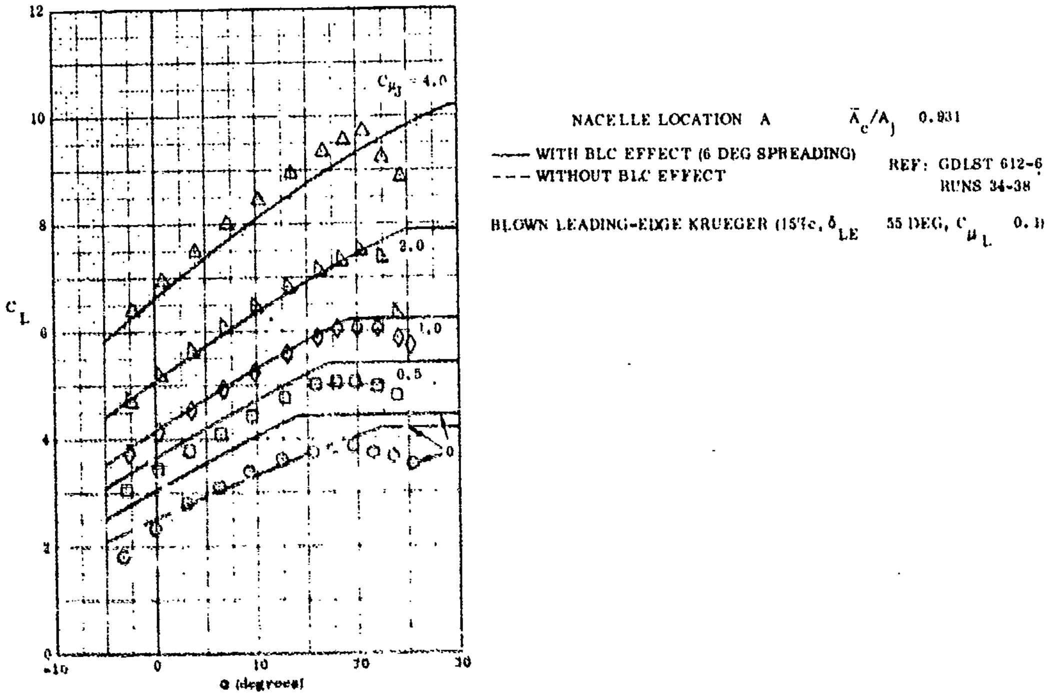

Figure 5-29. Correlation of Maximum Lift Generalized Methodology with EBF Test Data, $A = 8.0$, $\Lambda_{c/4} = 35$ Degrees, Triple-Slotted Flap (δ_f = 60 Degrees)

SECTION 6

DRAG METHODOLOGY

The total drag force coefficient, C_D, including jet thrust effects, is expressed as:

$$C_D = C_{D_{p_o}} + C_{D_i} - r\, C_\mu + C_{D_{RAM}} \qquad (6\text{-}1)$$

where

$C_{D_{P_o}}$	is the power-off minimum profile drag coefficient of the total aircraft including thrust recovery from leading-edge blowing.
C_{D_i}	is the power-on induced drag coefficient discussed in Section 6.1.
r	is the thrust recovery factor discussed in Section 6.2.
C_μ	is the overall gross jet momentum coefficient at the blowing nozzle for an IBF, or at the jet exit for EBF and MF/VT systems.
$C_{D_{RAM}}$	is momentum loss coefficient due to the inlet, ram drag. It is generally zero for the IBF system in the wind tunnel.

Methods for estimating the minimum profile drag coefficient, $C_{D_{P_o}}$, of the entire aircraft are not presented in the current methodology because methods of this type are published in numerous handbooks. In particular, the method outlined in Reference 6-1 may be applied to STOL transport configurations with multiple-slotted flaps and includes effects of Reynolds number, slot gap, Mach number, partial span, and fuselage cut-out and corrections to account for wing sweep and airfoil thicknesses. The methodology presented does not address the estimation of C_μ and $C_{D_{RAM}}$ which are assumed to be known from engine performance characteristics or from calibrations of the model jets and/or nozzles. All equations required to estimate the remaining terms in Equation 6-1 are shown in Figure 6-1,together with reference to specific equations in the text where the terminology is defined in detail.

EQUATION
NO.

(6-1) $$C_D = \underset{6.0}{C_{D_{p_o}}} + \underset{6.1}{C_{D_i}} - \underset{6.2}{r\, C_\mu} + \underset{6.0}{C_{D_{RAM}}}$$

(6-7) $$r = \sqrt[3]{\cos \delta_T} \text{ for } \delta_f \approx \delta_T \qquad \text{for MF/VT}$$

(6-8) $$= \cos \delta_T \text{ for } \delta_f < \delta_T$$

(6-9) $$r = \eta_s$$

$$\eta_s = 0.80 \qquad \text{for IBF}$$

(6-11) $$\eta_s = 0.4 \left[\cos \delta_f + \sqrt{\cos^2 \delta_f + 1.25} \right] \qquad \text{for EBF}$$

(6-10) $$\theta_s = \frac{\overline{A_c}}{A_j} \delta_f$$

(6-2) $$C_{D_i} = \frac{C_L^{\,2}}{\pi A e}$$

(6-3) $$e = \frac{\left[1 + \left(\delta_T^* / \epsilon \right) \frac{K_\Gamma C_\mu}{\pi A} \right]^2}{\left[1 + \left(\delta_T^* / \epsilon \right)^2 \frac{K_I C_\mu}{\pi A} \right]} e_o$$

(6-4) $$\delta_T^* = \frac{\overline{A_c}}{A_j} \epsilon + \left(1 - \frac{\overline{A_c}}{A_j} \right) \left(\delta_T + \alpha \right)$$

(6-5) $$\epsilon = \frac{2 \left[C_L - \left(1 - \overline{A_c}/A_j \right) C_\mu \sin \left(\alpha + \delta_T \right) \right]}{\left[\pi A + 2 \left(\overline{A_c}/A_j \right) C_\mu \right] e_o}$$

Figure 6-1. Drag Methodology

6.1 INDUCED DRAG

The induced drag coefficient, C_{D_i}, in Equation 6-1 is defined according to classical lifting line theory as:

$$C_{D_i} = \frac{C_L^2}{\pi A e} \tag{6-2}$$

where

C_L	is the overall lift coefficient of the entire system, including the jet reaction lift, as obtained from Equation 4-1.
A	is the aspect ratio of the wing based on the reference area, S.
e	is the induced drag factor (aerodynamic efficiency), which depends on blowing coefficient and the type of STOL system.

Equation 6-1 is used either power-on or power-off for the IBF, EBF, and MF/VT systems. As mentioned previously, effects of power for the various STOL systems may be included in Equation 6-2 through the definition of the induced drag factor, e. Thus, it may be readily demonstrated from the application of apparent mass concepts, together with the conservation of vertical momentum and energy, that the induced drag factor will be of the form:

$$e = \frac{\left[1 + \left(\delta_T^* / \epsilon\right) \dfrac{K_\Gamma C_\mu}{\pi A}\right]^2}{\left[1 + \left(\delta_T^* / \epsilon\right)^2 \dfrac{K_\Gamma C_\mu}{\pi A}\right]} e_o \tag{6-3}$$

where

δ^*_T	is the effective jet turning angle.
ϵ	is the average spanwise wing downwash angle at infinity
K_Γ	is equal to 2.0 for IBF and MF/VT systems and equal to 1.0 for EBF systems.
e_o	is the power-off aerodynamic efficiency.

Equation 6-3 includes a loss in jet thrust coefficient (or equivalently an increase in drag coefficient), which is given by:

$$C_\mu \;\; (1 - \cos \delta_T)$$

In addition, no interaction is assumed between the supercirculation lift and the reaction lift from the uncaptured part of the jet, and the normal small angle approximations have been made.

The effective jet turning angle, δ^*_T, depends on the jet nozzle deflection angle, δ_T, with respect to the wing reference plane (in the partial-capture-ratio EBF and MF/VT cases) and on the downwash angle, ϵ. Expressions for δ^*_T and ϵ are:

$$\delta_T^* = \frac{\overline{A_c}}{A_j}\,\epsilon + \left(1 - \frac{\overline{A_c}}{A_j}\right)\left(\delta_T + \alpha\right) \tag{6-4}$$

$$\epsilon = \frac{2\left[C_L - \left(1 - \overline{A_c}/A_j\right) C_\mu \sin\left(\alpha + \delta_T\right)\right]}{\left[\pi A + 2\left(\overline{A_c}/A_j\right) C_\mu\right] e_o} \tag{6-5}$$

where

$\bar{A}_c/A_j$ is the average jet capture ratio defined in Section 2.

In the limit of $\bar{A}_c/A_j = 1$, which is the case for IBF systems and for EBF systems with full capture, Equation 6-4 gives $\delta^*_T/\epsilon = 1.0$; hence, the induced drag factor, e, from Equation 6-3 reduces to the familiar idealized result of Spence and Maskell (Reference 6-2). Differentiating Equation 6-3 shows that the induced drag factor is a maximum for this value of δ^*_T/ϵ. Induced drag for the IBF system should therefore be less than the induced drag for either the EBF or MF/VT systems for which δ^*_T/ϵ may be either less than or larger than one. A second reason for higher induced drag for the EBF systems, even with full capture, is the highly peaked span load distribution encountered with the system. (See Figure 3-12.) The effect of this nonuniform span load on the EBF induced drag factor is not included in Equation 6-3. As shown in subsequent comparisons with test data, this effect is approximated by arbitrarily setting the coefficient of the C_μ in term K_Γ in Equation 6-3 to 1.0 for the EBF system.

Correlation of results from Equation 6-3 with test data is shown in Figure 6-2. For the IBF and EBF systems, this correlation indicates that good agreement with test data when a power-off induced drag factor, e_o between 0.8 and 1.0, is used as the base value. The lower value of this range corresponds to flaps at large deflection angle and with substantial separation (no BLC effectiveness), whereas the higher values correspond to flaps at low deflection and negligible separation (full BLC effectiveness). Determination of the particular value of e_o to use in Equation 6.3 for EBF and IBF systems should be based on test correlations for the particular flap system. Figure 6-2 also shows variation of the induced drag factor with C_μ for several EBF configurations. As noted in the preceding paragraph, improved correlation with Equation 6-3 is obtained by setting $K_\Gamma = 1.0$.

Correlation of the theory with test data for the MF/VT system is satisfactory at all but low values of the blowing coefficient, providing the power-off induced drag factor has been set equal to one. Since the discrepancy at low values of C_μ is apparently a BLC effect, it appears reasonable to use $e_o = 1$ when estimating induced drag of MF/VT systems with power on.

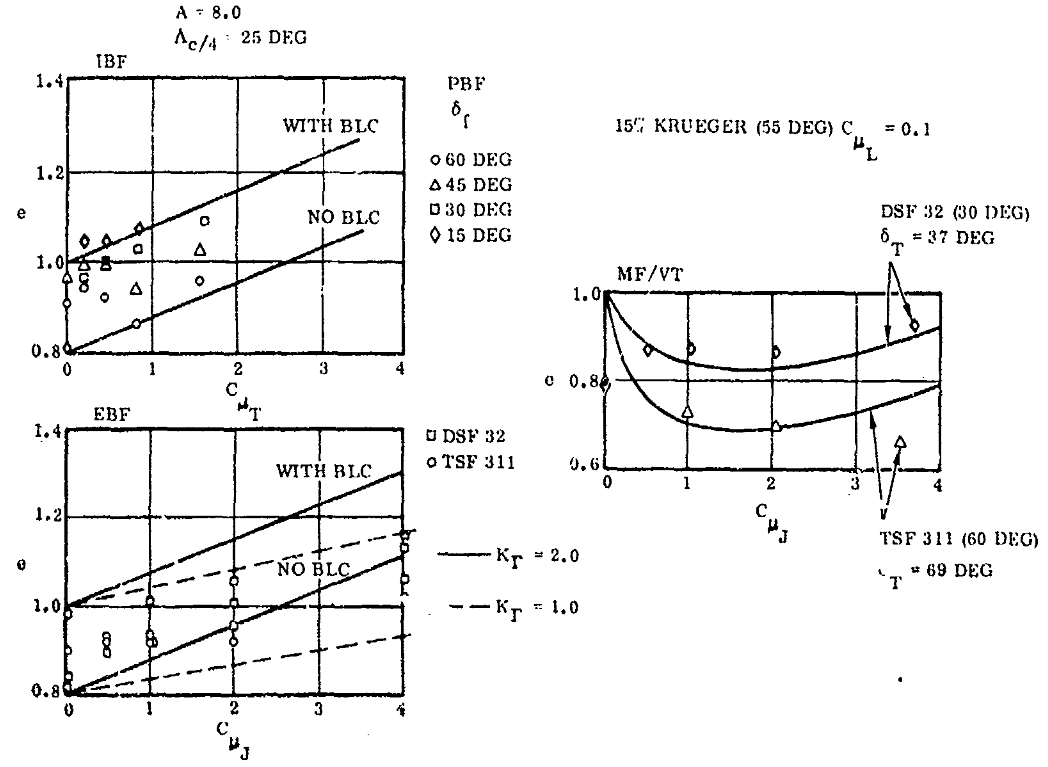

Figure 6-2. Induced Drag Correlation for IBF, EBF, and MF/VT Systems

SAMPLE PROBLEM

GIVEN: $\alpha = 10$ deg

A. EBF

$C_L = 5.932$

$c_\mu = 1.0$

$A = 8.0$

$e_o = 0.85$

$\delta_T = -3.5$ deg

$K_\Gamma = 1.0$

$\frac{\bar{A}_c}{A_j} = 0.935$

B. IBF

$C_L = 6.811$

$c_\mu = 1.0$ (Based on exposed area)

$= 0.868$ (Based on reference area)

$A = 8.0$

$e_o = 0.80$

$\frac{\bar{A}_c}{A_j} = 1.0$

$K_\Gamma = 2.0$

C. MF/VT

$C_L = 4.835$

$A = 8.0$

$e_o = 1.00$

$\frac{\bar{A}_c}{A_j} = 0.0$

$K_\Gamma = 2.0$

$\delta_T = 60$ deg

CALCULATE:

1. The downwash angle using Equation 6-5.

$$\epsilon = \frac{2\left[C_L - \left(1 - \overline{A_c}/A_j\right) C_\mu \sin\left(\alpha + \delta_T\right)\right]}{\left[\pi A + 2\left(\overline{A_c}/A_j\right) C_\mu\right] e_o} \qquad (6\text{-}5)$$

A. EBF

$$\epsilon = \frac{2[5.332 - (1.0 - 0.935)(1.0) \sin (10 - 3.5)]}{[(\pi)(8) + (2)(0.935)(1.0)]\ (0.85)}$$

$$= \frac{11.849}{22.952}$$

$$= 0.516 \text{ rad}$$

B. IBF

$$\epsilon = \frac{2[6.811 - (1.0 - 1.0)(0.868) \sin (10 - 3.5)]}{[(\pi)(6) + (2)(1.0)(0.868)]\ (0.80)}$$

$$= \frac{2(6.811)}{21.495}$$

$$= 0.634 \text{ rad}$$

C. MF/VT

$$\epsilon = \frac{2[4.835 - (1.0 - 0.0)(1.0) \sin (10 + 69)]}{[\pi (8) + (2)(0.0)(1.00)]\ (1.00)}$$

$$= \frac{7.707}{25.133}$$

$$= 0.307 \text{ rad}$$

2. Effective jet turning angle using Equation 6-4.

$$\delta_T^* = \frac{\overline{A_c}}{A_j} \epsilon + \left(1 - \frac{\overline{A_c}}{A_j}\right)\left(\delta_T + \alpha\right) \qquad (6\text{-}4)$$

A. EBF

$$\delta_T^* = (0.935)(0.516) + (1 - 0.935)\left(\frac{10 - 3.5}{57.295}\right)$$

$$= 0.490$$

B. IBF

$$\delta^* = (1.0)(0.634) + (1.0 - 1.0)(\delta_T + 10)$$

$$= 0.634$$

C. MF/VT

$$\delta^* = (0)(0.307) + (1.0 - 0.0)\left(\frac{69 + 10}{57.295}\right)$$

$$= 1.379$$

3. Induced drag factor using Equation 6-3.

$$e = \frac{\left[1 + \left(\delta_T^*/\epsilon\right)\frac{K_\Gamma C_\mu}{\pi A}\right]^2}{\left[1 + \left(\delta_T^*/\epsilon\right)^2 \frac{K_\Gamma C_\mu}{\pi A}\right]} e_o \qquad (6\text{-}3)$$

A. EBF

$$e = \frac{\left[1 + \left(\frac{0.490}{0.516}\right)(1.0)\left(\frac{1.0}{\pi(8)}\right)\right]^2}{\left[1 + \left(\frac{0.490}{0.516}\right)^2 (1.0)\left(\frac{1.0}{\pi(8)}\right)\right]} (0.85)$$

$$= \frac{1.077}{1.0359} (0.85)$$

$$= 0.884$$

B IBF

$$e = \frac{\left[1 + \left(\frac{0.634}{0.634}\right)(2.0)\left(\frac{0.868}{\pi(8)}\right)\right]^2}{\left[1 + \left(\frac{0.634}{0.634}\right)^2 (2.0)\left(\frac{0.868}{\pi(8)}\right)\right]} (0.80)$$

$$= \left(\frac{1.1429}{1.0691}\right)(0.80)$$

$$= 0.855$$

C. MF/VT

$$e = \frac{\left[1 + \left(\frac{1.379}{0.307}\right)(2.0)\left(\frac{1.0}{\pi(8)}\right)\right]^2}{\left[1 + \left(\frac{1.379}{0.307}\right)^2 (2.0)\left(\frac{1.0}{\pi(8)}\right)\right]} (1.0)$$

$$= \left(\frac{1.8427}{2.6056}\right)(1.0)$$

$$= 0.707$$

4. Induced drag using Equation 6-2.

$$C_{D_i} = \frac{C_L^{\;2}}{\pi A e} \tag{6-2}$$

A. EBF

$$C_{D_i} = \frac{(5.932)^2}{(\pi)(8)(0.884)}$$

$$= 1.584$$

B. IBF

$$C_{D_i} = \frac{(6.811)^2}{(\pi)(8)(0.855)}$$

$$= 2.159$$

C. MF/VT

$$C_{D_i} = \frac{(4.835)^2}{(\pi)(8)(0.707)}$$

$$= 1.316$$

6.2 THRUST RECOVERY

The thrust recovery factor, r, in the current methodology is defined as:

$$r = -d\,C_{D_P} / d\,C_\mu \tag{6-6}$$

where:

C_{D_P} is the power-on minimum profile drag coefficient.

C_μ is the gross jet momentum coefficient at the nozzle or jet exit.

The value of C_{D_P} is found by extrapolating the linear portion of the drag curve, plotted as C_L^2 versus $C_D - C_{D_{RAM}}$, to the zero lift coefficient as sketched in Figure 6-3. This definition of thrust recovery makes the thrust recovery factor independent of lift coefficient, but thrust recovery is closely coupled to the slope of the drag curve used in establishing the intercept at a lift coefficient of zero, or equivalently to the induced drag factor. However, errors introduced into the thrust recovery and induced drag factors by changes in slope $d\,C_D/d\,C_L^2$ tend to cancel when estimating the overall drag coefficient.

The thrust recovery factor includes jet thrust losses due to the additional skin friction and separation drag as the jet passes over the wing and flaps (scrubbing drag), and losses due to failure of the jet momentum to completely recover to the idealized downwash direction far behind the flap system. The thrust recovery factor also includes induced thrust losses from the fuselage cutout and nonuniform EBF jet spreading, which may be independent of angle of attack. Power-on as well as power-off partial-span flap effects such as aileron cutouts would be expected to introduce additional induced losses and to affect both the thrust recovery factor and the power-off minimum profile drag coefficient. Such partial-span flap effects are not included in the current methodology.

Based on test data from Reference 3-11, the thrust recovery factor for the MF/VT system may be approximated as:

$$r = \sqrt[3]{\cos \delta_T} \text{ for } \delta_f \approx \delta_T \tag{6-7}$$

$$r = \cos \delta_T \text{ for } \delta_f < \delta_T \tag{6-8}$$

For flap deflection angles much greater than the jet deflection angle ($\delta_f \gg \delta_T$), r is assumed equal to the EBF thrust recovery factor.

These equations are compared with the test data in Figure 6-4, where thrust recovery is plotted versus static turning angle for MF/VT systems. (The static turning angle is assumed equal to the jet deflection angle.) At a turning angle of about 70 degrees, thrust recovery decreases with a decrease in flap deflection, approaching the value of thrust recovery given in Equation 6-8 at the lowest flap angle of 30 degrees.

The thrust recovery factor for IBF systems is assumed equal to static turning efficiency, η_s:

$$r = \eta_s \tag{6-9}$$

The value of $\eta_s \simeq 0.8$ seems to fit test data from Reference 3-11 over a wide range of flap deflection angles, as shown in Figure 6-5a. Figure 6-5b shows the corresponding thrust recovery factors from Reference 3-11. Thrust recovery is shown to exceed static turning efficiency for these cases. This apparent discrepancy with Equation 6-9 occurs because thrust recovery includes a reduction in drag due to clean up of separation on the flaps, especially at large flap deflections, viz. BLC effect. This is also shown in Figure 6-5c, where thrust recovery at each flap deflection angle approaches the static efficiency value as blowing coefficient is increased. Therefore, if the power-off minimum drag coefficient, $C_{D_{P_o}}$, in Equation 6-1 does not include drag due to separation on the flap, the value of static turning efficiency for thrust recovery will evaluate the drag level adequately.

Thrust recovery for EBF systems is also assumed to be equal to static turning efficiency (Equation 6-9). Correlation of thrust recovery and static turning efficiency for EBF systems is shown in Figure 6-6, as obtained from test data in Reference 3-11. This data indicates that for double- and single-slotted flaps, thrust recovery is equal to or slightly greater than the static turning angle. For the triple-slotted flap configuration, however, thrust recovery is greater than the static turning efficiency by as much as 15 percent. This discrepancy could be due to the method of data analysis, where thrust recovery and the induced drag factor are interrelated as mentioned previously.

EBF static turning efficiency, η_s, as obtained from Reference 3-11 is plotted versus static turning angle, θ_s, for single-, double-, and triple-slotted flaps in Figure 6-7. Figure 6-7 also shows a theoretical relation from Reference 6-3 that estimates jet turning efficiency for a planar surface at the jet centerline. In the present methodology, jet turning angle, θ_s, is related to the flap deflection angle, δ_f, by:

$$\theta_s = \frac{\overline{A}_c}{A_j}\,\delta_f \tag{6-10}$$

Using Equation 6-10 in conjunction with Reference 6-3 leads to the following expression for η_s in terms of flap deflection angle.

$$\eta_s = 0.4 \left[\cos \delta_f + \sqrt{\cos^2 \delta_f + 1.25} \right] \tag{6-11}$$

Equation 6-11 correlates well with the test data, as indicated in Figure 6-7.

SAMPLE PROBLEM

GIVEN:

$\delta_f = 59.8$ deg

$\delta_T = 69$ deg (for MF/VT)

CALCULATE:

1. Thrust recovery for EBF using Equations 6-9 and 6-11.

$$r = \eta_s = 0.4 \left[\cos \delta_f + \sqrt{\cos^2 \delta_f + 1.25} \right] \tag{6-11}$$

$$= 0.4 \left[\cos\ (59.8) + \sqrt{(\cos\ [59.8])^2 + 1.25} \right]$$

$$= 0.6916$$

2. Thrust recovery for IBF using Equation 6-9.

$$r = \eta_s = 0.8 \tag{6-9}$$

3. Thrust recovery for MF/VT using Equation 6-7.

$$r = \sqrt[3]{\cos \delta_T} \tag{6-7}$$

$$= \sqrt[3]{\cos\ (69)}$$

$$= 0.7103$$

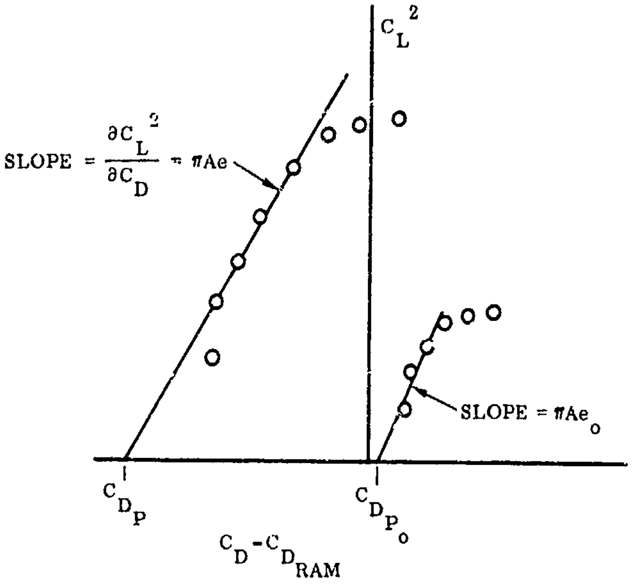

Figure 6-3. Definition of Induced Drag and Thrust Recovery Factors

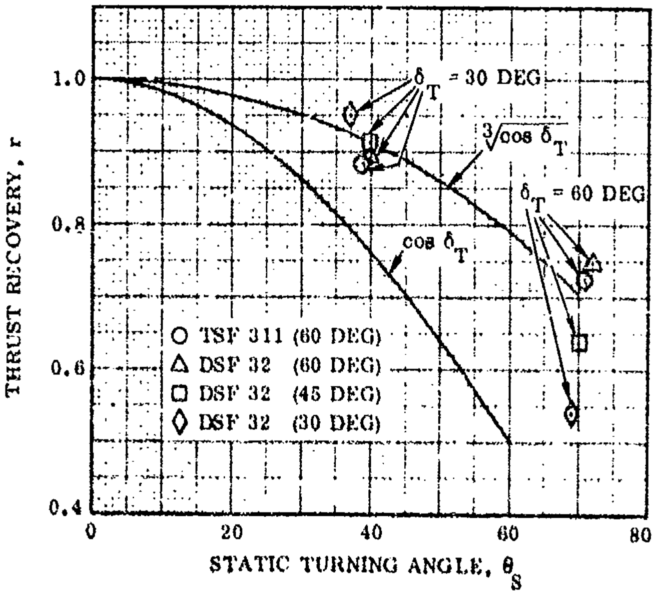

Figure 6-4. Thrust Recovery Correlation for MF/VT System

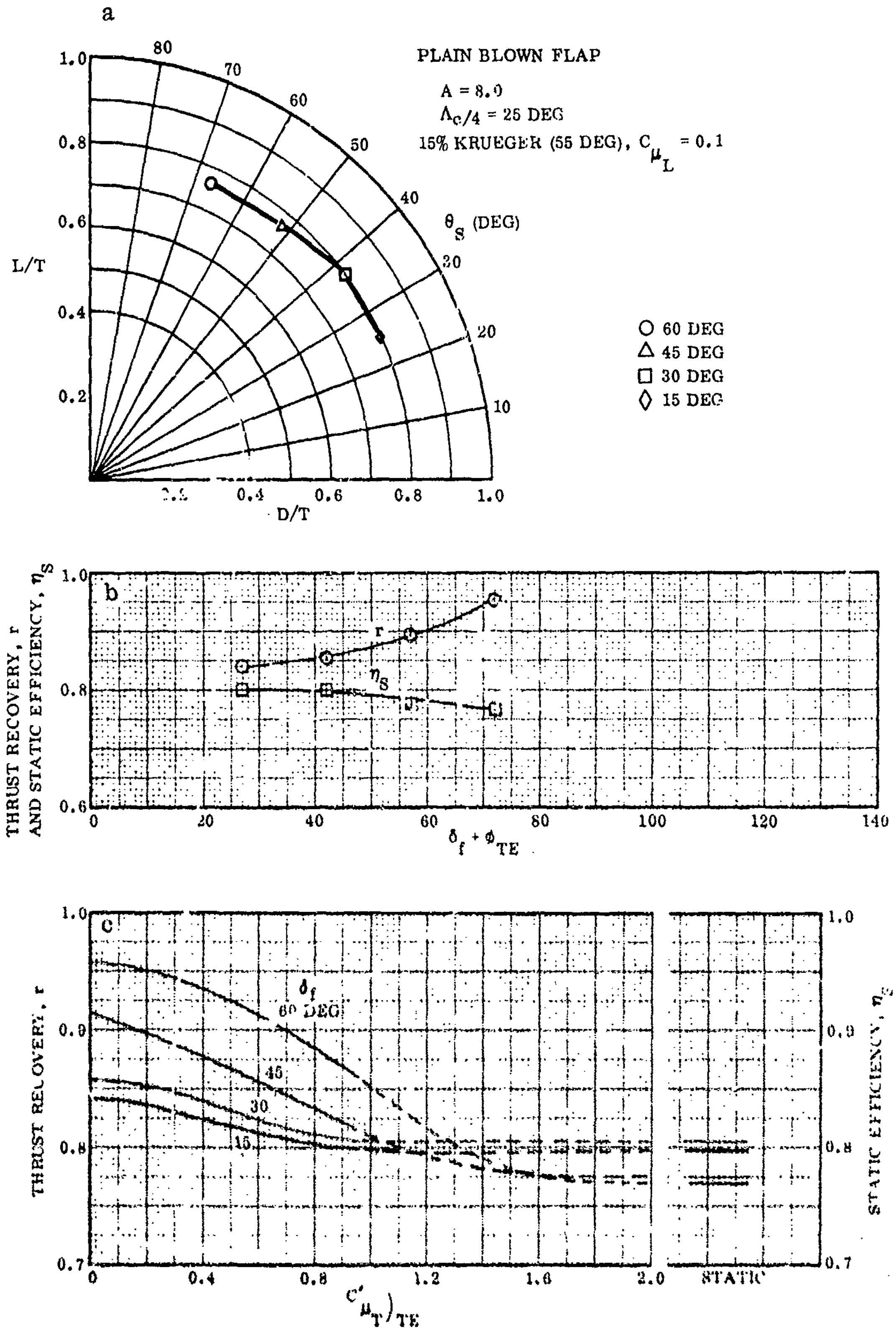

Figure 6-5. Thrust Recovery Correlation for IBF System

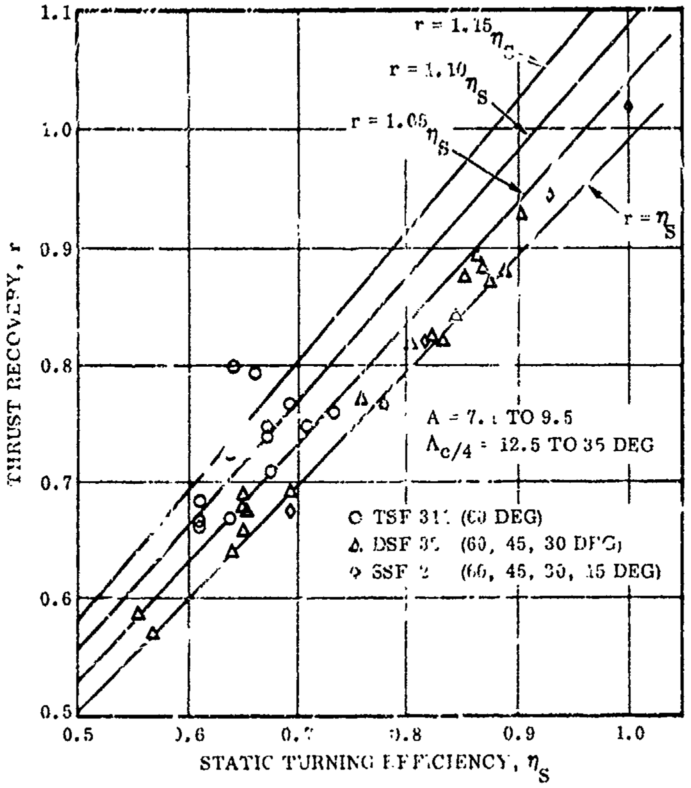

Figure 6-6. Correlation of Thrust Recovery with Static Turning Efficiency for EBF System

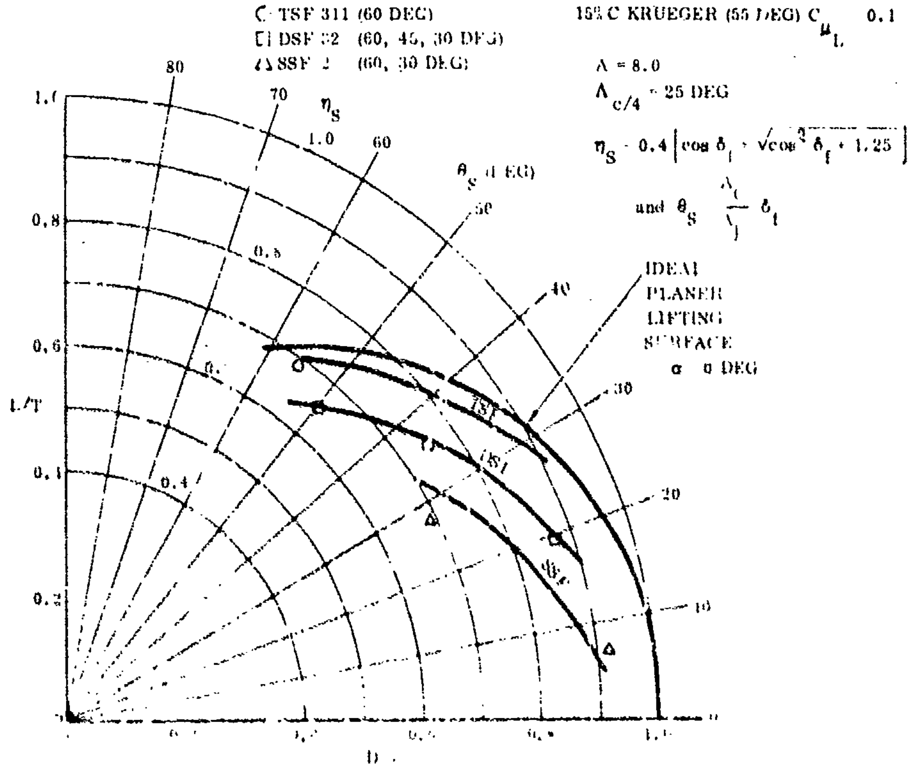

Figure 6-7. Static Turning Efficiency Correlation for EBF Systems

6.3 DRAG CORRELATION

The sample problem and correlations are for the wings described in Section 4.4

SAMPLE PROBLEM

GIVEN:

$C_{D_{p_o}} = 0.0$

$C_{D_{RAM}} = 0.0170$ for EBF

$C_{D_{RAM}} = 0.123$ for MF/VT

$C_{D_{RAM}} = 0.0$ for IBF

CALCULATE:

Total configuration drag using Equation 6-1.

$$C_D = C_{D_{p_o}} + C_{D_i} - r\,C_\mu + C_{D_{RAM}} \tag{6-1}$$

A. EBF

$C_\mu = 1.0$

$r = 0.6916$ from sample problem in Section 6.2.

$C_{D_i} = 1.584$ from sample problem in Section 6.1.

$C_D = 0.0 + 1.584 + 0.17 - (0.6916)(1.00)$

≈ 1.062

B. IBF

$C_\mu = 0.868$

$r = 0.8$ from sample problemin Section 6.2.

$C_{D_i} = 2.159$ from sample problem in Section 6.1.

$C_D = 0.0 + 2.159 + 0.0 - (0.868)(0.80)$

$= 1.465$

C. MF/VT

$C_\mu = 1.0$

$r = 0.7103$

$C_{D_i} = 1.316$

$C_D = 0.0 + 1.316 + 0.123 - (0.7103)(1.0)$

$= 0.729$

CORRELATIONS

Several assumptions have been made in the drag correlations with regard to the choice of aerodynamic parameters which are not explicitly defined in the methodology. Thus, the minimum-profile power-off drag coefficient, designated $C_{D_{Po}}$, has been assumed to be cancelled by the thrust component of the leading-edge jet momentum. Measured values for the RAM drag coefficient, $C_{D_{RAM}}$, as obtained from wind tunnel calibrations, have been included in the predicted drag levels for the EBF and MF/VT configurations because the wind tunnel balance readings include this drag contribution for these systems. The power-off induced drag factor, ϵ_0 (also termed aerodynamic efficiency), was taken as 0.8 for all IBF calculations, 0.85 for all EBF calculations, and 1.0 for all MF/VT calculations. A single value of ϵ_0 was used for each STOL system to simplify the calculations as much as possible, although improved agreement in drag might have been obtained for some configurations by referring to test data for the particular value of ϵ_0.

The EBF calculations for the wing with a triple-slotted flap (δ_f = 60 deg) are compared with test results in Figures 6-8 through 6-10. Figure 6-8, which is with the engines in the high position (Position A) for which the capture ratio is 0.935, indicates that the drag data compares reasonably well with the calculations for all values of C_μ and is relatively insensitive to the degree of assumed flow separation.

Figure 6-9 depicts a similar comparison but with the engines lowered to Position E, for which the capture ratio has been reduced to 0.579. In this case, the jet efflux no longer passes through the first flap slot. Drag data also compares well with the calculations at lift coefficients below stall.

Figure 6-10 compares the methodology and test results when the engines in Position E are tilted upward by 15 degrees so that the capture ratio is increased from 0.579 to 0.997.

Comparisons for double-slotted EBF systems of 30- and 60-degree deflections are shown in Figures 6-11 and 6-12, respectively. The engines are in Position A (high), for which the jets pass through the first flap slot. Data for the flaps at both deflections agrees well with the computations.

Figures 6-13 and 6-14 compare the methodology with test data for low-capture-ratio single-slotted flaps of 30 and 60 degrees of deflection, respectively. Although the jets are still in the high position, zero BLC effectiveness was assumed for power-on, because the jet efflux failed to pass through the single flap slot.

Figures 6-15 through 6-18 present correlations between methodology and test data for IBF systems with plain flaps of 15, 30, 45, and 60 degrees of deflection, respectively. As indicated in Figure 6-15, the methodology agrees reasonably well with the drag data for the 15-degree flap deflection. Similar agreement is shown in Figure 6-16 for the 30-degree flap deflection. Similar results are shown in Figure 6-17 for the 45-degree flap deflection and in Figure 6-18 for the 60-degree flap deflection.

Figures 6-19 and 6-20 compare methodology and test data for MF/VT configurations with the jets in a low and rearward position (Position F). The comparison in Figure 6-19 is for a double-slotted flap with 30 degrees of deflection and with an effective thrust vectoring angle of 37 degrees. Power-off data and calculations are similar to the power-off EBF comparison for the flap shown in Figure 6-11, except that ϵ_0 was taken equal to one for the MF/VT calculations, as discussed previously.

The comparisons in Figure 6-20 are for a triple-slotted flap with 60 degrees of deflection and with an effective thrust vectoring angle of 69 degrees.

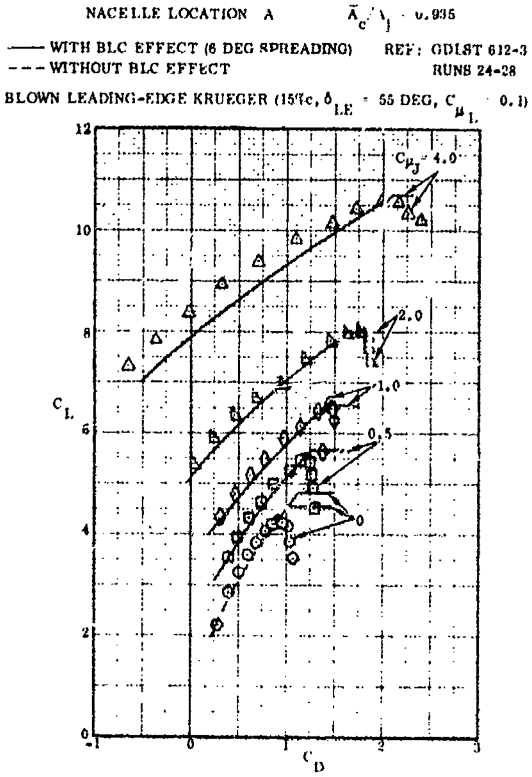

Figure 6-8. Correlation of Drag Generalized Methodology with EBF Test Data, A = 8, $\Lambda_{c/4}$ = 25 Degrees, Triple-Slotted Flap (δ_f = 60 Degrees), Nacelles High

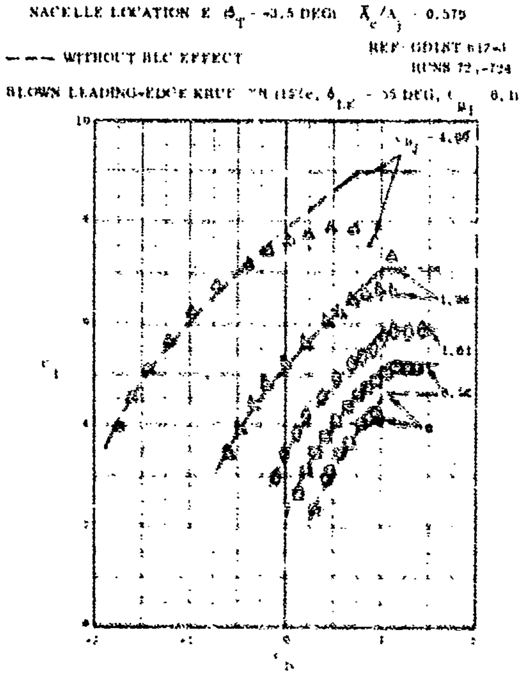

Figure 6-9. Correlation of Drag Generalized Methodology with EBF Test Data, A = 8, $\Lambda_{c/4}$ = 25 Degrees, Triple-Slotted Flap (δ_f = 60 Degrees), Nacelles Low

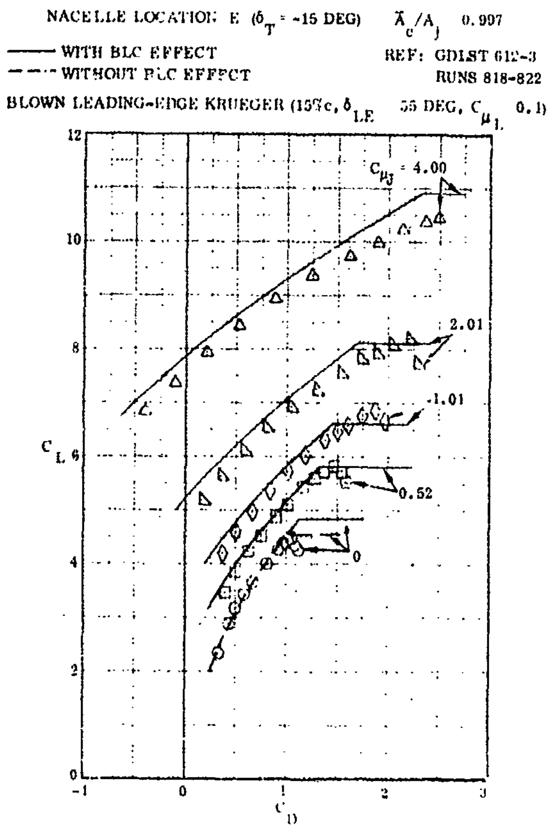

Figure 6-10, Correlation of Drag Generalized Methodology with EBF Test Data, A = 8, $\Lambda_{c/4}$ = 25 Degrees, Triple-Slotted Flap (δ_f = 60 Degrees), Nacelles Low with Thrust Deflected Upward 15 Degrees

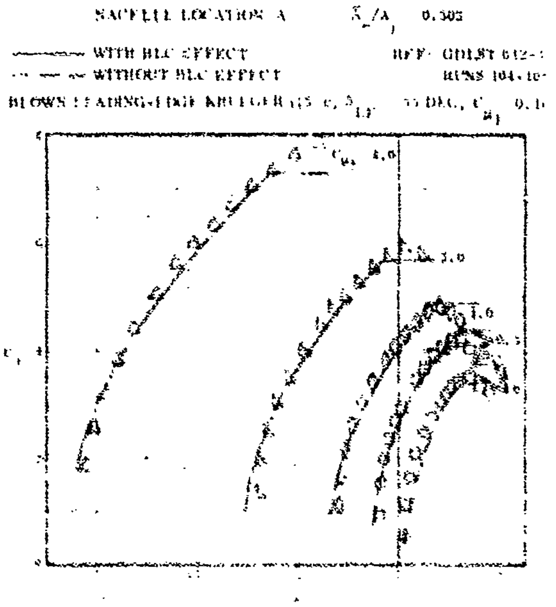

Figure 6-11. Correlation of Drag Generalized Methodology with EBF Test Data, A = 8, $\Lambda_{c/4}$ = 25 Degrees, Double-Slotted Flap (δ_f = 30 Degrees)

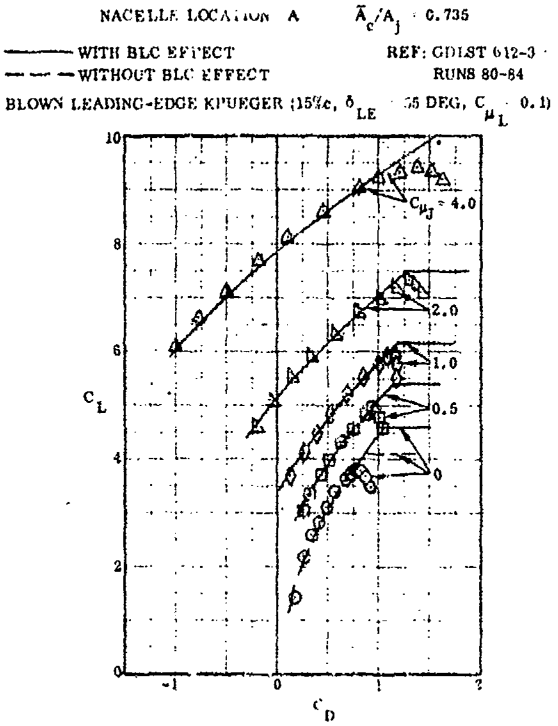

Figure 6-12. Correlation of Drag Generalized Methodology with EBF Test Data, A = 8, $\Lambda_{c/4}$ = 25 Degrees, Double-Slotted Flap (δ_f = 60 Degrees)

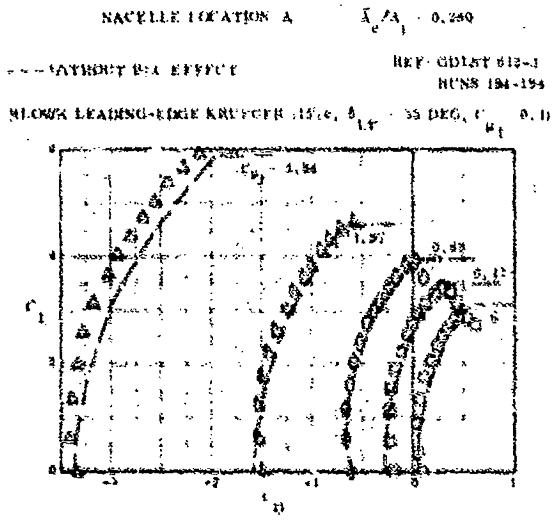

Figure 6-13. Correlation of Drag Generalized Methodology with EBF Test Data, A = 8, $\Lambda_{c/4}$ = 25 Degrees, Single-Slotted Flap (δ_f = 30 Degrees)

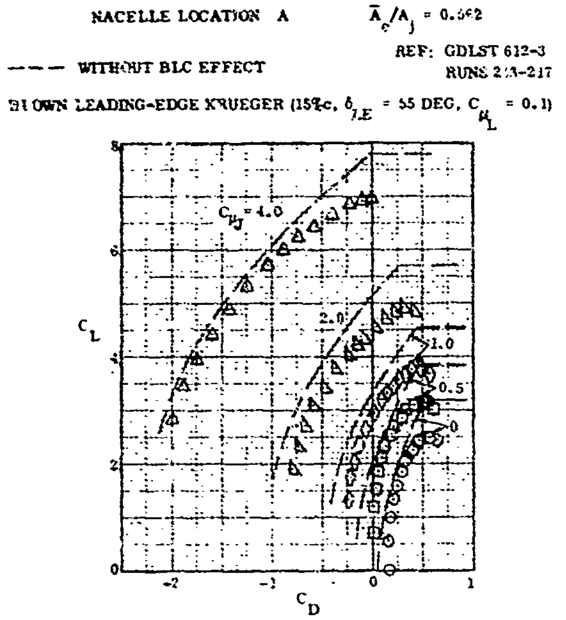

Figure 6-14. Correlation of Drag Generalized Methodology with EBF Test Data, A = 8, $\Lambda_{c/4}$ = 25 Degrees, Single-Slotted Flap (δ_f = 60 Degrees)

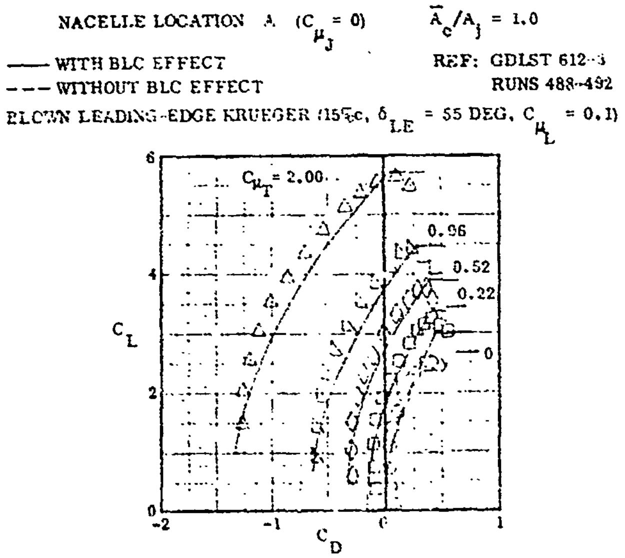

Figure 6-15. Correlation of Drag Generalized Methodology with IBF Test Data, A = 8, $\Lambda_{c/4}$ = 25 Degrees, Plain Blown Flap (δ_f = 15 Degrees)

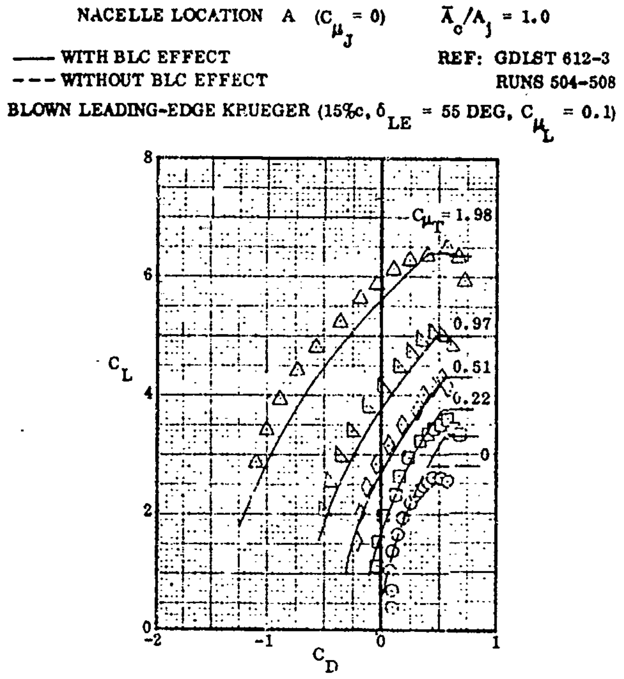

Figure 6-16. Correlation of Drag Generalized Methodology with IBF Test Data, A = 8, $\Lambda_{c/4}$ = 25 Degrees, Plain Blown Flap (δ_f = 30 Degrees)

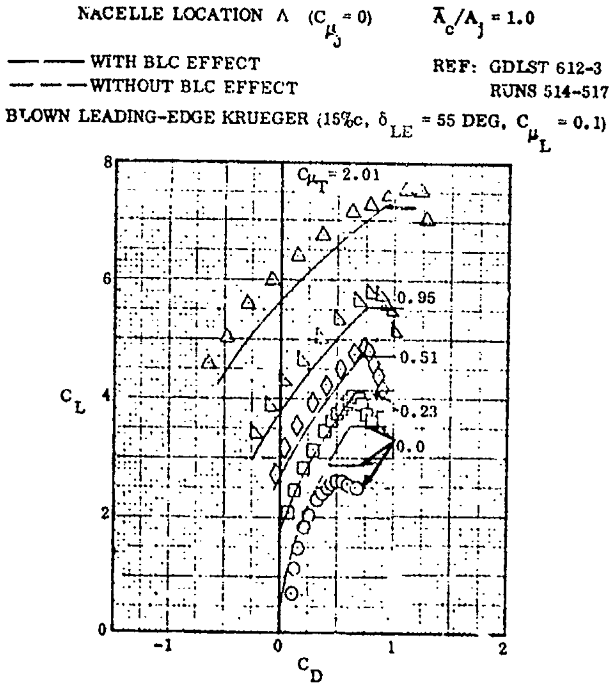

Figure 6-17. Correlation of Drag Generalized Methodology with EBF Test Data, A = 8, $\Lambda_{c/4}$ = 25 Degrees, Plain Blown Flap (δ_f = 45 Degrees)

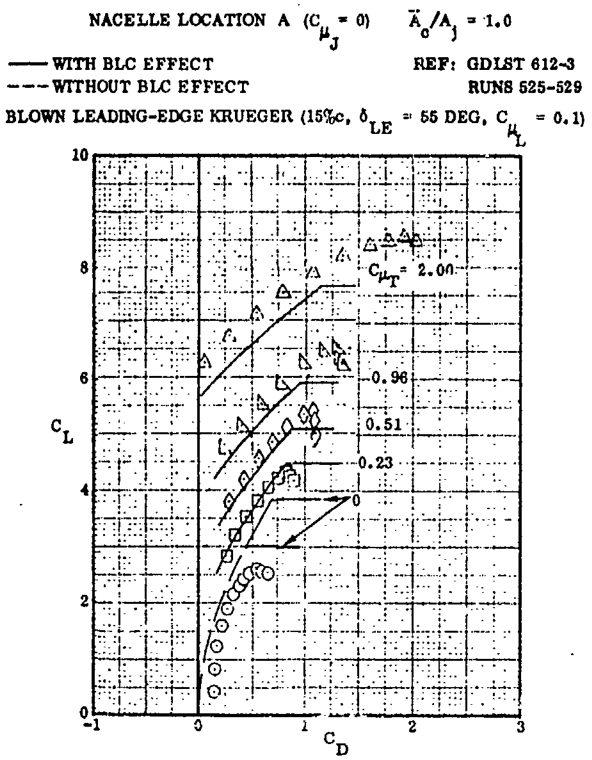

Figure 6-18. Correlation of the Drag Generalized Methodology with IBF Test Data, A = 8, $\Lambda_{c/4}$ = 25 Degrees, Plain Blown Flap (δ_f = 60 Degrees)

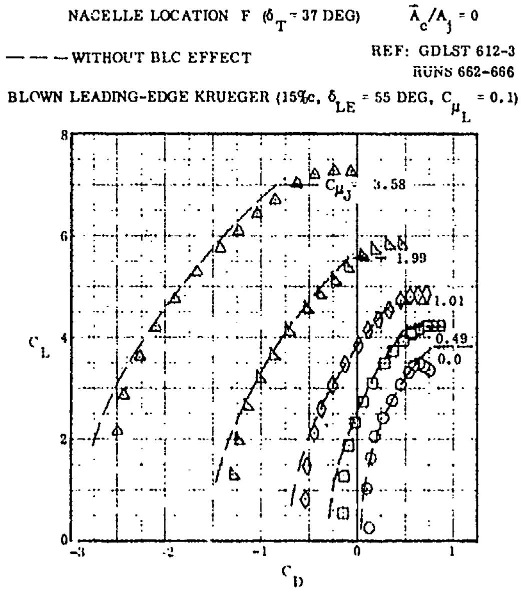

Figure 6-19. Correlation of Drag Generalized Methodology with MF/VT Test Data, A = 8, $\Lambda_{c/4}$ = 25 Degrees, Double-Slotted Flap (δ_f = 30 Degrees), Thrust Vectored Downward 37 Degrees

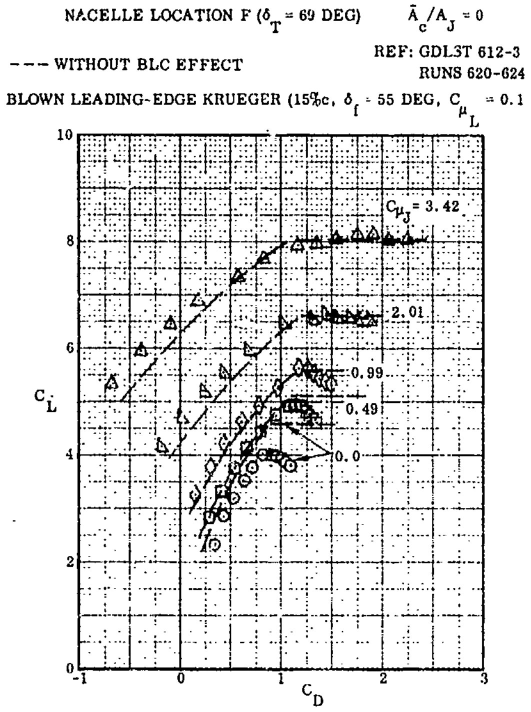

Figure 6-20. Correlation of Drag Generalized Methodology with MF/VT Test Data, A = 8, $\Lambda_{c/4}$ = 25 Degrees, Triple-Slotted Flap (δ_f = 60 Degrees), Thrust Vectored Downward 69 Degrees

SECTION 7

FLAP PITCHING MOMENT INCREMENTS

The basic problem in estimating pitching moment increments for the mechanical flap and IBF concepts is to determine the two-dimensional characteristics of their flap systems. Planform effects (i.e., aspect ratio and sweep) are overshadowed by the contributions from blowing on the IBF and by basic flap geometry on the mechanical flap. For the EBF concept, the most important consideration is to develop a rational mathematical model to represent engine exhaust plume impingement on the flaps. The effects of EBF planform variations are small in comparison with pitching moments produced by the powered lift system. The generalized methodology developed to solve these problems is discussed in the following paragraphs. Figure 7-1 shows the pitching moment methodology and the equations used.

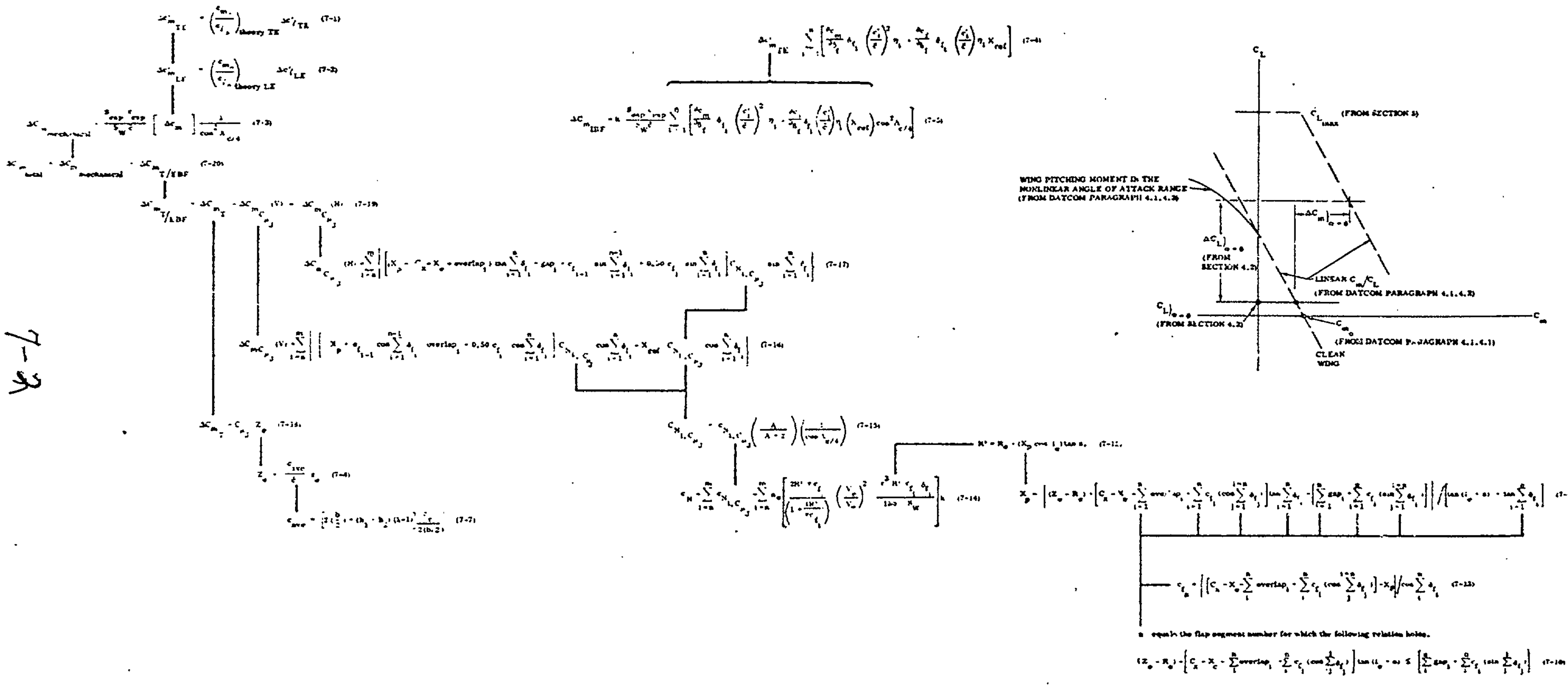

Figure 7-1. Pitching Moment Coefficient Methodology

~~7-2~~

7.1 MECHANICAL FLAP

The two-dimensional flap pitching moment increments at zero angle of attack for mechanical flaps are estimated by the methods in Reference 7-1. The methodology for pitching moments is developed parallel to the methods used for estimating the lift increments, which extend thin airfoil theory to cover multiple-slotted flaps with extensible chords. The trailing-edge flap incremental pitching moment at zero angle of attack is given by:

$$\Delta c'_{m_{TE}} = \left(\frac{c_{m_\delta}}{c_{\ell_\delta}}\right)_{\text{theory TE}} \Delta c'_{\ell_{TE}} \qquad (7\text{-}1)$$

where:

$\left(\frac{c_{m_\delta}}{c_{\ell_\delta}}\right)_{\text{theory TE}}$	is the trailing-edge flap center of pressure location from thin airfoil theory (Figure 7-2).
$\Delta c'_{\ell_{TE}}$	is the trailing-edge flap lift increment at zero angle of attack as defined by Equation 4-19. The flap efficiency factor, η, in Equation 4-19 is determined from Figures 4-8, 4-9, and 4-10 for single-, double-, and triple-slotted flaps.

The flap chord ratios and deflection angles for obtaining η from Figure 4-8, 4-10, and 4-11 are explained in Figure 4-11.

Pitching moment increment for a leading-edge flap is given by:

$$\Delta c'_{m_{LE}} = \left(\frac{c_{m_\delta}}{c_{\ell_\delta}}\right)_{\text{theory LE}} \Delta c'_{\ell_{LE}} \qquad (7\text{-}2)$$

where:

$\left(\frac{c_{m_\delta}}{c_{\ell_\delta}}\right)_{\text{theory LE}}$	is the leading edge flap center of pressure location from thin airfoil theory (Figure 7-2).
$\Delta c'_{\ell_{LE}}$	is the leading-edge flap lift increment at zero angle of attack as defined by Equation 4-22.

The three-dimensional test data on mechanical flaps did not indicate any appreciable effect of sweep. These effects are shown for power-off in Figure 7-6. An empirical correction factor was applied:

$$\Delta C'_{m_{\text{mechanical}}} = \frac{S_{exp}\, c_{exp}}{S_W\, \bar{c}} \left[\Delta c_m \right] \frac{1}{\cos^2 \Lambda_{c/4}} \qquad (7\text{-}3)$$

where:

S_W	is the wing area.
S_{exp}	is the exposed wing area
$\bar{c}$	is the mean aerodynamic chord.
c_{exp}	is the exposed mean aerodynamic chord.
Δc_m	is the two-dimensional pitching moment increment from Equation 7-1 or 7-2.

SAMPLE PROBLEM

GIVEN: Triple-Slotted Flap

FLAP GEOMETRY

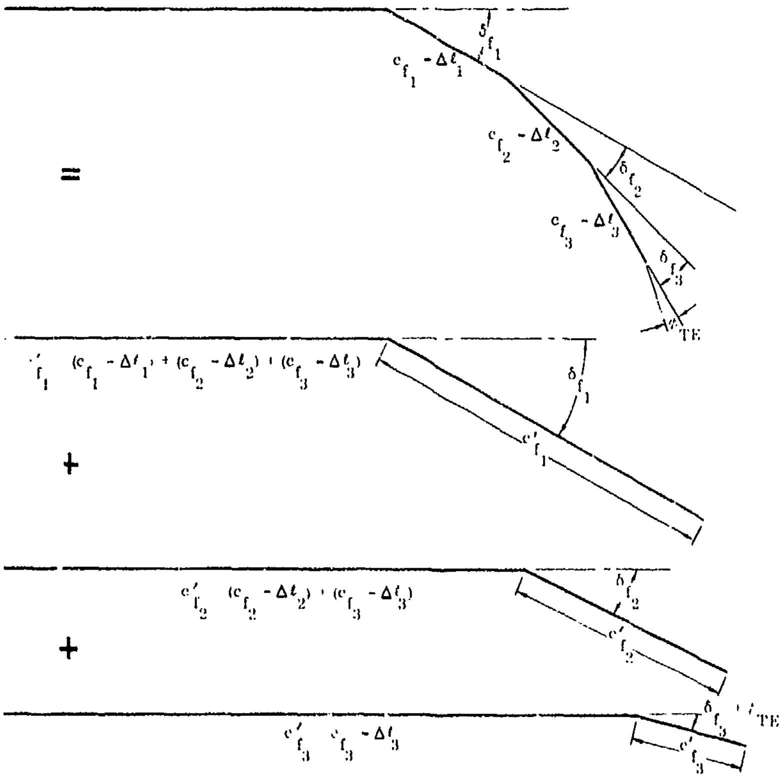

$c_x = 0.75\ \bar{c}$

$c_{f_1} = 0.287\ \bar{c}$

$c_{f_2} = 0.242\ \bar{c}$

$c_{f_3} = 0.244\ \bar{c}$

$\delta_{f_1} = 29.5$ deg

$\delta_{f_2} = 46.0$ deg

$\delta_{f_3} = 60.7$ deg

$\phi_{TE} = 0$ deg

WING GEOMETRY

$A = 8.0$ $\qquad \Lambda_{c/4} = 12.5$ deg

$S = 558$ sq in. $\qquad \bar{c} = 8.89$ in.

$S_{exp} = 480.6$ sq in. $\qquad c_{exp} = 8.44$ in.

CALCULATE:

$$c' = 1.523\ \bar{c}$$

$$\frac{c'_{f_1}}{c'} = 0.507$$

$$\frac{c'_{f_2}}{c'} = 0.319$$

$$\frac{c'_{f_3}}{c'} = 0.160$$

Obtain η from Figure 4-11 to determine Δc_{ℓ_f} from Equations 4-19 and 4-22,

then $\left(\frac{c_{m_\delta}}{c_{\ell_\delta}}\right)_{\text{Theory TE}}$ from Figure 7-2.

	c_{f_1}	c_{f_2}	c_{f_3}
η	0.77	0.77	0.77
Δc_{ℓ_f}	2.8852	3.5980	3.1831
$\left(\frac{c_{m_\delta}}{c_{\ell_\delta}}\right)_{\text{Theory TE}}$	-0.0954	-0.1488	-0.1979

Flap pitching moment increments from Equation 7-1.

$$\Delta c'_{m_{TE}} = \left(\frac{c_{m_\delta}}{c_{\ell_\delta}}\right)_{\text{theory TE}} \Delta c'_{\ell_{TE}} \qquad (7\text{-}1)$$

$$\Delta c_{m_1} = (-0.0954)\ (2.9852) = -0.2847$$

$$\Delta c_{m_2} = (-0.1488)\ (3.5980) = -0.5355$$

$$\Delta c_{m_3} = (-0.1979)\ (3.1831) = -0.6299$$

The total 2-D pitching moment increment is:

$$\Delta c_m\Big)_{\alpha = 0} = \Delta c_{m_1} + \Delta c_{m_2} + \Delta c_{m_3} = -1.4501$$

Test value = -1.4961

The three-dimensional case is calculated using Equation 7-3.

$$\Delta C'_{m_{\text{mechanical}}} = \frac{S_{\text{exp}}\ c_{\text{exp}}}{S_W\ \bar{c}} \left[\ \Delta c_m\ \right] \frac{1}{\cos^2 \Lambda_{c/4}} \qquad (7\text{-}3)$$

$$= \frac{480.6(8.44)}{558\ \ (8.89)}\ (-1.4501)\ \frac{1}{\cos^2 12.5} = -1.2440$$

Test value = -1.32

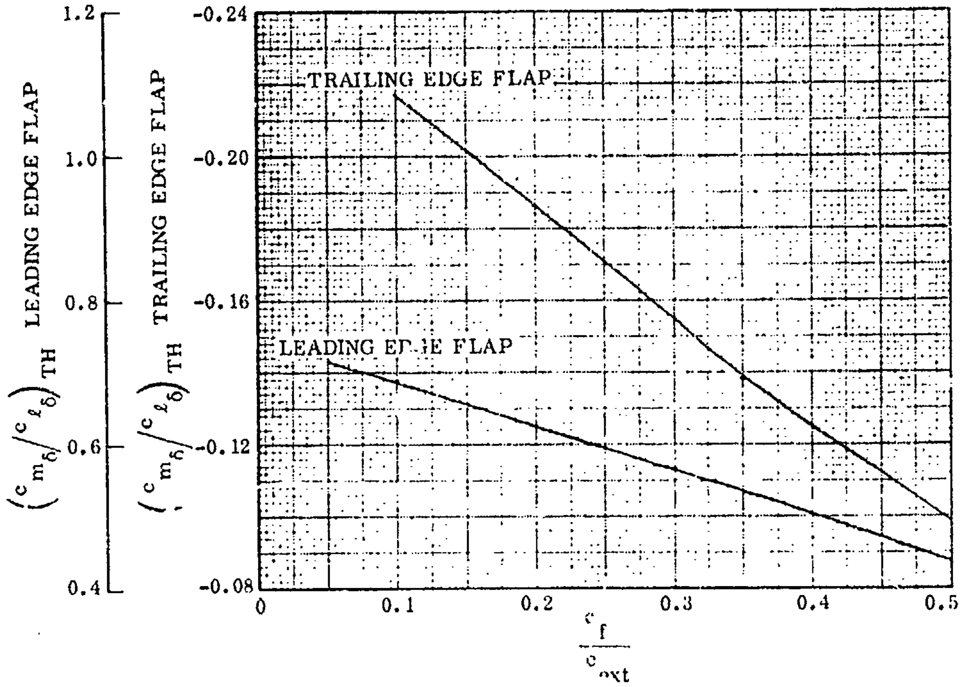

Figure 7-2. Flap Center of Pressure Location as given by Thin Airfoil Theory

7.2 INTERNALLY BLOWN FLAP

Spence's theory was used to determine two-dimensional pitching moment increments for the internally blown flap. The theory can be readily extended to include multiple-slotted flaps by methods analogous to those used for the mechanical flap. Mathematical superposition was discarded in favor of superposition as applied by the DATCOM. This was done to improve correlation. The following expression is used to calculate the moment increment.

$$\Delta c'_{m_{TE}} = \sum_{i=1}^{n} \left[\frac{\partial c_m}{\partial \delta_f} \delta_{f_i} \left(\frac{c'_i}{\bar{c}}\right)^2 \eta_i + \frac{\partial c_\ell}{\partial \delta_f} \delta_{f_i} \left(\frac{c'_i}{\bar{c}}\right) \eta_i X_{ref} \right] \qquad (7\text{-}4)$$

where:

c'_i	$= c_x + \sum_{1}^{i} c_{f_i}$, extended chord.
$\bar{c}$	is the mean aerodynamic chord.
X_{ref}	is the moment reference center as a fraction of the mean aerodynamic chord.
$\frac{\partial c_m}{\partial \delta_f}$ and $\frac{\partial c_\ell}{\partial \delta_f}$	are derivatives obtained from Figures 7-3 and 4-14.
n	is the number of flap elements from Figure 7-5.
η_i	is the efficiency factor for a flap segment at an angle δ'_{f_i} from Figure 7-4.
δ_{f_i}	is the flap segment angle in radians.
δ'_{f_i}	is equal to $\sum_{1}^{i} \delta_{f_i}$

The flap chord ratio values required to determine $\frac{\partial c_m}{\partial \delta_f}$ and $\frac{\partial c_\ell}{\partial \delta_f}$ from Figure 7-3 and 4-14, and the flap deflection angles to obtain η from Figure 7-4 are illustrated in Figure 7-5.

Changes in sweep and the percentage of spanwise flap blown are incorporated in the two-dimensional expression to form the following three-dimensional equation.

$$\Delta C_{m_{IBF}} = k \frac{S_{exp} c_{exp}}{S_W \bar{c}} \sum_{i=1}^{n} \left[\frac{\partial c_m}{\partial \delta_f} \delta_{f_i} \left(\frac{c'_i}{\bar{c}}\right)^2 \eta_i + \frac{\partial c_\ell}{\partial \delta_f} \delta_{f_i} \left(\frac{c'_i}{\bar{c}}\right) \eta_i \left(X_{ref}\right) \cos^2 \Lambda_{c/4} \right] \qquad (7\text{-}5)$$

where:

$\Lambda_{c/4}$ is the sweep at the quarter chord.

k is the span of the flaps expressed as a fraction of exposed wing span.

NACA TN4040 developed a method to three-dimensionalize two-dimensional pitching moment increments. This method was included in the IBF method and shows up as the $\cos^2 \Lambda c/4$ term.

SAMPLE PROBLEM

GIVEN: Triple-Slotted Flap with Blowing at the Knee of the First Flap Segment.

FLAP GEOMETRY

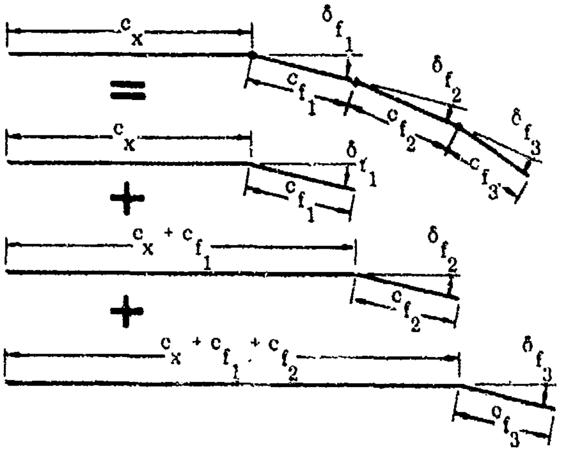

$c_x = 0.75c$

$c_{f_1} = 0.28c$ $\delta_{f_1} = 28$ deg

$c_{f_2} = 0.23c$ $\delta_{f_2} = 17$ deg

$c_{f_3} = 0.23c$ $\delta_{f_3} = 15$ deg

$$c'_i = c_x + \sum_1^i c_{f_i}$$

WING GEOMETRY

$A = 8.0$ $\Lambda_{c/4} = 12.5$ deg

$S_W = 558$ $\bar{c} = 8.30$

$S_{exp} = 480$ $c_{exp} = 8.44$

CALCULATE:

1. Flap chord ratios and deflections.

$$\frac{c_{f_1}}{c'_1} = \frac{28}{75 + 28} = 0.272$$

$$\frac{c_{f_2}}{c'_2} = \frac{23}{75 + 28 + 23} = 0.182$$

$$\frac{c_{f_3}}{c'_3} = \frac{23}{75 + 28 + 23 + 23} = 0.154$$

$$\delta_{f_1}' = \delta_{f_1} = 28 \text{ deg}$$

$$\delta_{f_2}' = \delta_{f_1} + \delta_{f_2} = 28 \text{ deg} + 17 \text{ deg} = 45 \text{ deg}$$

$$\delta_{f_3}' = \delta_{f_1} + \delta_{f_2} + \delta_{f_3} = 28 \text{ deg} + 17 \text{ deg} + 15 \text{ deg} = 60 \text{ deg}$$

2. $\frac{\partial c_\ell}{\partial \delta_f}$ and $\frac{\partial c_m}{\partial \delta_f}$ from Figures 4-14 and 7-3 for the specific flap chords and momentum coefficient and the η from Figure 7-7.

c_{f_1}/c_{ext_1}

C_{μ_T}	$\frac{\partial c_\ell}{\partial \delta_f}$	$\frac{\partial c_m}{\partial \delta_f}$	η
1.0	6.50	-3.05	0.95
2.0	8.45	-4.10	0.95
3.0	10.15	-5.10	0.95

c_{f_2}/c_{ext_2}

C_{μ_T}	$\frac{\partial c_\ell}{\partial \delta_f}$	$\frac{\partial c_m}{\partial \delta_f}$	η
1.0	5.85	-3.00	0.87
2.0	7.85	-4.15	0.87
3.0	9.65	-5.30	0.87

c_{f_3}/c_{ext_3}

C_{μ_T}	$\frac{\partial c_\ell}{\partial \delta_f}$	$\frac{\partial c_m}{\partial \delta_f}$	η
1.0	5.65	-3.0	0.80
2.0	7.65	-4.15	0.80
3.0	9.35	-5.30	0.80

3. Flap pitching moment increments from Equation 7-4.

$$\Delta c'_{m_{TE}} = \sum_{i=1}^{n} \left[\frac{\partial c_m}{\partial \delta_f} \delta_{f_i} \left(\frac{c'_i}{\bar{c}} \right)^2 \eta_i + \frac{\partial c_\ell}{\partial \delta_f} \delta_{f_i} \left(\frac{c'_i}{\bar{c}} \right) \eta_i X_{ref} \right] \qquad (7\text{-}4)$$

$c_\mu = 1.0$

$\Delta c_{m_1} = (-3.05)(0.488)(1.03)^2(0.95) + (6.5)(0.488)(1.03)(0.95)(0.25) = -0.7242$

$\Delta c_{m_2} = (-3.0)(0.296)(1.26)^2(0.87) + (5.85)(0.296)(1.26)(0.87)(0.25) = -0.7519$

$\Delta c_{m_3} = (-3.0)(0.262)(1.49)^2(0.80) + (5.65)(0.262)(1.49)(0.80)(0.25) = \underline{-0.9549}$

$\Delta c_{m_{total}} = -2.4310$

Test Value $= -2.3701$

$c_\mu = 2.0$

$\Delta c_{m_1} = (-4.10)(0.488)(1.03)^2(0.95) + (8.45)(0.488)(1.03)(0.95)(0.25) = -1.0078$

$\Delta c_{m_2} = (-4.15)(0.296)(1.26)^2(0.87) + (7.85)(0.296)(1.26)(0.87)(0.25) = -1.0599$

$\Delta c_{m_3} = (-4.15)(0.262)(1.49)^2(0.80) + (7.65)(0.262)(1.49)(0.80)(0.25) = \underline{-1.3338}$

$\Delta c_{m_{total}} = -3.4015$

Test Value $= -3.3691$

$c_\mu = 3.0$

$\Delta c_{m_1} = (-5.10)(0.488)(1.03)^2(0.95) + (10.15)(0.488)(1.03)(0.95)(0.25) = -1.2967$

$\Delta c_{m_2} = (-5.30)(0.296)(1.26)^2(0.87) + (9.65)(0.296)(1.26)(0.87)(0.25) = -1.3841$

$\Delta c_{m_3} = (-5.30)(0.262)(1.49)^2(0.80) + (9.35)(0.262)(1.49)(0.80)(0.25) = \underline{-1.7363}$

$\Delta c_{m_{total}} = -4.4171$

Test Value $= -4.3328$

4. Derivatives, efficiency factor, and flap span factor.

	C_{μ_T}	$\frac{\partial c_\ell}{\partial \delta_f}$	$\frac{\partial c_m}{\partial \delta_f}$	η	k
c_{f_1} / c'_1	1.6	7.70	-3.65	0.95	1.0
c_{f_2} / c'_2	1.6	7.20	-3.62	0.87	1.0
c_{f_3} / c'_3	1.6	7.00	-3.55	0.80	1.0

5. Three-dimensional pitching moment increments.

$$\frac{S_{exp}\, c_{exp}}{S_W\, \bar{c}} = \frac{480}{558}\;\frac{8.44}{8.80} = 0.818$$

$$\cos^2 \Lambda_{c/4} = \cos^2 12.5 = 0.953$$

$$\Delta C_{m_1} = (1)(0.818)[(-3.65)(0.488)(1.03)^2(0.95)+(7.70)(0.488)(1.03)(0.95)$$
$$(0.25)(0.953)] = -0.752$$

$$\Delta C_{m_2} = (1)(0.818)[(-3.62)(0.296)(1.26)^2(0.87)+(7.20)(0.296)(1.26)(0.87)$$
$$(0.25(0.953))] = -0.755$$

$$\Delta C_{m_3} = (1)(0.818)[(-3.55)(0.262)(1.49)^2(0.80)+(7.00)(0.262)(1.49)(0.80)$$
$$(0.25)(0.953)] = -0.925$$

The three-dimensional pitching moment increment is calculated with Equation 7-5.

$$\Delta C_{m_{IBF}} = k \; \frac{S_{exp} \, c_{exp}}{S_W \bar{c}} \sum_{i=1}^{n} \left[\frac{\partial c_m}{\partial \delta_f} \, \delta_{f_i} \left(\frac{c_i'}{\bar{c}} \right)^2 \eta_i + \frac{\partial c_\ell}{\partial \delta_f} \delta_{f_i} \left(\frac{c_i'}{\bar{c}} \right) \eta_i \left(X_{ref} \right) \cos^2 \Lambda_{c/4} \right] \quad (7\text{-}5)$$

$$\Delta C_{m_{IBF}} = \Delta C_{m_1} + \Delta C_{m_2} + \Delta C_{m_3}$$

$$= -0.752 - 0.755 - 0.925 = -2.432$$

Test value = -2.517

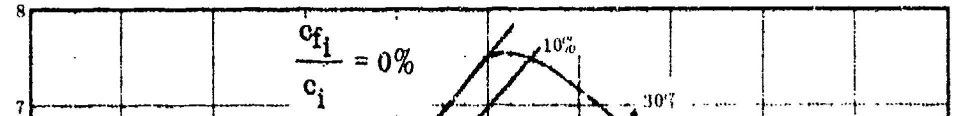

Figure 7-3. Pitching Moment Effectiveness About the Leading Edge for IBF from Spence's Theory, Two Dimensional

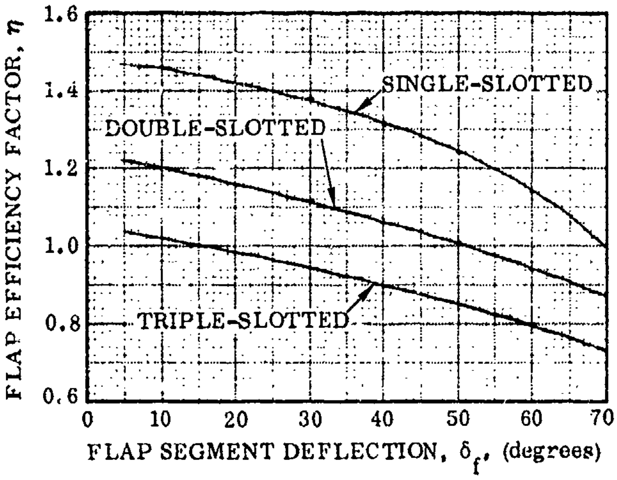

Figure 7-4. IBF Momentum Loss Chart, Two Dimensional

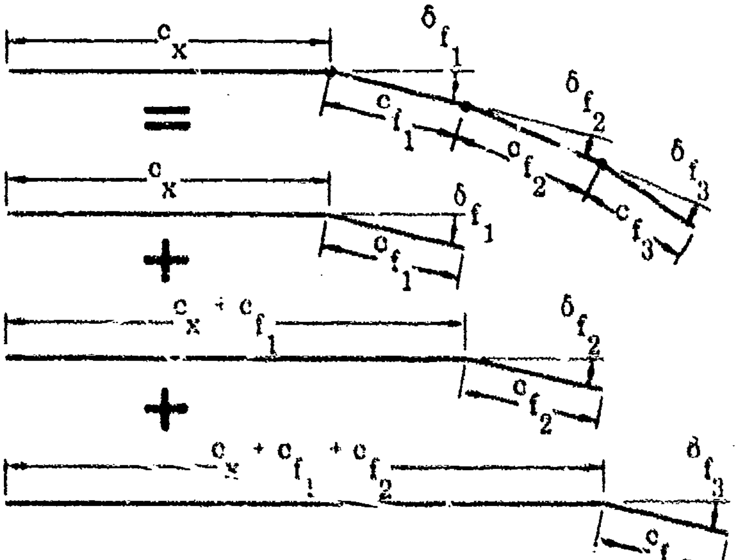

Figure 7-5. Triple-Slotted Flap Geometry

7.3 EXTERNALLY BLOWN FLAP

An EBF method was developed to predict the pitching moment increment due to a flap system that has jet engine exhaust impingement. Of the schemes attempted, none showed as much promise as the one in the following discussion. The increments are for zero angle of attack. The EBF test data is shown in Figure 7-6.

This method is totally dependent on wing-flap geometry and engine location. A totally mechanistic view of this system was adopted. The method consists of two parts:

> Part 1 calculates the contribution due that portion of the flaps influenced by the engines (Figure 7-7).
>
> Part 2 computes the portion that is not influenced by the engines.

The system for Part 1 is modeled by representing the portions of the flaps affected by the engine exhaust flow as semi-circular airfoils (Figure 7-8). The following simplifying assumptions were made:

1. No spillage along the flaps. The engine affects only the area in its expanding plume.
2. A 6-degree exhaust plume expansion angle.
3. Constant engine exhaust velocity in the plume for a specified power setting.
4. The exhaust velocity vector changes direction in the same manner as the flap segments.
5. Constant radius of the plume from its first impingement point.
6. Center of pressure at midchord for each flap segment.

Nomenclature for the flap geometry of the EBF is defined in Figure 7-9.

For constant pylon length, the vertical distance from the mean chord plane to the engine centerline relative to its local chord changes with engine spanwise location. Consequently, an average location for both engines was used.

$$c_{ave} = \left[\frac{b/2 - h_2 (1-\lambda)}{b/2} \, c_r + \frac{b/2 - h_1 (1-\lambda)}{b/2} \, c_r \right] \frac{1}{2} \qquad (7-6)$$

where:

$b/2$	is the wing semi-span.
$h_{1 \text{ or } 2}$	is the engine buttock line location.
λ	is the taper ratio.
c_r	is the wing root chord.

The equation is rearranged to the following expression:

$$c_{ave} = \left[2\left(\frac{b}{2}\right) + (h_1 + h_2)(\lambda - 1)\right]\frac{c_r}{2(b/2)} \qquad (7\text{-}7)$$

The vertical distance from MCP to the centerline of the engine at the exhaust plane for the average location, Z_e, is defined as a fraction of actual z_e:

$$Z_e = \frac{c_{ave}}{\bar{c}} z_e \qquad (7\text{-}8)$$

By affixing the origin of the coordinate system on the mean chord plane a distance X_e behind the leading edge, the equation describing each individual flap segment was defined as:

$$f_{z_m} = -x \tan \sum_{i}^{m} \delta_{f_i} + \left[C_x - X_e - \sum_{i}^{m} \text{overlap}_i + \sum_{i}^{m} c_{f_i} \left(\cos \sum_{j=1}^{i} \delta_{f_i}\right)\right] \tan \sum_{i}^{m} \delta_{f_i}$$

$$- \left[\sum_{i}^{m} \text{gap}_i + \sum_{i}^{m} c_{f_i} \left(\sin \sum_{j}^{i} \delta_{f_i}\right)\right] \qquad (7\text{-}9)$$

where:

m	is the number of flap elements.
C_x	is the distance from the leading edge to the leading edge of the first flap.
X_e	is the horizontal distance from the leading edge to the engine exhaust plane.
overlap_i	is the overlap between successive elements.
gap_i	is the gap between successive elements.

To determine the flap segment, n, on which the upper boundary of the engine exhaust first impinges, determine the value of n for which the following equation is true:

$$(Z_e - R_e) - \left[C_x - X_c - \sum_i^n \text{overlap}_i + \sum_i^n c_{f_i} \left(\cos \sum_j^i \delta_{f_j}\right)\right] \tan(i_e + s)$$

$$\leq \left[\sum_i^n \text{gap}_i + \sum_i^n c_{f_i} \left(\sin \sum_j^i \delta_{f_j}\right)\right] \qquad (7\text{-}10)$$

If no flap segment is in the exhaust flow, the scheme reduces to the mechanical flap model. Once the flap segment number is determined, the horizontal distance from the engine exhaust plane to the impingement point, X_p, is calculated:

$$X_p = \left\{(Z_e - R_e) + \left[C_x - X_e - \sum_{i=1}^n \text{overlap}_i + \sum_{i=1}^n c_{f_i} \left(\cos \sum_{j=1}^{i=n} \delta_{f_j}\right)\right] \tan \sum_{i=1}^n \delta_{f_i}\right.$$

$$\left. - \left[\sum_{i=1}^n \text{gap}_i + \sum_{i=1}^n c_{f_i} \left(\sin \sum_{j=1}^{i=n} \delta_{f_i}\right)\right]\right\} \Big/ \left[\tan(i_e + s) + \tan \sum_{i=1}^n \delta_{f_i}\right] \qquad (7\text{-}11)$$

The radius of the circular wing, R', is computed by:

$$R' = R_e + (X_p \cos i_e) \tan s, \qquad (7\text{-}12)$$

The portion of the n^th flap segment that is in the exhaust flow is calculated by:

$$c_{f_n} = \left\{\left[C_x - X_e - \sum_i^n \text{overlap}_i + \sum_i^n c_{f_i} \left(\cos \sum_j^{i=n} \delta_{f_j}\right)\right] \cdot X_p\right\} \Big/ \cos \sum_i^n \delta_{f_i} \qquad (7\text{-}13)$$

This value should be used for the effective chord of the nth flap segment in the remaining calculations.

The normal force on each flap segment for a given value of C_{μ_J} is determined from the modified Ribner formula for ring airfoils in nonaxial flow (Reference 7-2).

$$c_N = \sum_{i=n}^{m} c_{N_{i,C_{\mu_J}}} = \sum_{i=n}^{m} n_e \left[\frac{2R'/\pi c_{f_i}}{\left(1 + \frac{4R'}{\pi c_{f_i}}\right)} \left(\frac{V_e}{V_\infty}\right)^2 \frac{\pi^3 R' \; c_{f_i} \; \delta_{f_i}}{180 \quad S_W} \right] k \qquad (7\text{-}14)$$

where:

$c_{N_{i,C_{\mu_J}}}$ is the normal force coefficient for each flap segment.

n_e is the number of engines.

V_e is the engine exhaust velocity.

V_∞ is the free stream velocity.

k is equal to 0,625 $(C_{\mu_J})^{1/2}$

To compute the moment increment due to the externally blown flap, the normal force components times their respective moment arms are summed, assuming the normal forces act at the midchord of each segment.

Sweep and aspect ratio corrections are applied by:

$$C_{N_{i,C_{\mu_J}}} = c_{N_{i,C_{\mu_J}}} \left(\frac{A}{A+2}\right)\left(\frac{1}{\cos \Lambda_{c/4}}\right) \qquad (7\text{-}15)$$

The moment due to vertical force components is:

$$\Delta C_{mC_{\mu_J}}(V) = \sum_{i=n}^{m} \left\{ \left[X_p + c_{f_{i-1}} \cos \sum_{i=1}^{n-1} \delta_{f_i} - \text{overlap}_i \right.\right.$$

$$\left.\left. + 0.50 \; c_{f_i} \cos \sum_{i=1}^{n} \delta_{f_i} \right] C_{N_{i,C_{\mu_J}}} \cos \sum_{i=1}^{n} \delta_{f_i} - X_{ref} \; C_{N_{i,C_{\mu_J}}} \cos \sum_{i=1}^{n} \delta_{f_i} \right\} \qquad (7\text{-}16)$$

where:

X_{ref} is moment reference center.

The moment due to horizontal force components is:

$$\Delta C_{m_{C_{\mu_J}}}(H) = \sum_{i=n}^{m} \left\{ \left[(X_p - C_x + X_e + \text{overlap}_i) \tan \sum_{i=1}^{n} \delta_{f_i} + \text{gap}_i \right. \right.$$

$$\left. \left. + c_{f_{i-1}} \sin \sum_{i=1}^{n-1} \delta_{f_i} + 0.50\, c_{f_i} \sin \sum_{i=1}^{n} \delta_{f_i} \right] C_{N_{i,C_{\mu_J}}} \sin \sum_{i=1}^{n} \delta_{f_i} \right\} \qquad (7\text{-}17)$$

The direct thrust moment is:

$$\Delta C_{m_T} = C_{\mu_J} Z_e \qquad (7\text{-}18)$$

The moment due to the EBF portion is:

$$\Delta C_{m_{T/EBF}} = \Delta C_{m_T} - \Delta C_{m_{C_{\mu_J}}}(V) - \Delta C_{m_{C_{\mu_J}}}(H) \qquad (7\text{-}19)$$

The moment due to the area of the flap system that is undisturbed by the exhaust flow is computed with the linear theory previously discussed for the mechanical flap. The total expression, then, is:

$$\Delta C_{m_{total}} = \Delta C_{m_{mechanical}} + \Delta C_{m_{T/EBF}} \qquad (7\text{-}20)$$

SAMPLE PROBLEM

GIVEN: Triple-slotted flap on Wing No. 1 at Position E_3P_4

GEOMETRY

CONFIGURATION

$A = 8.0$ $\Lambda_{c/4} = 12.5$ deg $\lambda = 0.3874$

$S_W = 7.0534\,\bar{c}^2$ $\bar{c} = 8.895$ in. $c_r = 12.02$ in.

$b/2 = 33.406$ in. $h_1 = 10.40$ in. $h_2 = 17.5$ in.

$C_x = 0.75\bar{c}$ $X_e = 0.0\bar{c}$ $X_{ref} = 0.25\bar{c}$

$R_e = 0.1485\bar{c}$ $s = 6.0$ deg $i_e = 1.6$ deg

$z_e = 0.285\bar{c}$ $n_e = 4$ $m = 3$

FLAP (Same as in Sample Problem in Section 7.1)

$c_{f_1} = 0.287c$ $c_{f_2} = 0.242c$ $c_{f_3} = 0.244c$

$\delta_{f_1} = 29.5$ deg $\delta_{f_2} = 16.5$ deg $\delta_{f_3} = 14.7$ deg

$\text{Overlap}_1 = 0.0\bar{c}$ $\text{Overlap}_2 = 0.005\bar{c}$ $\text{Overlap}_3 = 0.009\bar{c}$

$\text{gap}_1 = 0.022\bar{c}$ $\text{gap}_2 = 0.022\bar{c}$ $\text{gap}_3 = 0.022\bar{c}$

ENGINE CHARACTERISTICS ($V_\infty = 115$ ft/sec)

$C_{\mu_J} = 1.0$

$V_e = 728$ ft/sec

CALCULATE:

1. Vertical distance from mean chord plane to centerline of engine at the exhaust plane with Equations 7-7 and 7-8.

$$c_{ave} = \left[2\left(\frac{b}{2}\right) + (h_1 + h_2)(\lambda - 1)\right] \frac{c_r}{2(b/2)}$$

$$= \left[2(33.406) + (10.4 + 17.5)(0.3874 - 1)\right] \frac{12.02}{2(33.406)} = 8.9451$$

and

$$Z_e = \frac{z_e}{\bar{c}} \, c_{ave}$$

$$= \frac{0.285}{8.895} (8.9451) = 0.2865$$

2. Flap segment on which the upper boundary of the engine exhaust first impinges with Equation 7-10. Try n = 1.

$$(Z_e - R_e) - \left[C_x - X_c - \sum_i^n \text{overlap}_i + \sum_i^n c_{f_i} \left(\cos \sum_j^i \delta_{f_j}\right)\right] \tan(i_c + s)$$

$$\leq \left[\sum_i^n \text{gap}_i + \sum_i^n c_{f_i} \left(\sin \sum_j^i \delta_{f_j}\right)\right]$$

Substituting:

$$(0.2866 - 0.1485) - \left[0.75 - 0.0 - 0.0 + 0.287 \cos 29.5\right].$$

$$\tan(1.6 + 6.0) \leq 0.022 + 0.287 \sin 29.5$$

Since $0.0047 \leq 0.1633$, the exhaust boundary does impinge on the first segment and n = 1.

3. Horizontal distance from the engine exhaust plane to the impingement point with Equation 7-11. (For this case, n = 1.)

$$X_p = \left\{ (Z_e - R_e) + \left[C_x - X_e - \sum_{i=1}^{n} \text{overlap}_i + \sum_{i=1}^{n} c_{f_i} \left(\cos \sum_{j=1}^{i=n} \delta_{\cdot}\right) \right] \tan \sum_{i=1}^{n} \delta_{f_i} - \left[\sum_{i=1}^{n} \text{gap}_i + \sum_{i=1}^{n} c_{f_i} \left(\sin \sum_{j=1}^{i=n} \delta_{f_i}\right) \right] \right\} \Big/ \left[\tan (i_e + s) + \tan \sum_{i=1}^{n} \delta_{i} \right]$$

$$X_p = \Big| (0.2866 - 0.1485) + (0.75 - 0.0 + 0.287 \cos 29.5) \tan 29.5$$

$$-(0.022 + 0.287 \sin 29.5) \Big| \; \Big| \tan (1.6 + 6.0) + \tan 29.5 \Big|$$

$$= 0.7728$$

4. Radius of the circular wing with Equation 7-12.

$$R' = R_c + (X_p \cos i_e) \tan s.$$

$$= 0.1485 + (0.7728 \cos 1.6) \tan 6.0$$

$$= 0.2297$$

5. Portion of the first flap segment that is in the exhaust flow with Equation 7-13. (For this case, n = 1.)

$$c_{f_n} = \left| \left[C_x - X_e - \sum_{i}^{n} \text{overlap}_i + \sum_{i}^{n} c_{f_i} \left(\cos \sum_{j}^{i=n} \delta_{f_j}\right) \right] - X_p \right| \Big/ \cos \sum_{i}^{n} \delta_{f_i}$$

$$= \Big| (0.75 - 0.0 - 0.0 + 0.287 \cos 29.5) - 0.7728 \Big| \Big/ \cos 29.5$$

$$= 0.2608$$

6. Normal force on each flap segment from Equation 7-14.

$$c_N = \sum_{i=n}^{m} c_{N_{i,C_{\mu_J}}} = \sum_{i=n}^{m} n_e \left[\frac{2R'/\pi c_{f_i}}{\left(1+\frac{4R'}{\pi c_{f_i}}\right)} \left(\frac{V_e}{V_\infty}\right)^2 \frac{\pi^3 R' c_{f_i} \delta_{f_i}}{180 \quad S_W} \right] k$$

$$c_{N_{1,1}} = (4) \left[\frac{2(0.2297)/\pi(0.2608)}{1+\{4(0.2297)\ /\pi(0.2608)\}} \left(\frac{728}{115}\right)^2 \frac{\pi^3 (0.2297)(0.2608)(29.5)}{180(7.0534)} \right]$$

$$\left[(0.625)(1.0)\right] = 1.1428$$

Similarly,

$$c_{N_{2,1}} = 0.6140$$

$$c_{N_{3,1}} = 0.5495$$

7. Wing aspect ratio and sweep effects for each flap section with Equation 7-15.

$$C_{N_{i,C_{\mu_J}}} = c_{N_{i,C_{\mu_J}}} \left(\frac{A}{A+2} \right) \left(\frac{1}{\cos \Lambda_{c/4}} \right)$$

$$C_{N_{1,1}} = 1.1428 \left(\frac{8.0}{8.0+2} \right) \left(\frac{1}{\cos (12.5)} \right) = 0.9364$$

Similarly,

$$C_{N_{2,1}} = 0.5033$$

$$C_{N_{3,1}} = 0.4504$$

8. Moment increments for each flap section, and sum with Equations 7-16 and 7-17.

$$\Delta C_{mC_{\mu_J}}(V) = \sum_{i=n}^{m} \left\{ \left[X_p + c_{f_{i-1}} \cos \sum_{i=1}^{n-1} \delta_{f_i} - \text{overlap}_i + 0.50\, c_{f_i} \cos \sum_{i=1}^{n} \delta_{f_i} \right] C_{N_{i,C_{\mu_J}}} \cos \sum_{i=1}^{n} \delta_{f_i} - X_{ref}\, C_{N_{i,C_{\mu_J}}} \cos \sum_{i=1}^{n} \delta_{f_i} \right\}$$

$$\Delta C_{m_{C_{\mu_J}}}(V) = \sum_{i=n}^{m} \Delta C_{m_{n,C_{\mu_J}}}(V)$$

$$\Delta C_{m_{1,1}}(V) = \left[0.7728 + 0.0 - 0.0 + 0.50\,(0.2608) \cos 29.5\right] (0.9364) \cos 29.5 - (0.25)(0.9364) \cos 29.5 = 0.519$$

Similarly,

$$\Delta C_{m_{2,1}}(V) = 0.289$$

$$\Delta C_{m_{3,1}}(V) = 0.212$$

$$\Delta C_{m_{C_{\mu_J}}}(V) = (0.519 + 0.289 + 0.212) = 1.020$$

$$\Delta C_{m_{C_{\mu_J}}}(H) = \sum_{i=n}^{m} \left\{ \left[(X_p - C_x + X_e + \text{overlap}_i) \tan \sum_{i=1}^{n} \delta_{f_i} + \text{gap}_i + c_{f_{i-1}} \sin \sum_{i=1}^{n-1} \delta_{f_i} + 0.50\, c_{f_i} \sin \sum_{i=1}^{n} \delta_{f_i} \right] C_{N_{i,C_{\mu_J}}} \sin \sum_{i=1}^{n} \delta_{f_i} \right\} \tag{7-17}$$

$$\Delta C_{m_{C_{\mu_J}}} (H) = \sum_{i=n}^{m} \Delta C_{m_{n,C_{\mu_J}}} (H)$$

$$\Delta C_{m_{1,1}} (H) = \Big[(0.7728 - 0.75 + 0.0 + 0.0) \quad \tan 29.5$$

$$+ 0.022 + 0.0 + 0.50\,(0.2608) \sin 29.5 \Big] (0.9364) \sin 29.5 = 0.0457$$

Similarly,

$$\Delta C_{m_{2,1}} (H) = 0.0986$$

$$\Delta C_{m_{3,1}} (H) = 0.1915$$

$$\Delta C_{m_{C_{\mu_J}}} = 0.0457 + 0.0986 + 0.1915 = 0.3358$$

9. Direct thrust moment with Equation 7-18.

$$\Delta C_{m_T} = C_{\mu_J} \; Z_e$$

$$\Delta C_{m_T} = 1.0\,(0.2865) = 0.2865$$

10. Total moment due to the EBF with Equation 7-19.

$$\Delta C_{m_{T/EBF}} = \Delta C_{m_T} - \Delta C_{m_{C_{\mu_J}}}(V) - \Delta C_{m_{C_{\mu_J}}}(H)$$

$$= 0.2865 - 1.020 - 0.3358$$

$$= -1.07$$

The mechanical flap increment from the sample problem in Section 7.1 is equal to -1.244. The total moment increment is determined with Equation 7-20.

$$\Delta C_{m_{total}} = \Delta C_{m_{mechanical}} + \Delta C_{m_{T/EBF}}$$

$$= -1.244 - 1.07 = -2.314$$

Test value = -2.395.

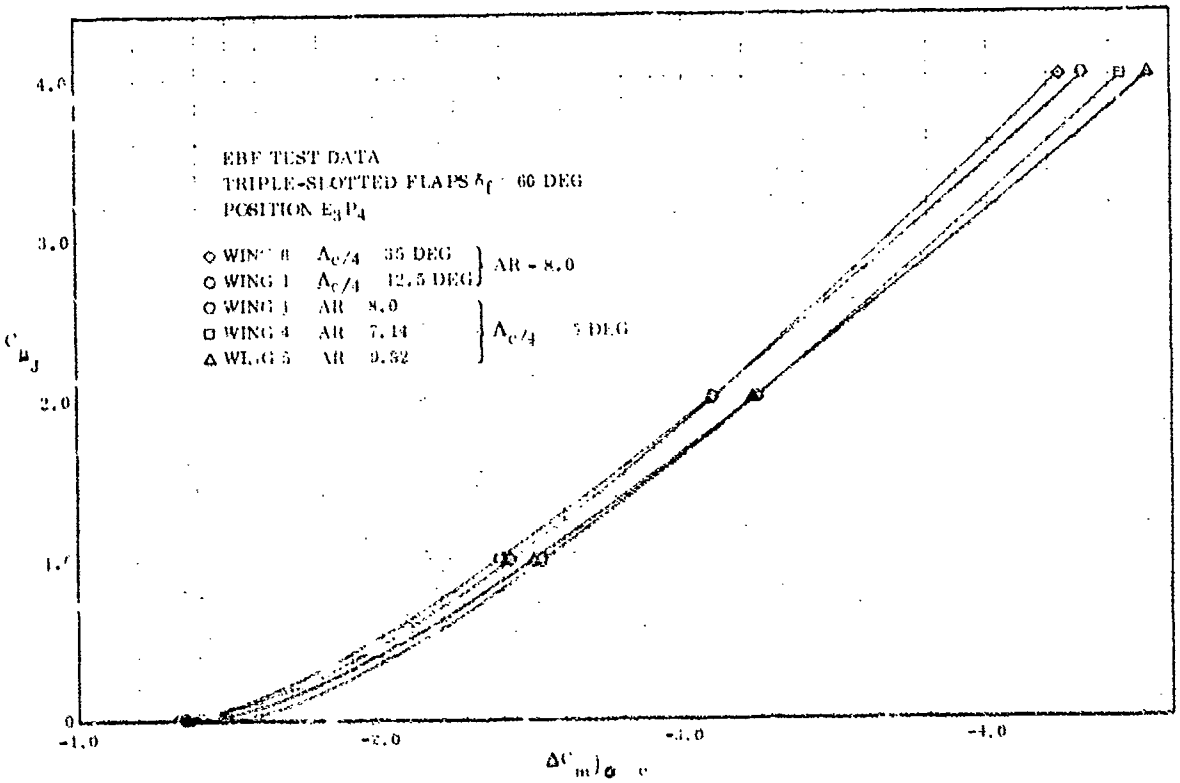

Figure 7-6. Effect of Aspect Ratio and Sweep on EBF Pitching Moment Increments

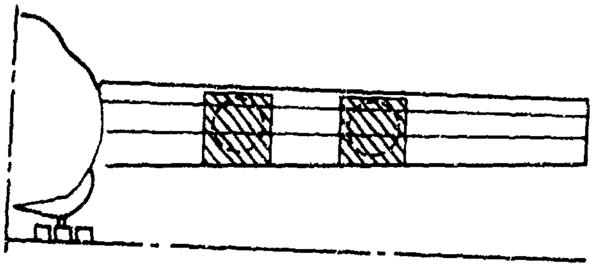

Figure 7-7. Flap Area Affected by the Engines on an EBF System

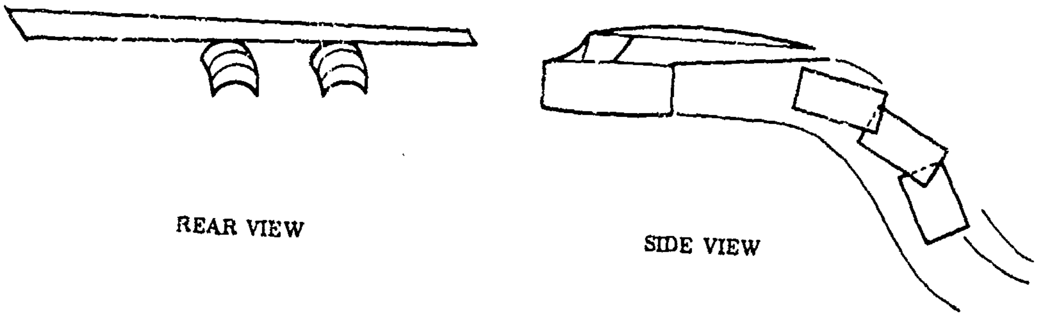

Figure 7-8. Representation of Engine Exhaust with Semicircular Airfoils

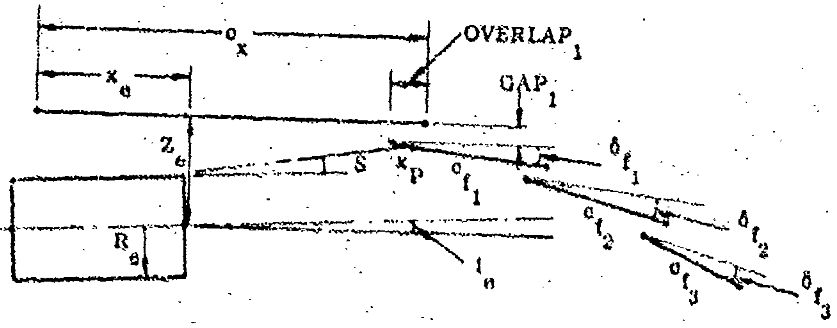

Figure 7-9. Definition of Flap Geometry for EBF

7.4 CORRELATION OF THREE-DIMENSIONAL FLAP INCREMENTS

Tables 7-1 through 7-3 show the correlations with test data for the mechanical, internally blown, and externally blown flaps. Table 7-1 shows the various combinations of flap configuration, aspect ratio and sweep for the mechanical flaps that were tested and correlated. Table 7-2 presents combinations of flap configuration, momentum coefficient, sweep, and aspect ratio for the internally blown flap. Table 7-3 has the added factor of engine configuration and position for the externally blown flap case.

Table 7-1. Mechanical Flap Data Correlation

δ_f (deg)	Flap Slots	A	$\Lambda_{c/4}$ (deg)	$\Delta C_m)_{\alpha=0}$ Test	$\Delta C_m)_{\alpha=0}$ Calculated	% Error
30	Double	8	12.5	-0.3965	-0.3965	14.2
60	Double	8	12.5	-0.9217	-0.6700	27.3
60	Triple	8	12.5	-1.3282	-1.2240	7.3
30	Single	8	25	-0.1806	-0.2614	44.7
60	Single	8	25	-0.1883	-0.3037	61.3
30	Double	8	25	-0.4888	-0.4836	1.0
60	Double	8	25	-0.9619	-0.7420	22.9
60	Triple	8	25	-1.4293	-1.3513	5.5
30	Double	9.5	25	-0.6215	-0.4685	24.6
60	Double	9.5	25	-0.9123	-0.7286	20.1
60	Triple	9.5	25	-1.4096	-1.3249	6.0
30	Double	7.14	25	-0.5804	-0.4922	15.2
60	Double	7.14	25	-0.8914	-0.7513	15.6
60	Triple	7.14	25	-1.3534	-1.3696	1.2
30	Double	8	35	-0.5800	-0.5638	2.9
60	Double	8	35	-0.9097	-0.8905	2.1
60	Triple	8	35	-1.3208	-1.5672	18.6

$$\text{Average Error} = \sum \frac{|\ \%\ \text{error}\ |}{n} = 17.1$$

Table 7-2. Internally Blown Flap Data Correlation

δ_f (deg)	Flap Slots	C_μ	$\Lambda_{c/4}$ (deg)	AR	k	$\Delta C_m)_{\alpha=0}$ Test	$\Delta C_m)_{\alpha=0}$ Calculated	% Error
30	Single	1	12.5	8.0	1.0	-1.1863	-1.11	6.4
30	Single	2	12.5	8.0	1.0	-1.434	1.32	7.9
30	Plain	1	12.5	8.0	1.0	-0.9519	-0.967	1.7
30	Plain	2	12.5	8.0	1.0	-1.354	-1.37	1.2
60	Plain	1	12.5	8.0	1.0	-1.59	-1.67	5.0
60	Plain	2	13.5	8.0	1.0	-2.240	-2.33	4.0
30	Plain	1	35.0	8.0	1.0	-1.129	-1.13	0.8
30	Plain	2	25.0	8.0	1.0	-1.591	-1.58	0.6
30	Plain	1	25.0	8.0	0.81	-0.888	-0.906	2.0
30	Plain	2	35.0	8.0	0.81	-1.298	-1.28	1.4
45	Plain	1	25.0	8.0	1.0	-1.564	-1.47	6.0
45	Plain	2	35.0	8.0	1.0	-2.159	-2.17	0.5
60	Plain	1	25.0	8.0	1.0	-1.888	-1.81	4.1
60	Plain	2	25.0	8.0	1.0	2.639	-2.48	6.0
60	Plain	1	25.0	8.0	0.81	1.440	-1.47	2.1
60	Plain	2	25.0	8.0	0.81	2.041	2.01	1.5

$$\text{Average Error} = \sum \frac{|\%\ \text{error}|}{n} = 3.19$$

Table 7-3. Externally Blown Flap Data Summary Substantiation Correlation

	Flap Slots	Engine Position	$\Lambda_{c/4}$	AR	C_{μ_J}	$\Delta C_m)_{\alpha=0}$ Test	$\Delta C_m)_{\alpha=0}$ Calculated	% Error
60	Triple	E_3P_4*	12.5	8.0	1	-2,395	-2,473	3.3
		E_3P_4*	12.5	8.0	2	-3,093	-3,126	1.1
		E_3P_4*	12.5	8.0	4	-4,316	-4,192	2.9
60	Double	E_3P_4*	12.5	8.0	1	-1,7673	-1,667	5.7
		E_3P_4*	12.5	8.0	2	-2,288	-2,213	3.3
		E_3P_4*	12.5	8.0	4	-3,124	-3,091	1.1
30	Double	E_3P_4*	25	8.0	1	-1.0013	-1,059	5.8
		E_3P_4*	25	8.0	2	-1.247	-1,377	10.4
		E_3P_4*	25	8.0	4	-1,594	-1,383	13.2
		E_3P_4*	25	9.519	1	-0,9235	-1.004	8.7
		E_3P_4*	25	9.519	2	-1,0431	-1,2829	23.0
		E_3P_4*	25	9.519	4	-1,2018	-1,2360	2.8
60	Double	E_3P_4*	25	9.519	1	-1,8238	-1,6035	12.1
		E_3P_4*	25	9.519	2	-2,3306	-2,1147	9.3
		E_3P_4*	25	9.519	4	-3,1516	-2,9306	7.0
60	Triple	E_3P_4*	25	9.519	1	-2,538	-2,3522	7.3
		E_3P_4*	25	9.519	2	-3,2379	-2,9547	8.7
		E_3P_4*	25	9.519	4	-4,4362	-3,9203	11.4
30	Double	E_3P_4*	25	7.14	1	-0,8698	-1.1328	30.2
		E_3P_4*	25	7.14	2	-0,9777	-1,499	53.3
		E_3P_4*	25	7.14	4	-1,1383	-1,564	37.4
60	Double	E_3P_4*	25	7.14	1	-1,8966	-1,7120	9.7
		E_3P_4*	25	7.14	2	-2,4133	-2,3057	4.5
		E_3P_4*	25	7.14	4	-3,3385	-3,2692	2.1
60	Triple	E_3P_4*	25	7.14	1	-2,5033	-2,4719	1.3
		E_3P_4*	25	7.14	2	-3,2313	-3,169	1.9
		E_3P_4*	25	7.14	4	-4,5320	-4,3127	4.8
30	Double	E_3P_4*	35	8.0	1	-0,8654	-1,1347	31.1
		E_3P_4*	35	8.0	2	-0,9857	-1,5246	54.7
		E_3P_4*	35	8.0	4	-1,1463	-1,5585	36.0
60	Double	E_3P_4*	35	8.0	1	-1,8036	-1,6745	7.2
		E_3P_4*	35	8.0	2	-2,3096	-2,2572	2.3
		E_3P_4*	35	8.0	4	-3,1212	-3,1997	2.5
	Triple	E_3P_4*	35	8.0	1	-2,4219	-2,3851	1.5
		E_3P_4*	35	8.0	2	-3,0923	-3,0726	0.7
		E_3P_4*	35	8.0	4	-4,2465	-4,1613	2.0
	Triple	E_7P_5†	12.5	8.0	1	-1,6116	-1,7158	6.7
		E_7P_5†	12.5	8.0	2	-1,7474	-1,7852	2.2
		E_7P_5†	12.5	8.0	4	-1,8496	-1,7819	3.7
	Triple	E_7P_5†	25	8.0	1	-1,5947	-1,5307	4.0
		E_7P_5†	25	8.0	2	-1,7123	-1,4959	2.6
		E_7P_5†	25	8.0	4	-1,6350	-1,3085	20.0

Average error = $\sum \frac{|\%\ \text{error}|}{n}$ = 10.94

---

* E_3P_4 - Short Cowl, Short Pylon

† E_7P_5 = Long Cowl, Long Pylon

SECTION 8

DOWNWASH

A simple, universal procedure is presented for the prediction of downwash at the horizontal tail. The procedure was developed on the basis of the conclusions and data trends determined from the downwash data analysis presented in Section 6 of Reference 8-1 and is shown in Figure 8-1. The referenced data analysis and the test data provided a sound basis for development of the downwash calculation procedure. Of fundamental importance is the fact that a major portion of the testing was accomplished using an auxiliary rake probe to measure tail flow-field characteristics for a wide variety of tail-off model configurations. The results from approximately 560 cases are summarized to substantiate the use of the procedure for 15 combinations of wing geometry, trailing-edge flap configuration, and type of lift augmentation system.

Static calibration runs provide data to determine the thrust recovery factor, r, and the turning angle, Θ, of the thrust vector. The availability of these thrust parameters for each configuration permits the direct thrust portion, $C_{L_{DT}}$, of the total lift coefficient, C_L, to be determined from one of the following expressions.

$$C_{L_{DT}} = C_{\mu_J} (r) \sin (\alpha_W + \Theta + i_W) \qquad (8\text{-}1)$$

or

$$C_{L_{DT}} = C_{\mu_T} (r) \sin (\alpha_W + \Theta + i_W) \qquad (8\text{-}2)$$

where:

C_{μ_J}	is the thrust coefficient (EBF or MF/VT).
C_{μ_T}	is the momentum coefficient (IBF).
α_W	is wing angle of attack.
i_W	is wing incidence angle.

The total lift coefficient attributable to direct thrust is subtracted from the total lift coefficient to determine the aerodynamic lift coefficient, $C_{L_{aero}}$.

The data analysis presented in Reference 3-11 indicates that the downwash behind a wing with a powered lift system remains a function of aerodynamic lift coefficient. Further, if proper adjustment is made to account for the downward displacement of

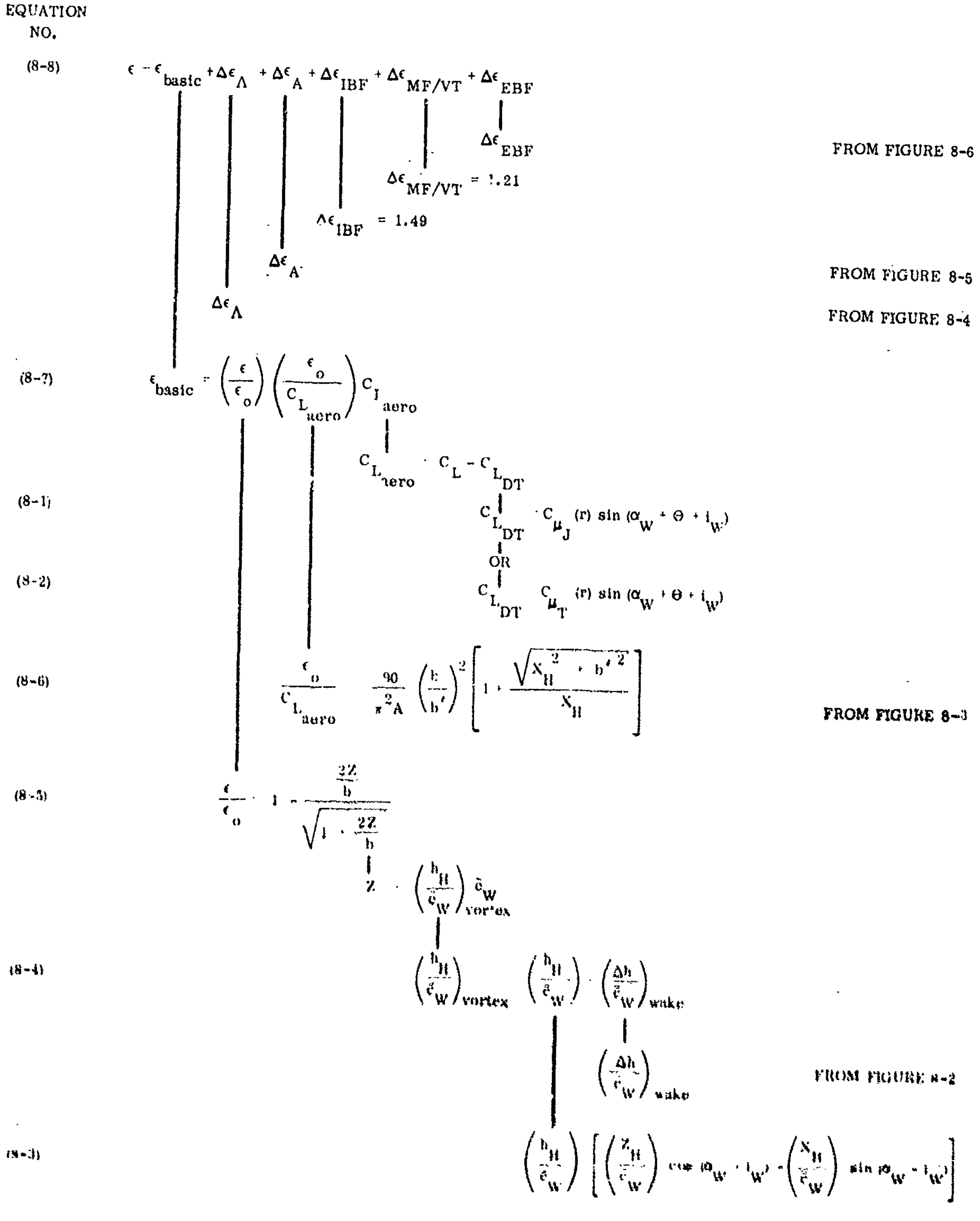

Figure 8-1. Downwash Methodology

the wing wake below the vortex plane due to increasing wing angle of attack, the downwash varies in a manner closely resembling the variation predicted by lifting-line theory for elliptical wing loading.

The adequacy of the procedure was tested with variations of wing aspect ratio and sweep angle. Displacement of the wing wake with respect to the vortex plane, at several longitudinal positions where the downwash angle had been measured, was represented as a function of wing normalized angle of attack. The wake displacement values were determined by an rms averaging of the values required to obtain perfect agreement between calculated and measured downwash angle. The final normalized version of the resulting wake displacement curves are presented in Figure 8-2. The wing angle of attack at which maximum aerodynamic lift coefficient, $\alpha_{W}\left(C_{L_{aero}}\right)_{max}$, is attained was used as the normalization factor for α_W. The normalized vertical displacement of any point from 0.25 $\bar{c}_W$ in stability axes was determined by using the following axis rotation equation.

$$\left(\frac{h_H}{\bar{c}_W}\right) = \left[\left(\frac{Z_H}{\bar{c}_W}\right)\cos\left(\alpha_W - i_W\right) - \left(\frac{X_H}{\bar{c}_W}\right)\sin\left(\alpha_W - i_W\right)\right] \qquad (8\text{-}3)$$

where:

Z_H is vertical displacement from 0.25 $\bar{c}_W$ in body-axis system.

X_H is longitudinal displacement from 0.25 $\bar{c}_W$ in body-axis system.

$\bar{c}_W$ is the wing mean aerodynamic chord.

The normalized vertical displacement of any point with respect to the vortex sheet was then determined as the algebraic sum of displacement from the 0.25 $\bar{c}_W$ reference plus the incremental displacement of the vortex sheet.

$$\left(\frac{h_H}{\bar{c}_W}\right)_{vortex} \quad \left(\frac{h_H}{\bar{c}_W}\right) + \left(\frac{\Delta h}{\bar{c}_W}\right)_{wake} \qquad (8\text{-}4)$$

where:

Δh is the incremental displacement of the vortex sheet.

Assuming an elliptical wing loading, the ratio of downwash at an arbitrary vertical location to the downwash in the wing wake is determined by lifting-line theory:

$$\frac{\epsilon}{\epsilon_o} = 1 - \frac{\frac{2Z}{b}}{\sqrt{1 + \frac{2Z}{b}}} \qquad (8\text{-}5)$$

where:

ϵ_o	is the downwash angle at the vortex plane.
Z	is the vertical displacement from the wing wake determined by $\left(\frac{h_H}{\bar{c}_W}\right)_{vortex} \bar{c}_W$.
b	is the wing span.

The following relationship was used to determine downwash at positions in the wake far enough downstream from 0.25 $\bar{c}_W$ to be suitable for locating the horizontal tail.

$$\frac{\epsilon_o}{C_{L_{aero}}} = \frac{90}{\pi^2 A}\left(\frac{b}{b'}\right)^2\left[1 + \frac{\sqrt{X_H^2 + b'^2}}{X_H}\right] \qquad (8\text{-}6)$$

where:

ϵ_o	is the downwash angle in the vortex plane (degrees).
$C_{L_{aero}}$	is the aerodynamic lift coefficient.
A	is the wing aspect ratio.
b'	is effective width of wake.
$\left(\frac{b'}{b}\right)$ =	0.785 due to assumed elliptic wing loading.

The downwash at the desired point is:

$$\epsilon_{basic} \quad \left(\frac{\epsilon}{\epsilon_o}\right)\left(\frac{\epsilon_o}{C_{L_{aero}}}\right)C_{L_{aero}} \qquad (8\text{-}7)$$

A comparison of measured downwash with calculated results revealed that if a single nominal curve was used to represent the theoretical variation of downwash angle with longitudinal displacement, the effects of wing aspect ratio and sweep angle can both be satisfactorily represented by simple downwash angle increments ($\Delta\epsilon_\Lambda$ and $\Delta\epsilon_A$) applicable for all practical values of thrust coefficient (C_{μ_J} = 0 through 4.0). The final curve selected to represent theoretical variation of normalized downwash with normalized longitudinal displacement in the vortex plane is presented in Figure 8-3. This figure was developed using a baseline aspect ratio of 8.0 in Equation 8-6.

Downwash angle increments for wing sweep angle ($\Delta\epsilon_\Lambda$) and aspect ratio ($\Delta\epsilon_A$) are presented in Figures 8-4 and 8-5, respectively.

The procedure was then applied to an IBF configuration. The difference between calculated and measured downwash, at point suitable for locating a tail, was minimized with a single constant value of incremental downwash ($\Delta\epsilon_{IBF}$ = 1.49 degrees) applicable for values of momentum coefficient, C_{μ_T} = 0 through 2.0. Similar results were obtained for the MF/VT, a triple-slotted flap with thrust vectored to 90 degrees ($\Delta\epsilon_{MF/VT}$ = 1.21 degrees).

Next, the procedure was applied to an EBF configuration that used a double-slotted flap at several deflection angles. The incremental value of downwash, for suitably locating a horizontal tail at any arbitrary point, was a function of thrust coefficient and flap deflection.

The normalized version of the downwash increment for EBF configurations ($\Delta\epsilon_{EBF}$) at various values of C_{μ_J} is presented in Figure 8-6 as a function of $\bar{A}_c/A_j$.

The following expression was developed to calculate downwash for lift-augmented systems:

$$\epsilon = \epsilon_{basic} + \Delta\epsilon_\Lambda + \Delta\epsilon_A + \Delta\epsilon_{IBF} + \Delta\epsilon_{MF/VT} + \Delta\epsilon_{EBF} \tag{8-8}$$

where:

ϵ_{basic}	is the primary downwash angle, Equation 8-7.
$\Delta\epsilon_\Lambda$	is the downwash angle increment for wing sweep angle effects obtained from Figure 8-4 as a function of $\Lambda_{c/4}$.
$\Delta\epsilon_A$	is the downwash angle increment for wing aspect ratio effects obtained from Figure 8-5 as a function of aspect ratio.

$\Delta\epsilon_{IBF}$ is the downwash angle increment for an IBF configuration and is equal to 1.49 degrees.

$\Delta\epsilon_{MF/VT}$ is the downwash angle increment for an MF/VT configuration ($\delta_T \approx 90$ degrees) and is equal to 1.21 degrees.

$\Delta\epsilon_{EBF}$ is the downwash angle increment for an EBF configuration and is obtained from Figure 8-6 as a function of averaged capture ratio, defined in Section 2, and the thrust coefficient, $C_{\mu_J} > 0$.

As indicated in Figure 8-6, no more than one of the three downwash angle increments related to the type of powered lift augmentation ($\Delta\epsilon_{IBF}$, $\Delta\epsilon_{MF/VT}$, or $\Delta\epsilon_{EBF}$) should have a non-zero value for any specific case.

SAMPLE PROBLEM

GIVEN: Externally blown flap configuration with a triple-slotted flap and leading-edge flap

$A = 8.0$

$b = 66.813$ in.

$\bar{c}_W = 8.895$ in.

$\Lambda_{c/4} = 25$ deg

$i_W = 3.5$ deg

$\alpha_W = 10.05$ deg

$\alpha_{W_{\left(C_{L_{aero}}\right)_{max}}} = 20.31$ deg

$X_H = 42.00$ in.

$Z_H = 12.89$ in.

$C_L = 7.1964$

$C_{\mu_J} = 2.0$

$C_\mu = 0.1$

$\delta_f = 60$ deg

$\delta_{LE} = 55$ deg

$\delta_T = 0$ deg

$\Theta = 56.46$ deg

$r = 0.6569$

$\bar{A}_c/A_j = 0.935$

CALCULATE:

1. Lift coefficient due to direct thrust with Equation 8-1.

$$C_{L_{DT}} = C_{\mu_J} (r) \sin (\alpha_W + \Theta + i_W)$$

$$= (2)(0.6569) \sin (3.5 + 56.46 + 10.05)$$

$$= 1.2346$$

2. Aerodynamic lift coefficient.

$$C_{L_{aero}} = C_L - C_{L_{DT}}$$

$$= 7.1964 - 1.2346$$

$$= 5.9610$$

3. Normalized vertical displacement above the 0.25 $\bar{c}_W$ reference point with Equation 8-3.

$$\left(\frac{h_H}{\bar{c}_W}\right) = \left[\left(\frac{Z_H}{\bar{c}_W}\right) \cos (\alpha_W - i_W) - \left(\frac{X_H}{\bar{c}_W}\right) \sin (\alpha_W - i_W)\right]$$

$$= \left[\left(\frac{12.390}{8.895}\right) \cos (10.05 - 3.50) - \left(\frac{42.00}{8.895}\right) \sin (10.05 - 3.50)\right]$$

$$= 0.9011$$

4. Normalized displacement of the vortex plane.

$$\frac{X_H}{\bar{c}_W} = \frac{42.00}{8.895} = 4.7218$$

$$\frac{\alpha_W}{\alpha_{W_{\left(C_{L_{aero}}\right)_{max}}}} = \frac{10.05}{20.31} = 0.4948$$

From Figure 8-1

$$\left(\frac{\Delta h}{\bar{c}_W}\right)_{wake} = 0.282$$

5. Vertical displacement of $0.25\ \bar{c}_H$ above the wing wake plane with Equation 8-4.

$$\left(\frac{h_H}{\bar{c}_W}\right)_{vortex} = \left(\frac{h_H}{\bar{c}_W}\right) + \left(\frac{\Delta h}{\bar{c}_W}\right)_{wake}$$

$$= 0.9011 + 0.283$$

$$= 1.1841$$

6. Theoretical ratio of downwash at $0.25\ \bar{c}_H$ to the downwash wake plane with Equation 8-5.

$$\frac{\epsilon}{\epsilon_o} = 1 - \frac{\frac{2Z}{b}}{\sqrt{1 + \frac{2Z}{b}}}$$

where $Z = \left(\frac{h}{\bar{c}_W}\right)\bar{c}_W = (1.1841)(8.895) = 10.533$ in.

$$\frac{2Z}{b} = \frac{(2)(10.533)}{66.813} = 0.3153$$

$$\frac{\epsilon}{\epsilon_o} = 1 - \frac{0.3153}{\sqrt{1 + \overline{0.31473}^2}}$$

$$= 0.6993$$

7. Effective theoretical ratio of downwash to aerodynamic lift coefficient on the wing wake plane.

$$\frac{\epsilon_o}{C_{L_{aero}}} = 4.035 \text{ from Figure 8-2 at } \frac{X_H}{\bar{c}_W} = 4.72$$

8. Basic downwash at 0.25 $\bar{c}_H$ with Equation 8-7.

$$\epsilon_{basic} = \left(\frac{\epsilon}{\epsilon_o}\right)\left(\frac{\epsilon_o}{C_{L_{aero}}}\right) C_{L_{aero}}$$

$$= (0.6993)(4.035)(5.9618)$$

$$= 16.82 \text{ deg}$$

9. Downwash increments.

$\Delta\epsilon_\Lambda \approx 0.00$ deg from Figure 8-4 for $\Lambda_{c/4} = 25$ deg

$\Delta\epsilon_A = 0.17$ deg from Figure 8-5 for $A = 8.0$

$\Delta\epsilon_{IBF} = 0.0$ deg (not applicable)

$\Delta\epsilon_{MF/VT} = 0.0$ deg from Figure 8-6 for $\delta_T = 0$ deg

$\Delta\epsilon_{EBF} = 0.0$ deg from Figure 8-6 for $\bar{A}_c/A_j = 0.935$, $C_{\mu_J} = 2.0$

The total downwash is calculated with Equation 8-8.

$$\epsilon = \epsilon_{basic} + \Delta\epsilon_\Lambda + \Delta\epsilon_A + \Delta\epsilon_{IBF} + \Delta\epsilon_{MF/VT} + \Delta\epsilon_{EBF}$$

$$= 16.82 + 0.17 + 0 + 0 + 0$$

$$= 16.99 \text{ deg}$$

Test Value = 17.02

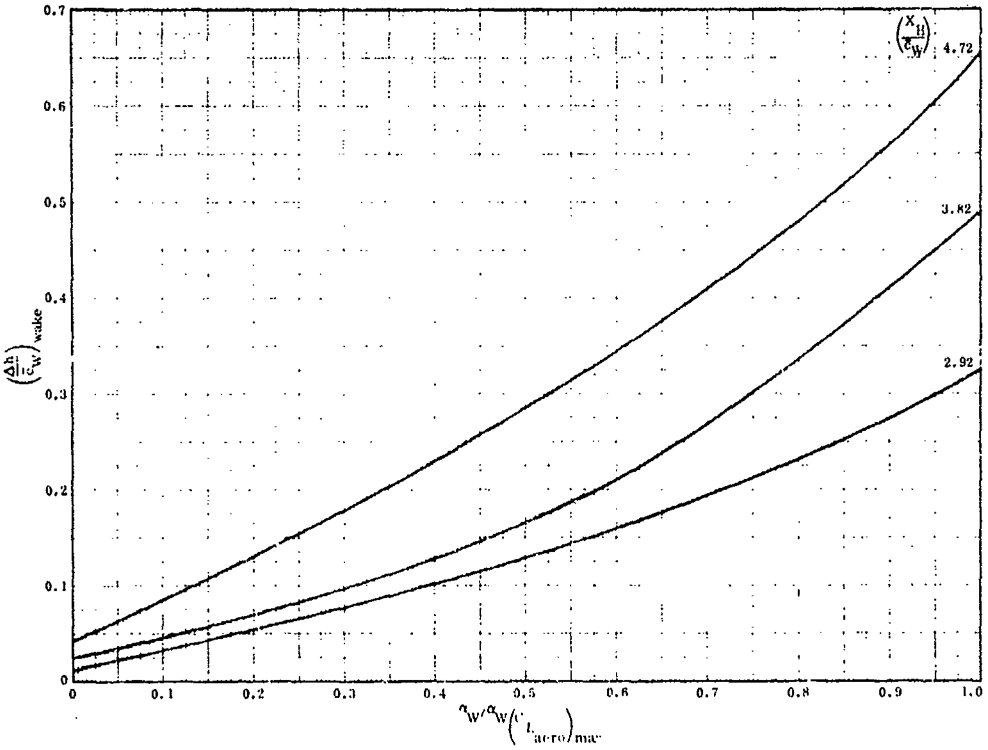

Figure 8-2. Variations of Normalized Vertical Displacement of Wake with Normalized Angle of Attack at Several Normalized Longitudinal Locations

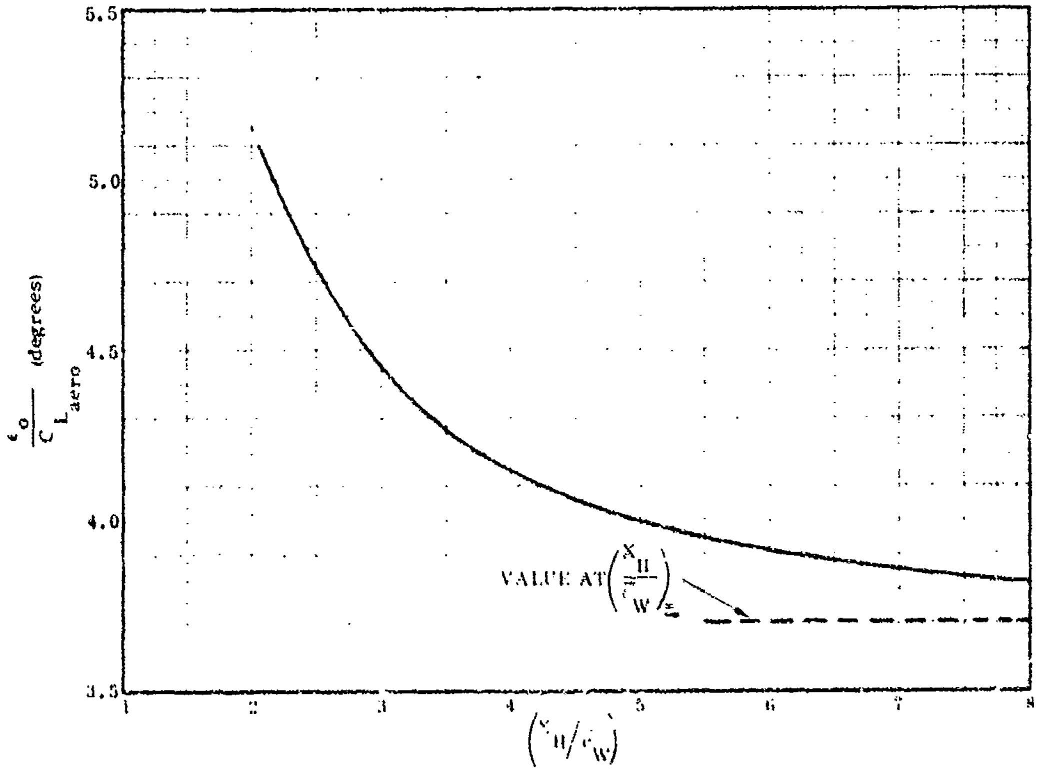

Figure 8-3. Theoretical Variation of Normalized Downwash Angle with Normalized Longitudinal Displacement in Vortex Plane

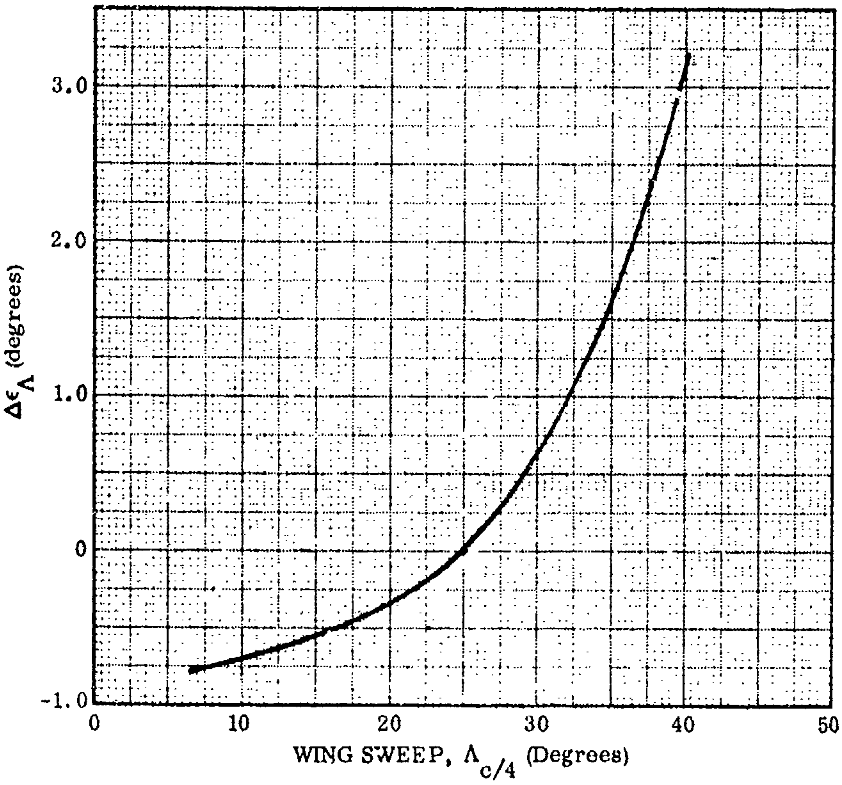

Figure 8-4. Downwash Angle Increment for Wing Sweep

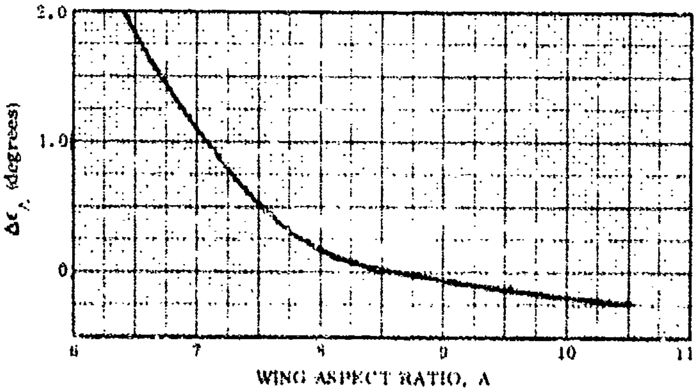

Figure 8-5. Downwash Angle Increment for Wing Aspect Ratio

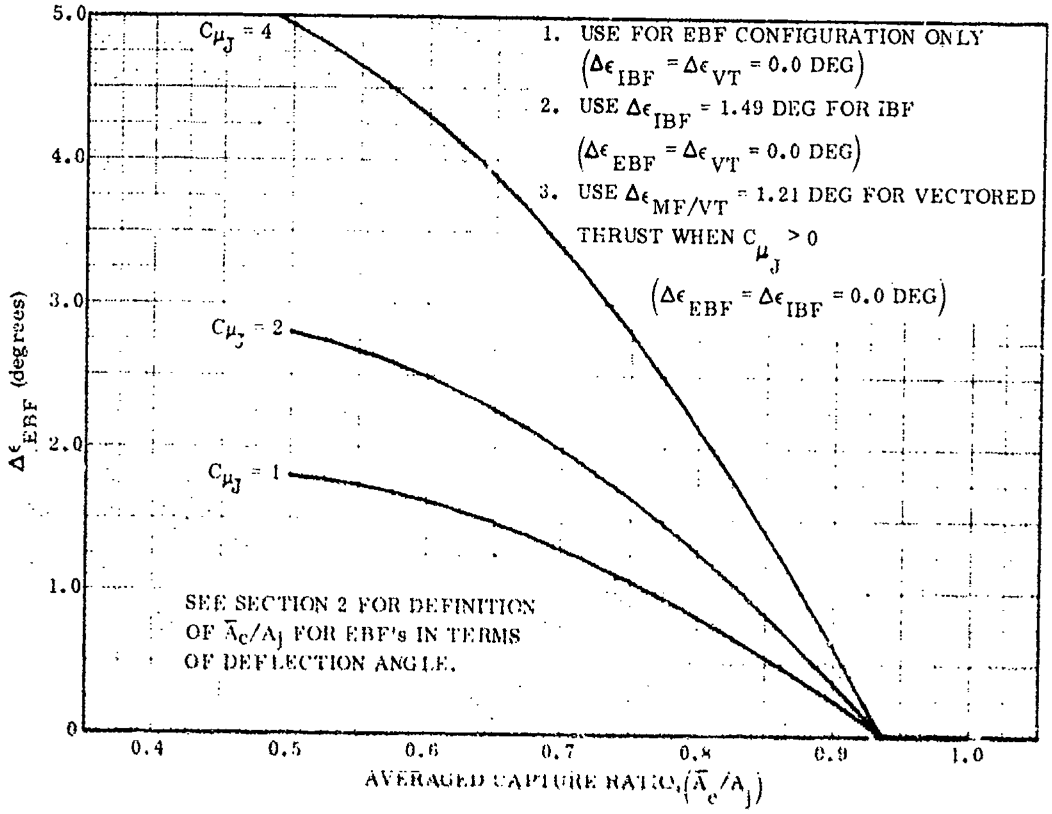

Figure 8-6. Downwash Angle Increment for Externally Blown Trailing Edge Flap Deflection at Various Values of Thrust Coefficient

CORRELATION

The results from approximately 560 cases similar to the sample calculation are compared with the measured values and summarized in Tables 8-1 through 8-5. Table 8-1 shows the 15 combinations of wing geometry and flap configuration for the different types of augmentation. Table 8-1 also indicates the appropriate tables to locate each combination.

Table 8-2, Sheets 1 through 5, presents the data for the various combinations of the externally blown flap configurations. Table 8-2, Sheets 1 through 3, generally indicates the relatively small effect of wing aspect ratio. The small effects of wing sweep are shown in Table 8-2, Sheets 2, 4, and 5. The effects on downwash of vectored thrust ($\delta_T \approx 90$ degrees) and for an internally blown plain flap are indicated in Tables 8-3 and 8-4, respectively.

Table 8-5, Sheets 1, 3, and 5, show the adequacy of the procedure in predicting downwash for the externally blown flap configuration when the T-type horizontal tail is a reasonable longitudinal distance from the wing. Similar comparisons are shown in Sheets 2, 4, and 6 for cases where the horizontal tail is vertically located close to the fuselage at the same longitudinal displacement. The adequacy of predicting downwash for the vertical locations of horizontal tail is shown in Sheets 7 and 8.

The largest differences between measured and calculated downwash angles occur at extreme values of wing normalized angle of attack. At low values, the nonlinear stalling effect induced by the leading-edge flap are just becoming significant.

Table 8-1. Summary of Configurations Substantiated

Table No. (Sheet)	Wing Aspect Ratio	Wing Sweep Angles c/4 (deg)	Type of Trailing-Edge Flap	Type Augmentation	Trailing-Edge Flap Deflection (deg)	Normalized Displacement Of 0.25 $\bar{c}_H$		Downwash Calculation	
						$\left(\frac{Z_H}{\bar{c}_W}\right)$	$\left(\frac{X_H}{\bar{c}_W}\right)$	Mean (% diff)	Standard Deviation (% diff)
8-2(1)	9.52	25	Triple Slotted	Externally Blown	60	1.45	4.72	-0.61	2.86
8-2(2)	8.00	25	Triple Slotted	Externally Blown	60	1.45	4.72	-0.61	4.23
8-2(3)	7.14	25	Triple Slotted	Externally Blown	60	1.45	4.72	-0.16	3.05
8-2(4)	8.0	12.5	Triple Slotted	Externally Blown	60	1.45	4.72	0.16	2.21
8-2(5)	8.0	35	Triple Slotted	Externally Blown	60	1.45	4.72	0.29	3.35
8-3	8.0	25	Triple Slotted	Vectored Thrust	60	1.45	4.72	0.04	3.67
8-4	8.0	25	Plain	Internally Blown	60	1.45	4.72	0.55	5.08
8-5(1)	8.0	25	Double Slotted	Externally Blown	60	1.45	4.72	2.00	4.49
8-5(2)	8.0	25	Double Slotted	Externally Blown	60	0.55	4.72	0.52	5.93
8-5(3)	8.0	25	Double Slotted	Externally Blown	45	1.45	4.72	-1.37	3.90
8-5(4)	8.0	25	Double Slotted	Externally Blown	45	0.55	4.72	0.54	7.15
8-5(5)	8.0	12.5	Double Slotted	Externally Blown	30	1.45	4.72	2.58	6.45
8-5(6)	8.0	12.5	Double Slotted	Externally Blown	30	0.55	4.72	-1.52	8.92
8-5(7)	8.0	12.5	Double Slotted	Externally Blown	30	1.45	2.92	2.07	7.04
8-5(8)	8.0	12.5	Double Slotted	Externally Blown	30	0.55	2.92	-5.85	6.25
					Downwash Calculation	Mean Value:		-0.09	—
						rms Value:		—	5.33

Table 8-2. Substantiation Data for Externally Blown Triple-Slotted Flap (Sheet 1)

A= 9.52 $\Lambda_{c/4}$ = 25 deg X_H = 4.72 $\bar{c}_W$ Z_H = 1.45 $\bar{c}_W$

δ_{LE} = 55 deg δ_f = 60 deg δ_T = 0 deg $\overline{A}_c/A_j$ = 0.935

C_{μ_J}	$\alpha_W/\alpha_{W\left(C_{L_{aero}}\right)max}$	$\epsilon_{measured}$	$\epsilon_{calculated}$	% Difference
4.0	-0.038	11.80	11.28	-4.41
	0.053	13.55	13.25	-2.21
	0.204	15.32	15.38	0.39
	0.355	17.64	17.55	-0.51
	0.480	19.77	20.11	1.72
	0.657	21.88	22.41	2.42
	0.805	23.92	24.78	3.60
	0.904	25.27	25.88	2.41
	1.000 (20.94 deg)	26.69	26.79	0.37
2.0	-0.116	10.22	9.65	-5.58
	0.040	11.75	11.45	-2.55
	0.193	13.59	13.38	-1.55
	0.347	15.36	15.34	-0.13
	0.500	17.41	17.24	-0.98
	0.652	19.08	19.39	1.62
	0.804	20.75	21.21	2.70
	0.902	21.99	22.09	0.64
	1.000 (20.46 deg)	23.27	22.36	-3.91
1.0	-0.142	8.63	8.58	-0.58
	0.031	10.35	10.08	-2.61
	0.206	12.07	11.76	-2.57
	0.375	13.44	13.38	-0.45
	0.548	15.22	15.19	-0.20
	0.719	16.66	16.74	0.48
	0.888	18.05	18.43	2.11
	1.000 (18.15 deg)	18.69	18.95	1.39
0	-0.181	5.53	5.08	-8.41
	0.003	7.26	6.89	-5.10
	0.182	8.77	8.40	-4.22
	0.359	9.93	9.71	-2.22
	0.536	10.91	10.91	0.00
	0.710	11.83	12.01	1.52
	0.884	12.79	13.05	2.03
	1.000 (19.55 deg)	12.88	13.40	4.04

Mean % Difference = -0.61

Standard Deviation = 2.86

Table 8-2. Substantiation Data for Externally Blown Triple-Slotted Flap (Sheet 2)

$A = 8.0$ $\Lambda_{c/4} = 25$ deg $X_H = 4.72\ \bar{c}_W$ $Z_H = 1.45\ \bar{c}_W$

$\delta_{LE} = 55$ deg $\delta_f = 60$ deg $\delta_T = 0$ deg $\overline{A_c/A_j} = 0.935$

C_{μ_J}	$\alpha_W/\alpha_W\left(C_{L_{aero}}\right)_{max}$	$\epsilon_{measured}$	$\epsilon_{calculated}$	% Difference
4.0	-0.097	11.43	11.44	0.09
	0.045	13.11	13.24	0.99
	0.199	15.28	15.37	0.59
	0.351	17.33	17.61	1.62
	0.502	19.58	19.89	1.58
	0.654	21.44	22.30	4.01
	0.803	23.62	24.42	3.39
	0.902	24.71	25.91	4.86
	1.000 (20.76 deg)	26.20	27.14	3.59
2.0	-0.124	9.73	9.69	-0.41
	0.031	11.54	11.39	-1.30
	0.186	13.42	13.13	-2.61
	0.340	15.09	14.84	-1.66
	0.495	17.02	17.01	-0.06
	0.648	18.91	18.84	-0.37
	0.801	20.59	20.88	1.41
	0.903	21.75	21.96	0.97
	1.000 (20.31 deg)	22.49	22.65	0.71
1.0	-0.152	8.31	8.50	2.29
	0.023	10.03	10.01	-0.20
	0.198	11.63	11.58	-0.43
	0.371	13.52	13.08	-3.25
	0.544	15.24	14.95	-1.90
	0.715	16.69	16.37	-1.92
	0.887	18.12	17.95	-0.94
	1.000 (18.01 deg)	19.03	18.70	-1.73
0	-0.188	6.02	4.87	-19.10
	-0.004	7.00	6.81	-2.71
	0.179	8.05	8.23	2.24
	0.356	10.68	9.53	-10.77
	0.534	10.77	10.78	0.09
	0.709	12.25	11.39	-2.94
	0.885	12.79	12.83	0.31
	1.000 (17.43 deg)	13.35	13.36	0.0
			Mean % Difference =	-0.61
			Standard Deviation =	4.23

Table 8-2. Substantiation Data for Externally Blown Triple-Slotted Flap (Sheet 3)

$A = 7.14$ $\Lambda_{c/4} = 25$ deg $X_H = 4.72\ \bar{c}_W$ $Z_H = 1.45\ \bar{c}_W$

$\delta_{LE} = 55$ deg $\delta_f = 60$ deg $\delta_T = 0$ deg $\overline{A_c/A_j} = 0.935$

C_{μ_J}	$\alpha_W / \alpha_{W\left(C_{L_{aero/max}}\right)}$	$\epsilon_{measured}$	$\epsilon_{calculated}$	% Difference
4.0	-0.112	11.14	11.49	3.14
	0.040	13.14	13.33	1.45
	0.192	15.24	15.35	0.72
	0.342	17.03	17.64	3.58
	0.493	19.07	19.68	3.20
	0.644	21.37	21.95	2.71
	0.795	23.23	24.23	4.30
	0.904	24.40	25.62	5.00
	1.000 (20.75 deg)	25.89	26.65	2.94
2.0	-0.130	9.71	10.00	2.99
	0.027	11.52	11.76	2.08
	0.181	13.45	13.29	-1.19
	0.336	15.41	15.01	-2.60
	0.491	17.09	17.00	-0.53
	0.645	18.97	18.97	0.00
	0.799	20.84	20.85	0.05
	0.900	21.88	22.07	0.87
	1.000 (20.18 deg)	22.75	22.68	-0.31
1.0	-0.157	8.47	8.92	5.31
	0.018	10.42	10.34	-0.77
	0.194	11.94	11.83	-0.92
	0.369	13.70	13.46	-1.75
	0.542	15.38	15.09	-1.89
	0.715	16.86	16.59	-1.60
	0.886	18.52	18.12	-2.61
	1.000 (17.88 deg)	19.41	18.77	-3.30
0	-0.193	5.29	5.35	1.13
	-0.007	7.22	7.23	0.14
	0.174	8.91	8.54	-4.15
	0.352	10.52	9.83	-6.56
	0.531	11.44	11.06	-3.32
	0.708	12.94	12.25	-5.31
	0.884	14.12	13.15	-6.87
	1.000 (17.43 deg)	14.11	13.50	-4.32
			Mean % Difference =	-0.16
			Standard Deviation =	3.05

Table 8-2. Substantiation Data for Externally Blown Triple-Slotted Flap (Sheet 4)

$A = 8.00$ $\Lambda_{c/4} = 12.5$ deg $X_H = 4.72\ \bar{c}_W$ $Z_H = 1.45\ \bar{c}_W$

$\delta_{LE} = 55$ deg $\delta_f = 60$ deg $\delta_T = 0$ deg $\overline{A_c}/A_j = 0.935$

C_{μ_J}	$\alpha_W/\alpha_W\left(C_{L_{aero}}\right)_{max}$	$\epsilon_{measured}$	$\epsilon_{calculated}$	% Difference
4.0	-0.110	11.17	10.91	-2.31
	0.043	12.95	12.86	-0.69
	0.196	14.94	14.87	-0.47
	0.349	17.29	17.06	-1.33
	0.500	19.31	19.32	0.05
	0.653	21.64	21.66	0.09
	0.802	23.99	23.81	-0.75
	0.902	25.17	24.99	-0.72
	1.000 (20.59 deg)	26.68	25.99	-2.59
2.0	-0.125	9.64	9.58	-0.62
	0.031	11.42	11.31	-0.96
	0.186	13.17	12.99	-1.37
	0.341	15.12	15.02	-0.66
	0.496	17.08	17.06	-0.12
	0.647	18.89	19.08	1.01
	0.800	20.65	20.74	0.44
	0.901	21.88	21.56	-1.46
	1.000 (20.22 deg)	22.59	22.37	-0.93
1.0	-0.135	8.80	8.53	-3.07
	0.022	10.13	10.08	-0.49
	0.180	11.86	11.69	-1.43
	0.336	13.49	13.41	-0.59
	0.492	15.45	15.13	-2.07
	0.647	16.96	16.83	-0.77
	0.800	17.63	18.13	2.84
	0.902	18.92	18.82	-0.53
	1.000 (19.39 deg)	18.80	18.86	0.32
0	-0.162	5.27	5.36	1.71
	0.001	6.91	6.95	0.58
	0.160	8.30	8.34	-0.60
	0.321	9.82	9.80	-0.20
	0.478	10.88	11.17	2.67
	0.636	11.66	12.26	5.15
	0.793	12.86	13.36	3.89
	0.897	13.17	14.00	6.30
	1.000 (19.46 deg)	13.57	14.32	5.53
			Mean % Difference =	0.16
			Standard Deviation =	2.21

Table 8-2. Substantiation Data for Externally Blown Triple-Slotted Flap (Sheet 5)

$A = 8.00$	$\Lambda_{c/4} = 35$ deg	$X_H = 4.72\ \bar{c}_W$	$Z_H = 1.45\ \bar{c}_W$
$\delta_{LE} = 55$ deg	$\delta_f = 60$ deg	$\delta_T = 0$ deg	$\overline{A_c}/A_j = 0.935$

C_{μ_J}	$\alpha_W/\alpha_W\left(C_{L_{aero}}\right)_{max}$	$\epsilon_{measured}$	calculated	% Difference
4.0	-0.112	10.98	10.72	-2.37
	0.041	12.97	12.44	-4.09
	0.195	14.94	14.34	-4.02
	0.347	16.87	16.37	-2.96
	0.499	19.05	18.44	-3.20
	0.650	20.99	20.66	-1.33
	0.802	22.99	22.80	-0.83
	0.902	24.13	24.19	0.25
	1.000 (20.72 deg)	25.32	25.26	-0.24
2.0	-0.128	9.47	9.37	-1.06
	0.026	11.14	10.90	-2.15
	0.182	13.00	12.54	-3.54
	0.337	14.63	14.34	-1.98
	0.492	16.55	16.15	-2.42
	0.645	18.30	17.96	-1.86
	0.797	19.89	19.83	-0.30
	0.899	21.03	20.84	-0.90
	1.000 (20.33 deg)	22.04	21.86	-0.82
1.0	-0.140	7.94	8.42	6.05
	0.016	9.99	9.76	-2.30
	0.174	12.29	11.23	-8.62
	0.331	12.91	12.82	-0.70
	0.436	14.51	14.42	-0.62
	0.642	15.87	16.12	1.58
	0.798	17.34	17.73	2.25
	0.900	18.10	18.72	3.43
	1.000 (20.02)	18.71	19.29	3.10
0	-0.174	5.14	5.36	4.28
	-0.008	6.57	6.80	3.50
	0.155	8.11	8.26	1.85
	0.316	9.38	9.57	2.03
	0.476	10.55	10.78	2.18
	0.636	11.58	11.97	3.37
	0.792	12.54	12.86	2.55
	0.898	12.55	13.51	7.65
	1.000 (19.41 deg)	12.33	13.90	12.73
			Mean % Difference =	0.29
			Standard Deviation =	3.86

Table 8-3. Substantiation Data for Triple-Slotted Flap with Vectored Thrust

$A = 8.00$	$\Lambda_{c/4} = 25$ deg	$X_H = 4.72\ \bar{c}_W$	$Z_H = 1.45\ \bar{c}_W$
$\delta_{LE} = 55$ deg	$\delta_f = 30$ deg	$\delta_T = 90$ deg	$\overline{A_c/A_j} = 0.935$

C_{μ_J}	$\alpha_W/\alpha_W\left(C_{L_{aero}}\right)_{max}$	$\epsilon_{measured}$	$\epsilon_{calculated}$	% Difference
3.4	-0.140	6.79	6.56	-3.39
	0.006	8.70	8.34	-4.14
	0.151	10.19	9.87	-3.14
	0.294	11.54	11.45	-0.78
	0.438	13.54	13.33	-1.55
	0.581	14.61	15.07	3.15
	0.722	16.54	16.64	0.60
	0.814	17.93	17.30	-3.51
	0.907	18.73	18.12	-3.26
	1.000 (21.83 deg)	19.68	18.83	-4.32
2.0	-0.186	6.67	6.69	0.30
	0.004	8.28	8.21	-0.85
	0.193	9.73	9.66	-0.72
	0.380	11.11	11.17	0.54
	0.568	12.81	12.81	0.00
	0.817	14.92	14.90	-0.13
	0.953	15.92	15.31	-3.83
	1.000 (16.70 deg)	17.01	15.90	-6.53
1.0	-0.179	6.14	6.60	7.45
	0.000	7.76	8.15	5.03
	0.179	9.14	9.61	5.14
	0.356	10.47	11.09	5.92
	0.534	11.93	12.50	4.78
	0.709	13.37	14.07	5.24
	0.886	14.78	15.69	6.16
	1.000 (17.65 deg)	15.64	16.15	3.26
0	-0.211	5.08	5.12	0.79
	-0.004	6.87	6.69	-2.62
	0.199	7.87	7.86	-0.13
	0.404	9.28	9.19	-0.97
	0.605	10.31	10.29	-0.19
	0.804	11.66	11.42	-2.06
	1.000 (15.36 deg)	12.50	11.89	-4.88

Mean % Difference = 0.04
Standard Deviation = 3.67

Table 8-4. Substantiation Data for Internally Blown Plain Flap

AR = 8.00	$\Lambda_{c/4}$ = 25 deg	$X_H = 4.72\ \bar{c}_W$	$Z_H = 1.45\ \bar{c}_W$
δ_{LE} = 55 deg	δ_f = 60 deg	δ_T = 0 deg	$A_c/A_j = 0.935$
			$C_{\mu_J} = 0$

C_{μ_T}	$\alpha_W/\alpha_W\left(C_{L_{aero}}\right)_{max}$	ϵ measured	ϵ calculated	% Difference
2.0	-0.113	10.42	11.47	10.08
	0.029	11.89	13.11	10.26
	0.169	13.86	14.74	7.91
	0.309	15.69	16.46	4.91
	0.449	17.66	18.24	3.28
	0.589	19.86	20.26	2.01
	0.727	22.00	21.96	-0.18
	0.819	23.06	23.05	-0.04
	0.910	24.32	23.83	-2.01
	1.000 (22.27 deg)	25.16	24.49	-2.26
1.0	-0.176	9.00	9.55	6.11
	0.021	10.55	10.91	3.41
	0.218	12.31	12.30	-0.08
	0.415	14.24	13.70	-3.79
	0.610	16.04	15.05	-6.17
	0.806	17.58	16.48	-6.26
	1.000 (15.84 deg)	19.15	17.00	-11.23
0.5	-0.193	7.40	8.12	9.73
	0.008	8.81	9.45	7.26
	0.209	10.57	10.80	2.18
	0.407	11.66	11.99	2.83
	0.607	13.42	13.25	-1.27
	0.804	14.64	14.51	-0.89
	1.000 (15.59 deg)	16.09	15.26	-5.16
0.2	-0.210	6.09	6.72	10.34
	-0.006	7.38	7.89	6.91
	0.198	8.93	9.10	1.90
	0.399	9.97	10.18	2.11
	0.601	11.31	11.38	0.62
	0.801	12.54	12.31	-1.83
	1.000 (15.34 deg)	13.47	13.08	-2.90
0	-0.156	2.40	2.47	2.92
	-0.030	3.55	3.43	-3.38
	0.096	4.76	4.54	-4.63
	0.221	5.95	5.65	-5.04
	0.346	6.69	6.72	0.45
	0.470	8.22	7.82	-4.87
	0.593	9.18	8.60	-6.32
	0.675	9.84	9.53	-3.15
	0.757	10.40	10.15	-2.40
	0.838	10.56	10.76	1.89
	0.919	11.22	11.22	0.00
	1.000 (34.90 deg)	11.48	11.54	0.52
			Mean % Difference =	0.55
			Standard Deviation	5.08

Table 8-5. Substantiation Data for Externally Blown Double-Slotted Flap (Sheet 1)

$A = 8.00$ $\Lambda_{c/4} = 25$ deg $X_H = 4.72\ \bar{c}_W$ $Z_H = 1.45\ \bar{c}_W$

$\delta_{LE} = 55$ deg $\delta_f = 60$ deg $\delta_T = 0$ deg $A_c/A_j = 0.828$

C_{μ_J}	$\alpha_W/\alpha_W\left(C_{L_{aero}}\right)_{max}$	$\epsilon_{measured}$	$\epsilon_{calculated}$	% Difference
4.0	0.029	12.23	12.35	0.98
	0.170	13.93	14.27	2.44
	0.310	16.04	16.33	1.81
	0.449	18.00	18.39	2.17
	0.589	20.39	20.66	1.32
	0.729	22.36	23.04	3.04
	0.820	23.37	24.21	3.59
	0.910	24.31	25.28	3.99
	1.000 (22.45 deg)	25.33	26.08	2.96
2.0	0.020	10.60	10.67	0.66
	0.177	12.47	12.25	-1.76
	0.332	14.26	13.93	-2.31
	0.489	16.19	15.85	-2.10
	0.644	17.95	17.70	-1.39
	0.798	19.26	19.41	0.78
	0.901	20.30	20.46	0.79
	1.000 (20.10 deg)	21.45	21.30	-0.70
1.0	0.011	9.30	9.19	-1.18
	0.170	11.28	10.63	-5.76
	0.327	12.58	12.17	-3.26
	0.485	13.83	13.78	-0.36
	0.640	15.91	15.40	-3.21
	0.796	17.91	16.97	-5.25
	0.898	17.63	17.75	0.68
	1.000 (19.83 deg)	18.41	18.28	-0.71
0	-0.016	5.94	5.14	-13.47
	0.149	7.21	6.44	-10.69
	0.309	8.33	7.44	-10.68
	0.469	9.50	8.66	-8.84
	0.629	10.79	9.99	-7.41
	0.790	12.07	11.22	-7.04
	0.865	12.47	11.91	-4.49
	1.000 (19.29 deg)	12.49	12.40	-0.72

Mean % Difference = 2.00

Standard Deviation = 4.19

Table 8-5. Substantiation Data for Externally Blown Double-Slotted Flap (Sheet 2)

$A = 8.00$ $\Lambda_{c/4} = 25$ deg $X_H = 4.72\ \bar{c}_W$ $Z_H = 0.55\ \bar{c}_W$

$\delta_{LE} = 55$ deg $\delta_f = 60$ deg $\delta_T = 0$ deg $\overline{A_c}/A_j = 0.935$

C_{μ_J}	$\alpha_W/\alpha_W\left(C_{L_{aero}}\right)_{max}$		$\epsilon_{measured}$	$\epsilon_{calculated}$	% Difference
4.0	0.029		16.11	16.04	-0.43
	0.170		18.39	18.53	0.76
	0.310		20.98	21.16	0.86
	0.449		23.02	23.70	2.95
	0.589		25.72	26.41	2.68
	0.729		27.80	29.18	4.96
	0.820		28.98	30.47	5.14
	0.910		29.82	31.59	5.94
	1.000	(22.45 deg)	30.42	32.38	6.44
2.0	0.020		14.04	13.93	-0.78
	0.177		16.35	16.01	-2.08
	0.332		18.28	18.12	-0.92
	0.489		20.57	20.54	-0.15
	0.644		22.93	22.76	-0.74
	0.798		24.43	24.75	1.31
	0.901		25.38	25.94	2.21
	1.000	(20.10 deg)	25.96	26.85	3.43
1.0	0.011		12.50	12.09	-3.29
	0.170		14.36	13.98	-2.65
	0.327		16.03	15.94	-0.56
	0.485		17.94	17.94	0.00
	0.640		19.77	19.89	0.61
	0.796		21.31	21.75	2.06
	0.898		21.57	22.66	5.06
	1.000	(19.83 deg)	21.99	23.13	5.18
	-0.016		7.35	6.88	-6.39
	0.149		9.50	8.59	-9.58
	0.309		11.02	9.87	-10.44
	0.469		12.70	11.42	-10.08
	0.629		13.72	13.06	-4.81
	0.790		15.22	14.52	-4.60
	0.895		14.89	15.33	2.96
	1.000		12.98	15.86	22.19

Mean % Difference = 0.52

Standard Deviation = 5.93

Table 8-5. Substantiation Data for Externally Blown Double-Slotted Flap (Sheet 3)

$A = 8.00$	$\Lambda_{c/4} = 25$ deg	$X_H = 4.72\ \bar{c}_W$	$\underline{Z_H} = 145\ \bar{c}_W$
$\delta_{LE} = 55$ deg	$\delta_f = 45$ deg	$\delta_T = 0$ deg	$A_c/A_j = 0.740$

C_{μ_J}	$\alpha_W / \alpha_{W\left(C_{L_{aero}}\right)_{max}}$	$\epsilon_{measured}$	$\epsilon_{calculated}$	% Difference
4.0	0.006	10.18	10.00	-1.77
	0.128	11.93	11.72	-1.76
	0.249	13.64	13.57	-0.51
	0.367	15.59	15.51	-0.51
	0.488	17.81	17.72	-0.51
	0.608	20.06	20.23	0.85
	0.687	21.46	21.61	0.70
	0.769	22.73	23.06	1.45
	0.846	24.37	24.91	2.22
	0.923	25.47	25.98	2.00
	1.000 (26.22 deg)	26.94	26.84	-0.37
2.0	0.001	8.84	8.50	-3.85
	0.133	10.32	10.00	-3.10
	0.265	12.13	11.58	-4.53
	0.395	13.64	13.41	-1.69
	0.526	15.57	15.20	-2.38
	0.657	17.48	17.46	-0.11
	0.742	18.19	18.51	1.76
	0.829	19.73	19.90	0.86
	0.915	20.76	20.92	0.77
	1.000 (23.92 deg)	21.67	21.84	0.78
1.0	-0.005	7.83	7.25	-6.13
	0.142	9.04	9.02	-0.22
	0.285	10.66	10.27	-3.66
	0.430	12.03	11.78	-2.08
	0.574	13.85	13.41	-3.18
	0.716	15.27	15.08	-1.24
	0.812	16.35	16.44	0.55
	0.907	17.03	17.15	0.70
	1.000 (21.68 deg)	17.79	18.06	1.52
0	-0.017	5.27	4.62	-12.33
	0.134	6.93	6.18	-10.82
	0.280	8.40	7.65	-8.93
	0.425	9.53	8.88	-6.82
	0.572	10.36	10.21	-1.45
	0.716	11.49	11.35	-1.22
	0.811	11.93	12.07	1.17
	0.906	12.64	12.67	0.24
	1.000 (21.28 deg)	11.86	13.07	10.20
			Mean % Difference	≈ -1.37
			Standard Deviation	≈ 3.90

Table 8-5. Substantiation Data for Externally Blown Double-Slotted Flap (Sheet 4)

$A = 8.00$ $\Lambda_{c/4} = 25$ deg $X_H = 4.72\ \bar{c}_W$ $Z_H = 0.55\ \bar{c}_W$

$\delta_{LE} = 55$ deg $\delta_f = 45$ deg $\delta_T = 0$ deg $A_c/A_j = 0.740$

C_{μ_J}	$\alpha_W/\alpha_W\left(C_{L_{aero}}\right)_{max}$	$\epsilon_{measured}$	$\epsilon_{calculated}$	% Difference
4.0	0.006	13.38	12.47	-6.80
	0.128	15.76	14.74	-6.47
	0.249	17.60	17.12	-3.11
	0.367	20.25	19.53	-3.51
	0.488	22.55	22.22	-1.46
	0.608	25.15	25.19	0.16
	0.687	26.67	26.76	0.34
	0.765	27.91	28.37	1.67
	0.846	29.62	30.45	2.80
	0.923	30.64	31.55	2.97
	1.000 (26.62 deg)	31.54	32.41	2.76
2.0	0.001	11.58	10.81	-6.65
	0.133	13.20	12.77	-3.26
	0.265	15.49	14.81	-4.39
	0.395	17.43	17.09	-1.95
	0.526	19.84	19.27	-2.97
	0.657	22.24	21.97	-1.21
	0.742	22.93	23.14	0.92
	0.829	23.95	24.72	3.22
	0.915	24.52	25.82	5.30
	1.000 (23.92 deg)	24.99	26.79	7.20
1.0	-0.005	10.26	9.57	-6.73
	0.142	11.74	11.32	-3.56
	0.285	13.86	13.26	-4.33
	0.430	15.52	15.15	-2.38
	0.574	17.27	17.14	-0.75
	0.716	18.97	19.12	0.79
	0.812	19.86	20.73	4.38
	0.907	19.79	21.50	8.64
	1.000 (21.68 deg)	20.09	22.50	12.00
0	-0.017	6.87	6.17	-10.19
	0.134	9.13	8.24	-9.75
	0.280	10.46	10.14	-2.97
	0.425	12.04	11.69	-2.91
	0.572	12.79	13.32	4.14
	0.716	13.60	14.65	7.72
	0.811	13.79	15.47	13.18
	0.906	12.51	16.10	28.70
	1.000 (21.28 deg)	11.32	16.52	----

Mean % Difference = 0.54
Standard Deviation = 7.15

Table 8-5. Substantiation Data for Externally Blown Double-Slotted Flap (Sheet 5)

$A = 8.00$ $\Lambda_{c/4} = 12.5$ deg $X_H = 4.72\ \bar{c}_W$ $\underline{Z_H} = 1.45\ \bar{c}_W$

$\delta_{LE} = 55$ deg $\delta_f = 30$ deg $\delta_T = 0$ deg $A_c/A_j = 0.502$

C_{μ_J}	$\alpha_W/\alpha_{W\left(C_{L_{aero}}\right)_{max}}$	$\epsilon_{measured}$	$\epsilon_{calculated}$	% Difference
4.0	0.099	7.79	9.11	16.94
	0.212	9.49	10.68	12.54
	0.326	11.30	12.43	10.00
	0.439	13.41	14.28	6.49
	0.551	15.62	16.34	4.61
	0.628	17.30	17.97	3.87
	0.702	18.88	19.40	2.75
	0.776	20.39	20.83	2.16
	0.851	21.71	22.35	2.95
	0.925	23.36	23.47	0.47
	1.000 (27.77 deg)	25.01	24.91	-0.41
2.0	0.099	6.64	7.33	10.39
	0.212	8.54	8.81	3.16
	0.326	10.07	10.50	4.27
	0.439	11.41	12.20	6.92
	0.553	13.55	14.22	4.94
	0.628	15.00	15.45	3.00
	0.703	16.21	16.86	4.01
	0.778	17.61	18.24	3.58
	0.851	18.84	19.70	4.56
	0.926	20.05	20.63	2.89
	1.000 (27.61 deg)	20.97	21.39	2.00
1.0	0.106	6.64	6.38	-3.92
	0.228	8.01	7.73	-3.50
	0.352	9.42	9.44	0.21
	0.474	10.87	11.01	1.29
	0.596	12.28	12.80	4.23
	0.678	13.69	14.08	2.85
	0.758	14.61	15.14	3.63
	0.839	15.65	16.40	4.86
	0.921	16.73	17.99	7.53
	1.000 (26.47 deg)	17.31	18.17	4.97
0	0.103	5.45	4.29	-21.28
	0.228	6.71	5.79	-13.71
	0.353	7.89	7.29	-7.60
	0.475	9.29	8.82	-5.06
	0.597	10.61	10.29	-3.02
	0.678	11.05	11.15	0.90
	0.760	11.74	12.08	2.90
	0.839	12.09	12.89	6.62
	0.920	12.82	13.69	6.79
	1.000 (26.25 deg)	13.30	14.30	7.52

Mean % Difference = 2.58

Standard Deviation = 6.45

Table 8-5. Substantiation Data for Externally Blown Double-Slotted Flap (Sheet 6)

$A = 8.00$ $\Lambda_{c/4} = 12.5$ deg $X_H = 4.72\ \bar{c}_W$ $Z_H = 0.55\ \bar{c}_W$

$\delta_{LE} = 55$ deg $\delta_f = 30$ deg $\delta_T = 0$ deg $A_c/A_j = 0.502$

C_{μ_J}	$\alpha_W/\alpha_W\left(C_{L_{aero}}\right)_{max}$	$\epsilon_{measured}$	$\epsilon_{calculated}$	% Difference
4.0	0.099	11.57	10.46	-9.59
	0.212	13.81	12.77	-7.53
	0.326	16.18	14.96	-7.54
	0.439	18.46	17.28	-6.39
	0.551	20.73	19.75	-4.73
	0.628	22.15	21.68	-2.12
	0.702	23.57	23.31	-1.10
	0.776	24.87	24.94	0.28
	0.851	26.01	25.37	-2.47
	0.925	27.03	27.89	3.18
	1.000 (27.77 deg)	28.57	29.42	2.98
2.0	0.099	10.23	9.04	-11.63
	0.212	12.25	10.94	-10.69
	0.326	14.15	13.07	-7.63
	0.439	16.11	15.21	-5.59
	0.553	17.83	17.65	-1.01
	0.628	19.16	19106	-0.52
	0.703	20.03	20.73	3.49
	0.778	21.06	22.24	5.60
	0.851	21.83	23.90	9.48
	0.926	23.11	24.83	7.44
	1.000 (27.61 deg)	26.10	25.61	-1.88
1.0	0.106	9.49	8.12	-14.44
	0.228	10.99	9.89	-10.01
	0.352	12.53	12.04	-3.91
	0.474	14.41	13.99	-2.91
	0.596	15.72	16.13	2.61
	0.678	16.68	17.63	5.70
	0.758	17.33	18.87	8.89
	0.839	18.25	20.29	11.18
	0.921	19.01	22.07	16.10
	1.000 (25.45 deg)	19.51	22.19	13.47
0	0.103	7.09	5.93	-29.78
	0.238	9.44	7.89	-16.42
	0.353	10.89	9.80	-10.01
	0.475	12.20	11.68	-4.96
	0.597	13.34	13.42	0.60
	0.678	13.72	14.47	5.47
	0.760	13.67	19.48	13.24
	0.839	12.32	16.36	----
	0.920	8.12	17.21	----
	1.000 (25.23 deg)	8.34	17.84	----

Mean % Difference = -1.52
Standard Deviation = -8.92

Table 8-5. Substantiation Data for Externally Blown Double-Slotted Flap (Sheet 7)

$A = 8.00$	$\Lambda_{c/4} = 12.5$ deg	$X_H = 2.92\ \bar{c}_W$	$Z_H = 1.45\ \bar{c}_W$
$\delta_{LE} = 55$ deg	$\delta_f = 30$ deg	$\delta_T = 0$ deg	$\bar{A}_c/A_j = 0.502$

C_{μ_J}	$\alpha_W/\alpha_W\left(C_{L_{aero}}\right)_{max}$	$\epsilon_{measured}$	$\epsilon_{calculated}$	% Difference
4.0	0.100	8.96	9.68	8.04
	0.213	10.55	11.26	6.73
	0.327	12.70	13.01	2.44
	0.440	14.51	14.88	2.55
	0.552	16.08	16.89	5.04
	0.628	17.22	18.21	5.75
	0.702	18.60	19.68	5.81
	0.777	19.75	20.99	6.28
	0.853	21.08	22.45	6.50
	0.927	22.59	23.77	5.22
	1.000 (27.77 deg)	24.30	24.86	2.30
2.0	0.098	8.03	8.01	-0.25
	0.212	9.69	9.44	-2.58
	0.326	11.01	11.11	0.91
	0.439	12.70	12.90	1.57
	0.553	14.18	14.76	4.09
	0.627	15.34	15.97	4.11
	0.702	16.68	17.26	3.48
	0.777	17.79	18.47	3.82
	0.857	18.78	19.62	4.47
	0.926	19.81	20.80	5.00
	1.000 (27.63 deg)	21.10	21.42	1.52
1.0	0.106	7.63	7.03	-7.86
	0.230	8.71	8.43	-3.21
	0.352	10.18	10.03	-1.47
	0.474	11.42	11.67	2.19
	0.597	12.96	13.35	3.01
	0.677	13.79	14.50	5.15
	0.759	14.76	15.67	6.17
	0.839	15.62	16.68	6.79
	0.921	16.48	17.82	8.13
	1.000 (25.48 deg)	17.31	18.58	7.34
0	0.103	6.44	4.93	-23.95
	0.227	7.58	6.46	-14.53
	0.350	9.02	7.89	-12.53
	0.472	9.99	9.39	-6.11
	0.596	11.02	10.89	-1.18
	0.674	11.77	11.62	-1.27
	0.756	12.06	12.35	2.40
	0.836	12.33	13.21	7.14
	0.916	12.58	13.98	11.18
	1.000 (25.27 deg)	12.46	14.55	16.85

Mean % Difference = 2.07

Standard Deviation = 7.04

Table 8-5. Substantiation Data for Externally Blown Double-Slotted Flap (Sheet 8)

$A = 8.00$ $\Lambda_{c/4} = 12.5$ deg $X_H = 2.92\ \bar{c}_W$ $Z_H = 0.55\ \bar{c}_W$

$\delta_{LE} = 55$ deg $\delta_f = 30$ deg $\delta_T = 0$ deg $\overline{A}_c/A_j = 0.502$

C_{μ_J}	$\alpha_W/\alpha_W\left(C_{L_{aero}}\right)_{max}$	$\epsilon_{measured}$	$\epsilon_{calculated}$	% Difference
4.0	0.100	12.76	11.45	-10.27
	0.213	14.42	13.51	-6.31
	0.327	17.44	15.81	-9.35
	0.440	19.47	18.16	-6.73
	0.552	21.78	20.65	-5.19
	0.628	23.34	22.34	-4.28
	0.702	24.88	24.03	-3.42
	0.777	26.11	25.51	-3.83
	0.853	27.91	27.20	-2.54
	0.927	30.01	28.77	-4.13
	1.000 (27.77 deg)	32.85	29.89	-9.01
2.0	0.098	11.39	9.94	-12.73
	0.212	13.39	11.82	-11.73
	0.326	15.50	13.94	-10.06
	0.439	17.44	16.19	-7.17
	0.553	19.47	18.51	-4.93
	0.627	20.68	19.97	-3.43
	0.702	22.00	21.49	-2.32
	0.777	23.14	22.95	-0.82
	0.857	24.48	24.29	-0.78
	0.926	26.43	25.51	-3.48
	1.000 (27.63 deg)	30.07	26.14	-13.07
1.0	0.106	10.50	8.97	-14.57
	0.230	12.26	10.81	-11.83
	0.357	13.86	12.84	-7.36
	0.474	15.67	14.95	-4.59
	0.597	17.38	17.00	-2.19
	0.677	18.58	18.37	-1.13
	0.759	19.36	19.80	2.27
	0.839	20.25	20.91	3.26
	0.921	21.15	22.21	5.01
	1.000 (25.48 deg)	22.19	23.04	3.83
0	0.103	8.94	6.74	-24.61
	0.227	10.59	8.78	-17.09
	0.350	12.26	10.62	-13.39
	0.472	13.76	12.49	-9.23
	0.595	14.91	14.34	-3.82
	0.674	15.41	15.18	-1.49
	0.755	15.39	16.06	4.35
	0.836	14.05	17.04	----
	0.916	13.21	17.89	----
	1.000 (25.27 deg)	10.08	18.45	----

Mean % Difference = -5.85

Standard Deviation = 6.25

SECTION 9

LATERAL-DIRECTIONAL STABILITY DERIVATIVES

The effects of powered-lift systems on lateral directional stability derivatives should be manifested through the wing contributions to C_{y_β}, C_{ℓ_β}, and C_{n_β}. In the current DATCOM, wing contributions to C_{y_β} and C_{n_β} are calculated from the method given in Reference 9-1. Experience with the method (and also the correlation curves given in the DATCOM) has indicated very poor correlation with test data. The recommended procedure for estimating C_{y_β} and C_{n_β} is to consider only the body and wing-body interference contributions, using the rationale that the wing terms are small. The DATCOM method for C_{ℓ_β}, taken from Reference 9-2, is dependent on the wing contributions and is primarily a function of sweep, dihedral angle, aspect ratio, and taper ratio. Experience with the method has shown it can predict C_{ℓ_β} to satisfactorily correlate with test data. A deficiency associated with the method is the lack of a technique for the power-off effects of high-lift devices on the static lateral-directional stability derivatives. A method for predicting these effects of high-lift devices is presented in Reference 9-3, but it has not proven very satisfactory.

The proposed methodology shown in Figure 9-1 consists of extending the charts from Reference 9-2 (for wing terms that are dependent on C_L) to include the effects of high-lift devices and powered-lift systems, based on the test data shown in Reference 3-11.

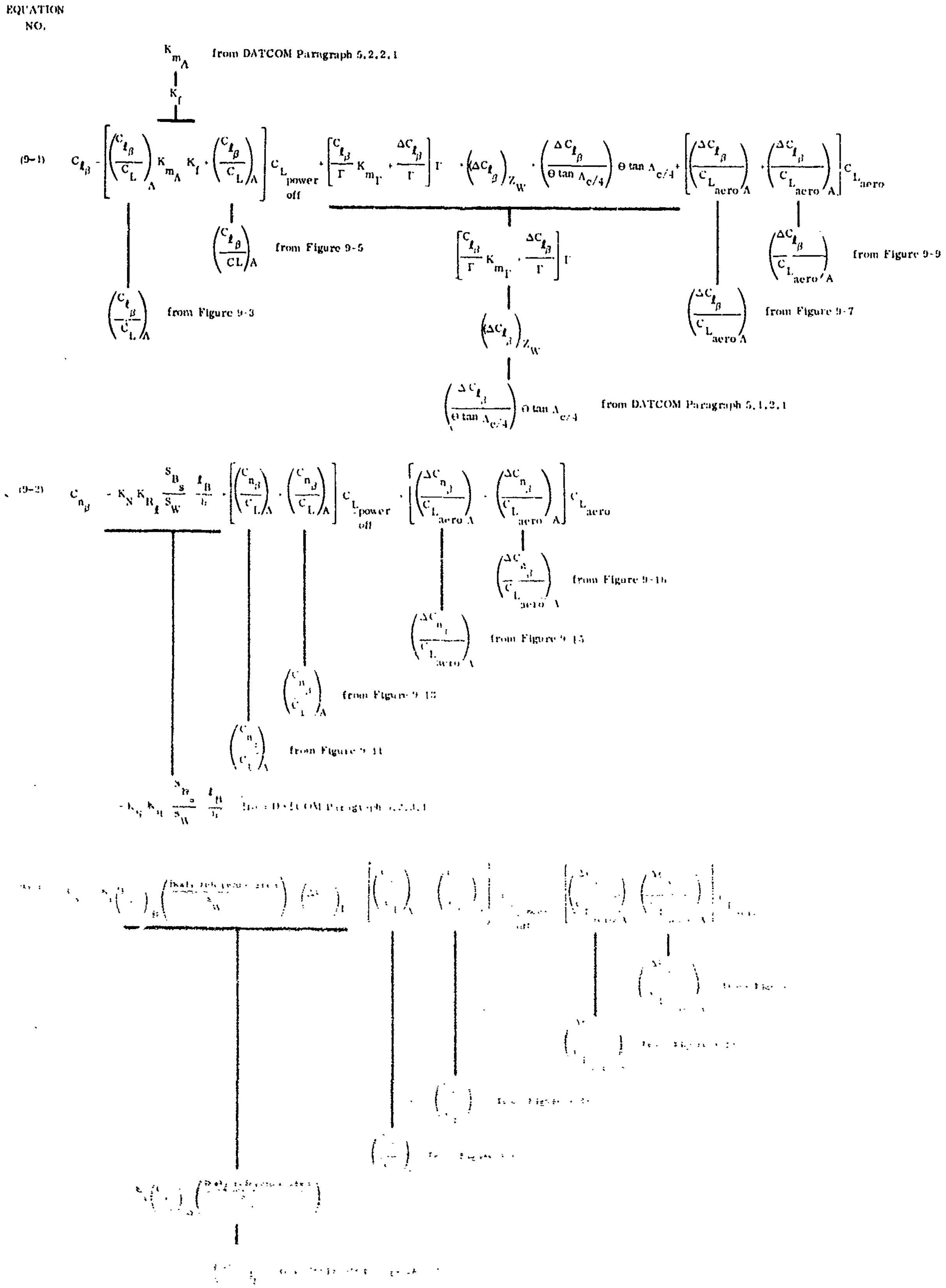

Figure 9-1. Stability Derivative Methodology

9.1 ROLLING MOMENT DUE TO SIDESLIP, C_{ℓ_β}

The methodology to estimate C_{ℓ_β} in Reference 9-2 basically consists of developing an analytical expression for predicting the effects of sweep. Aspect ratio effects were taken as the difference between experimental and calculated values for swept wings. The power-off problem is to determine the parameters $(C_{\ell_\beta}/C_L)_\Lambda$ and $(C_{\ell_\beta}/C_L)_A$ for wings with high-lift devices.

The basic data used to determine sweep effects on C_{ℓ_β} is shown in Figure 9-2. The slopes of $d(C_{\ell_\beta})/d(\Lambda_{c/4})$ were obtained from Figure 9-2 and converted to the parameter $(C_{\ell_\beta}/C_L)_\Lambda$ to produce the chart in Figure 9-3 (equivalent to Figure 5.1.2.1-27 in the DATCOM). The sweep angle has now been referenced to the midchord, and the curve for $\delta_f = 0$ is in good agreement with that presented in the DATCOM.

Aspect ratio effects were determined from configurations with a wing sweep of 25 degrees that had aspect ratios of 7.14, 8.00, and 9.52. The C_{ℓ_β} increment due to sweep was subtracted from total measured C_{ℓ_β} for these wings and the remainder plotted as a function of 1/A, for which the theory predicted an approximately linear relationship. The results are shown in Figure 9-4, from which Figure 9-5 was subsequently constructed (equivalent to Figure 5.1.2 1-28b in the DATCOM).

The effects of a powered-lift system (in this case, the EBF) were handled like those of the power-off case, by determining incremental values for C_{ℓ_β} arising from sweep and aspect ratio contributions with power on. In this case, the lift coefficient included only the aerodynamic terms, $C_{L_{aero}}$.

Basic data used to determine sweep effects with power on is shown in Figure 9-6, where $C\mu_J = 2.0$. The difference in the slopes, $d(C_{\ell_\beta})/d(\Lambda_{c/4})$, between the power on and power off cases were used to obtain the parameter $\left(\Delta C_{\ell_\beta}/C_{L_{aero}}\right)_\Lambda$ and a design chart for the sweep contribution with power on was constructed (Figure 9-7). Similarly, the effects of aspect ratio were determined, and the plot of $\left(\Delta C_{\ell_\beta}/C_{L_{aero}}\right)_A$ versus 1/A is shown in Figure 9-8.

The design chart for the aspect ratio contribution is presented in Figure 9-9. By using the design charts presented in this section and the existing DATCOM, C_{ℓ_β} for the wing/body is obtained from the relationship given in Equation 9-1.

$$C_{\ell_\beta} = \left[\left(\frac{C_{\ell_\beta}}{C_L}\right)_\Lambda K_{m_\Lambda} K_f + \left(\frac{C_{\ell_\beta}}{C_L}\right)_A\right] C_{L_{\substack{\text{power}\\ \text{off}}}} + \left[\frac{C_{\ell_\beta}}{\Gamma} K_{m_\Gamma} + \frac{\Delta C_{\ell_\beta}}{\Gamma}\right]\Gamma$$

$$+\left(\Delta C_{\ell_\beta}\right)_{Z_W} + \left(\frac{\Delta C_{\ell_\beta}}{\theta \tan \Lambda_{c/4}}\right)\theta \tan \Lambda_{c/4} + \left[\left(\frac{\Delta C_{\ell_\beta}}{C_{L_{\text{aero}}}}\right)_\Lambda + \left(\frac{\Delta C_{\ell_\beta}}{C_{L_{\text{aero}}}}\right)_A\right] C_{L_{\text{aero}}} \tag{9-1}$$

where:

$\left(\frac{C_{\ell_\beta}}{C_L}\right)_\Lambda$ is from Figure 9-3, or can be obtained from DATCOM for $\delta_f = 0$.

$\left(\frac{C_{\ell_\beta}}{CL}\right)_A$ is from Figure 9-5, or can be obtained from DATCOM for $\delta_f = 0$.

$\left(\frac{\Delta C_{\ell_\beta}}{C_{L_{\text{aero}}}}\right)_\Lambda$ is from Figure 9-7.

$\left(\frac{\Delta C_{\ell_\beta}}{C_{L_{\text{aero}}}}\right)_A$ is from Figure 9-9.

All remaining terms are obtained from DATCOM.

SAMPLE PROBLEM

GIVEN:

Triple-slotted flap, $\delta_f = 60$ deg

Engine Location F (low, aft)

$C_{L_{\text{power off}}} = 3.853$

$C_{L_{\text{aero}}} = 4.485$

CALCULATE:

Rolling moment due to sideslip, C_{ℓ_β}, through use of Equation 9-1.

$$C_{\ell_\beta} = \left[\left(\frac{C_{\ell_\beta}}{C_L}\right)_\Lambda K_{m_\Lambda} K_f + \left(\frac{C_{\ell_\beta}}{C_L}\right)_A\right] C_{L_{\text{power off}}} + \left[\frac{C_{\ell_\beta}}{\Gamma} K_{m_\Gamma} + \frac{\Delta C_{\ell_\beta}}{\Gamma}\right]\Gamma$$

$$+ \left(\Delta C_{\ell_\beta}\right)_{Z_W} + \left(\frac{\Delta C_{\ell_\beta}}{\theta \tan \Lambda_{c/4}}\right)\theta \tan \Lambda_{c/4} + \left[\left(\frac{\Delta C_{\ell_\beta}}{C_{L_{\text{aero}}}}\right)_\Lambda + \left(\frac{\Delta C_{\ell_\beta}}{C_{L_{\text{aero}}}}\right)_A\right] C_{L_{\text{aero}}} \qquad (9\text{-}1)$$

The following terms are obtained from DATCOM:

$$\left[\frac{C_{\ell_\beta}}{\Gamma} K_{m_\Gamma} + \frac{\Delta C_{\ell_\beta}}{\Gamma}\right]\Gamma = 0.00088 \text{ deg}^{-1}$$

$$\left(\Delta C_{\ell_\beta}\right)_{Z_W} = -0.00146 \text{ deg}^{-1}$$

$$\left(\frac{\Delta C_{\ell_\beta}}{\theta \tan \Lambda_{c/4}}\right)\theta \tan \Lambda_{c/4} = 0.000048 \text{ deg}^{-1}$$

The total of the above terms = $-0.000532 \text{ deg}^{-1}$.

The following information is obtained from the design charts.

$$\left(\frac{C_{\ell_\beta}}{C_L}\right)_\Lambda = -0.0021 \text{ deg}^{-1} \text{ from Figure 9-2.}$$

$$\left(\frac{C_{\ell_\beta}}{C_L}\right)_A = 0.00095 \text{ deg}^{-1} \text{ from Figure 9-4.}$$

$$\left(\frac{\Delta C_{\ell_\beta}}{C_{L_{aero}}}\right)_\Lambda = -0.00077 \text{ deg}^{-1} \text{ from Figure 9-6.}$$

$$\left(\frac{\Delta C_{\ell_\beta}}{C_{L_{aero}}}\right)_A = 0.00095 \text{ deg}^{-1} \text{ from figure 9-8.}$$

Using the above information:

$$\begin{aligned} C_{\ell_\beta} &= (-0.0021 + 0.00095)\ 3.853 + (-0.00077 + 0.00095)\ 4.485 - 0.000532 \\ &= -0.00416 \text{ deg}^{-1} \end{aligned}$$

Test value = $-0.00447 \text{ deg}^{-1}$

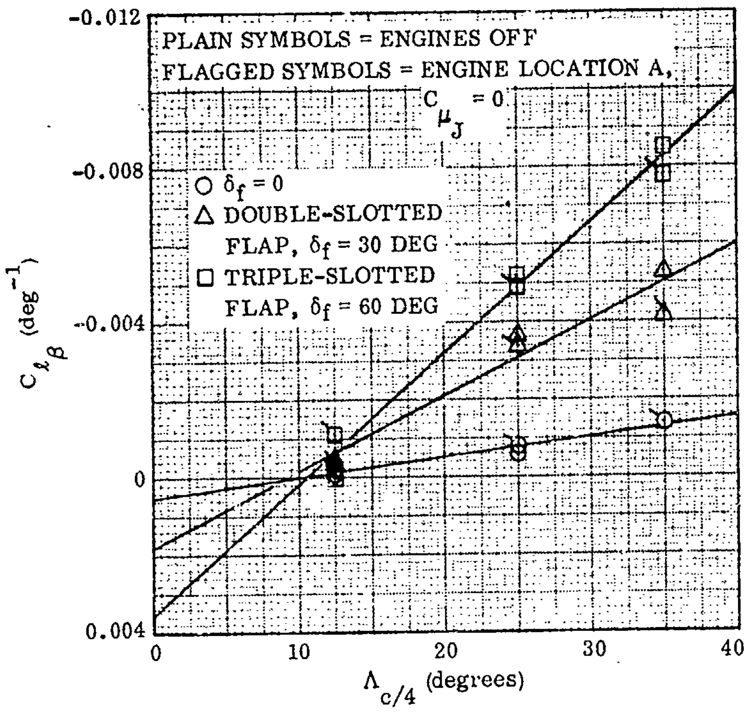

Figure 9-2. Effect of Sweep and High-Lift Devices on C_{ℓ_β}

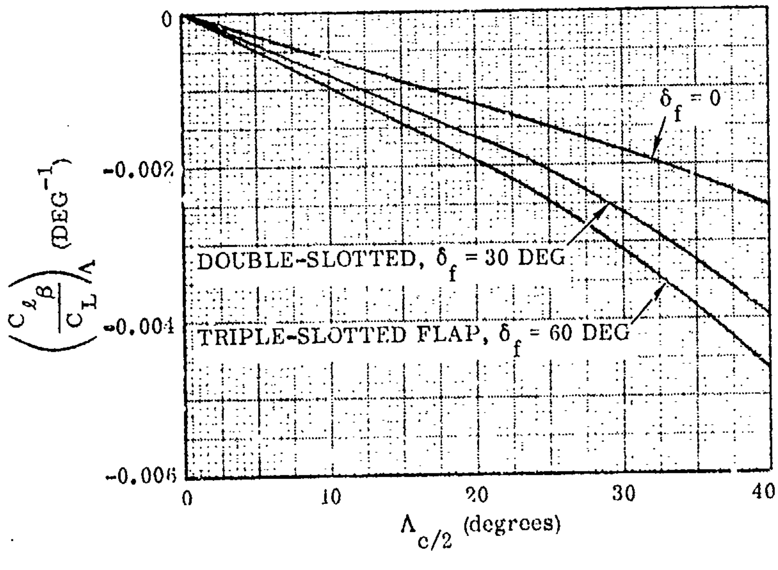

Figure 9-3. Wing Sweep Contribution to C_{ℓ_β}

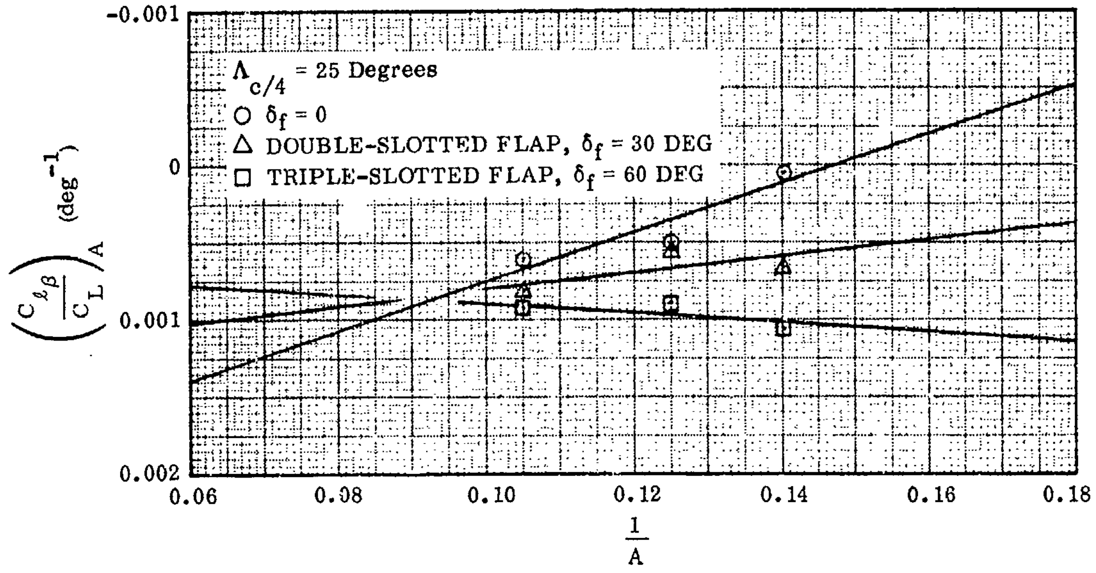

Figure 9-4. Effect of Aspect Ratio and High-Lift Devices on C_{ℓ_β}

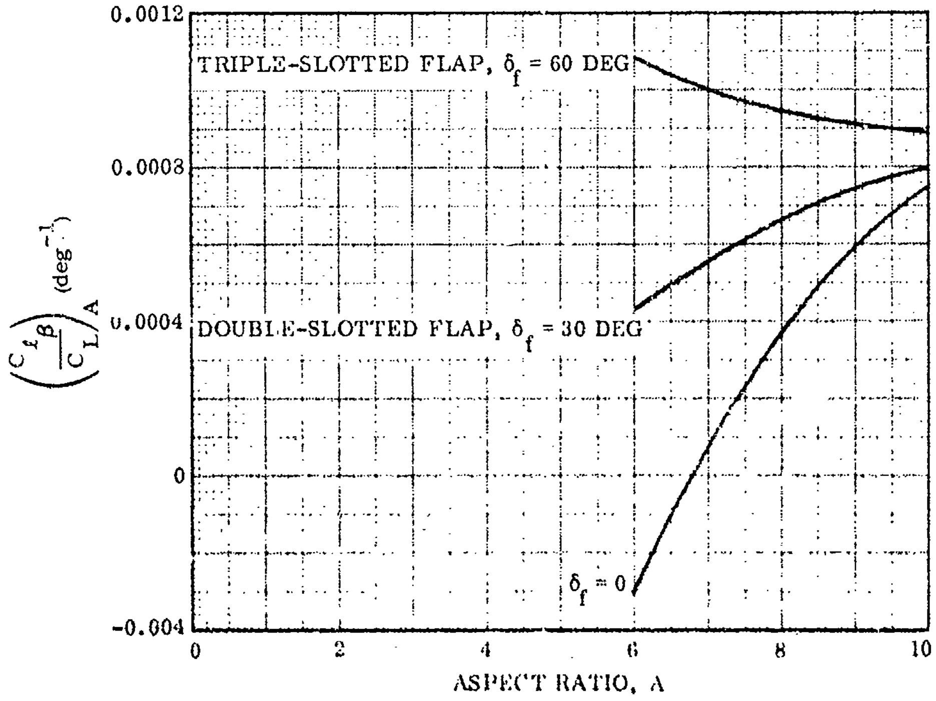

Figure 9-5. Aspect Ratio Contribution to C_{ℓ_β}

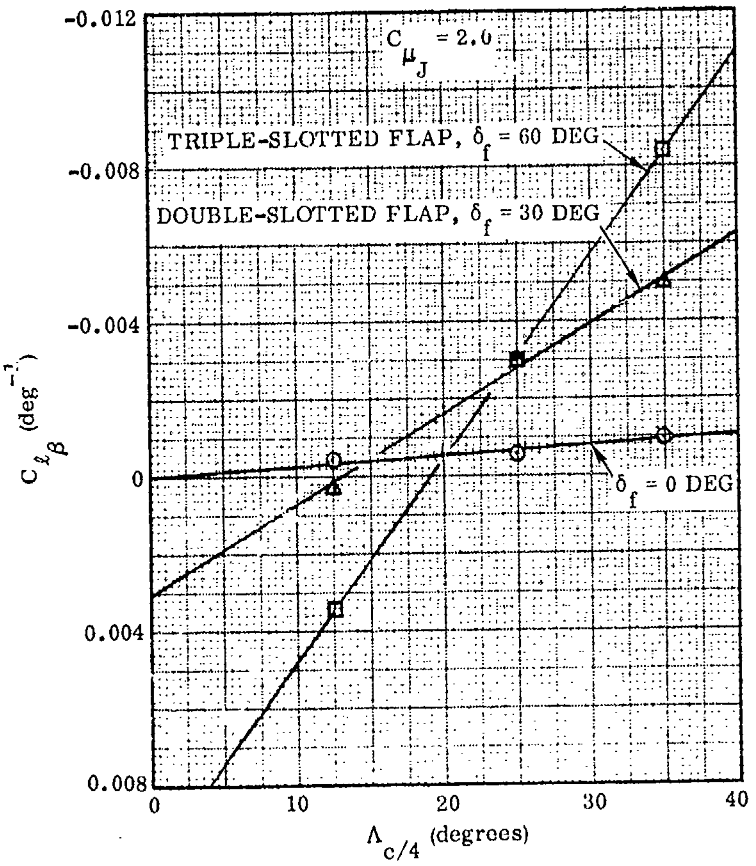

Figure 9-6. Effect of Sweep and High-Lift Devices on C_{ℓ_β}, $C_{\mu_J} = 2.0$

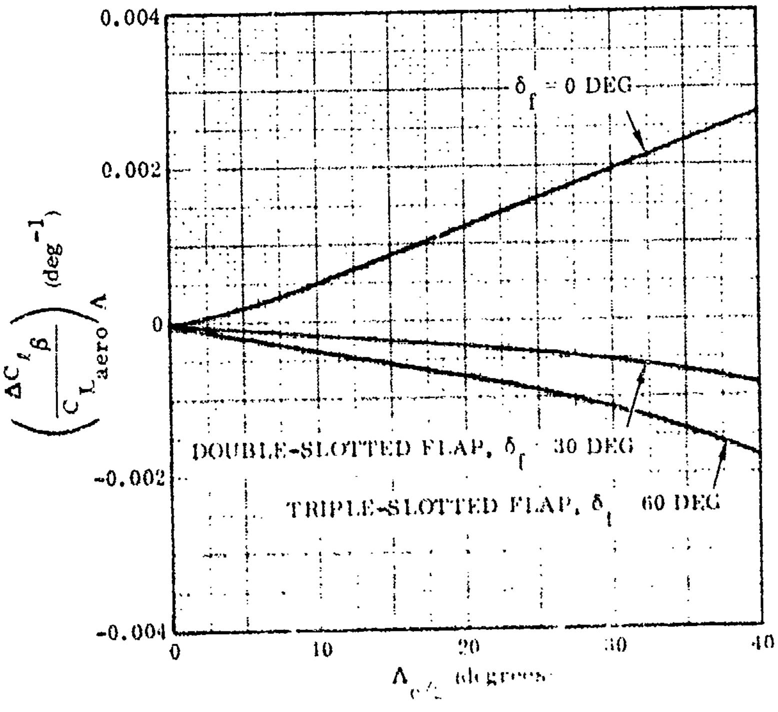

Figure 9-7. Wing Sweep Contribution to C_{ℓ_β} with Powered-Lift System

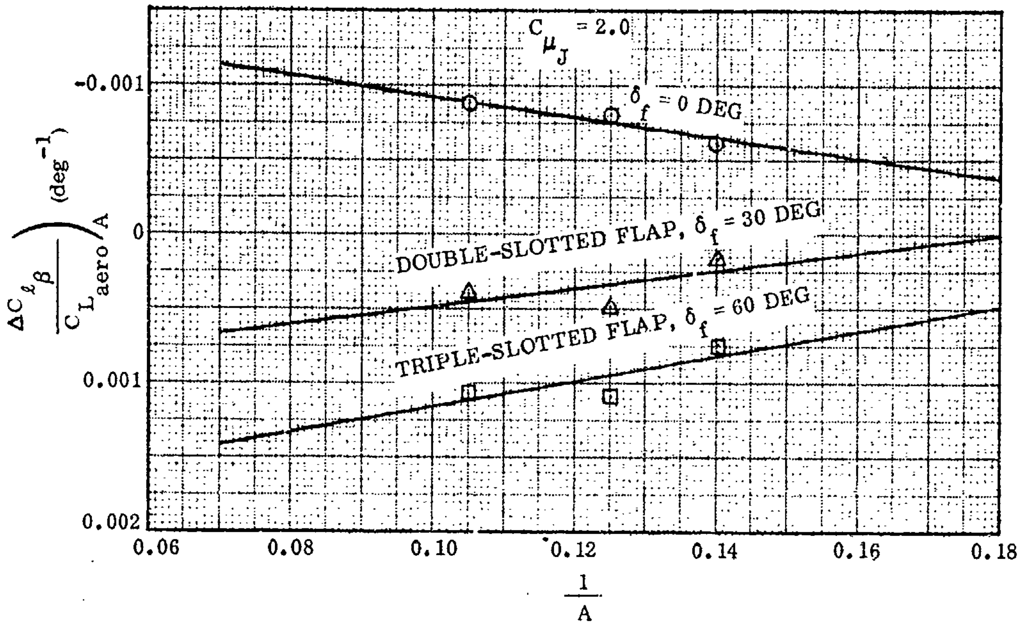

Figure 9-8. Effect of Aspect Ratio and High-Lift Devices on C_{ℓ_β}, $C_{\mu_J} = 2.0$

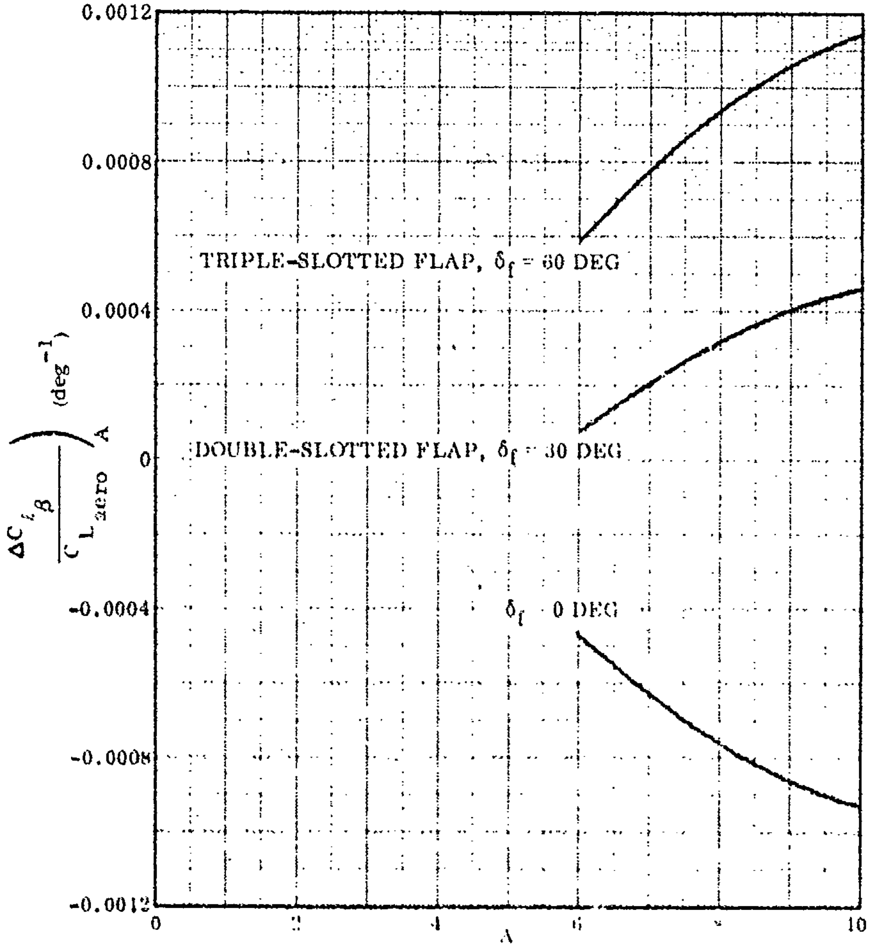

Figure 9-9. Aspect Ratio Contribution to C_{ℓ_β} with Powered-Lift System

9.2 YAWING MOMENT DUE TO SIDESLIP, C_{n_β}

It was noted previously that the equations for determining wing contributions to C_{n_β} given in DATCOM were considered inadequate. The test data has indicated that there is a large effect on C_{n_β} from high-lift devices and power. Since the mechanisms that induce these effects should be analogous to those that produce changes in C_{ℓ_β}, a similar approach to that used in Section 9.1 has been applied in determining C_{n_β}. The effects of sweep and high-lift devices are shown in Figure 9-10. Effects of the engine nacelles are also shown.

The resulting design chart for sweep effects on C_{n_β}, power off, is given in Figure 9-11. Aspect ratio contribution to C_{n_β} is derived from Figure 9-12, and the design chart for estimating this effect is presented as Figure 9-13. The increments for C_{n_β} due to the powered-lift system are given in Figures 9-14 through 9-17, where Figure 9-14 shows the test data used to determine sweep effects and Figure 9-15 is the corresponding design chart. Test data for aspect ratio effects is shown in Figure 9-16, and the design chart is in Figure 9-17.

The stability derivative, C_{n_β}, can now be obtained from the relationship in Equation 9-2.

$$C_{n_\beta} = - K_N K_{R_\ell} \frac{S_{B_s}}{S_W} \frac{\ell_B}{b} + \left[\left(\frac{C_{n_\beta}}{C_L}\right)_\Lambda + \left(\frac{C_{n_\beta}}{C_L}\right)_A\right] C_{L_{\substack{power\\off}}}$$

$$+ \left[\left(\frac{\Delta C_{n_\beta}}{C_{L_{aero}}}\right)_\Lambda + \left(\frac{\Delta C_{n_\beta}}{C_{L_{aero}}}\right)_A\right] C_{L_{aero}} \qquad (9-2)$$

where:

$- K_N K_R \frac{S_{B_s}}{S_W} \frac{\ell_B}{b}$ is obtained from Paragraph 5.2.3.1 of the DATCOM.

$\left(\frac{C_{n_\beta}}{C_L}\right)_\Lambda$ is from Figure 9-11.

$\left(\frac{C_{n_\beta}}{C_L}\right)_A$ is from Figure 9-13.

$$\left(\frac{\Delta C_{n_\beta}}{C_{L_{aero}}}\right)_\Lambda$$ is from Figure 9-15.

$$\left(\frac{\Delta C_{n_\beta}}{C_{L_{aero}}}\right)_A$$ is from Figure 9-16.

SAMPLE PROBLEM

GIVEN: Configuration defined for sample problem in Section 9.1.

CALCULATE:

Yawing moment due to sideslip, C_{n_β}, from Equation 9-2.

$$C_{n_\beta} = - K_N K_{R_\ell} \frac{S_{B_s}}{S_W} \frac{\ell_B}{b} + \left[\left(\frac{C_{n_\beta}}{C_L}\right)_\Lambda + \left(\frac{C_{n_\beta}}{C_L}\right)_A\right] C_{L_{\substack{power\\off}}} + \left[\left(\frac{\Delta C_{n_\beta}}{C_{L_{aero}}}\right)_\Lambda + \left(\frac{\Delta C_{n_\beta}}{C_{L_{aero}}}\right)_A\right] C_{L_{aero}} \tag{9-2}$$

$$-K_N K_{R_\ell} \frac{S_{B_s}}{S_W} \frac{\ell_B}{b} = -0.00277 \text{ deg}^{-1} \text{ (from DATCOM)}$$

$$\left(\frac{C_{n_\beta}}{C_L}\right)_\Lambda = 0.000242 \text{ deg}^{-1} \text{ from Figure 9-10.}$$

$$\left(\frac{C_{n_\beta}}{C_L}\right)_A = 0.00010 \text{ deg}^{-1} \text{ from Figure 9-12.}$$

$$\left(\frac{\Delta C_{n_\beta}}{C_{L_{aero}}}\right)_\Lambda = -0.00003 \text{ deg}^{-1} \text{ from Figure 9-14.}$$

$$\left(\frac{\Delta C_{n_\beta}}{C_{L_{aero}}}\right)_A = 0.00028 \text{ deg}^{-1} \text{ from Figure 9-16.}$$

Using the above information:

$$C_{n_\beta} = -0.00277 + (0.000242 + 0.00010)\ 3.853 + (-0.00003 + 0.00028)\ 4.435$$

$$= -0.000331 \text{ deg}^{-1}$$

Test value = $-0.00422 \text{ deg}^{-1}$

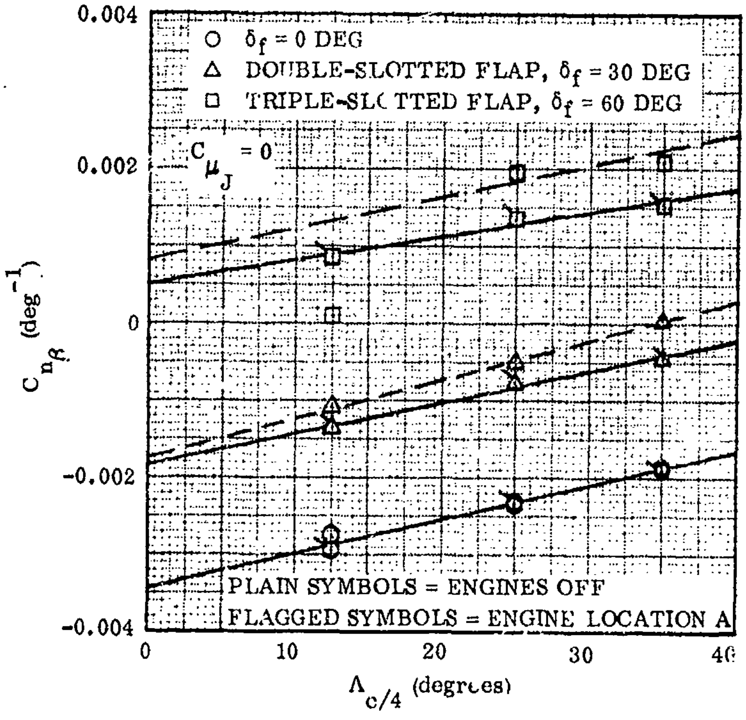

Figure 9-10. Effect of Sweep and High-Lift Devices on C_{n_β}, $C_{\mu_J} = 0$

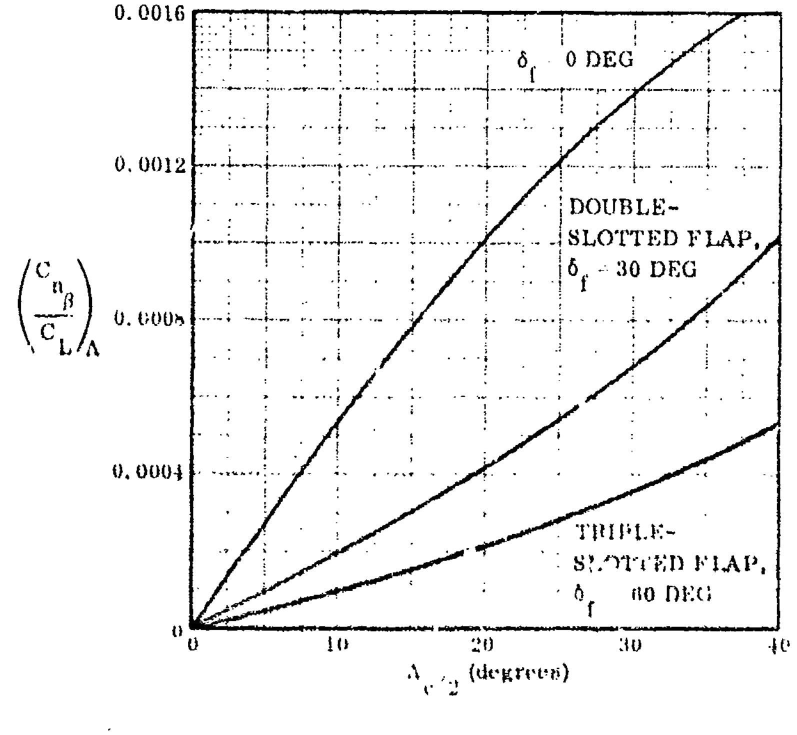

Figure 9-11. Wing Sweep Contribution to C_{n_β}, $C_{\mu_J} = 0$

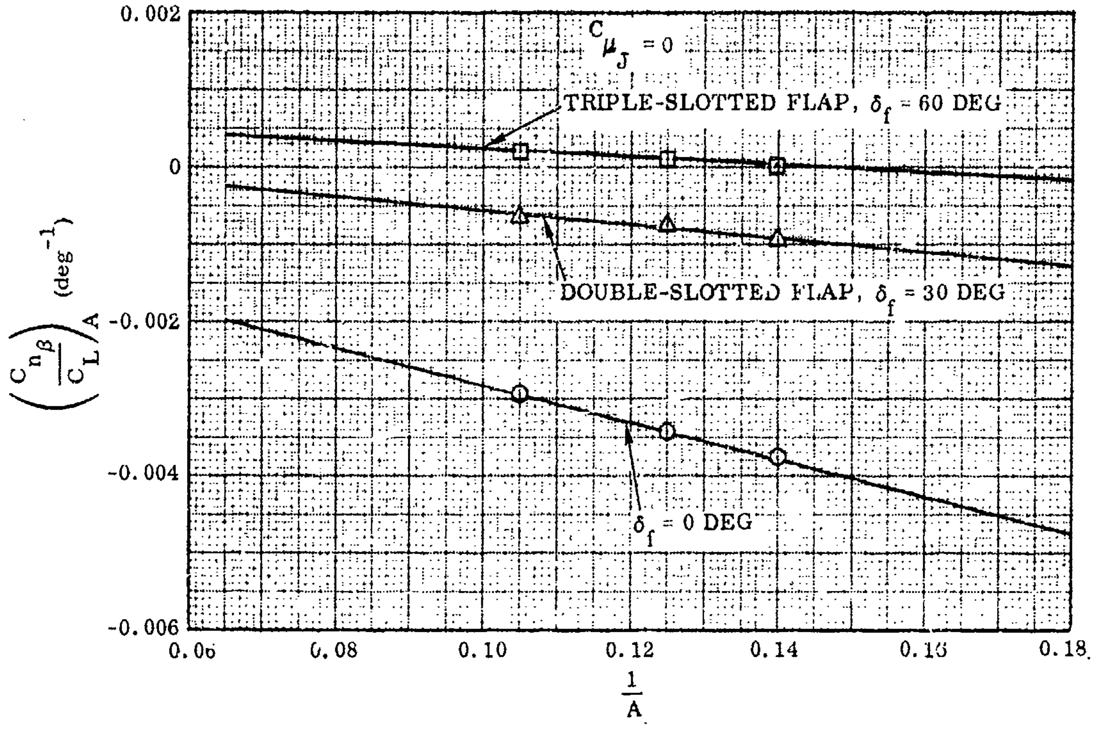

Figure 9-12. Effect of Aspect Ratio and High-Lift Devices on C_{n_β}, $C_{\mu_J} = 0$

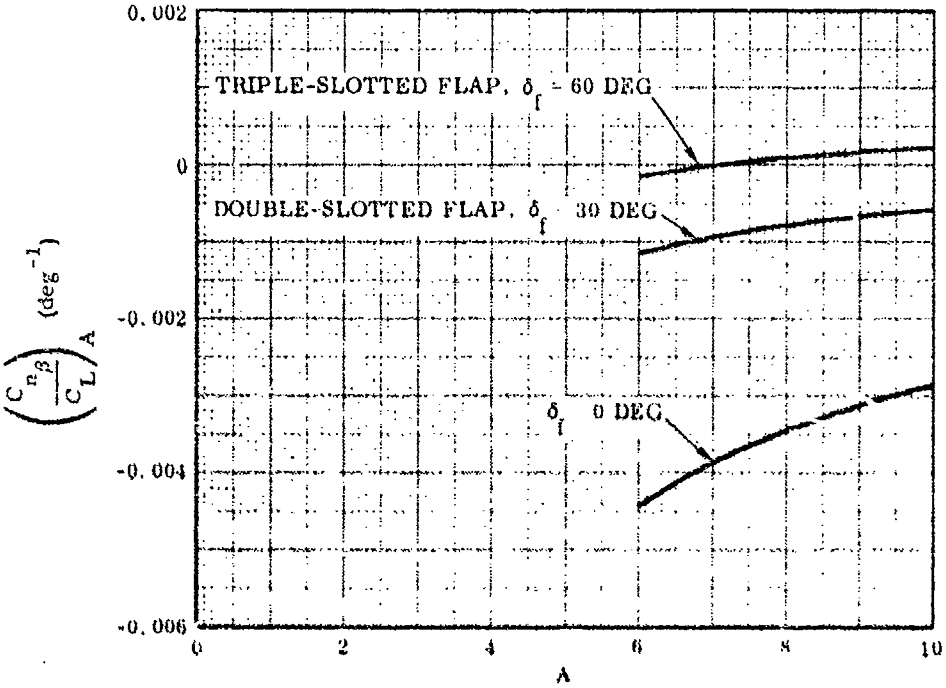

Figure 9-13. Aspect Ratio Contribution to C_{n_β}, $C_{\mu_J} = 0$

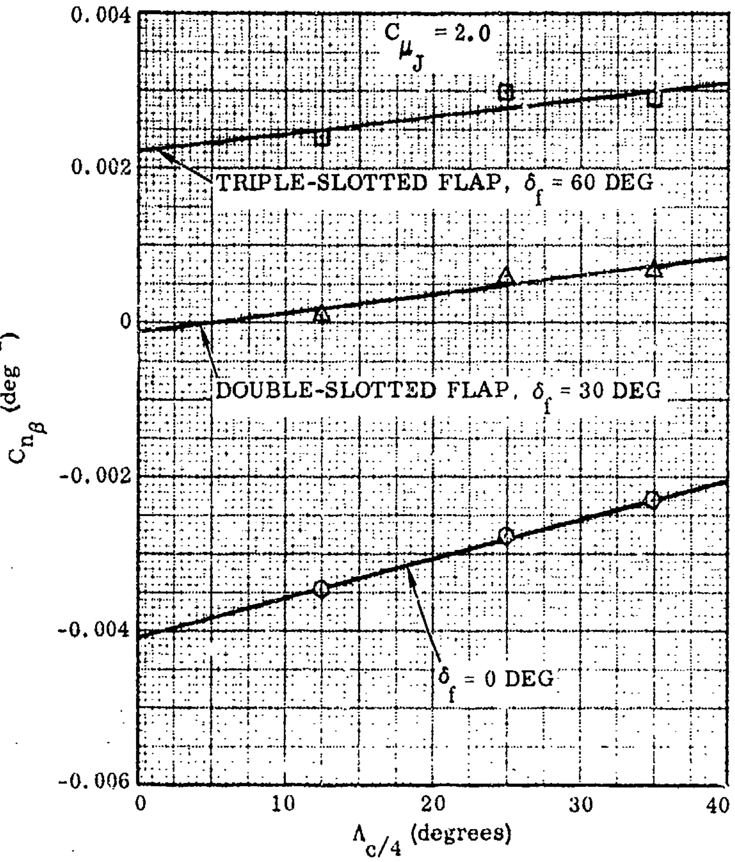

Figure 9-14. Effect of Sweep and High-Lift Devices on C_{n_β}, $C_{\mu_J} = 2$

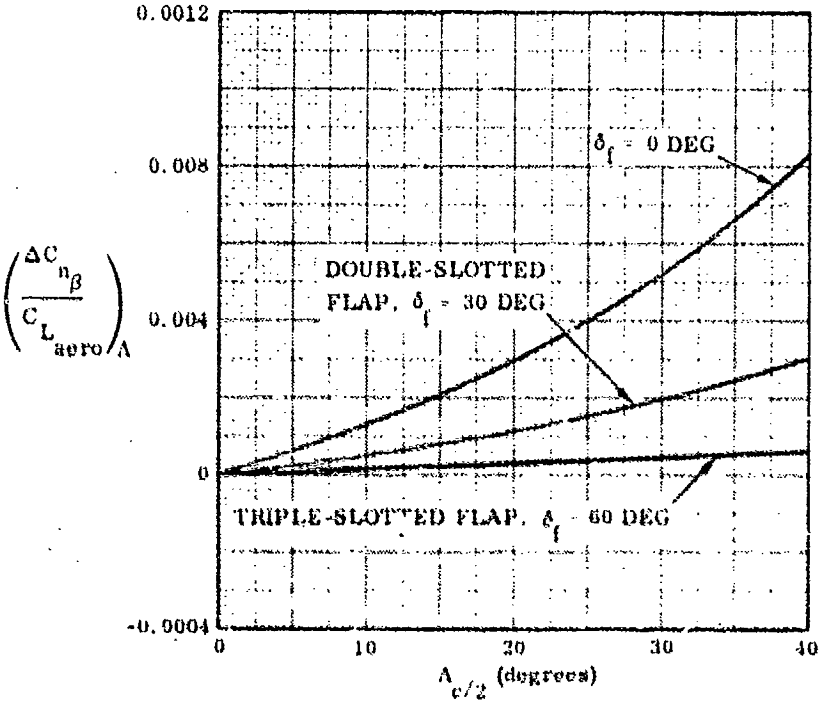

Figure 9-15. Wing Sweep Contribution to C_{n_β}, $C_{\mu_J} = 2$

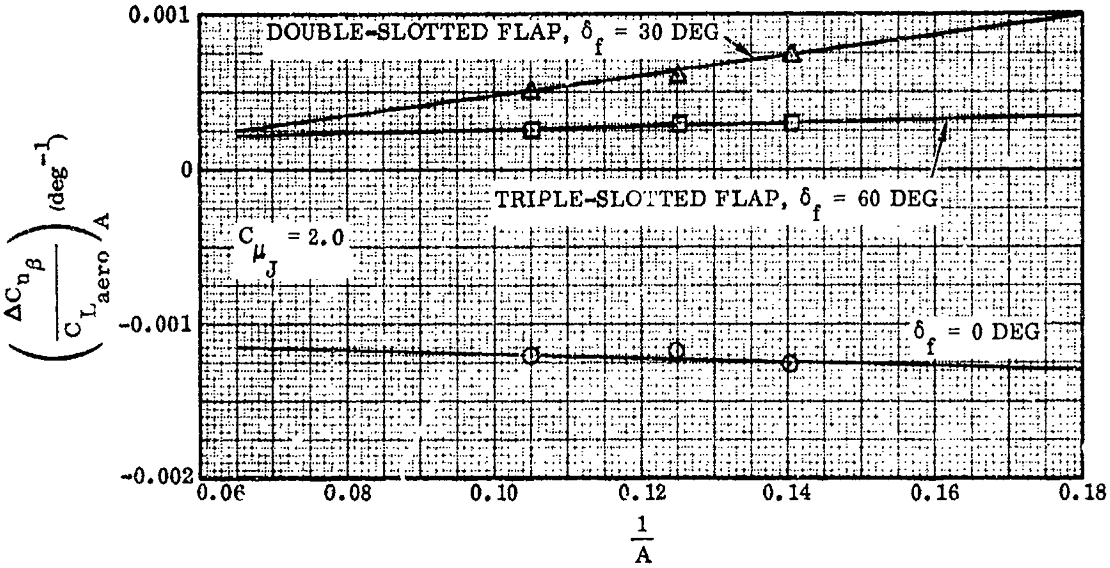

Figure 9-16. Effect of Aspect Ratio and High-Lift Devices on C_{n_β}, $C_{\mu_J} = 2$

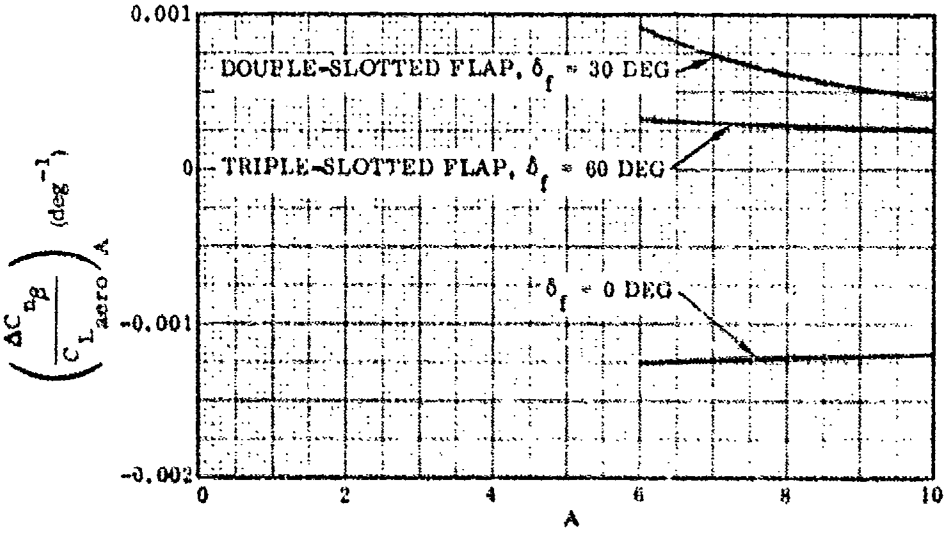

Figure 9-17. Aspect Ratio Contribution to C_{n_β} with Powered-Lift System

9.3 SIDE FORCE DUE TO SIDESLIP, C_{y_β}

Design charts for wing contributions to C_{y_β} were generated by following a procedure similar to that used to evaluate C_{ℓ_β} and C_{n_β}. Side force is inherently the least accurately determined static lateral-directional stability derivative because it produces the smallest load on the model balance system, which causes poor resolution of this force component. Fortunately, C_{y_β} does not influence aircraft flying qualities to the same extent as C_{ℓ_β} and C_{n_β}. The data presented for determining C_{y_β} is shown in the following figures.

1. Figure 9-18. Test data for determining sweep effects and the influence of high-lift devices, power off.
2. Figure 9-19. Design chart for wing sweep contribution to C_{y_β}, power off.
3. Figure 9-20. Test data used to establish aspect ratio effects, power off.
4. Figure 9-21. Design chart for aspect ratio contribution to C_{y_β}, power off.
5. Figure 9-22. Test data to establish increments due to powered-lift systems on the sweep contribution.
6. Figure 9-23. Design chart for sweep contribution to C_{y_β} with a powered-lift system.
7. Figure 9-24. Test data to establish aspect ratio effects with powered-lift system.
8. Figure 9-25. Design chart for aspect ratio contribution, with powered-lift system.

The stability derivative, C_{y_β}, can now be obtained from the relationship in Equation 9-3.

$$C_{y_\beta} = K_i \left(C_{y_\beta}\right)_B \left(\frac{\text{Body reference area}}{S_W}\right) + \left(\Delta C_{y_\beta}\right)_\Gamma$$

$$+ \left[\left(\frac{C_{y_\beta}}{C_L}\right)_\Lambda + \left(\frac{C_{y_\beta}}{C_L}\right)_A\right] C_{L_{\text{power off}}} + \left[\left(\frac{\Delta C_{y_\beta}}{C_{L_{\text{aero}}}}\right)_\Lambda + \left(\frac{\Delta C_{y_\beta}}{C_{L_{\text{aero}}}}\right)_A\right] C_{L_{\text{aero}}} \qquad (9-3)$$

where:

The first two terms are obtained from Paragraph 5.2.1.1 of the DATCOM.

$\left(\frac{C_{y_\beta}}{C_L}\right)_\Lambda$ is from Figure 9-19.

$\left(\frac{C_{y_\beta}}{C_L}\right)_A$ is from Figure 9-21.

$\left(\frac{\Delta C_{y_\beta}}{C_{L_{aero}}}\right)_\Lambda$ is from Figure 9-23.

$\left(\frac{\Delta C_{y_\beta}}{C_{L_{aero}}}\right)_A$ is from Figure 9-25.

SAMPLE PROBLEM

GIVEN: Same configuration as for sample problems in Sections 9.1 and 9.2.

CALCULATE:

Side force due to sideslip, C_{y_β}, from Equation 9-3.

$$C_{y_\beta} = K \left(C_{y_\beta}\right)_B \left(\frac{\text{Body reference area}}{S_W}\right) + \left(\Delta C_{y_\beta}\right)_\Gamma$$

$$+ \left[\left(\frac{C_{y_\beta}}{C_L}\right)_\Lambda + \left(\frac{C_{y_\beta}}{C_L}\right)_A\right] C_{L_{\substack{power\\ off}}} + \left[\left(\frac{\Delta C_{y_\beta}}{C_{L_{aero}}}\right)_\Lambda + \left(\frac{\Delta C_{y_\beta}}{C_{L_{aero}}}\right)_A\right] C_{L_{aero}} \qquad (9\text{-}3)$$

$$K_i \left(C_{y_\beta}\right)_B \left(\frac{\text{Body refererence area}}{S_W}\right) = -0.0080 \text{ deg}^{-1} \text{ (from DATCOM)}$$

$\left(\Delta C_{y_\beta}\right)_\Gamma$ = 0.00035 deg^{-1} (from DATCOM)

Total of above terms = −0.00765 deg^{-1}.

$\left(\frac{C_{y_\beta}}{C_L}\right)_A$ = 0.00122 deg^{-1} from Figure 9-18.

$\left(\frac{C_{y_\beta}}{C_L}\right)_A$ = −0.00532 deg^{-1} from Figure 9-20.

$\left(\frac{\Delta C_{y_\beta}}{C_{L_{\text{aero}}}}\right)_A$ = 0.00195 deg^{-1} from Figure 9-22.

$\left(\frac{\Delta C_{y_\beta}}{C_{L_{\text{aero}}}}\right)_A$ = −0.0036 deg^{-1} from Figure 9-24.

Using the above information:

$$\begin{aligned} C_{y_\beta} &= (0.00122 + 0.00532)\ 3.853 + (0.00195 - 0.0036)\ 4.485 - 0.00765 \\ &= -0.03085 \text{ deg}^{-1} \end{aligned}$$

Test value = −0.03109 deg^{-1}.

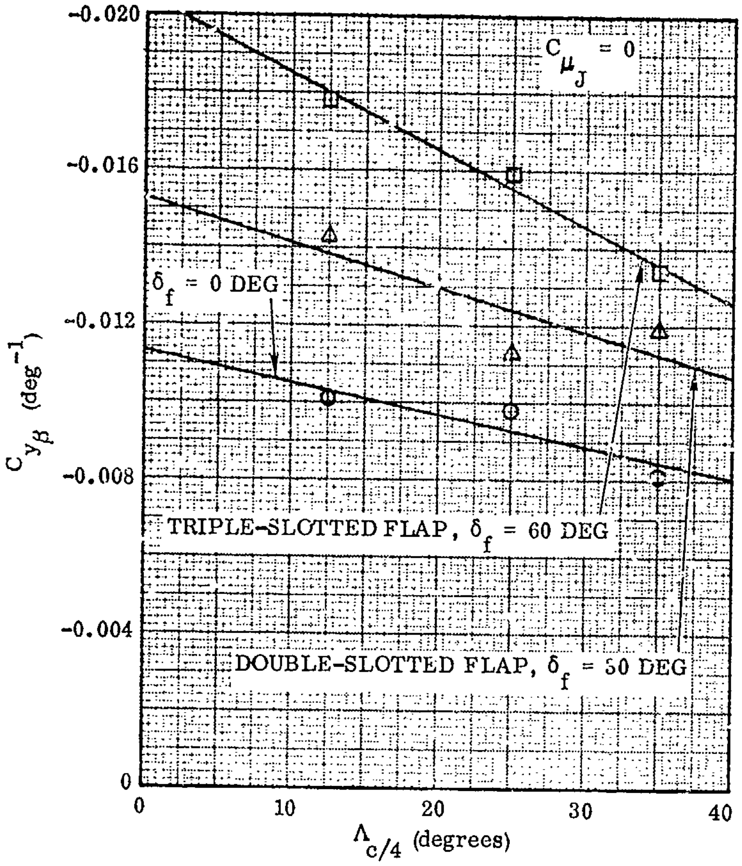

Figure 9-18. Effect of Sweep and High-Lift Devices on C_{y_β}, $C_{\mu_J} = 0$

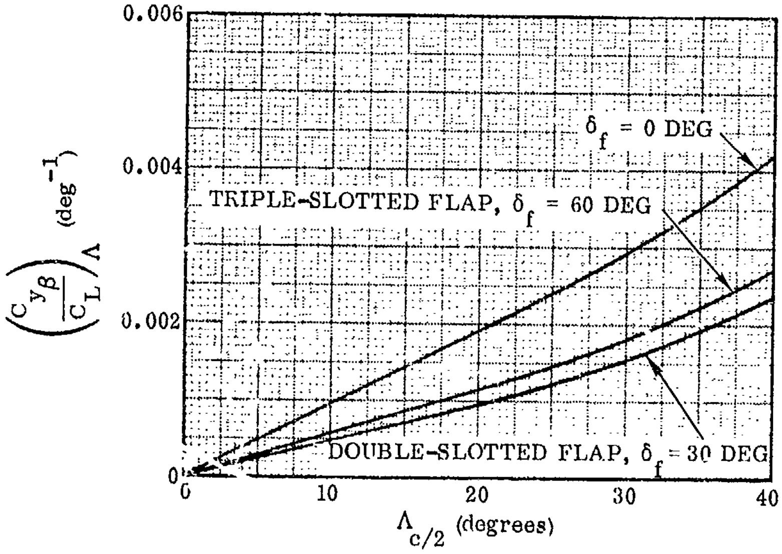

Figure 9-19. Sweep Contribution to C_{y_β}, $C_{\mu_J} = 0$

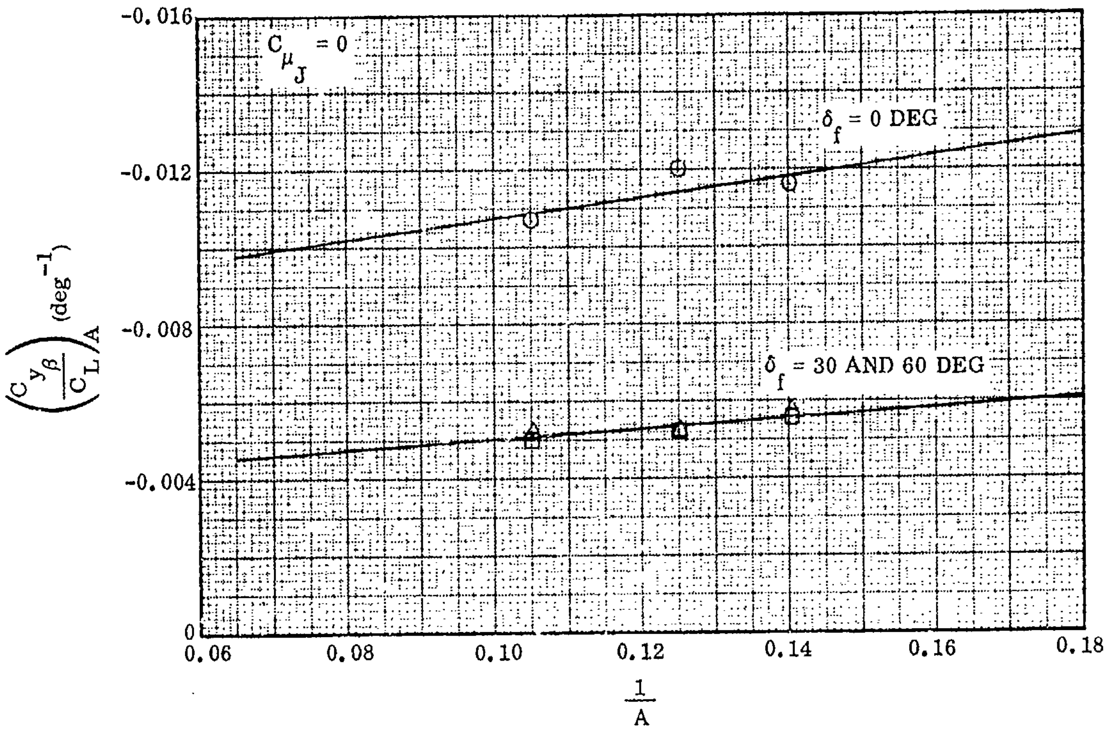

Figure 9-20. Effect of Aspect Ratio and High-Lift Devices on C_{y_β}, $C_{\mu_J} = 0$

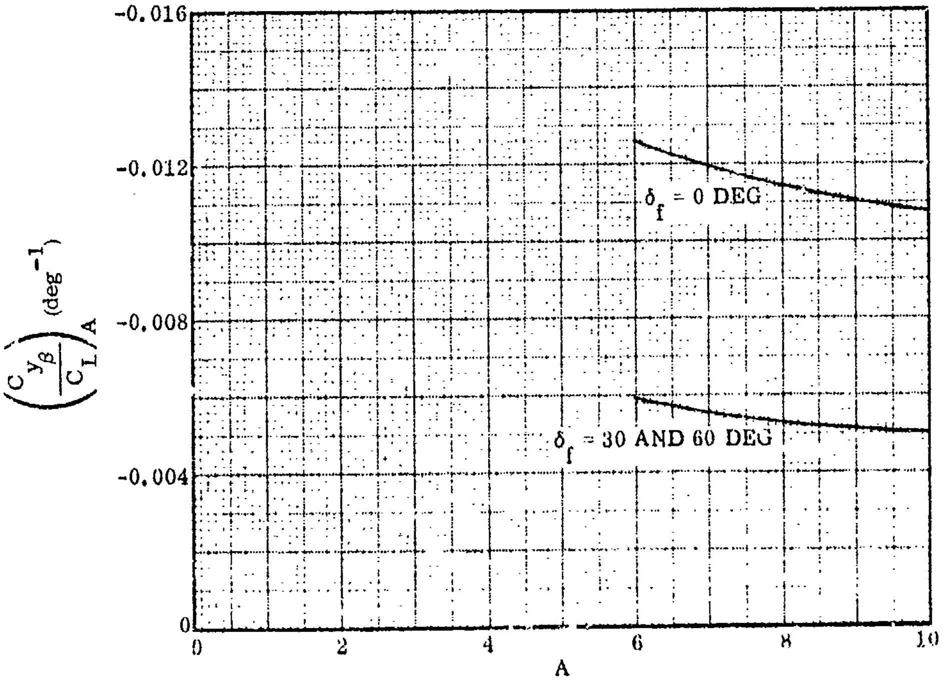

Figure 9-21. Aspect Ratio Contribution to C_{y_β}, $C_{\mu_J} = 0$

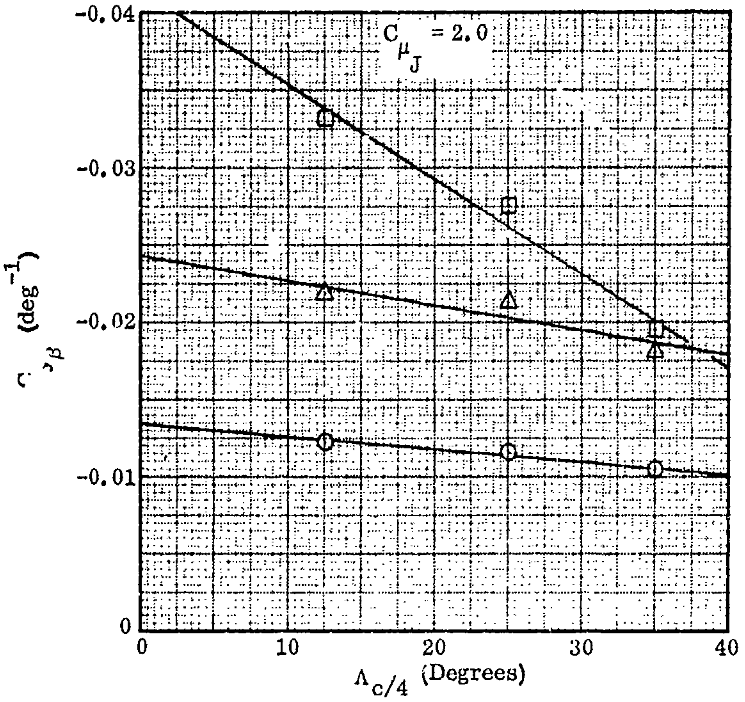

Figure 9-22. Effect of Sweep and High-Lift Devices on C_{y_β}, $C_{\mu_J} = 2$

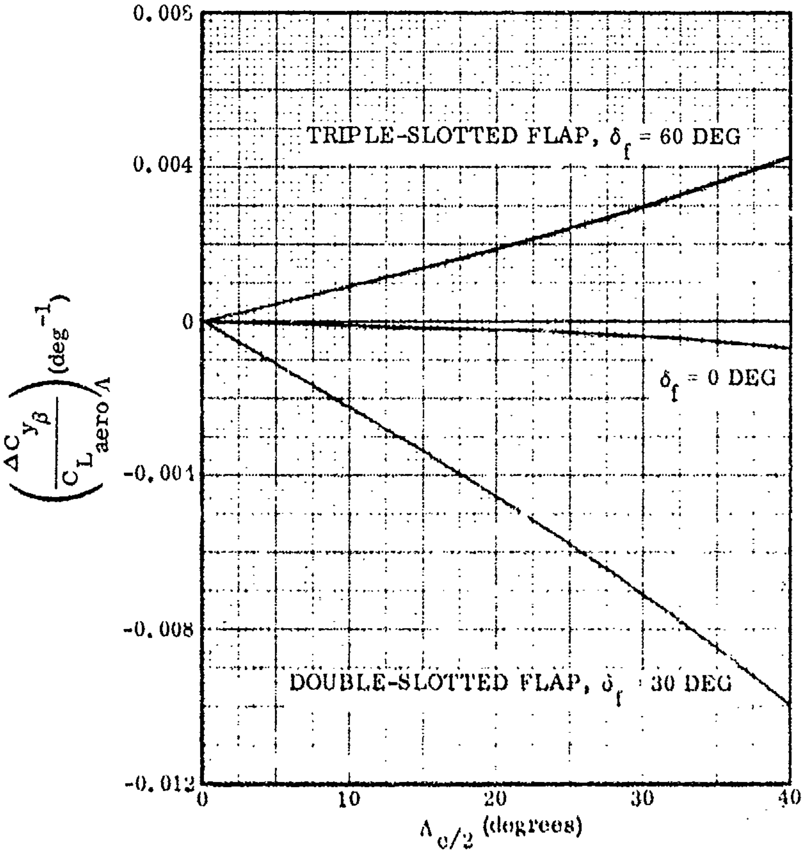

Figure 9-23. Sweep Contribution to C_{y_β} with Powered-Lift System

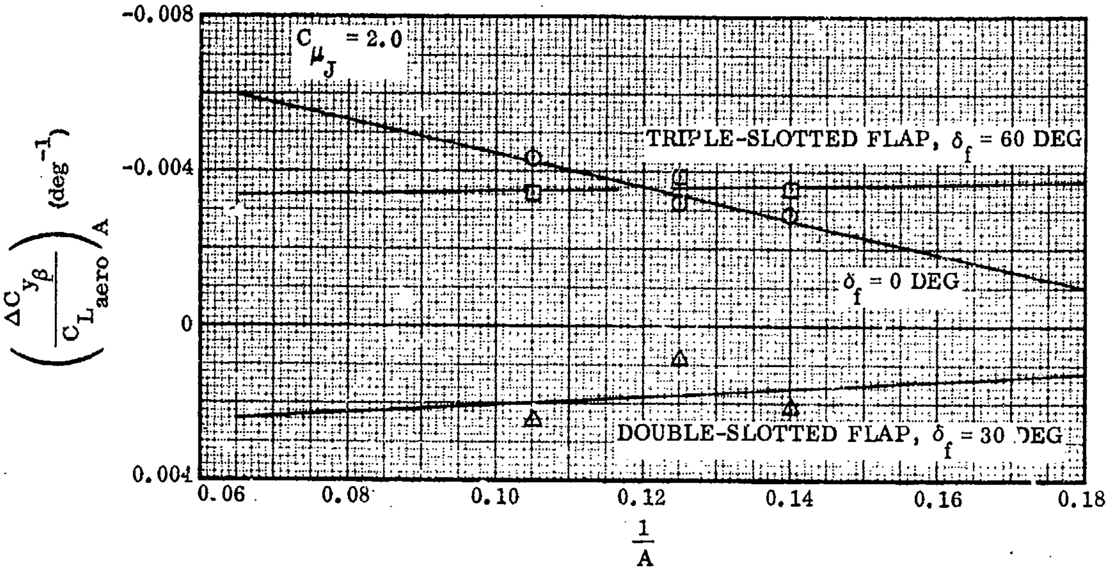

Figure 9-24. Effect of Aspect Ratio and High-Lift Devices on C_{y_β}, $C_{\mu_J} = 2$

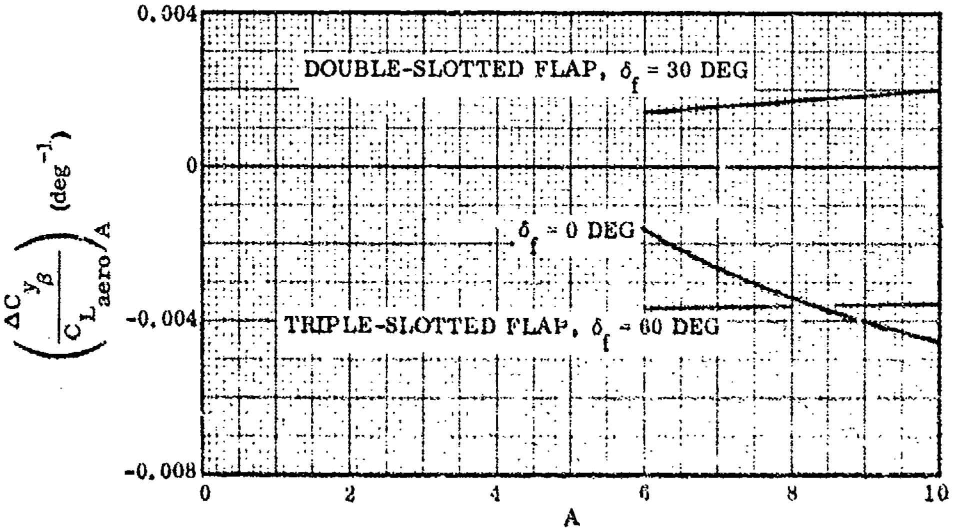

Figure 9-25. Aspect Ratio Contribution to C_{y_β} with Powered-Lift System

9.4 DATA CORRELATION FOR LATERAL-DIRECTIONAL STABILITY DERIVATIVES

The comparisons of calculated and test values for C_{ℓ_β}, C_{n_β} and C_{y_β} are shown in Tables 9-1, 9-2 and 9-3, respectively. The errors obtained for C_{ℓ_β} and C_{y_β} for the power-on case are approximately equal to those indicated in DATCOM for the power-off case. However, the predicted C_{n_β} values generally show more instability than the test data. The predicted C_{n_β} values can be made close to the test values by adding a constant value of 0.0015 deg^{-1} to each predicted value.

Table 9-1. Data Substantiation for C_{ℓ_β}

$\Lambda_{c/4}$ (deg)	Flap Slots	δ_f (deg)	$\left(C_{\ell_\beta}\right)_{CALC} \times 10^{-3}$	$\left(C_{\ell_\beta}\right)_{TEST} \times 10^{-3}$	$\Delta C_{\ell_\beta} \times 10^{-3}$
25	Double	30	-3.55	-3.192	0.358
25	Double	30	-3.55	-2.488	1.062
25	Double	30	-3.52	-3.424	0.096
25	Double	30	-3.53	-3.125	0.405
25	Double	60	-3.72	-3.988	-0.268
25	Triple	60	-4.16	-4.470	-0.310
25	Triple	60	-4.27	-3.416	0.854
25	Double	60	-3.71	-4.136	-0.426
25	Triple	60	-4.48	-2.717	1.763
35	--	0	-0.597	-1.16	-0.563
35	--	0	-0.507	-1.31	-0.803
35	--	0	-0.553	-0.61	-0.057
35	Double	30	-5.496	-4.95	0.546
35	Double	60	-8.788	-6.80	1.988
35	Triple	60	-9.572	-6.81	2.762

$$\Delta C_{\ell_{\beta_{ave}}} = \sum \frac{\left|\Delta C_{\ell_\beta} \times 10^{-3}\right|}{n} = 0.817 \times 10^{-3}$$

Table 9-2. Data Substantiation for C_{n_β}

$\Lambda_{c/4}$ (deg)	Flap Slots	δ_f (deg)	$\left(C_{n_\beta}\right)_{CALC} \times 10^{-3}$	$\left(C_{n_\beta}\right)_{TEST} \times 10^{-3}$	$\Delta C_{n_\beta} \times 10^{-3}$
25	Double	30	-2.43	-1.684	0.746
25	Double	30	-2.35	-0.845	1.505
25	Double	30	-3.06	-1.297	1.763
25	Double	30	-3.04	-1.138	1.902
25	Double	60	-1.07	2.339	3.409
25	Triple	60	-0.33	4.223	4.553
25	Triple	60	-0.44	4.061	4.501
25	Double	60	-1.03	2.731	3.761
25	Triple	60	-0.23	-1.935	-1.705
35	--	0	-1.902	-2.18	-0.278
35	--	0	-1.421	-2.78	-1.359
35	--	0	-1.268	-2.09	-0.822
35	Double	30	0.969	0.79	-0.179
35	Double	60	2.578	3.37	0.792
35	Triple	60	2.574	2.67	0.096

$$\Delta C_{n_{\beta_{ave}}} = \sum \frac{\left|\Delta C_{n_\beta} \times 10^{-3}\right|}{n} = 1.825 \times 10^{-3}$$

Table 9-3. Data Substantiation for C_{y_β}

$\Lambda_{c/4}$ (deg)	Flap Slots	δ_f (deg)	$\left(C_{y_\beta}\right)_{CALC} \times 10^{-3}$	$\left(C_{y_\beta}\right)_{TEST} \times 10^{-3}$	$\Delta C_{y_\beta} \times 10^{-3}$
25	Double	30	-26.85	-16.53	10.32
25	Double	30	-27.29	-14.27	13.02
25	Double	30	-22.79	-14.34	8.45
25	Double	30	-22.96	-14.76	8.20
25	Double	60	-24.70	-25.00	-0.30
25	Triple	60	-30.85	-32.01	-1.16
25	Triple	60	-30.19	-31.09	-0.90
25	Double	60	-25.00	-25.53	-0.53
25	Triple	60	-32.03	-18.83	13.20
35	--	0	-9.224	-10.29	-1.066
35	--	0	-6.865	-12.75	-5.885
35	--	0	-6.082	-11.43	-5.348
35	Double	30	-24.00	-17.03	6.97
35	Double	60	-12.410	-24.38	-11.97
35	Triple	60	-13.364	-24.23	-10.866

$$\Delta C_{y_{\beta_{ave}}} = \sum \frac{\left|\Delta C_{y_\beta} \times 10^{-3}\right|}{n} = 6.55 \times 10^{-3}$$

SECTION 10

CONCLUSIONS

A general methodology has been developed for predicting the low speed aerodynamic and stability characteristics of STOL transport aircraft. The methodology is applicable to the EBF, IBF and MF/VT STOL concepts. The basic procedures, which predict the lift curve versus angle of attack, maximum lift coefficient, induced drag, thrust recovery, pitching moment, and downwash angle are easily hand-calculated for a single case or programmed on a small computer to calculate a large number of configurations. The methodology has been evaluated by comparing its results with wind tunnel test data obtained under the current STOL program for EBF, IBF and MF/VT configurations over a range of jet momentum coefficients from zero to four and with a wide variety of jet nacelle locations and trailing flap configurations.

The following conclusions are based largely on the results of numerous correlations indicated in Sections 4 through 9.

1. The lift and induced drag characteristics of EBF, IBF, and MF/VT configurations are estimated reasonably well by using the EBF/IBF analogy method and the assumption that only the portion of the jet momentum captured by the flaps contributes to the supercirculatory lift.
2. The assumption made in the methodology that there is no supercirculation (favorable lift interference) from the jet momentum not captured by the flaps agrees well with the EBF test data for partial capture. The methodology underpredicts the MF/VT lift at high jet momentum coefficients, indicating some favorable interference for the latter system — especially when the thrust vectoring angle is close to the flap deflection angle.
3. EBF lift values are relatively insensitive to the assumed extent of spanwise jet spreading. The assumption in the methodology of a minimum jet expansion angle of 6 degrees gave satisfactory agreement for the EBF comparisons.
4. The methodology utilizes previous empirical correlations of flap turning efficiency to account for effects of boundary layer separation on flap effectiveness and on lift curve slope. These correlations tend to overestimate the adverse effects of separation on lift for the triple- and double-slotted flap configurations.

5. Plain IBF configurations at $C_{\mu_T} \geq 0.5$ have effectively eliminated flap separation effects on lift and achieved the full potential-flow theory values of lift, including supercirculation effects, beyond this jet momentum coefficient.

6. EBF-system nacelles must be located so that the jet exhaust penetrates the first flap slot to be effective in eliminating flap separation effects on lift and achieves a BLC effect over the entire flapped span of the wing for $C_{\mu_J} \geq 1.0$.

7. The assumption, for maximum lift, that stall occurs when the pressure loading near the leading edge reaches the same value as at the stall condition with flaps retracted and with no blowing was found to lead to a satisfactory prediction of maximum lift coefficient under the following conditions:

   - Separation must be assumed at or behind the knee of the leading edge device rather than at the leading edge of the wing.
   - Effects of power on maximum lift coefficient include the influence on the downwash angle on the pressure loading, as introduced into the current methodology.
   - Stall does not occur over the trailing flaps.

8. The methodology assumes that the aerodynamic efficiency (induced drag factor) increases with increasing jet momentum coefficient one-half as fast for the EBF configuration (because of the peaky spanloading) as for the IBF cases.

9. Detailed methods for predicting the power-off minimum profile drag coefficient and the power-off induced drag factor are not included and must be found from either test results or alternative procedures.

10. The defined thrust recovery is the negative of the rate of change of minimum profile drag coefficient with jet momentum coefficient and is independent of lift coefficient. The test values are sensitive to the assumed induced drag factors when the drag curve is nonparabolic.

    The thrust recovery in the methodology is approximately the same as the jet static turning efficiency for both the EBF and IBF configurations. In the IBF case, a value of thrust recovery equal to 80 percent was found to be satisfactory for all flap deflections angles up to 60 degrees (jet upper surface angles of 72 degrees). For the EBF case, the thrust recovery was correlated with a theoretical equation for the idealized static turning efficiency of a planar wing.

11. The methods for the mechanical flap two-dimensional flap-pitching moment increments were not greatly affected by the planform variations so the three-dimensional values were obtained by applying rudimentary 3-D corrections. The

method for internally blown flaps with multiple chord segments was developed through an extension of Spence's theory. The mathematical model for the externally blown flap configuration appears to give satisfactory results for the flap slots immersed in the engine exhaust.

12. The extensive tail wake rake surveys indicated that the downwash behaved in accordance with the trends predicted by simple lifting line theory. A tail downwash methodology was developed, utilizing lifting line equations with a correction to account for vertical displacement of the wing wake. Powered-lift systems effects were accounted for by normalizing downwash angle with respect to aerodynamic lift (i.e., lift coefficient with direct thrust terms removed) to furnish impressive correlations.

13. The method presented in DATCOM for predicting C_{ℓ_β} was extended to include the effects of high-lift systems and the incremental effects of the powered lift. Analogous curves were also developed to predict the wing contributions to C_{n_β} and C_{n_β}. Satisfactory correlations with test data were achieved for C_{ℓ_β} and C_{y_β} but further improvement is required for C_{n_β}.

A recommended Phase II program is described in detail in Volume I, Configuration Definition Report.

SECTION 11

REFERENCES

3-1 USAF Stability and Central DATCOM, October 1960 with revisions through February 1972.

3-2 K. E. Marks, Method for Calculating Wing High-Lift Characteristics Using Nonlinear Section Data, Convair Aerospace report GDC-ERR-1560, San Diego, Calif, December 1970.

3-3 T. Strand, The Jet Flap — Review and Extension, Convair Aerospace report ZA-255, November 1957.

3-4 R. A. Hartunian, The Finite Aspect Ratio Jet Flap, Cornell Aeronautical Laboratory report AI-1190-A-3, October 1959.

3-5 K. P. Kerney, "A Theory of the High-Aspect-Ratio Jet Flap," AIAA Journal, Vol 9, No. 3, March 1971, pp 431-435.

3-6 W. H. Gallaher, Three-Dimensional Jet Flap Theory with Partial Span Flaps, Convair Aerospace report GDCA-ERR-1752, San Diego, Calif, December 1972.

3-7 A. Das, Tragflachentheorie fur Tragflugel mit Strahlklappen, Jahrbach 1960, der Wiss. Gesellschaft fur Luftfahrt, pp 112-133, 1960, or: Lifting Surface Theory for Wings with Jet Flaps, National Research Council of Canada, NRC-77-1122, 1964.

3-8 E. S. Levinsky, Wing-in-Jet Method and Fortran Program for STOL Aircraft with Externally Blown Flaps, Convair Aerospace report GDCA-ERR-1750, San Diego, Calif, December 1972.

3-9 E. S. Levinsky and J. C. Ramsey, Methodology for Estimating STOL Aircraft High Lift Systems Characteristics, AIAA Paper No. 72-779, AIAA 4th Aircraft Design, Flight Test, and Operations Meeting, August 7-9, 1972.

3-10 E. S. Levinsky, Evaluation of Two-Dimensional Mechanical and Internally Blown Flap Airfoil Data with and without Leading Edge, Convair Aerospace report GDCA-ERR-1751, San Diego, Calif, December 1972.

3-11 J. C. Ramsey and E. C. Laudeman, et. al., STOL Tactical Aircraft Investigation, Vol IV, "Wind Tunnel Data Analysis," Convair Aerospace report GDCA-DHG73-001, 31 January 1973.

3-12 C. C. Smith, Jr., Pressure Distributions on an External-Flow Jet Augmented Flap STOL Model, NASA LWP-908, October 1970.

3-13 G. C. Green and B. Perry, "Aerodynamic Loads Measurements on Ext. Blown Flaps STOL Model," in STOL Technical Conference Slides. October 1972.

3-14 L. Ting, C. H. Liu and G. Kleinstein, "Interference of Wing and Multipropellers", *AIAA Journal*, Vol 10, No. 7, July 1972, pp 906-914.

3-15 F. Chow, E. Krause, C. H. Liu and J. Mao, "Numerical Investigations of an Airfoil in a Nonuniform Stream", *Journal of Aircraft*, Vol 7, No. 6, November-December 1970, pp 531-537.

3-16 G. R. Ludwig and J. C. Erickson, Jr., "Numerical Investigation of an Airfoil in a Nonuniform Stream", *Journal of Aircraft*, Vol 8, No. 11, November 1971, p 874.

3-17 C. A. Schollenberger, *Analysis and Interaction of Jets and Airfoils in Two Dimensions*, AIAA Paper 72-777, August 1972.

3-18 D. A. Spence, "The Lift on a Thin Airfoil with a Jet-Augmented Flap," *Aeronautical Quarterly*, Vol 9, Pt 3, August 1958, pp 287-299.

Also, Royal Aircraft Establishment Technical Note No. 2450, May 1956.

3-19 F. Thomas, *Untersuchungen über die Erhohung des Auftriebes von Tragflügeln mittels Grenzschichlbeeinflussung durch Ausblasen*, Z. Flug Wiss, Vol 10, 1962, pp 46-65.

4-1 D. A. Spence, "The Lift-Coefficient of a Thin Jet-Flapped Wing," *Proceedings of the Royal Aeronautical Society*, Series A, Vol 238, No. 1212, 1956, pp 46-68.

4-2 D. A. Spence, *A Treatment of the Jet Flap by Thin-Aerofoil Theory*, Royal Aircraft Establishment, report 2568, November 1955.

4-3 D. A. Spence, "Some Simple Results for Two-Dimensional Jet Flap Aerofoils," *Aeronautical Quarterly*, Vol IX, Pt 4, November 1958, pp 395-406.

4-4 J. Hebert, et. al., *Effects of High Lift Devices on V/STOL Aircraft Performance*, USAAVLABS Technical Report 70-33A, Vol 1, June 1969.

4-5 Wenzinger, C. J., and Harris, T. A., "Wind-Tunnel Investigation of an NACA 23012 Airfoil with Various Arrangements of Slotted Flaps," NACA TR 664, 1939.

4-6 Wenzinger, C. J. and Garavain, W., "Wind-Tunnel Investigation of an NACA 23012 Airfoil with a Slotted Flap and Three types of Auxiliary Flap," NACA TR679, 1939.

4-7 Harris, T.A. and Recant, I. G., "Wind-Tunnel Investigation of NACA 23012, 23021, and 23030 Airfoils Equipped With 40-Percent Chord Double Slotted Flaps," NACA 723, 1941.

4-8 Lowry, J. G., "Wind-Tunnel Investigation of an NACA 23012 Airfoil With Several Arrangements of Slotted Flaps With Extended Lips," NACA TN808, 1941.

4-9 Cahill, J. F., "Two-Dimensional Wind-Tunnel Investigation of Four Types of High-Lift Flap on an NACA 65-210 Airfoil Section," NACA TN1191, Feb. 1947.

4-10 Unpublished General Dynamics/Convair Data.

4-11 Unpublished Canadair Data.

5-1 P. H. Perry, *A Review of Some Published Data on the External-Flow Jet-Augmented Flap*, with Appendix by D. N. Foster, Royal Aircraft Establishment Report 70240, December 1970.

5-2 D. J. Moorhouse, "A Practical Look at the Stall and High Lift Operation of Externally Blown Flap STOL Transport Configurations," presented at the AGARD Conference on *Fluid Dynamics of Aircraft Stalling*, Lisbon, Portugal, April 1972.

6-1 *Aerospace Handbook*, Aerospace report FZA-381-II, Fort Worth, Texas, October 1972.

6-2 F. C. Maskell and D. A. Spence, "A Theory of the Jet Flap in Three Dimensions," *Proceedings of Royal Society*, Series A, Vol 251, No. 1266, June 1959.

Also Royal Aircraft Establishment report Aero 2612, September 1958.

6-3 T. Strand, E. S. Levinsky and M. H. Y. Wei, "Unified Performance Theory for V/STOL Aircraft in Equilibrium Flight, Part I and II," *Journal of Aircraft*, Vol 4, No. 2 and 3, March-April, May-June 1967.

7-1 J. Hebert, et. al., *Effects of High-Lift Devices on V/STOL Aircraft Performance*, USAAVLABS Technical Report 70-33A, October 1970.

7-2 H. S. Ribner, "The Ring Airfoil in Nonaxial Flow," *Journal of the Aeronautical Sciences*, September 1947.

8-1 J. C. Ramsey and E. C. Laudeman, et. al., *STOL Tactical Aircraft Investigation*, Vol IV, "Wind Tunnel Data Analysis," Convair Aerospace report GDCA-DHG73-001, 31 January 1973.

9-1 T. A. Toll and M. J. Queijo, *Approximate Relations and Charts for Low Speed Stability Derivatives of Swept Wings*, NACA TN 1581, 1948.

9-2 E. C. Polhamus and W. C. Sleeman, Jr., *The Rolling Moment Due to Sideslip of Swept Wings at Subsonic and Transonic Speeds*, NASA TN D-209, February, 1960.

9-3 J. H. Lichtenstein and J. L. Williams, Effect of High-Lift Devices on the Static-Lateral-Stability Derivatives of a 45-Degree Sweptback Wing of Aspect Ratio 4.0 and Taper Ratio 0.6 in Combination with a Body, NACA TN 2819, November 1952.